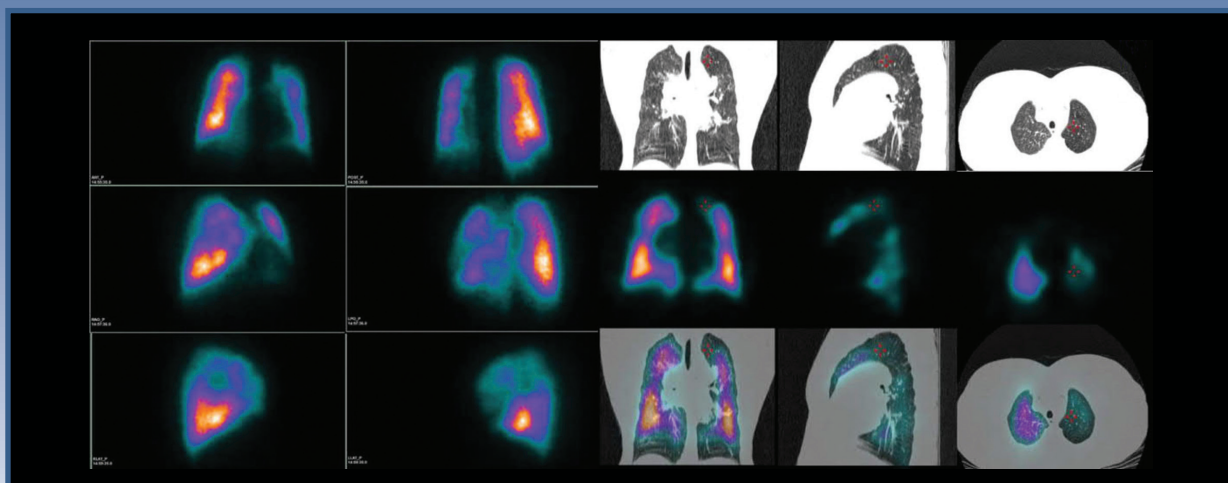


Nuclear Medicine

R · E · V · I · E · W

merged with Problems of Nuclear Medicine

MEiN: 40 pkt.



See page 121

ISSN 1506–9680

2021, Volume 24, Number 2

e-ISSN 1644–4345

Journal of Polish, Serbian, Hungarian, Bulgarian
and Macedonian Societies of Nuclear Medicine



Nuclear Medicine

R · E · V · I · E · W

merged with *Problems of Nuclear Medicine**

Editor-in-Chief

G. Kamiński (Warszawa, Poland)

Deputy Editor-in-Chief

M. Dziuk (Warszawa, Poland)

J. Kunikowska (Warszawa, Poland)

National Editors

I. Garai (Debrecen, Hungary)

D. Huić (Zagreb, Croatia)

D. Sobic Saranovic (Belgrade, Serbia)

Board of Editors:

V. Artiko (Belgrade, Serbia)

R.P. Baum (Bad Berka, Germany)

O. Belohlavek (Prague, Czech Republic)

B. Birkenfeld (Szczecin, Poland)

K. Borbély (Budapest, Hungary)

J. Braziewicz (Kielce, Poland)

J. Buscombe (London, United Kingdom)

J.M. Carrill (Santander, Spain)

I. Carrio (Barcelona, Spain)

A. Celler (Vancouver, Canada)

A. Chiti (Rozzano, Italy)

B. Chrapko (Lublin, Poland)

A. Cuocolo (Naples, Italy)

C.S. Cutler (Columbia, United States)

G. De Vincentis (Rome, Italy)

E. Dziuk (Warszawa, Poland)

R. Howman-Giles (Sydney, Australia)

A. Hubalewska-Dydejczyk (Kraków, Poland)

B. Jarzab (Gliwice, Poland)

W. Kloc (Gdańsk, Poland)

W. Knapp (Hannover, Germany)

V.N. Korsunsky (Moscow, Russia)

M. Kostkiewicz (Kraków, Poland)

I. Kozłowicz-Gudzińska (Warszawa, Poland)

O. Kraft (Ostrava, Czech Republic)

L. Królicki (Warszawa, Poland)

J. Kuśmierek (Łódź, Poland)

J. Lepej (Banska Bystrica, Slovak Republic)

A. Lewiński (Łódź, Poland)

T. Maina (Athens, Greece)

B. Małkowski (Bydgoszcz, Poland)

R. Mikołajczak (Otwock-Świerk, Poland)

M. Myslivecek (Olomuc, Czech Republic)

V. Obradović (Belgrade, Serbia)

A.K. Padhy (Singapore)

E. Piperkova (Sofia, Bulgaria)

A. Płachcińska (Łódź, Poland)

Z. Rajkovic (Banja Luka, Bosnia & Herzegovina)

F. Rogowski (Białystok, Poland)

D. Rubello (Rovigo, Italy)

M. Ruchala (Poznań, Poland)

M.M. Saw (Singapore)

A. Signore (Rome, Italy)

H. Sinzinger (Vienna, Austria)

A. Soricelli (Italy)

A. Sowa-Staszczak (Kraków, Poland)

D.A. Stanescu (Bucharest, Romania)

M. Studniarek (Gdańsk, Poland)

A. Syrenicz (Szczecin, Poland)

I. Szilvasi (Budapest, Hungary)

K. Toth (Warszawa, Poland)

J.H. Turner (Fremantle, Australia)

I. Velikyan (Uppsala, Sweden)

M. Vlajkovic (Nis, Serbia)

P. Vlcek (Praha, Czech Republic)

The Scientific Committee of the journal is being created and the list of the scientific council members contains the persons who have declared willingness to collaborate.

Secretary

A. Krajewska (Warszawa, Poland)

Editorial Office

Wojskowy Instytut Medyczny

ul. Szaserów 128, 04-141 Warszawa

e-mail: nmr@viamedica.pl

Managing Editor

K. Klimek (Gdańsk, Poland)

*Following the agreement concluded on 23 February 2011 between the Polish Society of Nuclear Medicine and Via Medica Sp. z o.o. the journal „Nuclear Medicine Review” has merged with „Problemy Medycyny Nuklearnej”, a journal published since 1987.

Nuclear Medicine Review (ISSN 1506-9680, e-ISSN 1644-4345) is published twice a year by VM Media sp. z o.o., VM Group sp. k., Grupa Via Medica

ul. Świętokrzyska 73, 80-180 Gdańsk, Poland

tel: (+48 58) 320 94 94, fax: (+48 58) 320 94 60; e-mail: redakcja@viamedica.pl, marketing@viamedica.pl

http://www.viamedica.pl

Advertising. For details on media opportunities within this journal please contact the advertising sales department, ul. Świętokrzyska 73, 80-180 Gdańsk, Poland

tel: (+48 58) 320 94 52, e-mail: marketing@viamedica.pl

The Editors accept no responsibility for the advertisement contents.

Single issues requests should be send to e-mail: prenumerata@viamedica.pl. Electronic orders option available at: www.nmr.viamedica.pl



© Via Medica 2021

All rights reserved, including translation into foreign languages. No part of this periodical, either text or illustration, may be used in any form whatsoever. It is particularly forbidden for any part of this material to be copied or translated into a mechanical or electronic language and also to be recorded in whatever form, stored in any kind of retrieval system or transmitted, whether in an electronic or mechanical form or with the aid of photocopying, microfilm, recording, scanning or in any other form, without the prior written permission of the publisher. The rights of the publisher are protected by national copyright laws and by international conventions, and their violation will be punishable by penal sanctions.

Indexation: Crossref, DOAJ (Directory of Open Access Journals), EMBASE, ESCI (Emerging Sources Citation Index), Index Copernicus (100.00), MEDLINE, Polish Medical Bibliography, Ministry of Science and Higher Education (40), Scopus, Ulrich's Periodicals Directory.

Editorial policies and author guidelines are published on journal website: www.journals.viamedica.pl/nuclear_medicine_review



20-0825-001-001

Nuclear Medicine

R · E · V · I · E · W

merged with *Problems of Nuclear Medicine**

2021, Volume 24, Number 2

Editorial V

Original articles

Leili Zarifmahmoudi, Hamidreza Ghorbani, Ramin Sadeghi, Salman Soltani, Kayvan Sadri, Mahmoud Tavakkoli, Maliheh Keshvari
Sentinel lymph node biopsy in upper tract urothelial cancers: an experience with intraoperative radiotracer injection 41

Chrissa Sioka, Christos Moulías, Paraskevi V. Voulgari, Andreas Fotopoulos, Ioannis D. Bassukas
Single photon emission computed tomography myocardial perfusion imaging in patients with moderate to severe psoriasis 46

Ahmed Fathala, Abdulaziz Alsugair, Moheieldin Abouzied, Ahmed Almuhaideb
Patterns of [¹⁸F]FDG myocardial uptake in oncology patients as a predictor of myocardial ischaemia on stress myocardial perfusion imaging 51

Marco Ravanelli, Alberto Grammatica, Guido Squassina, Francesco Bertagna, Domenico Albano, Davide Lancini, Paolo Bosio, Angelo Zigliani, Giorgio Maria Agazzi, Roberto Maroldi, Piero Nicolai, Raffaele Giubbini, Cesare Piazza, Davide Farin
Value of [¹⁸F]FDG PET-CT in the follow-up of surgically treated oral tongue squamous cell carcinoma: single centre cohort analysis on 87 patients 58

Maciej Kolodziej, Marek Saracyn, Arkadiusz Lubas, Dorota Brodowska-Kania, Andrzej Mazurek, Mirosław Dziuk, Jolanta Dymus, Grzegorz Kaminski
Evaluation of the usefulness of positron emission tomography (PET/CT) with [¹⁸F]fluorodeoxyglucose ([¹⁸F]FDG) performed to detect recurrence and/or metastasis of differentiated thyroid cancer in patients with increased thyroglobulin concentration and negative ¹³¹I whole-body scintigraphy — a preliminary study 63

Sonya Sergieva, Radoslav Mangalgiev, Milena Dimcheva, Kamen Nedev, Zahary Zahariev, Bozhil Robev
SPECT-CT imaging with [^{99m}Tc]PSMA-T4 in Patients with recurrent prostate cancer 70

Reviews

Narges Jokar, Abdullatif Amini, Mohammadreza Ravanbod, Maryam Barekat, Hossein Shooli, Ali Gholamrezanezhad, Majid Assadi
State-of-the-art modalities in cardio-oncology: insight from a nuclear medicine approach 82

Sara Kurkowska, Bożena Birkenfeld, Hanna Piwowarska-Bilska
Physical quantities useful for quality control of quantitative SPECT/CT imaging 93

Ebru Salmanoglu
The role of [¹⁸F]FDG PET/CT for gastric cancer management 99

Clinical vignettes

Inci Uslu Biner, Ebru Tatci, Ozlem Ozmen, Mujgan Guler, Fatma Benli
Presentation of genital tuberculosis detected on [¹⁸F]FDG PET-CT scan resembling a primary gynaecological tumour and metastases 104

Hadis Mohammadzadeh Kosari, Seyed Rasoul Zakavi, Somayeh Barashki, Hesamoddin Roustaei Firouzabad, Saeedeh Ataei Nakhaei, Kamran Aryana
Incidental finding of a dermoid cyst in a whole-body iodine scan: importance of using I131 SPECT/CT in the differentiated thyroid carcinoma 106

Punit Sharma, Indranil Ghosh
[¹⁸F]FDG PET-CT findings in an unusual case of synchronous double primary lung cancer of different histologies 108

Fariba Jafari, Mehrosadat Alavi
Incidental detection of COVID-19 associated pneumonia by [^{99m}Tc]UBI scintigraphy 110

Mehrosadat Alavi, Fariba Jafari
Incidental detection of COVID-19 associated pneumonia by thyroid scintigraphy 113

<i>Olgierd Chrabanski, Tomasz Golab</i> Infection of aortobifemoral bypass graft implanted 20 years ago proved by labeled leukocytes SPECT-CT.....	115
<i>Mohsen Arabi, Hanieh Zamani, Masume Soltanabadi, Leila Kalhor</i> [^{99m} Tc]MIBI scintigraphy in a patient with thyroid follicular neoplasm: a case report and review of literature.....	118
<i>Marylin Acuña Hernandez, Tatiana Morales Avellaneda, Jorge Andres Navaez Gomez, Liset Sanchez Orduz</i> Findings in [^{99m} Tc]MAA SPECT/CT in the diagnosis and follow-up of pulmonary embolism after infection by SARS-CoV-2 (COVID-19).....	120
<i>Aleksandra Ledwon, Przemysław Soczomski, Ewa Paliczka-Cieślak, Aleksandra Blewaska, Daria Handkiewicz-Junak</i> False-positive radioiodine uptake in breasts in a female haemodialysis patient	122
<i>Georgios Meristoudis, Ioannis Ilias, Evangelia Zaromytidou, Emmanouil Alevroudis, Athanasios Notopoulos</i> Cholethorax with biliopleural communication detected on [^{99m} Tc]mebrofenin hepatobiliary scintigraphy.....	124



Dear Sirs and Madams,

I would like to announce the “summer” issue of „Nuclear Medicine Review” in 2021. The first chapter consists of six original articles. It opens — written by Iranian colleagues one — who concluded that the sentinel node mapping in upper tract urothelial cancers (UTUC) using a radiotracer as the mapping material is feasible. Injection technique (intra-vesical approach vs peri-tumoral injection after exposure of the tumor) and location of the tumor (proximal vs distal) may affect the feasibility of the technique.

The second one, by Greek scientists titled *Single photon emission computer tomography myocardial perfusion imaging in patients with moderate to severe psoriasis* shows that these patients have similar rate of abnormal Summed Scores for Stress scans (SSS) compared to control patients. However, the difference between SSS and scans for rest are significantly lower in patients with psoriasis. It indicates compromised reversibility of resting perfusion defects.

The next paper from Saudi Arabia indicates that the physiological myocardial [^{18}F]FDG uptake in fasting oncology patients is variable. The regional myocardial [^{18}F]FDG uptake pattern is the most frequent pattern associated with myocardial ischemia on stress single photon emission CT (SPECT) myocardial perfusion imaging (MPI). The agreement between regional FDG uptake and presence of ischemia on SPECT is fair.

The fourth article — from Italy — analyzes the value of [^{18}F]FDG PET-CT in the follow-up of surgically treated oral tongue squamous cell carcinoma. The results demonstrate a change in

diagnostic strategy — as decided by the multidisciplinary team — in about one fifth of patients. These results should prompt in designing a rational surveillance schedule in surgically treated patients with oral tongue squamous cell cancer.

From Poland, we received a paper which concludes that: PET/CT with [^{18}F]FDG is a useful tool for detection of non-radioiodine avid recurrence and/or metastases of Differentiated Thyroid Cancer. The concentration of baseline (natTg) and stimulated Thyroglobulin (sTg) is highly correlated with positive result of PET/CT with [^{18}F]FDG. The concentration of natTg is comparable with sTg in predicting a positive result of PET/CT with [^{18}F]FDG. The cut-off point for positive result of PET/CT for natTg was 1.36 ng/mL and for sTg was 7.05 ng/mL.

The next one is from Bulgaria. It concerns about the SPECT-CT Imaging with [$^{99\text{m}}\text{Tc}$]PSMA in Patients with Recurrent Prostate Cancer and indicates that this method is useful for the diagnosis and restaging of recurrent disease, in consideration of Radio Ligand Therapy and in monitoring of treatment.

In our magazine there are three reviews from Iran, Poland and Turkey concerning (respectively): State of The Art Modalities in Cardio-Oncology, Physical quantities useful for quality control of quantitative SPECT/CT imaging and The role of [^{18}F]FDG PET/CT for gastric cancer management.

Clinical Vignette Chapter shows ten interesting cases. Some of them resemble that COVID-19 pandemic hasn't stopped yet.

In the end of my letter, I wish you a happy summer vacation!

Yours,

Grzegorz Kamiński

G. Kamiński

Editor-in-Chief

Nuclear Medicine Review

Sentinel lymph node biopsy in upper tract urothelial cancers: an experience with intraoperative radiotracer injection

Leili Zarifmahmoudi¹, Hamidreza Ghorbani², Ramin Sadeghi¹, Salman Soltani², Kayvan Sadri¹, Mahmoud Tavakkoli², Maliheh Keshvari²

¹Nuclear Medicine Research Center, Mashhad University of Medical Sciences, Mashhad, Iran

²Kidney Transplantation Complications Research Center, Mashhad University of Medical Sciences, Mashhad, Iran

[Received 7 V 2020; Accepted 28 VI 2021]

ABSTRACT

Background: The feasibility of the sentinel node mapping in upper tract urothelial cancers (UTUC) was evaluated, using a radiotracer as the mapping material.

Material and methods: To identify the sentinel lymph nodes, 37 MBq of [^{99m}Tc] phytate was injected in five patients with the renal pelvis or ureter cancer, who were candidates for ureterectomy and lymphadenectomy. The radiotracer was injected in a peritumoral fashion following the surgical exposure of the tumour. The sentinel lymph nodes were detected using a hand-held gamma probe.

Results: By intraoperatively injecting the radiotracer immediately after surgical exposure of the tumour, at least one sentinel lymph node could be detected in each patient, and the detection rate was 100%. The location of sentinel nodes was in the paracaval, renal hill, retro-aortic, para-aortic, common iliac, and external iliac areas, which was dependent on the tumour location. No false-negative case was identified.

Conclusions: Sentinel node mapping is feasible in UTUC. Injection technique (intra-vesical approach vs peri-tumoral injection after exposure of the tumour) and location of the tumour (proximal vs distal) may affect the technique's feasibility.

KEY words: lymphoscintigraphy; nuclear medicine; ureter; renal pelvis; sentinel lymph node biopsy; lymphadenectomy

Nucl Med Rev 2021; 24, 2: 41–45

Introduction

Urothelial carcinomas can be originated from lower (bladder and urethra) or upper (pyelocaliceal cavities and ureter) parts of the urinary tract [1]. Bladder carcinomas (lower tract urothelial carcinomas) account for 90–95% of the urinary tract malignancies; however, the upper urinary tract (UUT) transitional cell carcinoma (TCC) is an uncommon type of malignancies and accounts for 5–10% of urinary tract cancers [2, 3]. Tumours of the ureter are particularly rare compared to bladder cancer or renal pelvis tumours, despite sharing common histopathology and similar risk factors [4].

The most common treatment option for high-grade tumours originate in the upper ureter and renal pelvis, is nephroureterectomy followed by regional lymph node dissection (LND); however, due to the low incidence of the upper tract urinary carcinoma (UTUC), the indication and extent of LND is not standardized [5]. The risk of lymph node involvement increases with the T stage of the disease, and up to 60% of UTUCs demonstrate local invasion at diagnosis [6]. LND is recommended to be performed based on the laterality and tumour location following nephroureterectomy; however, due to variable lymphatic drainage and lack of consensus on anatomical boundaries, the potential benefit of routine LND on survival or disease recurrence remains controversial [7, 8].

Sentinel lymph node mapping procedure is used for detecting the first lymph node in the path of lymphatic drainage of cancers. This technique reveals the pathological status of the regional lymph nodes for the better staging of the disease, determining the treatment strategy, and preventing the unnecessary LND. Sentinel lymph node biopsy is routinely performed for breast cancer,

Correspondence to: Hamidreza Ghorbani
 Kidney Transplantation Complications Research Center, Mashhad University of Medical Sciences, Mashhad, Iran
 e-mail: Ghorbanibr@mums.ac.ir

malignant melanoma, gynaecological, and penile tumours; however, for other urologic genitourinary carcinomas, it is still under investigation [9–14].

The present study evaluated the feasibility of sentinel node mapping in UTUC using a radiotracer as the mapping material.

Material and methods

This study was approved by the ethics committee of Mashhad University of Medical Sciences under the number 940295. Between 2016 and 2019, all the admitted UTUC patients at the urology department of Imam Reza Hospital, Mashhad, Iran, were included. All the patients gave their informed consent before inclusion in the study. Patients with negative lymph node involvement before the surgery, based on clinical and radiological evaluations (cN0, cM0) were included. The exclusion criteria were positive lymph nodes metastasis and a history of chemotherapy or radiotherapy.

Radiotracer injection

Following anaesthesia, 37 MBq of [^{99m}Tc]phytate in two divided doses (0.5 mL each) were used as the radiotracer. In the first four patients with TCC of the distal part of the ureter, the radiotracer was injected sub-mucosally in the peritumoral area of the tumour through ureteroscopy. These patients were excluded from the study due to sentinel lymph node detection failure. The injection technique was changed in five other patients: the radiotracer was injected into two peritumoral sites following the tumour's exposure (Tab. 1, Fig. 1).

Sentinel node biopsy

The mean time between the tracer injection and performing intraoperative sentinel lymph node mapping was one hour. Following the excision of the ureter and kidney and before starting lymphadenectomy, a hand-held gamma probe (SURGIGUIDE, Partonegar Persia) was used to measure the radioactivity and perform sentinel node biopsy. The sentinel lymph nodes were defined as any lymph node with an in-vivo count of at least ten times higher than the background (thigh). These nodes were dissected and counted again ex-vivo. The dissected lymph nodes were put on

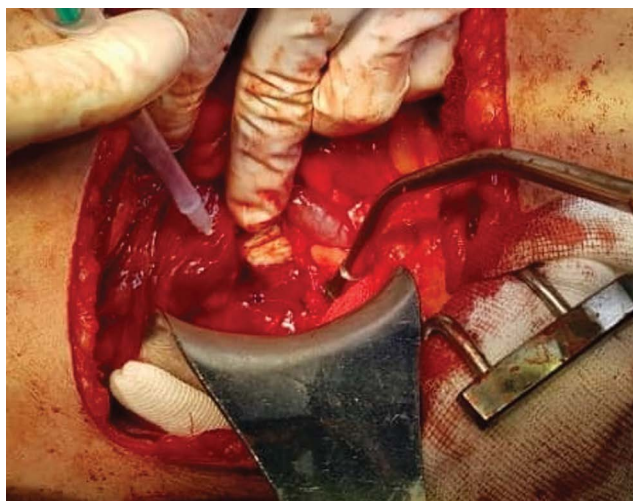


Figure 1. Injection of the radiotracer in a patient with mid-urethral tumour, after the surgical exposure of the tumour

the tip of the gamma probe while the probe was pointed to the ceiling. All the lymph nodes with ex-vivo count five times higher than the background (thigh) were eventually determined as the sentinel lymph node.

After harvesting the detected sentinel lymph nodes, the surgical area was searched again to confirm the complete sentinel lymph node removal.

Regional lymphadenectomy was performed based on the surgeon's decision to assess the false-negative rate. For the left-sided renal pelvis, upper ureteral, and mid-urethral tumours, the lymphadenectomy dissection area covered para-aortic, pre-aortic, and inter-aortocaval nodes from the renal hilum to the aortic bifurcation. For the right-sided renal pelvis and upper ureteral tumours, mid-urethral tumours lymph nodes of the paracaval, precaval, and interaortocaval areas from the renal hilum to the aortic bifurcation are considered for lymphadenectomy. Common iliac, external iliac, obturator, and hypogastric lymph nodes of each side of the pelvic are also dissected for mid to distal ureteral tumours.

Table 1. Detailed data of the included patients

Patients	Gender	age	Tumor location	kidney	Tumor stage	Tumor larger diameter (cm)	Detection of the SN	SN location	Number of SN	Involvement of SN	Involvement of lymph nodes
1	M	53	Middle	right	T3	2.5	Yes	Paracaval	3	Yes 1/3	Yes (paracaval)
2	M	74	Proximal	Left	T1	2.7	Yes	Renal hill	2	No	No
3	M	40	Renal pelvis (proximal)	Right	T3	4 × 2	Yes	Renal hill	2	No	No
4	M	80	Distal	Right	T2	4.5	Yes	Common iliac external iliac	2	No	No
5	F	48	Renal pelvis (proximal)	left	T2	4	Yes	Retroaort and Paraaort	2	No	No

SN — sentinel node

Histopathological investigation

The pathologists examined the excised lymph nodes and specimen; all dissected tissues were formalin-fixed, paraffin-embedded, and serially sectioned for haematoxylin-eosin staining. The histopathological status of the sentinel nodes was compared with the other dissected lymph nodes.

Evaluated indices (detection rate and false-negative rate)

The primary endpoints of the study were sentinel node detection rate and false-negative rate (FNR).

The detection rate was measured as the ratio of all cases with at least one detected sentinel node to all included patients. The false-negative rate was measured as the ratio of patients with involved non-sentinel lymph nodes despite pathologically free sentinel lymph nodes to all patients with involved nodes and at least one harvested sentinel node [15, 16].

Results

Five patients with renal pelvis or ureter cancer were included; four patients were male, and one was female with a mean age of 59.

The tumour was localized in proximal ureter in two patients, distal ureter in one patient, and middle ureter in one patient.

Demographic data and information regarding the sentinel lymph node detection are summarized in Table 1.

Detection rate

In all patients with the peritumorally injection of the radiotracer following the surgical exposure of the tumour, at least one sentinel node was detected. The detection rate was 100% in these five patients, and eleven (median = 2) sentinel lymph nodes were dissected in total (Fig. 1).

All the patients with no detected sentinel node were injected through the ureteroscopy at two sites around the visible tumour; so, the detection rate was zero in UTUC patients with ureteroscopic injections; these patients were excluded from the study.

The detected sentinel nodes were in the paracaval lymph nodes (patient 1), renal hilum lymph nodes (patients 2 and 3), retro aortic and para-aortic lymph nodes (patient 5), and common iliac and external iliac lymph nodes (patient 4).

False-negative rate

One patient (number 1) had pathological involvement of the dissected sentinel lymph node. The detected sentinel nodes were in paracaval area (three sentinel nodes), and one showed tumoral involvement. Based on the pathology report, the non-sentinel paracaval lymph nodes dissected in this patient were also pathologically involved.

No lymph node involvement was noted in the remaining four patients (no false-negative result).

Discussion

Upper urinary tract TCCs are among the rare types of genitourinary tumours which develop in the renal pelvis and ureter and might be associated with bladder cancer. To the authors' knowledge, they evaluated the feasibility of the sentinel node mapping approach for

the first time in patients with UTUC including, patients with TCCs in the proximal, middle, and distal parts of the ureter and also in the renal pelvis. They used Tc-99m phytate as the mapping material, and no blue dye was used due to the reported adverse reaction to the blue dye injection [17, 18].

The detection rate in this study was highly dependent on the injection method of the radiotracer. In patients with the ureteroscopic injection of the tracer, no sentinel node could be identified intra-operatively. So, these patients were excluded from the study and changed the injection technique. In the remaining patients (five patients) with radiotracer injection following the tumour exposure during the surgery, at least one sentinel node could be identified. These results are most likely due to the technical difficulty of injection through a ureteroscope. The movement of the radiotracer in the lymphatic system is reasonably fast, which ensures a successful mapping using an intra-operative injection of the tracer [19–21].

Although LND is performed for better staging of the tumour, due to the low prevalence of UTUC, the curative role of LND continues to be debated, and LND is not currently performed in all patients worldwide. In patients with the T1 stage of the disease, there might be a low probability of the LN metastases, and LND does not seem to improve the staging. All the current evidence on UTUC is based on retrospective studies with a limited study population. To precisely determine the indication of LND and its optimal template, which varies according to the location of the disease, more extensive studies should be performed [22–27]. Although the LND template has been studied previously, there is no standardized template for LND, and it is dependent on the site of the affected ureter [1, 28].

Based on the present results, sentinel lymph nodes as the first lymph nodes which receive the metastatic cells were located in the renal hilum, retro-aortic, and para-aortic lymph nodes of the patients with TCCs in the proximal part of the left ureter or the left renal pelvis. However, in two patients with TCCs in the middle part of the right ureter and the right renal pelvis, the detected sentinel lymph nodes were in paracaval and right renal hilum lymph nodes. The sentinel lymph nodes in one of the study patients with TCC in the distal part of the right ureter was in the common iliac and external iliac lymph nodes. The present results were in accordance with the previous studies in this regard. Kondo et al. [22] proposed that the paracaval, retrocaval, and interaortocaval nodes have a higher risk of metastases in patients with the right renal pelvis and upper two-thirds of the ureter tumours and should be included in the LND template. On the other hand, the renal hilum and para-aortic nodes in patients with left renal pelvis tumours should be considered in the LND template.

We included only patients with no lymph node involvement based on preoperative imaging; however, these modalities have shown limited accuracy for preoperative LN staging or identifying patients with LN invasion [29, 30]. LND in patients with UTUC is highly surgeon-dependent due to inaccurate prediction tools, and sentinel lymph node mapping might be of value to find the metastatic status of the regional lymph nodes. This study showed that sentinel node could be detected in all the UTUC patients with the intraoperative injection of the radiotracer mapping, and sentinel lymph node mapping might be a feasible method in patients with tumours in different parts of the ureter or renal pelvis. However, more extensive studies (preferably multicentral) are needed before any definitive conclusion.

The major limitation of the present study was the low sample size due to the low incidence of UTUC. However, to the authors' knowledge, this study is the first study on intraoperative sentinel lymph node mapping in UTUC tumours, which obtained promising results.

Conclusions





Sentinel node mapping is feasible in UTUC. Injection technique (intra-vesical approach vs peri-tumoral injection after exposure of the tumour) and location of the tumour (proximal vs distal) might affect the technique's feasibility.

References

- Rouprêt M, Babjuk M, Compérat E, et al. European Association of Urology guidelines on upper urinary tract urothelial carcinoma: 2017 update. *Eur Urol.* 2018; 73(1): 111–122, doi: [10.1016/j.eururo.2017.07.036](https://doi.org/10.1016/j.eururo.2017.07.036), indexed in Pubmed: [28867446](https://pubmed.ncbi.nlm.nih.gov/28867446/).
- Babjuk M, Böhle A, Burger M, et al. EAU guidelines on non-muscle-invasive urothelial carcinoma of the bladder: update 2016. *Eur Urol.* 2017; 71(3): 447–461, doi: [10.1016/j.eururo.2016.05.041](https://doi.org/10.1016/j.eururo.2016.05.041), indexed in Pubmed: [27324428](https://pubmed.ncbi.nlm.nih.gov/27324428/).
- Siegel RL, Miller KD, Jemal A. Cancer Statistics, 2017. *CA Cancer J Clin.* 2017; 67(1): 7–30, doi: [10.3322/caac.21387](https://doi.org/10.3322/caac.21387), indexed in Pubmed: [28055103](https://pubmed.ncbi.nlm.nih.gov/28055103/).
- Greenlee RT, Murray T, Bolden S, et al. Cancer statistics, 2000. *CA Cancer J Clin.* 2000; 50(1): 7–33, doi: [10.3322/canjclin.50.1.7](https://doi.org/10.3322/canjclin.50.1.7), indexed in Pubmed: [10735013](https://pubmed.ncbi.nlm.nih.gov/10735013/).
- Spieß PE, Agarwal N, Bangs R, et al. Bladder cancer, version 5.2017, NCCN clinical practice guidelines in oncology. *J Natl Compr Canc Netw.* 2017; 15(10): 1240–1267, doi: [10.6004/jnccn.2017.0156](https://doi.org/10.6004/jnccn.2017.0156), indexed in Pubmed: [28982750](https://pubmed.ncbi.nlm.nih.gov/28982750/).
- Leow JJ, Liu Z, Tan TW, et al. Optimal management of upper tract urothelial carcinoma: current perspectives. *Onco Targets Ther.* 2020; 13: 1–15, doi: [10.2147/OTT.S225301](https://doi.org/10.2147/OTT.S225301), indexed in Pubmed: [32021250](https://pubmed.ncbi.nlm.nih.gov/32021250/).
- Stein JP, Lieskovsky G, Cote R, et al. Radical cystectomy in the treatment of invasive bladder cancer: long-term results in 1,054 patients. *J Clin Oncol.* 2001; 19(3): 666–675, doi: [10.1200/JCO.2001.19.3.666](https://doi.org/10.1200/JCO.2001.19.3.666), indexed in Pubmed: [11157016](https://pubmed.ncbi.nlm.nih.gov/11157016/).
- Zigeuner R, Pummer K. Urothelial carcinoma of the upper urinary tract: surgical approach and prognostic factors. *Eur Urol.* 2008; 53(4): 720–731, doi: [10.1016/j.eururo.2008.01.006](https://doi.org/10.1016/j.eururo.2008.01.006), indexed in Pubmed: [18207315](https://pubmed.ncbi.nlm.nih.gov/18207315/).
- Zarifm Mahmoudi L, Ghorbani H, Sadri K, et al. Sentinel node biopsy in urothelial carcinoma of the bladder: systematic review and meta-analysis. *Urol Int.* 2019; 103(4): 373–382, doi: [10.1159/000497310](https://doi.org/10.1159/000497310), indexed in Pubmed: [30836375](https://pubmed.ncbi.nlm.nih.gov/30836375/).
- Hassanzade M, Attaran M, Treglia G, et al. Lymphatic mapping and sentinel node biopsy in squamous cell carcinoma of the vulva: systematic review and meta-analysis of the literature. *Gynecol Oncol.* 2013; 130(1): 237–245, doi: [10.1016/j.ygyno.2013.04.023](https://doi.org/10.1016/j.ygyno.2013.04.023), indexed in Pubmed: [23612317](https://pubmed.ncbi.nlm.nih.gov/23612317/).
- Sadeghi R, Gholami H, Zakavi SR, et al. Accuracy of sentinel lymph node biopsy for inguinal lymph node staging of penile squamous cell carcinoma: systematic review and meta-analysis of the literature. *J Urol.* 2012; 187(1): 25–31, doi: [10.1016/j.juro.2011.09.058](https://doi.org/10.1016/j.juro.2011.09.058), indexed in Pubmed: [22088350](https://pubmed.ncbi.nlm.nih.gov/22088350/).
- Kadkhodayan S, Hasanzadeh M, Treglia G, et al. Sentinel node biopsy for lymph nodal staging of uterine cervix cancer: a systematic review and meta-analysis of the pertinent literature. *Eur J Surg Oncol.* 2015; 41(1): 1–20, doi: [10.1016/j.ejso.2014.09.010](https://doi.org/10.1016/j.ejso.2014.09.010), indexed in Pubmed: [25454828](https://pubmed.ncbi.nlm.nih.gov/25454828/).
- Sadeghi R, Tabasi KT, Bazaz SMM, et al. Sentinel node mapping in the prostate cancer. Meta-analysis. *Nuklearmedizin.* 2011; 50(3): 107–115, doi: [10.3413/nukmed-0339-10-07](https://doi.org/10.3413/nukmed-0339-10-07), indexed in Pubmed: [21264441](https://pubmed.ncbi.nlm.nih.gov/21264441/).
- Ansari M, Rad MA, Hassanzadeh M, et al. Sentinel node biopsy in endometrial cancer: systematic review and meta-analysis of the literature. *Eur J Gynaecol Oncol.* 2013; 34(5): 387–401, indexed in Pubmed: [24475571](https://pubmed.ncbi.nlm.nih.gov/24475571/).
- Sadeghi R. Sentinel node mapping diagnostic studies warrant a unique reporting criteria: comment on Xiong et al. systematic review. *Eur J Surg Oncol.* 2014; 40(8): 1025–1026, doi: [10.1016/j.ejso.2014.03.031](https://doi.org/10.1016/j.ejso.2014.03.031), indexed in Pubmed: [24857379](https://pubmed.ncbi.nlm.nih.gov/24857379/).
- Zarifm Mahmoudi L, Sadeghi R. Re: radio-guided lymph node mapping in bladder cancer using SPECT/CT and intraoperative -Probe methods. *Clin Nucl Med.* 2017; 42(4): 327, doi: [10.1097/RLU.0000000000001485](https://doi.org/10.1097/RLU.0000000000001485), indexed in Pubmed: [27997419](https://pubmed.ncbi.nlm.nih.gov/27997419/).
- Ramin S, Azar FP, Malihe H. Methylene blue as the safest blue dye for sentinel node mapping: emphasis on anaphylaxis reaction. *Acta Oncol.* 2011; 50(5): 729–731, doi: [10.3109/0284186X.2011.562918](https://doi.org/10.3109/0284186X.2011.562918), indexed in Pubmed: [21413854](https://pubmed.ncbi.nlm.nih.gov/21413854/).
- Jangjoo A, Forghani MN, Mehrabibahar M, et al. Anaphylaxis reaction of a breast cancer patient to methylene blue during breast surgery with sentinel node mapping. *Acta Oncol.* 2010; 49(6): 877–878, doi: [10.3109/02841861003769964](https://doi.org/10.3109/02841861003769964), indexed in Pubmed: [20429734](https://pubmed.ncbi.nlm.nih.gov/20429734/).
- Sadeghi R, Forghani MN, Memar B, et al. How long the lymphoscintigraphy imaging should be continued for sentinel lymph node mapping? *Ann Nucl Med.* 2009; 23(6): 507–510, doi: [10.1007/s12149-009-0284-y](https://doi.org/10.1007/s12149-009-0284-y), indexed in Pubmed: [19588215](https://pubmed.ncbi.nlm.nih.gov/19588215/).
- Aliakbarian M, Memar B, Jangjoo A, et al. Factors influencing the time of sentinel node visualization in breast cancer patients using intradermal injection of the radiotracer. *Am J Surg.* 2011; 202(2): 199–202, doi: [10.1016/j.amjsurg.2010.06.035](https://doi.org/10.1016/j.amjsurg.2010.06.035), indexed in Pubmed: [21810501](https://pubmed.ncbi.nlm.nih.gov/21810501/).
- Jangjoo A, Forghani MN, Mehrabibahar M, et al. Comparison of early and delayed lymphoscintigraphy images of early breast cancer patients undergoing sentinel node mapping. *Nucl Med Commun.* 2010; 31(6): 521–525, indexed in Pubmed: [20429094](https://pubmed.ncbi.nlm.nih.gov/20429094/).
- Kondo T, Nakazawa H, Ito F, et al. Impact of the extent of regional lymphadenectomy on the survival of patients with urothelial carcinoma of the upper urinary tract. *J Urol.* 2007; 178(4 Pt 1): 1212–1217, doi: [10.1016/j.juro.2007.05.158](https://doi.org/10.1016/j.juro.2007.05.158), indexed in Pubmed: [17698147](https://pubmed.ncbi.nlm.nih.gov/17698147/).
- Brausi MA, Gavioli M, De Luca G, et al. Retroperitoneal lymph node dissection (RPLD) in conjunction with nephroureterectomy in the treatment of infiltrative transitional cell carcinoma (TCC) of the upper urinary tract: impact on survival. *Eur Urol.* 2007; 52(5): 1414–1418, doi: [10.1016/j.eururo.2007.04.070](https://doi.org/10.1016/j.eururo.2007.04.070), indexed in Pubmed: [17507148](https://pubmed.ncbi.nlm.nih.gov/17507148/).
- Roscigno M, Cozzarini C, Bertini R, et al. Prognostic value of lymph node dissection in patients with muscle-invasive transitional cell carcinoma of the upper urinary tract. *Eur Urol.* 2008; 53(4): 794–802, doi: [10.1016/j.eururo.2008.01.008](https://doi.org/10.1016/j.eururo.2008.01.008), indexed in Pubmed: [18207313](https://pubmed.ncbi.nlm.nih.gov/18207313/).
- Roscigno M, Shariat SF, Freschi M, et al. Assessment of the minimum number of lymph nodes needed to detect lymph node invasion at radical nephroureterectomy in patients with upper tract urothelial cancer. *Urology.* 2009; 74(5): 1070–1074, doi: [10.1016/j.urology.2009.04.084](https://doi.org/10.1016/j.urology.2009.04.084), indexed in Pubmed: [19883824](https://pubmed.ncbi.nlm.nih.gov/19883824/).
- Roscigno M, Shariat SF, Margulis V, et al. The extent of lymphadenectomy seems to be associated with better survival in patients with nonmetastatic upper-tract urothelial carcinoma: how many lymph nodes should be removed? *Eur Urol.* 2009; 56(3): 512–518, doi: [10.1016/j.eururo.2009.06.004](https://doi.org/10.1016/j.eururo.2009.06.004), indexed in Pubmed: [19559518](https://pubmed.ncbi.nlm.nih.gov/19559518/).
- Miyake H, Hara I, Gohji K, et al. The significance of lymphadenectomy in transitional cell carcinoma of the upper urinary tract. *Br J Urol.* 1998; 82(4): 494–498, doi: [10.1046/j.1464-410x.1998.00800.x](https://doi.org/10.1046/j.1464-410x.1998.00800.x), indexed in Pubmed: [9806176](https://pubmed.ncbi.nlm.nih.gov/9806176/).
- Roscigno M, Brausi M, Heidenreich A, et al. Lymphadenectomy at the time of nephroureterectomy for upper tract urothelial cancer. *European Urology.* 2011; 60(4): 776–783, doi: [10.1016/j.eururo.2011.07.009](https://doi.org/10.1016/j.eururo.2011.07.009).

29. Secin FP, Koppie TM, Salamanca JI, et al. Evaluation of regional lymph node dissection in patients with upper urinary tract urothelial cancer. *Int J Urol.* 2007; 14(1): 26–32, doi: [10.1111/j.1442-2042.2006.01664.x](https://doi.org/10.1111/j.1442-2042.2006.01664.x), indexed in Pubmed: [17199856](https://pubmed.ncbi.nlm.nih.gov/17199856/).
30. Lughezzani G, Jeldres C, Isbarn H, et al. A critical appraisal of the value of lymph node dissection at nephroureterectomy for upper tract urothelial carcinoma. *Urology.* 2010; 75(1): 118–124, doi: [10.1016/j.urology.2009.07.1296](https://doi.org/10.1016/j.urology.2009.07.1296), indexed in Pubmed: [19864000](https://pubmed.ncbi.nlm.nih.gov/19864000/).

Single photon emission computed tomography myocardial perfusion imaging in patients with moderate to severe psoriasis

Chrissa Sioka¹, Christos Moulias², Paraskevi V. Voulgari³, Andreas Fotopoulos¹, Ioannis D. Bassukas²

¹Department of Nuclear Medicine, Medical School, University Hospital of Ioannina, Greece

²Department of Skin and Venereal Diseases, Medical School, University Hospital of Ioannina, Greece

³Rheumatology Clinic, Department of Internal Medicine, Medical School, University of Ioannina, Greece

[Received 24 VI 2021; Accepted 09 VI 2021]

Abstract

Background: Psoriasis is a chronic inflammatory disorder with an increased risk for coronary artery disease (CAD). This retrospective study aimed to evaluate the rate of myocardial ischaemia in patients with psoriasis subjected to myocardial perfusion imaging (MPI).

Material and methods: Twelve patients with moderate to severe psoriasis that had MPI were compared to 395 MPIs randomly retrieved from our MPIs pool data. All patients had a [^{99m}Tc]tetrofosmin stress — rest single-photon emission computer tomography ([^{99m}Tc]SPECT). Summed difference scores (SDS) were calculated for stress (SSS), rest (SRS) and their difference (SDS = SSS – SRS).

Results: There was no significant difference in the frequency of abnormal MPI SPECT outcomes between patients with vs. without psoriasis (6/12 vs 214/395 respectively; $p = 0.778$). From the evaluation of SSS, SRS and SDS, only the SDS scores of inadequately compensated resting perfusion defects were significantly lower in patients with psoriasis ($p = 0.012$).

Conclusions: Patients with moderate-to-severe psoriasis had a similar rate of abnormal SSS scans compared to control patients. However, the SDS scans were significantly lower in patients with psoriasis indicating compromised reversibility of resting perfusion defects. Larger controlled studies are needed to verify these observations.

KEY words: psoriasis; myocardial perfusion imaging; SPECT; myocardial ischaemia; perfusion defects

Nucl Med Rev 2021; 24, 2: 46–50

Introduction

Psoriasis is a chronic, recurrent, multifactorial inflammatory skin disorder with a complex co-morbidities profile, which includes increased coronary artery disease (CAD) risk [1]. The higher prevalence of cardiovascular risk factors is translated into a higher CAD burden [2], the higher lifetime risk of a major adverse

cardiovascular event (MACE) and a higher cardiovascular mortality rate, however, the latter only in patients with severe disease and/or psoriatic arthritis [3].

Whenever feasible, coronary angiography (CA) remains the gold standard for the diagnosis of CAD. Alternatively, non-invasive cardiovascular imaging methods are important for the prediction of future MACE in patients with CA contraindications. Among them, myocardial perfusion imaging (MPI) single photon emission computed tomography (SPECT) is probably the modality with the highest impact to detect a silent myocardial ischaemic region [4]. To date, MPI data has been only occasionally reported in patients with psoriasis [5, 6]. This retrospective study aimed to evaluate the myocardial status in patients with moderate-to-severe psoriasis utilizing MPI.

Correspondence to: Andreas Fotopoulos
Department of Nuclear Medicine, Medical School,
University Hospital of Ioannina, Greece
e-mail: professor.fotopoulos@yahoo.com

Material and methods

By comparing the medical records of the Nuclear Medicine and Dermatology Departments we identified 12 MPIs study outcomes in 12 patients with a history of moderate-to-severe psoriasis. Since the prevalence rate of all psoriasis cases in the reference population is approximately 3% [7], we additionally retrieved randomly MPI results of 395 patients without psoriasis which formed the control group independent of their medical history, cardiac or other diseases. Thus, this yielded the study population of 407 patients, which included approximately 3% (12/407) of the patient group and 97% (395/407) of the control group. The assumption was that randomly selected that large control group of patients with other medical conditions could better balance any variations in patient characteristics between the 2 groups.

All MPIs (inpatients and control individuals) were performed after requisition by a cardiologist for a variety of reasons, using a 1-day imaging protocol according to published guidelines [8], with stress protocol consisted either of a dynamic exercise — Bruce protocol treadmill exercise test or a pharmacological exercise with dipyridamole or dobutamine. The injected dose was 8 mCi [^{99m}Tc] tetrofosmin at stress and 20 mCi [^{99m}Tc]tetrofosmin at rest. Forty minutes later, the images were acquired via a 90°-angled dual-head camera, using a collimator with 64 stops and 25 s per projection over a 180° arc. Subsequently, the images were reconstructed without attenuation correction as previously reported [9].

Images were visually evaluated by two nuclear medicine specialists, applying a 5-point severity scoring scale from normal (score = 0) to absent (score = 4) perfusion to a 17 segments polar myocardium map as previously reported [10, 11].

Summed stress scores (SSS), summed rest scores (SRS) and summed difference scores (SDS) was valued for semiquantitative visual analysis. Summed scores over the 17 myocardium segments (range: 0–64) were evaluated separately for stress [SSS reflects both stress-induced and resting perfusion defects (*i.e.*, ischaemia + infarct)] and rest (SRS-resting perfusion defects (*i.e.*, reflecting scar/hibernating myocardium or artifact)] images. In addition, their difference [SDS = SSS – SRS, a measure of reversibility in response to exercise or pharmacologic stress, (*i.e.*, ischaemia)], was additionally calculated. SSS scores ≥ 4 were considered to indicate myocardial ischaemia — ('pathologic' MPI), graded further as mild ($4 \leq \text{SSS} < 9$), moderate ($9 \leq \text{SSS} < 14$) and severe for $\text{SSS} \geq 4$ [12]. Comparisons of traits of interest between patients with vs. without psoriasis were quantified by Fisher's exact, χ^2 - and Mann-Whitney U- tests. The impact of sex (male, female), age ('elderly', *i.e.* > 65, versus younger patients) and psoriasis (yes, no) on the MPI scores was inferred with 'generalized linear' and for the dichotomous outcome 'pathologic' MPI with logistic regression models respectively. All statistical tests were calculated with the SPSSv26 software at a significance level $p < 0.05$.

Results

Relevant demographic and laboratory findings of the 12 psoriasis patients [6 men and 6 women; mean age: 70.7 years; psoriasis area and severity index (PASI) score: 19.2] are summarized in Supplementary Table 1. Patients with psoriasis were significantly older at the time of MPI (in average about 10 years, $p = 0.001$,

Mann-Whitney U-test; Tab. 2) Psoriatic patients had also increased inflammation parameters, C-reactive protein (CRP; average: 10.4) and erythrocyte sedimentation rate (ESR; average: 39.1), which reflect disease activity. In addition, most patients with psoriasis had traditional risk factors for CAD such as increased cholesterol levels and diabetes mellitus and some of them a history of cardiac morbidity (Tab. 1).

There was no significant difference in the frequency of abnormal MPI outcomes between patients with vs. without psoriasis (6/12 vs 214/395 respectively; $p = 0.778$, Fisher's exact test) or the distributions of the different MPI assessed degrees of myocardial ischaemia ($p = 0.756$; χ^2 -test). From the 3 parameters of the MPI evaluation (SSS, SRS and SDS), only the SDS scores differed between patients with and without psoriasis, with SDS being significantly lower in patients with psoriasis ($p = 0.012$, Mann-Whitney U-test; Tab. 2 and Fig. 1). Moreover, the above impact of psoriasis on the SDS scores was substantiated further by analysing the impact of age, sex and psoriasis on the MPI scores with regression

Table 1. Demographic, clinical and laboratory characteristics of $n = 12$ patients with psoriasis

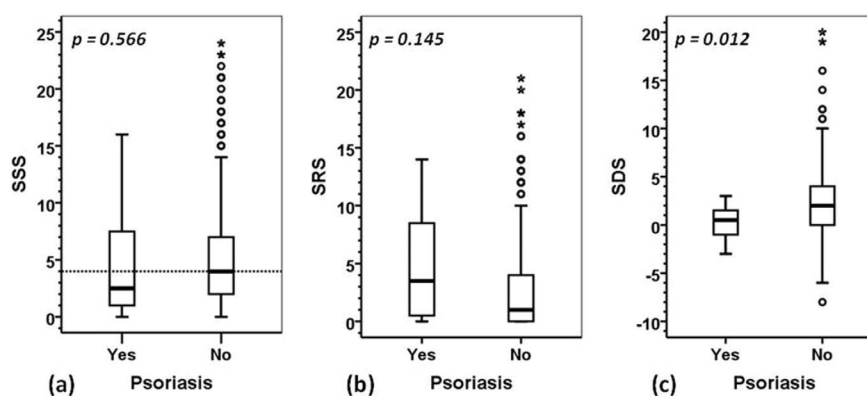
	Range		
	Mean (SEM ¹)	Min	Max
Age (year)	70.7 (1.8)	56	78
Sex (number)	6 Male / 6 Female		
Psoriasis characteristics			
PASI	19.2 (2.7)	10	35
Psoriatic arthritis (number)	1 / 12		
Acrodermatitis continua (number)	1 / 12		
ESR ¹ (mm/h)	39.1 (5.5)	19	72
CRP ¹ (mg/l, normal values: 0–6)	10.4 (1.8)	2	20
Elevated CRP (number)	8 / 12		
Cholesterol (mg/dl)			
Total cholesterol	198.7 (17.9)	87	267
LDL ¹	116.7 (15.0)	26	176
HDL ¹	42.0 (3.1)	25	56
LDL / HDL	2.7 (0.3)	1.0	3.6
Triglycerides	205.3 (16.3)	109	255
Glucose (mg/dl)	168.4 (20.2)	92	308
Psoriasis treatment (number)			
Topical psoriasis treatment (number)	12/12		
Systemic psoriasis treatment (number)	12/12		
Systemic <i>per os</i> ² (number)	10/12		
Biological ³ (number)	10/12		
CVD ¹			
Myocardial infarction (number)	2/12		
Heart insufficiency (number)	1/12		
Aorta insufficiency (number)	2/12		
Atrial fibrillation (number)	2/12		

¹Abbreviations. CRP — C-reactive protein, CVD: cardiovascular disease, ESR — erythrocyte sedimentation rate, HDL — high-density lipoprotein, LDL — low-density lipoprotein, SEM — standard error of the mean. ²acitretin, apremilast ³Adalimumab, efalizumab, etanercept, infliximab, secukinumab, ustekinumab

Table 2. Comparison of age at SPECT MPI conduction and SPECT MPI myocardial ischemia scores between patients with psoriasis and controls (mean [SEM]; p-values: Mann-Whitney U-test)

	All patients (n = 407)			Elderly patients (age > 65; n = 134)		
	Psoriasis n = 12	Control n = 395	p	Psoriasis n = 12	Control n = 124	p
SSS ¹	70.7 [1.80]	60.0 [0.60]	0.001		Not applicable	
SRS ¹	4.92 [1.55]	5.33 [0.26]	0.566	5.10 [1.77]	5.90 [0.49]	0.478
SDS ¹	4.67 [1.34]	2.91 [0.20]	0.145	4.60 [1.47]	3.75 [0.41]	0.410
MPI ²	0.25 [0.52]	2.43 [0.12]	0.012	0.50 [0.58]	2.16 [0.26]	0.022

¹SPECT MPI ischaemia score: generalized linear model; ²myocardial ischaemia (pathologic MPI): logistic regression model; MPI — pathologic myocardial perfusion by MPI SPECT (SSS \geq 4); SRS — Ischaemia reversibility scores, SDS = SSS – SRS; SEM — Standard Error of the Mean; SRS — Summed Rest Score; SSS — Summed Stress Score; SRS: Summed Rest Score; SDS — Ischaemia reversibility scores, SDS = SSS – SRS; MPI — pathologic myocardial perfusion by MPI SPECT (SSS \geq 4), SEM — Standard Error of the Mean.

**Figure 1.** Box-plot diagrams of SPECT MPI summed scores of patients with vs. without psoriasis (p: significance; Mann-Whitney U-test);

A. SSS: ischaemia scores at stress. Dashed line: score limit for ischaemia; **B.** SRS: ischaemia scores at rest; **C.** SDS: scores of reversibility of stress ischaemia (SDS = SSS – SRS); MPI — myocardial perfusion imaging; SPECT — single photon emission computed tomography

models. Of these three factors, male sex was the most important and universal predictor of myocardial ischaemia (Tab. 3). However, psoriasis remains a significant independent predictor of the SDS ($p = 0.023$). Finally, older age was a significant predictor only of a higher degree of resting perfusion defects (SRS score; $p = 0.016$).

Discussion

To the best of the authors' knowledge, this is the first report of the results of cardiologist's indicated MPI tests in patients with moderate-to-severe psoriasis. The main outcome of this study is a comparable prevalence of myocardial ischaemia (around 50%) in patients with and without psoriasis, even though the former patients were significantly older at the time of the MPI conduction. However, the compromised myocardial oxygenation of the patients with moderate-to-severe psoriasis seems to be already established at a younger age. Employing MPI Zutt et al. [6], found a comparable rate of ischaemia (56%) in 50 prospectively examined much younger psoriasis patients (average 49.3 years, *i.e.*, about 20 years younger compared to the present cohort) with a similar disease burden. In this context, it is worth noting that Yalcin et al. [5], reported no pathologic MPI results in 28 much younger patients (average age: 41.2 years) with a rather mild psoriasis at the time of examination.

However, an association between cardiovascular disease and psoriasis is detected most consistently among patients with severe psoriasis. A systematic review and meta-analysis in which classification as severe psoriasis was based upon surrogate markers (*e.g.*, a requirement for systemic treatment or hospital admission) found support for an increased risk for myocardial infarction, cardiovascular mortality, and stroke among patients with severe psoriasis [13]. In contrast to severe psoriasis, studies evaluating the relationship between milder disease and cardiovascular morbidity have yielded less consistent findings [14]. A longer duration of disease may be an additional risk factor for adverse cardiovascular events [15].

The rationale for a correlation between psoriasis and atherosclerotic disease is not well understood. Although the increased prevalence of main risk factors for cardiovascular disease, in patients with psoriasis likely contributes to the elevated risk for atherosclerosis, the role of chronic inflammation in the pathogenesis of both disorders may also be a key factor [16].

In a systematic review and meta-analysis that pooled the results of four studies, all-cause cardiovascular mortality was significantly greater in patients with severe psoriasis than in the general population [13]. A fifth study that reported a hazard ratio from the multivariate analysis offered additional support; the cohort study of approximately 3600 patients with moderate-to-severe psoriasis (defined as psoriasis treated with systemic therapy) and

Table 3. Parameters (standard errors) of best-fit regression models of the effect of age (> 65 vs. ≤ 65), sex (male vs. female) and psoriasis (yes vs. no) on the summed ischemia severity scores by SPECT MPI and on the diagnosis of a pathologic MPI test outcome (p = significance level).

	Age	p	Sex	p	Psoriasis	p
SSS ¹	0.46 (0.48)	0.340	5.12 (0.46)	0.000	-1.29 (1.34)	0.330
SRS ¹	0.91 (0.38)	0.016	3.79 (0.36)	0.000	0.81 (1.04)	0.436
SDS ¹	-0.45 (0.34)	0.180	1.35 (0.32)	0.000	-2.11 (0.93)	0.023
MPI ²	-0.33 (0.23)	0.183	1.64 (0.23)	0.000	-0.41 (0.65)	0.534

SSS: Summed Stress ischemia Score; SRS: Summed Rest ischemia Score; SDS: Ischemia reversibility score (SDS = SSS - SRS); MPI: pathologic myocardial perfusion by MPI SPECT (SSS ≥ 4). 1SPECT MPI ischemia score: Generalized linear model 2Myocardial ischemia (pathologic MPI): Logistic regression model

14,330 control patients without a history of psoriasis, found that patients with severe psoriasis were more likely than controls to die from the cardiac or cerebrovascular disease [17, 18].

Our present MPI findings demonstrated that older patients with moderate-to-severe psoriasis exhibited significantly less reversible ischaemia at rest, compared to the control group. In the light of these observations, the question arises whether therapies with a systemic anti-inflammatory impact, like anti-tumour necrosis factor-alpha antibodies agents, might attenuate and eventually prevent the evolution of myocardial ischaemia as a function of disease duration and severity and ultimately reduce the MACE risk [16].

Conclusion

In summary, we found a similar rate of myocardial ischaemia during stress in patients with moderate-to-severe psoriasis compared to control patients, but with less reversibility of ischaemia at rest. These findings are preliminary and their exact aetiology still unclear. The main limitation of this retrospective study is the small number of index patients. Larger, controlled studies are needed to verify our observations and inquire about the role of MPI studies in the evaluation of myocardial ischaemia in patients with psoriasis.

Conflict of interest

None declared.

Disclosure

None.

Funding

None.

References

- Boehncke WH, Schön M. Psoriasis. *The Lancet*. 2015; 386(9997): 983–994, doi: [10.1016/s0140-6736\(14\)61909-7](https://doi.org/10.1016/s0140-6736(14)61909-7), indexed in Pubmed: [26025581](https://pubmed.ncbi.nlm.nih.gov/26025581/).
- Fernández-Armenteros JM, Gómez-Arbonés X, Buti-Soler M, et al. Psoriasis, metabolic syndrome and cardiovascular risk factors. A population-based study. *J Eur Acad Dermatol Venereol*. 2019; 33(1): 128–135, doi: [10.1111/jdv.15159](https://doi.org/10.1111/jdv.15159), indexed in Pubmed: [29953676](https://pubmed.ncbi.nlm.nih.gov/29953676/).
- Raaby L, Ahlehoff O, de Thurah A. Psoriasis and cardiovascular events: updating the evidence. *Arch Dermatol Res*. 2017; 309(3): 225–228, doi: [10.1007/s00403-016-1712-1](https://doi.org/10.1007/s00403-016-1712-1), indexed in Pubmed: [28213804](https://pubmed.ncbi.nlm.nih.gov/28213804/).
- Varadaraj G, Chowdhary GS, Ananthkrishnan R, et al. Diagnostic accuracy of stress myocardial perfusion imaging in diagnosing stable ischemic heart disease. *J Assoc Physicians India*. 2018; 66(8): 40–44, indexed in Pubmed: [31324083](https://pubmed.ncbi.nlm.nih.gov/31324083/).
- Yalcin H, Balci DD, Ucar E, et al. Myocardial perfusion is preserved in patients with psoriasis without clinically evident cardiovascular disease. *J Eur Acad Dermatol Venereol*. 2009; 23(7): 798–802, doi: [10.1111/j.1468-3083.2009.03178.x](https://doi.org/10.1111/j.1468-3083.2009.03178.x), indexed in Pubmed: [19470047](https://pubmed.ncbi.nlm.nih.gov/19470047/).
- Zutt M, Rudolph H, Kaune KM, et al. Myocardial scintigraphy — a method for detecting cardiac comorbidity in psoriasis patients? *J Dtsch Dermatol Ges*. 2016; 14(10): 1007–1014, doi: [10.1111/ddg.12892](https://doi.org/10.1111/ddg.12892), indexed in Pubmed: [27767272](https://pubmed.ncbi.nlm.nih.gov/27767272/).
- Bassukas I, Mavridou K, Evangelou T, et al. The prevalence of psoriasis among elderly individuals: more questions than answers. *Ageing Research*. 2011; 2(1): e1, doi: [10.4081/ar.2011.e1](https://doi.org/10.4081/ar.2011.e1).
- Arumugam P, Harbinson M, Reyes E, et al. Procedure guidelines for radionuclide myocardial perfusion imaging with single-photon emission computed tomography. *Nucl Med Commun*. 2013; 34(8): 813–826, doi: [10.1097/MNM.0b013e32836171eb](https://doi.org/10.1097/MNM.0b013e32836171eb), indexed in Pubmed: [23719150](https://pubmed.ncbi.nlm.nih.gov/23719150/).
- Fotopoulos A, Petrikis P, Iakovou I, et al. The impact of depression and anxiety in prognosis of patients undergoing myocardial perfusion imaging with 99mTc tetrofosmin SPECT for evaluation of possible myocardial ischemia. *Nucl Med Rev Cent East Eur*. 2020; 23(2): 58–62, doi: [10.5603/NMR.a2020.0014](https://doi.org/10.5603/NMR.a2020.0014), indexed in Pubmed: [33007091](https://pubmed.ncbi.nlm.nih.gov/33007091/).
- Sioka C, Exarchopoulos T, Tasiou I, et al. Myocardial perfusion imaging with (99 m)Tc-tetrofosmin SPECT in breast cancer patients that received postoperative radiotherapy: a case-control study. *Radiat Oncol*. 2011; 6: 151, doi: [10.1186/1748-717X-6-151](https://doi.org/10.1186/1748-717X-6-151), indexed in Pubmed: [22067743](https://pubmed.ncbi.nlm.nih.gov/22067743/).
- Fotopoulos A, Papadimitropoulos K, Papadopoulos A, et al. Myocardial ischemia in female patients with rheumatoid arthritis assessed with single photon emission tomography-myocardial perfusion imaging. *Nucl Med Rev Cent East Eur*. 2019; 22(1): 8–13, doi: [10.5603/NMR.2019.0001](https://doi.org/10.5603/NMR.2019.0001), indexed in Pubmed: [31482536](https://pubmed.ncbi.nlm.nih.gov/31482536/).
- Giannopoulos S, Markoula S, Sioka C, et al. Detecting myocardial ischemia with technetium-tetrofosmin myocardial perfusion imaging in ischemic stroke. *Neurohospitalist*. 2017; 7(4): 164–168, doi: [10.1177/1941874417704752](https://doi.org/10.1177/1941874417704752), indexed in Pubmed: [28974994](https://pubmed.ncbi.nlm.nih.gov/28974994/).
- Samarasekera EJ, Neilson JM, Warren RB, et al. Incidence of cardiovascular disease in individuals with psoriasis: a systematic review and meta-analysis. *J Invest Dermatol*. 2013; 133(10): 2340–2346, doi: [10.1038/jid.2013.149](https://doi.org/10.1038/jid.2013.149), indexed in Pubmed: [23528816](https://pubmed.ncbi.nlm.nih.gov/23528816/).
- Dowlatshahi EA, Kavousi M, Nijsten T, et al. Psoriasis is not associated with atherosclerosis and incident cardiovascular events: the Rotterdam Study. *J Invest Dermatol*. 2013; 133(10): 2347–2354, doi: [10.1038/jid.2013.131](https://doi.org/10.1038/jid.2013.131), indexed in Pubmed: [23492918](https://pubmed.ncbi.nlm.nih.gov/23492918/).

15. Egeberg A, Skov L, Joshi AA, et al. The relationship between duration of psoriasis, vascular inflammation, and cardiovascular events. *J Am Acad Dermatol.* 2017; 77(4): 650–656.e3, doi: [10.1016/j.jaad.2017.06.028](https://doi.org/10.1016/j.jaad.2017.06.028), indexed in Pubmed: [28826925](https://pubmed.ncbi.nlm.nih.gov/28826925/).
16. Reich K. The concept of psoriasis as a systemic inflammation: implications for disease management. *J Eur Acad Dermatol Venereol.* 2012; 26(Suppl 2): 3–11, doi: [10.1111/j.1468-3083.2011.04410.x](https://doi.org/10.1111/j.1468-3083.2011.04410.x), indexed in Pubmed: [22356630](https://pubmed.ncbi.nlm.nih.gov/22356630/).
17. Abuabara K, Azfar RS, Shin DB, et al. Cause-specific mortality in patients with severe psoriasis: a population-based cohort study in the U.K. *Br J Dermatol.* 2010; 163(3): 586–592, doi: [10.1111/j.1365-2133.2010.09941.x](https://doi.org/10.1111/j.1365-2133.2010.09941.x), indexed in Pubmed: [20633008](https://pubmed.ncbi.nlm.nih.gov/20633008/).
18. Ntusi NAB, Francis JM, Sever E, et al. Anti-TNF modulation reduces myocardial inflammation and improves cardiovascular function in systemic rheumatic diseases. *Int J Cardiol.* 2018; 270: 253–259, doi: [10.1016/j.ijcard.2018.06.099](https://doi.org/10.1016/j.ijcard.2018.06.099), indexed in Pubmed: [30017519](https://pubmed.ncbi.nlm.nih.gov/30017519/).

Patterns of [¹⁸F]FDG myocardial uptake in oncology patients as a predictor of myocardial ischaemia on stress myocardial perfusion imaging

Ahmed Fathala¹, Abdulaziz Alsugair, Moheieldin Abouzied², Ahmed Almuhaideb
 King Faisal Hospital, Riyadh, Saudi Arabia

[Received 5 X 2020; Accepted 15 III 2021]

Abstract

Background: There is variable cardiac uptake observed on oncological ¹⁸F-fluorodeoxyglucose ([¹⁸F]FDG) positron emission/computed tomography (PET/CT). The main purpose of this study is to evaluate patterns of overnight fasting myocardial [¹⁸F]FDG uptake in oncological PET/CT and analyse the relationship between myocardial [¹⁸F]FDG uptake and myocardial ischaemia on stress single-photon emission CT (SPECT) myocardial perfusion imaging (MPI).

Material and methods: A total of 362 subjects underwent both oncological PET/CT and stress SPECT MPI within 3 months of each other. Subjects with focal-mass-like [¹⁸F]FDG myocardial uptake raising the suspicion of cardiac metastasis and subjects with coronary artery disease (CAD) were excluded. The myocardial [¹⁸F]FDG uptake was classified into four patterns.

Results: Abnormal SPECT MPI was noted in 91 (25%) patients; 220 (61%) patients had completely absent [¹⁸F]FDG uptake, 80 (22%) had diffuse [¹⁸F]FDG uptake, 39 (11%) had focal on diffuse [¹⁸F]FDG uptake, and 23 (6%) had focal or regional myocardial [¹⁸F]FDG uptake, the regional [¹⁸F]FDG myocardial uptake was the most predictive of myocardial ischaemia on SPECT MPI, and there were positive associations between age, sex, hypertension, tobacco smoking, hypercholesterolemia, and left ventricular ejection, a fair agreement was noted between the focal or regional FDG uptake and presence of ischaemia on SPECT, $K = 0.394$ (95% CI 0.164 to 0.189).

Conclusions: Based on the presented findings, the physiological myocardial [¹⁸F]FDG uptake in fasting oncology patients is variable. The regional myocardial [¹⁸F]FDG uptake pattern is the most frequent pattern associated with myocardial ischaemia on stress SPECT MPI, however, the agreement between regional FDG uptake and presence of ischaemia on SPECT is fair.

KEY words: myocardial ischaemia; myocardial [¹⁸F]FDG uptake; oncological PET/CT; CAD risk stratification

Nucl Med Rev 2021; 24, 2: 51–57

Introduction

While normal myocardial ¹⁸F-fluorodeoxyglucose ([¹⁸F]FDG) activity can be defined as absent or diffusely, focally, or regionally increased, myocardial [¹⁸F]FDG uptake in oncology patients is non-uniform and variable [1]. There is high spatial and temporal heterogeneity of the

[¹⁸F]FDG myocardial metabolism patterns in cancer patients free of cardiac disease [2]. This variability may occur in daily cardiac evaluation, and it may affect the interpretation of cardiac studies in certain disease evaluations, such as cardiac sarcoidosis and myocardial viability [3]. Some data suggest that metabolic alteration may occur in oncology patients; for example, metabolic alteration in cardiac glucose uptake may arise in patients with Hodgkin's lymphoma independent of skeletal muscle uptake [4]. The regional myocardial uptake in patients with stable angina is homogeneously low and comparable to that of healthy subjects [5]. However, in patients with ischaemic cardiomyopathy or severe re-perfused myocardial injury, the myocardial utilization at rest is increased because the oxidative metabolism is reduced. In this case, to

Correspondence to: Ahmed Fathala
 King Faisal Specialist Hospital and Research Centre,
 PO Box 3354, Riyadh 11211
 phone: +966 55-253-2402; fax: +96-64-422-481
 e-mail: ahm35799@hotmail.com

support adenosine triphosphate production from glycolysis, the primary substrate of energy metabolism becomes glucose [6, 7].

Studies have also shown that, in patients with severe coronary artery disease (CAD) and unstable angina, myocardial glucose utilization is enhanced in the absence of clinical, electrocardiographic, or detectable perfusion evidence of acute ischaemia [8]. Also, studies have shown that patients with clinical suspicion of CAD have a higher incidence of focal myocardial uptake and coronary artery calcification but the FDG uptake is often observed in sites remote from those with calcification [9]. However, it is difficult to diagnose the presence of an ischaemic myocardium by fasting [^{18}F]FDG positron emission/computed tomography (PET/CT) imaging alone because the glucose metabolism in the fasting state is quite heterogeneous, even in normal myocardium [10, 11]. Myocardial glucose utilization increases in many conditions, such as myocardial ischaemia, pressure overload, and during exercise; myocardial regional ischaemia leads to the translocation of both glucose transporters, GLUT 4 and GLUT 1, to the sarcolemma in vivo; also, myocardial ischaemia stimulates adenosine monophosphate-activated protein kinase, which may increase cardiac glucose uptake [12]. Thus, the authors wanted to explore the [^{18}F]FDG myocardial uptake patterns in routine overnight fasting oncology patients, and it was hypothesized that focal or regional myocardial [^{18}F]FDG uptake would be associated with myocardial ischaemia on stress single-photon emission CT (SPECT) myocardial perfusion imaging (MPI) due to the myocardial metabolic shift from oxidation of free fatty acid to glucose uptake. Finally, the authors wanted to explore whether the level of blood glucose at the time of injection of [^{18}F]FDG would have any influence on the myocardial [^{18}F]FDG uptake.

Material and methods

Population and study design

This retrospective study was approved by the hospital institutional review board. Subjects who underwent both oncological PET/CT and stress SPECT MPI within 3 months of each other were identified through a search of the radiology and cardiology database for appropriate clinical indications between January 2017 and December 2019. Ten patients were excluded because they had a focal-mass-like [^{18}F]FDG myocardial uptake raising the suspicion of cardiac metastasis or tumour involvement; this needed further correlative imaging with other imaging modalities, such as echocardiography or cardiac magnetic resonance imaging. A stress/rest SPECT MPI was performed for clinically appropriate indication per referring physicians such as symptomatic patients with chest pain and high-risk patients undergoing major surgery for pre-operative risk stratification. Also, patients with established CAD, such as patients with prior myocardial infarction, prior coronary artery bypass surgery (CABG), or prior percutaneous coronary intervention (PCI), were excluded.

[^{18}F]FDG PET/CT imaging

All patients fasted overnight before the PET/CT studies. For imaging, 370–740 MBq (10–20 mCi) of [^{18}F]FDG was injected intravenously, and scanning started 60 minutes later. No intravenous contrast was administered. The studies were conducted

on a hybrid PET/CT scanner (GE, Discovery, Wisconsin, USA). All patients were in a supine position. CT images were acquired from the head to mid-thigh using the following standard parameters: 10 Kvp; current, 180 mA; pitch, 0.981:1; and single round tube rotation, 0.85. CT data were used for attenuation correction and PET images were reconstructed using ordered-subsets expectation maximization (OSEM); 2 iterations, 20 subsets, and a matrix size of 128×128 pixels were used in the reconstruction. To assess the myocardial [^{18}F]FDG uptake, the images were reconstructed with attenuation correction, reoriented, and displayed in traditional cardiac planes (short axis, vertical long axis, and horizontal long axis) for interpretation; the myocardial [^{18}F]FDG uptake was classified into the four following patterns: pattern 1, completely absent or mild myocardial [^{18}F]FDG uptake (Fig. 1a); pattern 2, diffuse (moderate or intense) myocardial [^{18}F]FDG uptake (Fig. 1b); pattern 3, patchy or multifocal myocardial [^{18}F]FDG uptake (Fig. 1c); and pattern 4, focal or regional myocardial [^{18}F]FDG uptake (anterior and septal myocardial [^{18}F]FDG uptake, lateral wall myocardial [^{18}F]FDG uptake, or inferior wall myocardial [^{18}F]FDG uptake (Fig. 1d).

Stress SPECT MPI acquisition and analysis

Patients underwent rest-stress myocardial perfusion imaging studies with either two-conductive separate day or low-dose high-dose same-day protocol. The acquisition parameters and post-processing were performed according to the guidelines of the American Society of Nuclear Cardiology (ASNC) for nuclear cardiology procedures [13]. The images were analysed in consensus by experienced nuclear medicine physicians in short, vertical, and horizontal views utilizing Auto SPECT (Cedars-Sinai Medical Center, Los Angeles, California). A reversible defect was defined as a perfusion defect on stress images that partially or completely reversible on rest images in two or more contiguous segments. A fixed perfusion defect was defined as a perfusion defect on stress images in two or more contiguous segments that persist on rest images. An abnormal perfusion scan was taken to indicate the presence of a reversible or fixed defect or both. Finally, gated short-axis images were processed with quantitative SPECT software, to measure the ejection fraction. In the visual analysis, the 17 segments were scored for perfusion defects on a 4-point system (0 = normal; 1 = mild; 2 = moderate; and 3 = severe), for both the stress and rest images. The perfusion defects based on perfusion scores at stress and rest were used to form the final interpretation of the studies. Perfusion abnormalities in the apical, anterior wall and septal perfusion defect were considered left anterior descending (LAD) artery territory; a lateral wall defect indicated left circumflex (LCX) artery territory, and an inferior wall perfusion defect indicated right coronary artery (RCA) territory.

Statistical analysis

Statistical analysis was performed using SPSS version 20 (IBM, USA). Continuous variables were reported as means \pm standard deviation, and categorical variables were reported as percentages. Group means were compared using the *t*-test, and the association between categorical variables was assessed using the Chi-square test. Binomial logistic regression was performed to ascertain the effects of age, sex, hypertension, hypercholesterolemia, tobacco smoking, left ventricular ejection fraction, myocardial [^{18}F]FDG

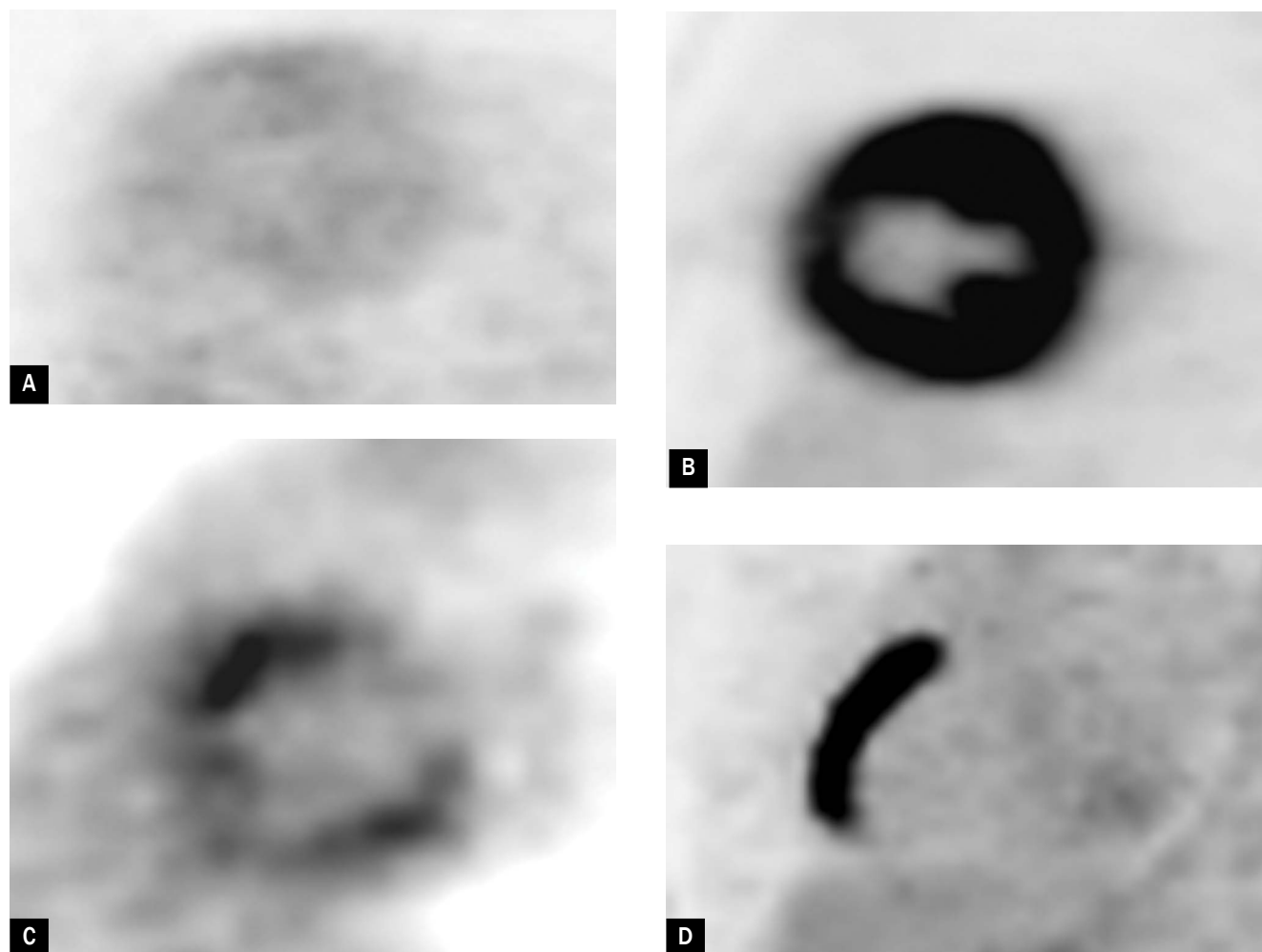


Figure 1. Selected axial [¹⁸F]FDG PET images demonstrating four patterns of myocardial FDG uptake; **A.** Completely absent myocardial [¹⁸F]FDG uptake; **B.** Diffuse intense myocardial [¹⁸F]FDG uptake; **C.** Patchy with focal myocardial [¹⁸F]FDG uptake; **D.** Regional/focal [¹⁸F]FDG uptake in the septal and anteroseptal wall (arrow)

uptake, and abnormal SPECT MPI. Cohen's K was run to determine if there was an agreement between focal/ regional myocardial FDG uptake and the presence of ischaemia on myocardial stress SPECT in 9 patients. The Type I error rate was set at 5%.

Results

Baseline characteristics of study subjects

A total of 362 subjects were included in the study; the average age was 65 ± 10 -years, and 219/362 (60.5%) patients were male. In addition, the mean blood glucose level at the time of FDG injection was 104 ± 36 mg, and the mean left ventricular ejection fraction was $57 \pm 9\%$. Furthermore, 24.3% 91/362 (25%) patients had abnormal SPECT MPI consistent with stress-induced myocardial ischaemia. Among the study subjects, 210/362 (58%) patients were hypertensive, 195/362 (53%) were diabetic, 42/362 (12%) smoked, and only 5/362 (1.4%) had a positive family history of CAD (Tab. 1). Type of cancer and oncological indication for FDG PET/CT are summarized in Table 2.

Table 1. Patient characteristics (N = 362)

Factor	Total number, %
Gender	
Male	219 (60.5%)
Female	143 (39.5%)
Age, years \pm SD	65 ± 10
CAD risk actors	
Hypertension	210 (58%)
Diabetes mellitus	195 (54%)
Hypercholesterolemia	68 (16%)
Smoking	42 (11.6%)
Family history of CAD	5 (1.4%)
LVEF%, mean \pm SD	57 ± 9
Mean blood Glucose at the injection of [¹⁸ F]FDG mmol/L \pm SD	104 ± 36
Abnormal SPECT, number, %	91 (25%)

CAD — indicates coronary artery disease; [¹⁸F]FDG — fluorodeoxyglucose; LVEF — left ventricular ejection fraction; SD — standard deviation; SPECT — single-photon emission computed tomography

Table 2. Type of oncologic indication for FDG PET/CT study, sample study (n = 362)

Type of Malignancy	Number	Percent [%]
Head and neck	47	12.9
Breast	67	18.5
Lung	21	5.8
GI/GU	53	14.6
Lymphoma	54	14.9
Others	120	33.1
Total	362	100

Patterns of myocardial [¹⁸F]FDG uptake and its relationship with blood glucose level

The mean blood glucose level was 104 ± 36 . Moreover, 220/362 (61%) of the study subjects had completely absent or mild [¹⁸F]FDG myocardial uptake, 80/362 (22%) had diffuse myocardial [¹⁸F]FDG uptake, 39/362 (11%) had patchy or multifocal myocardial [¹⁸F]FDG uptake, and 23/362 (6%) had regional myocardial [¹⁸F]FDG uptake. There was no statistically significant association between the glucose level and pattern of myocardial [¹⁸F]FDG uptake, $p = 0.762$ (Tab. 3).

Relationship between the pattern of myocardial [¹⁸F]FDG uptake and myocardial ischaemia on stress SPECT MPI

A significant statistical association was noted between the pattern of myocardial [¹⁸F]FDG uptake and myocardial ischaemia on stress SPECT MPI, $p = .025$; the most predictive pattern of myocardial [¹⁸F]FDG uptake associated with ischaemia was regional

or focal myocardial [¹⁸F]FDG, in 14/23 (39%) patients. The percentages of other patterns observed on stress SPECT MPI were relatively low; for example, the percentage of patients with a complete absence of myocardial [¹⁸F]FDG uptake was 20%.

Relationship between CAD risk factors and myocardial ischaemia on stress SPECT MPI

There was a statistically significant association between the patient age, male gender, hypertension, hypercholesterolemia, and tobacco smoking and abnormal SPECT MPI. In contrast, there was no association between diabetes mellitus and a history of CAD and abnormal SPECT MPI (Tab. 3).

Logistic regression predicting likelihood of SPECT based on CAD risk factors, left ventricle ejection fraction, and [¹⁸F]FDG uptake

Binomial logistic regression was performed to ascertain the effects of age, sex, hypertension, hypercholesterolemia, tobacco smoking, (left ventricular ejection fraction LVEF), and myocardial [¹⁸F]FDG uptake on the SPECT results. Of the seven predictive variables, only age, hypercholesterolemia, smoking, LVEF, and [¹⁸F]FDG uptake were associated with abnormal SPECT (Tab. 4).

The agreement between focal myocardial FDG uptake and presence of ischaemia on SPECT

Cohen's K was run to determine if there was an agreement between focal/regional myocardial FDG uptake and presence of ischaemia on myocardial stress SPECT in 9 patients, there was an agreement between 6 patients with focal FDG uptake and the presence of ischaemia on SPECT, however, there

Table 3. Baseline characteristics of patients with normal and abnormal SPECT

Characteristic	Overall (N = 362)	Patients with normal SPECT 271	Patients with abnormal SPECT 91	p-value
Demographics				
Age, (SD) [y]	65 ± 10	63 ± 10	68 ± 10	0.00001
Male	219	151	68	0.001
Female	143	120	23	
Hypertension	210	141	69	0.000
Diabetes mellitus	195	141	54	0.226
Hypercholesterolemia	28	30	58	0.0001
Smoking	42	18	42	0.0001
Family history of CAD	5	2	3	0.070
SPECT				
LVEF [%]	57 ± 9	58 ± 7	51 ± 7	0.0001
[¹⁸F]FDG- PET/CT				
Blood glucose level	104 ± 36	104 ± 36	103 ± 7	0.762
Myocardial FDG uptake				0.025
Total Absent	220	175	45	
Diffuse uptake	80	53	27	
Focal on diffuse uptake	39	29	10	
Focal/regional uptake	23	14	9	

CAD — indicates coronary artery disease; [¹⁸F]FDG — fluorodeoxyglucose; LVEF — left ventricular ejection fraction; SD — standard deviation; SPECT — single-photon emission computed tomography

Table 4. Logistic regression predicting the likelihood of SPECT based on CAD risk factors, LVEF, and [¹⁸F]FDG uptake

	p-value	Odds ratio	95% confidence interval of odds ratio	
			Lower	Upper
Age	0.012	1.039	1.009	1.070
Sex	0.45	0.519	0.273	0.966
Hypertension	0.055	0.534	0.882	1.014
Hypercholesterolemia	0.000	0.258	0.126	0.526
Smoking	0.000	0.233	0.105	0.514
LVEF	0.000	0.924	0.897	0.953
FDG uptake	0.023	1.405	1.049	1.881

CAD — indicates coronary artery disease; [¹⁸F]FDG — fluorodeoxyglucose; LVEF — left ventricular ejection fraction; SD P-value standard deviation; SPECT — single-photon emission computed tomography

Table 5. The agreement between Focal myocardial [¹⁸F]FDG uptake and presence of ischaemia on SPECT

	Regional FDG uptake	Concordant FDG uptake and Ischaemia	Discordant FDG uptake and no ischaemia
LAD	4	3	1
LCX	2	1	1
RCA	3	2	1
Total	9	6	3

[¹⁸F]FDG — fluorodeoxyglucose; LAD — left anterior descending coronary artery; LCX — left circumflex artery; RCA — right coronary artery; SPECT — single-photon emission computed tomography

was a discordant between FDG uptake and ischaemia on 3 patients. a fair agreement was noted between the FDG uptake and presence of ischaemia on SPECT, $K = 0.394$ (95% CI: 0.164 to 0.189) (Tab. 4 and 5).

Discussion

In this study, it was found that up to 61% of overnight fasting routine oncology patients had absent to mild myocardial [¹⁸F]FDG uptake; the remaining 39% of patients had variable physiological patterns. No association was found between blood glucose level at the time of [¹⁸F]FDG intravenous injection and pattern of myocardial [¹⁸F]FDG uptake, and finally and most importantly, a significant statistical association was found between the pattern of myocardial [¹⁸F]FDG uptake and the presence of myocardial ischaemia on stress SPECT MPI; the most significant predictive pattern of myocardial [¹⁸F]FDG uptake for myocardial ischaemia was regional or focal myocardial [¹⁸F]FDG uptake. However, the agreement between focal or regional FDG uptake and the presence of myocardial ischaemia is fair, $K = 0.394$. Studies have shown that the myocardial glucose uptake during fasting is variable, which reflects the availability and flexibility of myocardial substrate utilization [14, 15]. Among the 362 subjects in this study, 220 subjects had completely absent or minimal [¹⁸F]FDG uptake; these results were consistent with previous studies.

Understanding myocardial [¹⁸F]FDG uptake variability is crucial in the interpretation of myocardial viability, cardiac sarcoidosis, and [¹⁸F]FDG PET/CT studies for the detection of coronary atherosclerosis. Fasting alone cannot explain the variability of myocardial metabolism, which may be due in part to the level of substrates, such as glucose and free fatty acids; physiological and cellular processes, such as myocardial blood flow; and levels of hormones, such as insulin, glucagon, dopamine and thyroxine [3]. One study showed that ageing, left ventricular hypertrophy, diabetes mellitus, and obesity cause alterations in substrate metabolism of either glucose or fatty acids [16]. In addition, hypertensive patients with increased cardiac workload may have a metabolic shift favouring glucose oxidation over fatty acids [17].

Our study showed that, despite overnight fasting, 39% of the study subjects had different physiologic patterns of myocardial [¹⁸F]FDG uptake. This finding is somewhat consistent with the results of another study, in which 38% of enrolled individuals still demonstrated physiological myocardial [¹⁸F]FDG uptake despite prolonged fasting of up to 18 hours [18]. A high-fat, low-carbohydrate diet may facilitate the switching of the myocardial substrate metabolism from glucose to fatty acids [14, 19]. Despite these results, the optimum dietary manipulation before [¹⁸F]FDG PET/CT study for certain indications, such as evaluation of cardiac sarcoidosis, has not been defined or standardized [20].

Our study showed a significant association between the [¹⁸F]FDG myocardial uptake pattern and the presence of myocardial ischaemia on stress SPECT MPI, particularly in terms of regional or focal myocardial [¹⁸F]FDG. Studies have shown that CAD is associated with left ventricular uptake in oncology patients in a fasting state; the association between myocardial ischaemia and regional myocardial [¹⁸F]FDG uptake is due to stimulation of glycolysis and suppression of fatty acid oxidation by the ischaemic myocardium [21]. This metabolic shift is a prerequisite for continued energy production and cell survival. It appears that these alterations in the myocardial substrate may persist after the resolution of myocardial ischaemia in so-called ischaemia memory [22, 23]. One study suggested that this metabolic fingerprint appears superior to perfusion imaging for the detection of CAD and assigning a prognosis in patients with established CAD, and metabolic imaging with [¹⁸F]FDG or [¹²³I]beta methyl-P-iodophenyl pentadecanoic acid ([¹²³I]BMIPP) has been used for ischaemia detection during stress testing [24–27]. However, despite these promising studies about metabolic imaging for the detection of myocardial ischaemia, several questions remain to be answered, such as the optimal imaging protocol and a significant amount of diagnostic or prognostic data obtained from these metabolic studies that might alter patient management. Nevertheless, these results suggest that patients with regional myocardial [¹⁸F]FDG uptake at a relatively increased risk of myocardial ischaemia compared with other patterns, such as diffuse uptake or minimal [¹⁸F]FDG uptake, may benefit from further testing with stress SPECT MPI to diagnose myocardial ischaemia.

Study limitations

Our study is retrospective, and it has some limitations. The number of enrolled subjects was relatively small, which weakens the strength of the presented findings, especially for patients with regional [¹⁸F]FDG uptake and positive SPECT MPI for myocardial

ischaemia. Although the research looked at 362 patients who underwent both oncological PET/CT and stress SPECT MPI within 3 months, despite this limitation, the present finding is worth noting because it is the first study comparing the correlation of myocardial [¹⁸F]FDG uptake in oncological patients and the presence of myocardial ischaemia on stress SPECT MPI. The stress SPECT MPI results were not correlated with other cardiac imaging studies, such as those involving invasive coronary angiography or coronary CT angiography. The duration of overnight fasting in hours was not reported, since this variable was not controlled. The documented information in the chart was reviewed, but clearly, the duration of fasting could be quite variable from one patient to another. Finally, the myocardial [¹⁸F]FDG uptake was evaluated visually and not quantitatively because the myocardial [¹⁸F]FDG location and severity were evaluated.

Conclusions

Based on the presented findings, the physiological myocardial [¹⁸F]FDG uptake in overnight fasting oncology patients is quite variable. While a complete absence or minimal [¹⁸F]FDG uptake is the commonest pattern, the variability may affect the interpretation of cardiac sarcoidosis involvement or myocardial viability studies. Thus, further dietary manipulation and/or extended prolonged fasting before these studies must be considered. The regional myocardial FDG uptake pattern is the commonest pattern associated with myocardial ischaemia on stress SPECT MPI. However, there was a fair agreement between the focal FDG myocardial FDG uptake and the presence of ischaemia on SPECT. Therefore, patients with regional FDG uptake on oncological PET/CT may benefit from additional studies to exclude myocardial ischaemia. Exploration of the relationship between regional [¹⁸F]FDG uptake and myocardial ischaemia must be explored in a larger cohort to determine the relationship between variable myocardial FDG uptake in overnight fasting oncologic patients and the presence of ischaemia on SPECT MPI.

Conflict of interest

The authors declare that they do not have a conflict of interest.

Acknowledgments











We acknowledge Prof. Egesta Lopci, MD, PHD, PET and Nuclear Medicine Department, IRCCs Istituto Clinico Humanitas, Milano, Italy for her help in the statistical analysis and comments on the manuscript.

References

- Maurer AH, Burshteyn M, Adler LP, et al. How to differentiate benign versus malignant cardiac and paracardiac 18F FDG uptake at oncologic PET/CT. *Radiographics*. 2011; 31(5): 1287–1305, doi: [10.1148/rg.315115003](https://doi.org/10.1148/rg.315115003), indexed in Pubmed: [21918045](https://pubmed.ncbi.nlm.nih.gov/21918045/).
- Inglese E, Leva L, Matheoud R, et al. Spatial and temporal heterogeneity of regional myocardial uptake in patients without heart disease under fasting conditions on repeated whole-body 18F-FDG PET/CT. *J Nucl Med*. 2007; 48(10): 1662–1669, doi: [10.2967/jnumed.107.041574](https://doi.org/10.2967/jnumed.107.041574), indexed in Pubmed: [17873124](https://pubmed.ncbi.nlm.nih.gov/17873124/).
- Thut DP, Ahmed R, Kane M, et al. Variability in myocardial metabolism on serial tumor (18)F-FDG PET/CT scans. *Am J Nucl Med Mol Imaging*. 2014; 4(4): 346–353, indexed in Pubmed: [24982820](https://pubmed.ncbi.nlm.nih.gov/24982820/).
- Heckmann MB, Totakhel B, Finke D, et al. Evidence for a cardiac metabolic switch in patients with Hodgkin's lymphoma. *ESC Heart Fail*. 2019; 6(4): 824–829, doi: [10.1002/ehf2.12475](https://doi.org/10.1002/ehf2.12475), indexed in Pubmed: [31278857](https://pubmed.ncbi.nlm.nih.gov/31278857/).
- Camici P, Ferrannini E, Opie LH. Myocardial metabolism in ischemic heart disease: basic principles and application to imaging by positron emission tomography. *Prog Cardiovasc Dis*. 1989; 32(3): 217–238, doi: [10.1016/0033-0620\(89\)90027-3](https://doi.org/10.1016/0033-0620(89)90027-3), indexed in Pubmed: [2682779](https://pubmed.ncbi.nlm.nih.gov/2682779/).
- Schwaiger M, Schelbert HR, Ellison D, et al. Sustained regional abnormalities in cardiac metabolism after transient ischemia in the chronic dog model. *J Am Coll Cardiol*. 1985; 6(2): 336–347, doi: [10.1016/s0735-1097\(85\)80169-8](https://doi.org/10.1016/s0735-1097(85)80169-8), indexed in Pubmed: [3874892](https://pubmed.ncbi.nlm.nih.gov/3874892/).
- Lopaschuk GD, Stanley WC. Glucose metabolism in the ischemic heart. *Circulation*. 1997; 95(2): 313–315, doi: [10.1161/01.cir.95.2.313](https://doi.org/10.1161/01.cir.95.2.313), indexed in Pubmed: [9008441](https://pubmed.ncbi.nlm.nih.gov/9008441/).
- Araujo LI, Camici P, Spinks TJ, et al. Abnormalities in myocardial metabolism in patients with unstable angina as assessed by positron emission tomography. *Cardiovasc Drugs Ther*. 1988; 2(1): 41–46, doi: [10.1007/BF00054251](https://doi.org/10.1007/BF00054251), indexed in Pubmed: [3154693](https://pubmed.ncbi.nlm.nih.gov/3154693/).
- Garcia JR, Soler M, Fuertes S, et al. [Incidence of focal myocardial (18) F-FDG uptake and correlation with coronary calcifications by PET/CT]. *Rev Esp Med Nucl*. 2011; 30(1): 8–13, doi: [10.1016/j.rem.2010.09.002](https://doi.org/10.1016/j.rem.2010.09.002), indexed in Pubmed: [21208695](https://pubmed.ncbi.nlm.nih.gov/21208695/).
- de Groot M, Meeuwis APW, Kok PJM, et al. Influence of blood glucose level, age and fasting period on non-pathological FDG uptake in heart and gut. *Eur J Nucl Med Mol Imaging*. 2005; 32(1): 98–101, doi: [10.1007/s00259-004-1670-2](https://doi.org/10.1007/s00259-004-1670-2), indexed in Pubmed: [15605289](https://pubmed.ncbi.nlm.nih.gov/15605289/).
- Gropler RJ, Siegel BA, Lee KJ, et al. Nonuniformity in myocardial accumulation of fluorine-18-fluorodeoxyglucose in normal fasted humans. *J Nucl Med*. 1990; 31(11): 1749–1756, indexed in Pubmed: [2230987](https://pubmed.ncbi.nlm.nih.gov/2230987/).
- Young LH, Russell RR, Yin R, et al. Regulation of myocardial glucose uptake and transport during ischemia and energetic stress. *Am J Cardiol*. 1999; 83(12A): 25H–30H, doi: [10.1016/s0002-9149\(99\)00253-2](https://doi.org/10.1016/s0002-9149(99)00253-2), indexed in Pubmed: [10750583](https://pubmed.ncbi.nlm.nih.gov/10750583/).
- Dorbala S, Di Carli MF, Delbeke D, et al. SNMMI/ASNC/SCCT guideline for cardiac SPECT/CT and PET/CT 1.0. *J Nucl Med*. 2013; 54(8): 1485–1507, doi: [10.2967/jnumed.112.105155](https://doi.org/10.2967/jnumed.112.105155), indexed in Pubmed: [23781013](https://pubmed.ncbi.nlm.nih.gov/23781013/).
- Williams G, Kolodny GM. Suppression of myocardial 18F-FDG uptake by preparing patients with a high-fat, low-carbohydrate diet. *AJR Am J Roentgenol*. 2008; 190(2): W151–W156, doi: [10.2214/AJR.07.2409](https://doi.org/10.2214/AJR.07.2409), indexed in Pubmed: [18212199](https://pubmed.ncbi.nlm.nih.gov/18212199/).
- Lee HY, Nam HY, Shin SK. Comparison of myocardial F-18 FDG uptake between overnight and non-overnight fasting in non-diabetic healthy subjects. *Jpn J Radiol*. 2015; 33(7): 385–391, doi: [10.1007/s11604-015-0428-z](https://doi.org/10.1007/s11604-015-0428-z), indexed in Pubmed: [25981760](https://pubmed.ncbi.nlm.nih.gov/25981760/).
- Herrero P, Gropler RJ. Imaging of myocardial metabolism. *J Nucl Cardiol*. 2005; 12(3): 345–358, doi: [10.1016/j.nuclcard.2005.03.010](https://doi.org/10.1016/j.nuclcard.2005.03.010), indexed in Pubmed: [15944540](https://pubmed.ncbi.nlm.nih.gov/15944540/).
- Mäki MT, Haaparanta MT, Luotolahti MS, et al. Glucose uptake in the chronically dysfunctional but viable myocardium. *Circulation*. 1996; 93(9): 1658–1666, doi: [10.1161/01.cir.93.9.1658](https://doi.org/10.1161/01.cir.93.9.1658), indexed in Pubmed: [8653871](https://pubmed.ncbi.nlm.nih.gov/8653871/).
- Masuda A, Naya M, Manabe O, et al. Administration of unfractionated heparin with prolonged fasting could reduce physiological 18F-fluorodeoxyglucose uptake in the heart. *Acta Radiol*. 2016; 57(6): 661–668, doi: [10.1177/0284185115600916](https://doi.org/10.1177/0284185115600916), indexed in Pubmed: [26339041](https://pubmed.ncbi.nlm.nih.gov/26339041/).
- Harisankar CN, Mittal BR, Agrawal KL, et al. Utility of high fat and low carbohydrate diet in suppressing myocardial FDG uptake. *J Nucl Cardiol*. 2011; 18(5): 926–936, doi: [10.1007/s12350-011-9422-8](https://doi.org/10.1007/s12350-011-9422-8), indexed in Pubmed: [21732228](https://pubmed.ncbi.nlm.nih.gov/21732228/).
- Chareonthitawee P, Beanlands RS, Chen W, et al. Joint SNMMI-ASNC Expert Consensus Document on the Role of F-FDG PET/CT in Cardiac Sarcoid

- Detection and Therapy Monitoring. *J Nucl Med.* 2017; 58(8): 1341–1353, doi: [10.2967/jnumed.117.196287](https://doi.org/10.2967/jnumed.117.196287), indexed in Pubmed: [28765228](https://pubmed.ncbi.nlm.nih.gov/28765228/).
21. Neely JR, Morgan HE. Relationship between carbohydrate and lipid metabolism and the energy balance of heart muscle. *Annu Rev Physiol.* 1974; 36: 413–459, doi: [10.1146/annurev.ph.36.030174.002213](https://doi.org/10.1146/annurev.ph.36.030174.002213), indexed in Pubmed: [19400669](https://pubmed.ncbi.nlm.nih.gov/19400669/).
22. Abbott BG, Liu YH, Arrighi JA. [¹⁸F]Fluorodeoxyglucose as a memory marker of transient myocardial ischaemia. *Nucl Med Commun.* 2007; 28(2): 89–94, doi: [10.1097/MNM.0b013e328013eaa5](https://doi.org/10.1097/MNM.0b013e328013eaa5), indexed in Pubmed: [17198348](https://pubmed.ncbi.nlm.nih.gov/17198348/).
23. McNulty PH, Jagasia D, Cline GW, et al. Persistent changes in myocardial glucose metabolism in vivo during reperfusion of a limited-duration coronary occlusion. *Circulation.* 2000; 101(8): 917–922, doi: [10.1161/01.cir.101.8.917](https://doi.org/10.1161/01.cir.101.8.917), indexed in Pubmed: [10694532](https://pubmed.ncbi.nlm.nih.gov/10694532/).
24. Kawai Y, Tsukamoto E, Nozaki Y, et al. Significance of reduced uptake of iodinated fatty acid analogue for the evaluation of patients with acute chest pain. *J Am Coll Cardiol.* 2001; 38(7): 1888–1894, doi: [10.1016/s0735-1097\(01\)01634-5](https://doi.org/10.1016/s0735-1097(01)01634-5), indexed in Pubmed: [11738290](https://pubmed.ncbi.nlm.nih.gov/11738290/).
25. He ZX, Shi RF, Wu YJ, et al. Direct imaging of exercise-induced myocardial ischemia with fluorine-18-labeled deoxyglucose and Tc-99m-sestamibi in coronary artery disease. *Circulation.* 2003; 108(10): 1208–1213, doi: [10.1161/01.CIR.0000088784.25089.D9](https://doi.org/10.1161/01.CIR.0000088784.25089.D9), indexed in Pubmed: [12939208](https://pubmed.ncbi.nlm.nih.gov/12939208/).
26. Abramson BL, Ruddy TD, de Kemp RA, et al. Stress perfusion/metabolism imaging: A pilot study for a potential new approach to the diagnosis of coronary disease in women. *Journal of Nuclear Cardiology.* 2000; 7(3): 205–212, doi: [10.1016/s1071-3581\(00\)70008-0](https://doi.org/10.1016/s1071-3581(00)70008-0).
27. Dilsizian V, Bateman TM, Bergmann SR, et al. Metabolic imaging with beta-methyl-p-[(123)I]-iodophenyl-pentadecanoic acid identifies ischemic memory after demand ischemia. *Circulation.* 2005; 112(14): 2169–2174, doi: [10.1161/CIRCULATIONAHA.104.530428](https://doi.org/10.1161/CIRCULATIONAHA.104.530428), indexed in Pubmed: [16186423](https://pubmed.ncbi.nlm.nih.gov/16186423/).

Value of [¹⁸F]FDG PET-CT in the follow-up of surgically treated oral tongue squamous cell carcinoma: single centre cohort analysis on 87 patients

Marco Ravanelli¹, Alberto Grammatica², Guido Squassina¹, Francesco Bertagna³, Domenico Albano³, Davide Lancini², Paolo Bosio², Angelo Zigliani¹, Giorgio Maria Agazzi¹, Roberto Maroldi¹, Piero Nicolai⁴, Raffaele Giubbini³, Cesare Piazza², Davide Farina¹

¹Department of Radiology, University of Brescia, Brescia, Italy

²Department of Otorhinolaryngology — Head and Neck Surgery, University of Brescia, Brescia, Italy

³Department of Nuclear Medicine, University of Brescia, Brescia, Italy

⁴Section of Otorhinolaryngology — Head and Neck Surgery, Department of Neurosciences, University of Padua, Padua, Italy

[Received 13 X 2020; Accepted 12 VII 2021]

ABSTRACT

Background: To evaluate the diagnostic performance of [¹⁸F]fluorodeoxyglucose positron emission tomography/computed tomography ([¹⁸F]FDG-PET/CT) scan in detecting local recurrences in patients with surgically treated oral tongue squamous cell cancer (OTSCC).

Material and methods: Eighty-seven patients who had undergone surgery for OTSCC were monitored clinically and [¹⁸F]FDG-PET/CT and magnetic resonance (MR). PET uptakes were classified as functional (Type A), suspicious (Type B), or highly suggestive of local recurrence (Type C). A multidisciplinary team (MDT) evaluated case-by-case the surveillance strategy based on PET uptake.

Results: Fifty-nine patients presented FDG-PET uptake during follow-up: this report was significantly more frequent in patients who received flap reconstruction than in those without (73% vs 50%; $p = 0.05$). In 13 patients with Type A ($n = 1$), Type B ($n = 9$), and Type C ($n = 3$) uptakes an additional MR was considered preferable and discovered recurrence in 12. PET-CT had 9 true positives, 17 false positives, 71 true negatives, and no false-negative, resulting in sensitivity, specificity, positive (PPV) and negative predictive values (NPV) of 100%, 80.7%, 34.6%, and 100%.

Conclusions: The present results demonstrated a change in diagnostic strategy, as decided by the MDT, in about one-fifth of patients. The results should prompt in designing a rational surveillance schedule in surgically treated OTSCC.

KEY words: tongue carcinoma; PET/CT; [¹⁸F]FDG PET/CT; magnetic resonance imaging

Nucl Med Rev 2021; 24, 2: 58–62

Introduction

The incidence of oral tongue squamous cell carcinoma (OTSCC) is increasing worldwide and, although the peak is seen around the 6th decade, there is evidence of its increasing occurrence among the youngest, presumably due to early initiation of

smoking habits and alcohol consumption [1–3]. The therapeutic management of this type of tumour has not changed substantially in the last few decades and mainly relies on surgery alone for early T categories, while multimodal approaches (surgery followed by radiotherapy [RT] or chemoradiotherapy [CRT]) are applied to more advanced lesions. Surgical management of T1-T2 OTSCC consists of surgical excision with wide free margins (ranging between 1 and 2 cm) [4], while in case of larger tumours with a depth of invasion (DOI) superior to 10 mm (staged as T3 or higher according to the 8th Edition of the AJCC-UICC TNM Staging System) [5] some authors systematically perform a compartmental

Correspondence to: Domenico Albano
Department of Nuclear Medicine, University of Brescia, Brescia, Italy
e-mail: doalba87@libero.it

hemiglossopelvectomy to improve loco-regional control [6–8]. This surgical technique aims to the “en bloc” removal of the entire hemitongue and floor of mouth compartment along with its connective, neuromuscular, vascular, and lymphatic structures (also known as the T-N tract) connecting it to the adjacent neck levels. As a mandatory step after compartmental resection, a free or pedicled flap reconstruction is required, which frequently produces a certain degree of distortion of the anatomical configuration of the residual hemitongue and floor of the mouth [9, 10].

Computed tomography (CT) and magnetic resonance (MR) are the imaging modalities of choice in the pretreatment setting [11–14], the latter being more sensitive and specific, especially in terms of DOI evaluation [15]. According to the National Comprehensive Cancer Network (NCCN) guidelines [16] [¹⁸F]fluorodeoxyglucose positron emission tomography/CT ([¹⁸F]FDG-PET/CT) should also be considered in the preoperative evaluation of advanced (III–IV) stages due to a higher probability of unfavourable scenarios such as contralateral and/or lower neck lymph node metastases, and distant disease. During OTSCC follow-up, imaging plays also an essential role, especially in the detection of submucosal relapses, which may be missed at clinical evaluation. However, the algorithm for post-treatment follow-up is still a matter of debate. NCCN guidelines assert that annual repetition of the pretreatment imaging modality may be indicated in areas difficult to be appropriately visualized on clinical examination. As a general rule, the higher contrast resolution of MR is expected to improve the differentiation between muscle, scar, flap and recurrent tumour, as compared to CT [17]. On the other hand, in a large multicentric study, Mehanna et al. [18] demonstrated that [¹⁸F]FDG-PET/CT performed 3 months after CRT can replace planned neck dissection in a significant number of patients thanks to its very high negative predictive value (NPV) in assessing nodal metastases. Furthermore, [¹⁸F]FDG-PET/CT is unsurpassed to rule out distant metastases.

The role of PET/CT in assessing local control after surgery, however, has not been widely investigated. Müller et al. [19] compared contrast-enhanced CT, unenhanced PET/CT, and the combination of PET and contrast-enhanced CT in the follow-up of a small cohort of oral cancer patients after surgical treatment and flap reconstruction, finding that a combination of techniques gave the best performance in assessing loco-regional control. However, the issue of false-positive uptake in the floor of the mouth caused by different physiological factors should be considered, as recently suggested by Haerle et al. [20].

The aim of this study is therefore to investigate the role of [¹⁸F]FDG-PET/CT in monitoring local control in a cohort of patients surgically treated for OTSCC.

Material and methods

The local Institutional Review Board approved this retrospective observational study.

Patients

The clinical and follow-up records of 87 patients (56 men, 31 women; age range, 45–87 years; mean, 67 years) surgically treated for OTSCC in the Department of Otorhinolaryngology-Head and Neck Surgery of a tertiary referral academic Institution between December 2012 and February 2017, were retrospectively reviewed.

Patient baseline characteristics, type of treatment delivered, T, N and surgical margins features of the primary tumour are detailed in Table 1.

Follow-up policy

According to the NCCN guidelines [16], the institutional follow-up protocol consisted of clinical examination (every 2 months for the first 2 years, every 4 months for the third year, and then every 6 months until the 5th year) and imaging (PET-CT 3 months after surgery, MR at 9 months, then, alternatively, PET-CT and MR, every 6 months for 2 years and every year until the 5th year).

Patients with suspicious or positive findings at imaging were discussed in the multidisciplinary team (MDT) and submitted to:

- biopsy and PET-CT when a suspect was raised on the routine follow-up MR;
- MR when a suspect was raised on the routine follow-up PET-CT;
- watchful-waiting when the level of a suspect on either MR or PET-CT was considered low after the MDT review.

Only patients for whom PET-CT and MR studies were available and with at least 1 year of follow-up were included in the present study. The Median follow-up time was 36 months (range 12–90 months)

Table 1. Patient baseline characteristics and type of surgery

Age, mean (range)	67 (45–87)
Sex M:F	56:31
Type of surgery	
hemiglossopelvectomy	57 (67%)
transoral partial glossectomy	22 (25%)
anterior pelvectomy	3 (3%)
mandibulectomy	3 (3%)
total glossectomy	2 (2%)
Reconstruction flaps n = 68	
Radial Forearm free flap	29 (42.5%)
Antero Lateral thigh free flap	26 (38%)
Fibula free flap	3 (4.5%)
Lateral Dorsi free flap	3 (4.5%)
Facial artery myo-mucosal flap	1 (1.5%)
Scapular composite osteocutaneous fla	2 (3%)
Tranverse Rectus Myocutaneous free flap	2 (3%)
Iliac crest	2 (3%)
T stage*	
T1	13 (15%)
T2	20 (23%)
T3	39 (45%)
T4a	15 (17%)
N stage*	
N0	48 (55%)
N1	10 (11%)
N2a	2 (2%)
N2b	9 (10%)
N2c	3 (3%)
N3b	15 (17%)

*AJCC cancer staging, 8th ed.

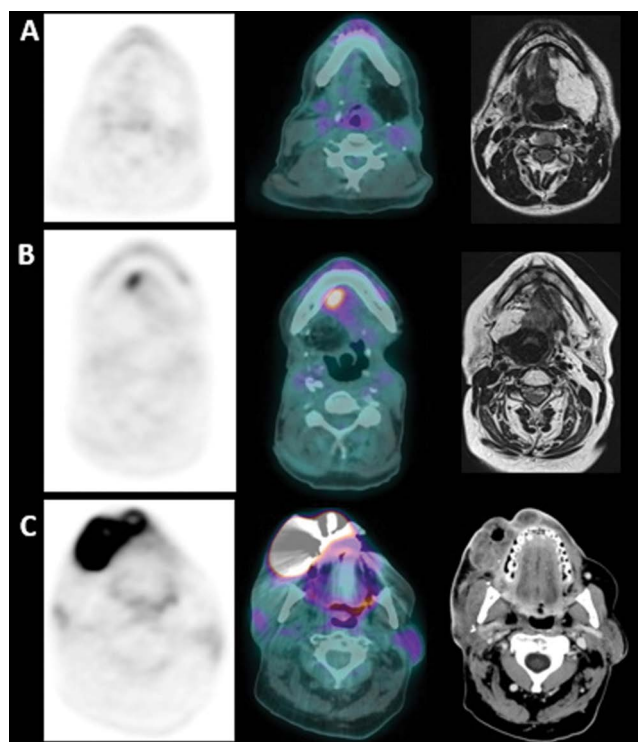


Figure 1. A. A representative case of type-A functional FDG uptake in the oral cavity (axial PET, PET/CT fused and contrast-enhanced images); B. in a 48-year old male treated for left-side tongue cancer. An example of type-B suspicious uptake on the left side in a 66-year old male treated for tongue carcinoma (axial PET, PET/CT fused and T-2 MRI images); C. A case of type-C FDG uptake on the right lip and cheek consistent with relapse (axial PET, PET/CT fused and T-2 MRI images)

PET-CT imaging and interpretation

PET-CT was performed after at least 6 hours fasting and with a glucose level lower than 150 mg/dL. The activity of 3.5–4.5 MBq/kg of [¹⁸F]FDG was administered intravenously and images were acquired 60 ± 10 minutes after injection of the radiotracer. Imaging was from the vertex to the mid-thigh using a Discovery 690 or a Discovery ST PET-CT system (General Electric Company, Milwaukee, WI, USA) with standard parameters (CT: 80 mA, 120 kV without contrast; 2.5–4 minutes per bed with a PET-step of 15 cm). The reconstruction was performed in a 128 × 128 matrix and with a 60 cm field of view. Patients were instructed to void before imaging acquisition, while no oral or intravenous contrast agents were administered or bowel preparation used for any patient. PET images were analysed visually by two nuclear medicine physicians with more than 15 years of experience in head and neck imaging. Every focal radiotracer uptake different from the physiological distribution and higher than background was regarded as suspicious or highly suggestive of recurrent disease. In case of discordant opinions, a third nuclear medicine physician was consulted. When present, PET uptakes in the oral cavity were classified as functional (Type A), suspicious (Type B), or highly suggestive of neoplastic recurrence (Type C) (Figure 1). In the case of highly suggestive uptakes, MR was used to confirm the diagnosis and possibly stage the relapse.

An MDT composed of radiologists, nuclear medicine physicians, head and neck surgeons, and medical and radiation

oncologists evaluated each case with PET radiotracer uptake to decide whether further diagnostic assessment by MR was necessary. The decision was made in consensus and was based on site of uptake, clinical and endoscopic findings, and re-assessment of the fusion CT scans.

MR imaging and interpretation

All the examinations were performed on a 1.5 T scanner (MagnetomAera, Siemens Healthcare, Erlangen, Germany). The MR protocol included: T2-weighted sequences on the axial and coronal planes (and/or sagittal plane, when necessary), T1-weighted, diffusion-weighted imaging (DWI), and post-contrast 3D fat-saturated gradient echo (VIBE) on the axial plane; the latter was also reconstructed on coronal and sagittal planes.

MR studies were reported by a team of five radiologists with extensive experience in head and neck imaging. A recurrence was suspected in the presence of nodular lesion with contrast enhancement and restriction at DWI. T2 hypointense tissue with faint contrast enhancement and no DWI restriction was a scar. T2 hyperintense tissue with variable contrast enhancement and increased water diffusivity at DWI was inflammatory oedema or granulation tissue.

The standard of reference was histology for resected or biopsied lesions and long-term follow-up in the case of negative PET-CT and MR studies.

Statistical analysis

Descriptive statistics were used for patients' characteristics, type of surgery, and type of PET uptake. The diagnostic performance of PET-CT was assessed in terms of sensitivity, specificity, PPV, and NPV. A Chi-square test was used to compare the frequency of PET uptake in patients with and without reconstruction by pedicled or free flaps. The threshold of statistical significance was set at 0.05. Statistical analyses were performed using Medcalc statistic software (Mariakerke, Belgium)

Results

A pathological diagnosis of local recurrence was diagnosed in 9 (10%) patients: in 2 of these (22%), PET-CT identified a subclinical local recurrence during routine follow-up while, in the remaining 7, the recurrence was clinically evident and PET-CT and MR were performed just to confirm and appropriately stage the disease.

A total of 208 PET-CT reports were screened in such a cohort of 87 patients. In 59 (68%) patients FDG uptake in the oral cavity was seen at PET-CT during follow-up; in detail, uptake was present in 49 (73%) patients who received flap reconstruction and in 10 (50%) without ($p = 0.05$). The characteristics of PET uptake are summarized in Table 2.

In 13 (22%) patients with PET uptake in the oral cavity, the MDT agreed to change the routine follow-up schedule by prescribing an additional MR scan. In 12 (92%) cases, MR was triggered by a Type B (9 patients) or Type C (3 patients) uptake. In one patient, MR was performed despite the PET uptake having been classified as Type A, because of clinical suspicion. In one case of Type C uptake, the MDT opted for a surveillance policy due to the patient's poor general condition.

Table 2. Summary of types of PET radiotracer uptake, additional MRI needed and final diagnoses

PET uptake in the oral cavity	59/87 33/59 type A 15/59 type B 11/59 type C
Need for additional MRI	13/87 9/13 type B uptake 3/13 type C uptake 1/13 type A uptake (clinically suspicious recurrence)
Additional MRI results	11/13 negative 7/11 type B 3/11 type C 1/11 type A 1/13 positive: type B 1/13 suspicious: type B
The final diagnosis in patients with additional MRI	12/13 negative (negative MRI or suspicious in 1 case) 1/13 recurrence (positive MRI)

In 12 (92%) cases with PET uptake in the oral cavity, the final diagnosis was no recurrence, while in one a recurrence was confirmed. In 12 cases, MR agreed with the final diagnosis. In one, MR findings were considered suspicious and a short-term follow-up was suggested. Long-term follow up confirmed no recurrence (one false positive) (Table 2). The single case of Type C uptake in which the MDT opted for watchful waiting showed no recurrence on long-term follow-up

Diagnostic performance of PET-CT

When considering no uptake and Type-A uptake as negative findings, and Type B and C uptake as positive findings, PET-CT had 9 true positives, 17 false positives, 71 true negatives, and no false-negative, resulting in a sensitivity, specificity, PPV, and NPV of 100%, 80.7%, 34.6%, and 100%, respectively. If the 7 cases in which PET-CT was used to stage clinically evident recurrences are excluded, PPV drops down to 10.5%, while the other statistical descriptors remain unchanged. In 13 cases, an inconclusive PET triggered an additional MR scan: in 12 of them, the final diagnosis turned out to be negative.

Discussion

In the absence of strict indications, even on international guidelines, the schedule and results of imaging follow-up of OTSCC are variable and largely influenced by factors like the type and number of patients treated, local facilities, geographic, and economic constraints. Clinical surveillance is universally considered the mainstay: in some centres, imaging is performed only in clinically suspicious cases, whereas in others it is fully integrated into the follow-up strategy also of clinically negative patients. In the authors' centre, a scheduled follow-up consisting of clinical examination and alternating [¹⁸F]FDG-PET/CT and MR scans has been adopted. The first imaging examination in the follow-up timeline, namely [¹⁸F]FDG-PET/CT, is performed 3 months after surgery, as suggested by the international guidelines, to limit false-positive results related to inflammatory changes [16].

While confirming the very high NPV of [¹⁸F]FDG-PET/CT in assessing local recurrences, the results of this study raise concerns about the very low PPV caused by the high number of false-positive results. Several PET radioisotope uptakes were reported as physiological (Type A) by nuclear medicine physicians experienced in head and neck imaging and were considered negative for this analysis. The presence of such physiological uptake has been described by Haerle et al. [20], who reported a strong prevalence of FDG uptake at the level of the mylohyoid muscle.

This is probably due to its activation during deglutition which, unlike chewing and talking, is an involuntary movement and thus cannot be completely avoided during the FDG uptake phase.

The largest portion of Type B PET uptakes (15 out of 59) did not determine changes of the standard follow-up protocol after discussion within the MDT: based on free pathological margins on the specimen, absence of symptoms, and unequivocally negative clinical evaluation, no additional study was prescribed. Only one (11%) patient with Type B uptake, further investigated with an additional MR scan, had a pathologically proven diagnosis of recurrence. Moreover, in 4 cases with Type C uptake (3 submitted to an additional MR, and once submitted to watchful waiting policy) recurrences were negative. These results question the possibility to make an accurate distinction between pathological and non-pathological uptakes, even in a tertiary care hospital with well-equipped nuclear medicine and experienced physicians.

In patients with flap reconstruction, among which the incidence of suspicious PET uptakes was significantly higher, the most common site for FDG uptake was seen deep in the floor of the mouth, near the interface between native tissue and flap. Such finding was retrospectively explained as a compensatory hyperactivation of the contralateral extrinsic oral muscles which, in such a distorted and asymmetric anatomy, may retract the flap. In line with these observations, Müller et al. [19] analysed a small cohort of 17 oral cancer patients who underwent surgery followed by reconstruction to demonstrate the added value of contrast-enhanced CT compared with standard FDG-PET with unenhanced CT. They found that by using contrast-enhanced CT, the specificity increased from 58% to 89%. This suggests that contrast-enhanced CT performed simultaneously with PET or as a second step, can improve the interpretation of PET findings and help to reduce the number of false-positive findings. In the authors' protocol, only plain CT was performed simultaneously with PET. CT images were used to assess the presence of solid tissue with mass effect at the uptake site but did not provide information about tissue vascularization. Although the absence of information provided by contrast enhancement may be a limitation of this study, it must be emphasized that simultaneous acquisition of PET and contrast-enhanced CT is not a routine procedure in most centres (for example, it is not feasible with old scanners), and the separate acquisition of contrast-enhanced CT or MR as a second step would impact on logistics and costs.

In this study, state-of-the-art MR proved to be a very accurate technique in clarifying suspicious PET findings and, in most cases, ruled out local relapse. This result does not imply an overall superiority of MR compared to [¹⁸F]FDG-PET/CT as the latter is very effective in assessing nodal and distant spread.

The main strength of this study is the relatively large number of homogeneously treated OTSCC patients, all followed by the same MDT with a PET/CT scan, while its main limitation is represented by its retrospective design. Moreover, semiquantitative analysis of PET uptake based on standardized uptake value was not performed given that, so far, no studies are establishing its usefulness in this setting. Despite the above-mentioned limitations, however, the results of this study suggest a more rational use of PET/CT, which might be reserved to patients with a high risk of distant metastases or to those in whom, for neck treatment, a watchful waiting policy is preferred over prophylactic dissection [18].

In times of economic constraints, a compelling evaluation of the real efficacy of a given follow-up policy in cancer patients is mandatory. For what concerns advanced OTSCC, which is currently often treated with all the available therapeutic modalities and reconstructive techniques, an expensive follow-up based on the liberal use of PET-CT (plus clinical examination and MR when needed) seems unjustified in terms of clinical benefits.

References

1. Myers JN, Elkins T, Roberts D, et al. Squamous cell carcinoma of the tongue in young adults: increasing incidence and factors that predict treatment outcomes. *Otolaryngol Head Neck Surg.* 2000; 122(1): 44–51, doi: [10.1016/S0194-5998\(00\)70142-2](https://doi.org/10.1016/S0194-5998(00)70142-2), indexed in Pubmed: [10629481](https://pubmed.ncbi.nlm.nih.gov/10629481/).
2. Annertz K, Anderson H, Björklund A, et al. Incidence and survival of squamous cell carcinoma of the tongue in Scandinavia, with special reference to young adults. *Int J Cancer.* 2002; 101(1): 95–99, doi: [10.1002/ijc.10577](https://doi.org/10.1002/ijc.10577), indexed in Pubmed: [12209594](https://pubmed.ncbi.nlm.nih.gov/12209594/).
3. Paderno A, Morello R, Piazza C. Tongue carcinoma in young adults: a review of the literature. *Acta Otorhinolaryngol Ital.* 2018; 38(3): 175–180, doi: [10.14639/0392-100X-1932](https://doi.org/10.14639/0392-100X-1932), indexed in Pubmed: [29984792](https://pubmed.ncbi.nlm.nih.gov/29984792/).
4. Chong V. Oral cavity cancer. *Cancer Imaging.* 2005; 5 Spec No A: S49–S52, doi: [10.1102/1470-7330.2005.0029](https://doi.org/10.1102/1470-7330.2005.0029), indexed in Pubmed: [16361136](https://pubmed.ncbi.nlm.nih.gov/16361136/).
5. Brierley JD, Gospodarowicz MK, Wittekind CT. TNM classification of malignant tumours - 8th edition. Wiley-Blackwell, Oxford 2017.
6. Calabrese L, Bruschini R, Giugliano G, et al. Compartmental tongue surgery: Long term oncologic results in the treatment of tongue cancer. *Oral Oncol.* 2011; 47(3): 174–179, doi: [10.1016/j.oraloncology.2010.12.006](https://doi.org/10.1016/j.oraloncology.2010.12.006), indexed in Pubmed: [21257337](https://pubmed.ncbi.nlm.nih.gov/21257337/).
7. Piazza C, Grammatica A, Montalto N, et al. Compartmental surgery for oral tongue and floor of the mouth cancer: Oncologic outcomes. *Head Neck.* 2019; 41(1): 110–115, doi: [10.1002/hed.25480](https://doi.org/10.1002/hed.25480), indexed in Pubmed: [30536781](https://pubmed.ncbi.nlm.nih.gov/30536781/).
8. Piazza C, Montalto N, Paderno A, et al. Is it time to incorporate 'depth of infiltration' in the T staging of oral tongue and floor of mouth cancer? *Curr Opin Otolaryngol Head Neck Surg.* 2014; 22(2): 81–89, doi: [10.1097/MCO.0000000000000038](https://doi.org/10.1097/MCO.0000000000000038), indexed in Pubmed: [24504225](https://pubmed.ncbi.nlm.nih.gov/24504225/).
9. Calabrese L, Giugliano G, Bruschini R, et al. Compartmental surgery in tongue tumours: description of a new surgical technique. *Acta Otorhinolaryngol Ital.* 2009; 29(5): 259–264, indexed in Pubmed: [20162027](https://pubmed.ncbi.nlm.nih.gov/20162027/).
10. Tagliabue M, Gandini S, Maffini F, et al. The role of the T-N tract in advanced stage tongue cancer. *Head Neck.* 2019; 41(8): 2756–2767, doi: [10.1002/hed.25761](https://doi.org/10.1002/hed.25761), indexed in Pubmed: [30942940](https://pubmed.ncbi.nlm.nih.gov/30942940/).
11. Sarrion Pérez MG, Bagán JV, Jiménez Y, et al. Utility of imaging techniques in the diagnosis of oral cancer. *J Craniomaxillofac Surg.* 2015; 43(9): 1880–1894, doi: [10.1016/j.jcms.2015.07.037](https://doi.org/10.1016/j.jcms.2015.07.037), indexed in Pubmed: [26325616](https://pubmed.ncbi.nlm.nih.gov/26325616/).
12. Paiva RR, Figueiredo PT, Leite AF, et al. Oral cancer staging established by magnetic resonance imaging. *Braz Oral Res.* 2011; 25(6): 512–518, doi: [10.1590/s1806-83242011000600007](https://doi.org/10.1590/s1806-83242011000600007), indexed in Pubmed: [22147231](https://pubmed.ncbi.nlm.nih.gov/22147231/).
13. Rajesh A, Khan A, Kendall C, et al. Can magnetic resonance imaging replace single photon computed tomography and computed tomography in detecting bony invasion in patients with oral squamous cell carcinoma? *Br J Oral Maxillofac Surg.* 2008; 46(1): 11–14, doi: [10.1016/j.bjoms.2007.08.024](https://doi.org/10.1016/j.bjoms.2007.08.024), indexed in Pubmed: [18029069](https://pubmed.ncbi.nlm.nih.gov/18029069/).
14. Burkill GJC, Evans RM, Raman VV, et al. Modern radiology in the management of head and neck cancer. *Clin Oncol (R Coll Radiol).* 2016; 28(7): 440–450, doi: [10.1016/j.clon.2016.03.003](https://doi.org/10.1016/j.clon.2016.03.003), indexed in Pubmed: [27156741](https://pubmed.ncbi.nlm.nih.gov/27156741/).
15. Murakami R, Shiraishi S, Yoshida R, et al. Reliability of MRI-derived depth of invasion of oral tongue cancer. *Acad Radiol.* 2019; 26(7): e180–e186, doi: [10.1016/j.acra.2018.08.021](https://doi.org/10.1016/j.acra.2018.08.021), indexed in Pubmed: [30268718](https://pubmed.ncbi.nlm.nih.gov/30268718/).
16. Fenton M, Foote RL, Gillison ML, et al. NCCN Guidelines Version 1.2019 Head and Neck Cancers. www.nccn.org/professionals/physician_gls/pdf/head-and-neck.pdf.
17. Oda M, Tanaka T, Kito S. Recent advances of the diagnostic images for oral cancers. In: Harris S. ed. *Oral cancer: causes, diagnosis and treatment*, 1st ed. Nova Science Publishers, New York 2011.
18. Mehanna H, Wong WL, McConkey CC, et al. PET-NECK Trial Management Group. PET-CT surveillance versus neck dissection in advanced head and neck cancer. *N Engl J Med.* 2016; 374(15): 1444–1454, doi: [10.1056/NEJMoa1514493](https://doi.org/10.1056/NEJMoa1514493), indexed in Pubmed: [27007578](https://pubmed.ncbi.nlm.nih.gov/27007578/).
19. Müller J, Hüllner M, Strobel K, et al. The value of (18) F-FDG-PET/CT imaging in oral cavity cancer patients following surgical reconstruction. *Laryngoscope.* 2015; 125(8): 1861–1868, doi: [10.1002/lary.25326](https://doi.org/10.1002/lary.25326), indexed in Pubmed: [25892275](https://pubmed.ncbi.nlm.nih.gov/25892275/).
20. Haerle SK, Hany TF, Ahmad N, et al. Physiologic [18F]fluorodeoxyglucose uptake of floor of mouth muscles in PET/CT imaging: a problem of body position during FDG uptake? *Cancer Imaging.* 2013; 13(1): 1–7, doi: [10.1102/1470-7330.2013.0001](https://doi.org/10.1102/1470-7330.2013.0001), indexed in Pubmed: [23425816](https://pubmed.ncbi.nlm.nih.gov/23425816/).

Evaluation of the usefulness of positron emission tomography with [¹⁸F]fluorodeoxyglucose performed to detect non-radioiodine avid recurrence and/or metastasis of differentiated thyroid cancer — a preliminary study

Maciej Kolodziej¹, Marek Saracyn¹, Arkadiusz Lubas², Dorota Brodowska-Kania¹, Andrzej Mazurek³, Mirosław Dziuk³, Jolanta Dymus⁴, Grzegorz Kaminski¹

¹Department of Endocrinology and Isotope Therapy, Military Institute of Medicine, Warsaw, Poland

²Department of Internal Medicine, Nephrology and Dialysis, Military Institute of Medicine, Warsaw, Poland

³Nuclear Medicine Department, Military Institute of Medicine, Warsaw, Poland

⁴Department of Laboratory Diagnostics, Military Institute of Medicine, Warsaw, Poland

[Received 1 VII 2021; Accepted 12 VII 2021]

Abstract

Background: About 30% of patients with disseminated differentiated thyroid cancer (DTC) may experience a loss of iodine uptake. It is associated with higher aggressiveness of the tumour and a reduced 10-year survival rate. The diagnosis of non-radioiodine avid DTC metastases remains a diagnostic challenge. A helpful technique for this diagnosis is positron emission tomography with 2-[¹⁸F]fluoro-2-deoxy-D-glucose (PET/CT with [¹⁸F]FDG). On the other hand, there are still discussions about the clinical value of using exogenous thyroid-stimulating hormone (TSH) stimulation before PET/CT with [¹⁸F]FDG.

The aim of the study was the assessment of the usefulness of PET/CT with [¹⁸F]FDG under TSH suppression and stimulation of TSH performed in the detection of non-radioiodine avid DTC metastases, as well as determination of the thyroglobulin concentration under suppression and stimulation of TSH, which influences the result of PET/CT with [¹⁸F]FDG in patients with non-radioiodine avid DTC.

Material and methods: Retrospective analysis of 37 PET/CT with [¹⁸F]FDG performed in patients with DTC diagnosed and treated at the Department of Endocrinology and Isotope Therapy of the Military Institute of Medicine from January 2018 to July 2020. Of these, PET/CT with [¹⁸F]FDG under exogenous rhTSH stimulation was performed in 22 patients and PET/CT with [¹⁸F]FDG under TSH suppression in 15 was performed. In all analyzed patients, the result of diagnostic whole-body scintigraphy (WBS) using 80 MBq ¹³¹I under rhTSH stimulation was negative, and the concentration of thyroglobulin after stimulation (sTg) was greater than 1.0 ng/mL.

Correspondence to: Maciej Kolodziej
 Department of Endocrinology and Isotope Therapy,
 Military Institute of Medicine, Warsaw, Poland
 e-mail: mkolodziej@wim.mil.pl

Results: In the group of patients examined under TSH suppression, non-radioiodine avid in PET/CT with [¹⁸F]FDG were found in 6 out of 15 patients (40%) and in the group of patients examined under rhTSH stimulation in 10 out of 22 patients (45%). The differences between the groups were not statistically significant. The analysis of the receiver operating characteristic (ROC) curves allowed to determine the cut-off point for the positive result of PET/CT performed under TSH suppression with sTg concentration of 11.03 ng/mL. In the group of studies performed under rhTSH stimulation, the cut-off point for sTg was 6.3 ng/mL. There was no statistically significant difference between the baseline thyroglobulin (natTg) and sTg levels and the positive PET/CT result. The administration of rhTSH before the PET/CT examination also had no statistically significant effect on the maximum standard uptake value (SUVmax) of the dominant lesion identified in the PET/CT.

Conclusions: 1) PET/CT with [¹⁸F]FDG is a useful tool for detection of non-radioiodine avid recurrence and/or metastases of DTC. 2) The concentration of natTg and sTg is highly correlated with a positive result of PET/CT with [¹⁸F]FDG. 3) The concentration of natTg is comparable with sTg in predicting a positive result of PET/CT with [¹⁸F]FDG. 4) The cut-off point for a positive result of PET/CT for natTg was 1.36 ng/mL and for sTg was 7.05 ng/mL.

KEY words: differentiated thyroid cancer; human recombinant TSH; thyroglobulin; whole-body scintigraphy; PET/CT; [¹⁸F]FDG; non-radioiodine avid thyroid cancer

Nucl Med Rev 2021; 24, 2: 63–69

Introduction

The concentration of thyroglobulin after stimulation of TSH (sTg) combined with whole-body diagnostic scintigraphy (WBS) using radioiodine (¹³¹I) is a recognized method that allows the follow-up of patients after ablative treatment of differentiated thyroid cancer (DTC) [1]. When the concentration of sTg is increased and there is no ¹³¹I uptake foci in WBS performed under endogenous or exogenous TSH stimulation, the non-radioiodine avid disease is suspected. It is an indication for positron emission tomography (PET/CT) with 2-[¹⁸F]fluoro-2-deoxy-D-glucose ([¹⁸F]FDG) [2]. Loss of iodine uptake may affect about 30% of patients with disseminated DTC [3, 4]. Such changes can be characterized by a poorer differentiation, usually higher aggressiveness and could show greater dynamics. The detection of non-radioiodine avid metastases is associated with a reduction in the 10-year survival rate [3, 5, 6]. The sensitivity and specificity of PET/CT with [¹⁸F]FDG for this type of lesions is assessed as 68.4%–100% and 66.7%–98.5%, respectively [4, 7–12]. Studies show a strong correlation between the concentration of sTg and the presence of foci of increased metabolism of [¹⁸F]FDG in PET/CT [4, 13, 14].

Aim

The study aimed to compare the effectiveness of PET/CT with [¹⁸F]FDG performed under TSH suppression and recombinant human TSH (rhTSH) stimulation in detecting non-radioiodine avid foci of DTC in patients with a negative result of WBS with ¹³¹I and increased concentration sTg.

The aim of the study was also a determination of the thyroglobulin concentration under suppression and stimulation of TSH, which influences the result of PET/CT with [¹⁸F]FDG in patients with non-radioiodine avid DTC.

Material and methods

The study was approved by the local Bioethics Committee at the Military Medical Chamber in Warsaw. A retrospective analysis of 37

PET/CT examinations with [¹⁸F]FDG was performed between January 2018 and July 2020 in the group of patients of the Department of Endocrinology and Isotope Therapy of the Military Institute of Medicine in Warsaw (Tab. 1) after surgery and adjuvant treatment with ¹³¹I due to DTC. PET/CT was performed in patients who, during follow-up after the adjuvant therapy, showed an increased concentration of baseline thyroglobulin (natTg) and/or sTg and a negative result of the WBS performed after administration of 80 MBq ¹³¹I. No recurrence and/or suspicious lymph nodes were found on ultrasound examination of the neck in any of the patients in the study group.

Of the analysed group, 40.5% (15/37) had PET/CT with [¹⁸F]FDG performed under TSH suppression, and 59.5% (22/37) under rhTSH stimulation (Thyrogen 0.9 mg administered twice intramuscularly with an interval of 24 hours).

PET/CT with [¹⁸F]FDG was performed at the Mazovian PET/CT Center *Affidea* in Warsaw. Post-stimulation PET/CT acquisition was performed 24 hours after the administration of the second dose of rhTSH.

PET/CT was performed 60 minutes after administration of 4 MBq/kg of [¹⁸F]FDG on a hybrid Discovery 710 64-row scanner from General Electric Medical Systems.

The following parameters were used in the tomographic part of PET/CT: voltage: 140 kV, intensity (automatically adjusted to the patient's weight): 40–100 mA, noise index: 22, the thickness of the tomographic layer in CT for absorption correction: 3.75 mm reconstructed to 1.25 mm, time lamp rotation: 0.8 s. The iterative reconstruction method was used in the PET study: the number of subsets: 18, the number of iterations: 3, the size of the matrix: 256 × 256. The Time-of-Flight technique was used to improve the image contrast concerning noise.

Assessments of TSH (reference values: 0.27–4.2 μ IU/mL) and Tg (reference values: 3.5–77 ng/mL) were performed at the Department of Laboratory Diagnostics of the Military Institute of Medicine using the electrochemiluminescence method (ECLIA) on the cobas e601 device from ROCHE Diagnostics, using ROCHE Diagnostics reagents. According to the DTC treatment

Table 1. Groups characteristic

Feature	natPET/CT (n = 15)	sPET/CT (n = 22)
Mean age	46 years	53 years
Sex	F = 13, M = 2	F = 17, M = 5
Histological type:		
— papillary	13	19
— follicular	2	3
Primary lesion (TNM):		
— T1a	1	0
— T1b	5	3
— T1m	4	7
— T2	0	2
— T3 i T4	4	8
— Tx	1	2
Lymph node involvement (TNM):		
— N0	4	6
— N1	9	10
— Nx	2	6
Metastasis presence (TNM):		
— M0	12	21
— M1	3	1
Number of patients with repeated therapy	10	18
Mean number of therapies per patient	2.4	2.7
Mean activity per therapy [GBq]	3.98	4.17
Mean total activity per patient [GBq]	9.55	11.38

guidelines, sTg concentrations above 1.0 ng/mL during follow-up were considered abnormal, which was one of the qualification criteria for PET/CT.

Ultrasound examinations were performed at the Department of Endocrinology and Isotope Therapy of the Military Institute of Medicine on the Acuson X150 device from Siemens with the use of a linear probe with a frequency of 8 MHz.

The WBSs were performed at the Department of Nuclear Medicine of the Military Institute of Medicine using NM/CT 870DR or Infinia VCHWK4 gamma-cameras from General Electric Medical System. The following parameters were used during the WBS: detector configuration: H-mode, energy window: 364 keV \pm 10%, collimator: high-energy general-purpose (HEGP), body contour: on, scan mode: continuous, exposure time per pixel: 320 s, speed: 7 cm/min, matrix: 256 \times 1024, acquisition zoom: 1.

The obtained results were presented in the form of a mean with standard deviations or a median with extreme values, depending on the fulfilment of the normal distribution conditions. Nominal variables are presented in the form of numbers with a frequency of occurrence. The compliance of the distribution of variables with the normal distribution was checked using the Shapiro-Wilk test. The correlation analysis was performed using the Pearson test for variables with a distribution close to the normal, otherwise, the Spearman test was used. Differences of nominal variables between groups were tested using the Chi-square test, and quantitative variables using the Student's t-test for unrelated variables. To identify the cut-off points for the studied variables, ROC analysis was performed. The results of the performed tests were considered significant for the two-sided $p < 0.05$. All statistical analyses were performed using the Statistica v.12 package (Statsoft, Cracow, Poland).

Results

Among 37 PET/CT examinations with [^{18}F]FDG, 15 were under TSH suppression (native-PET/CT — natPET/CT), and 22 were performed under rhTSH stimulation (stimulated-PET/CT — sPET/CT). In the natPET/CT group, 6 (6/15 — 40%) positive results were obtained (natPET/CT+) (Fig. 1, 2). The remaining studies in this group (9/15 — 60%) were assessed as negative (natPET/CT-) and did not show any foci of increased metabolism of [^{18}F]FDG related to the DTC. In the group of sPET/CT, 10 (10/22 — 45%) positive results (sPET/CT+) were obtained, finding foci of pathological [^{18}F]FDG uptake, which may correspond to recurrence or

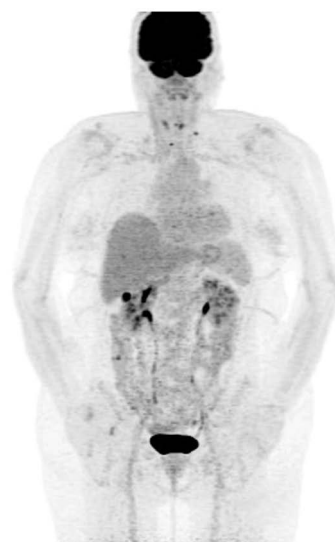


Figure 1A. PET/CT maximum intensity projection (MIP) performed under TSH suppression — accumulation of the [^{18}F]FDG in the left cervical and right mediastinal lymph nodes

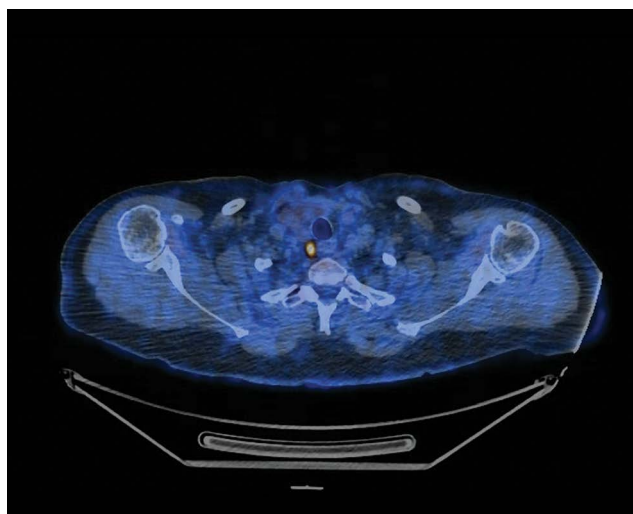


Figure 1B. PET/CT axial fusion projection performed under TSH suppression — accumulation of the [^{18}F]FDG in the right mediastinal lymph node



Figure 2A. PET/CT maximum intensity projection (MIP) performed under TSH suppression — multiple pulmonary metastasis

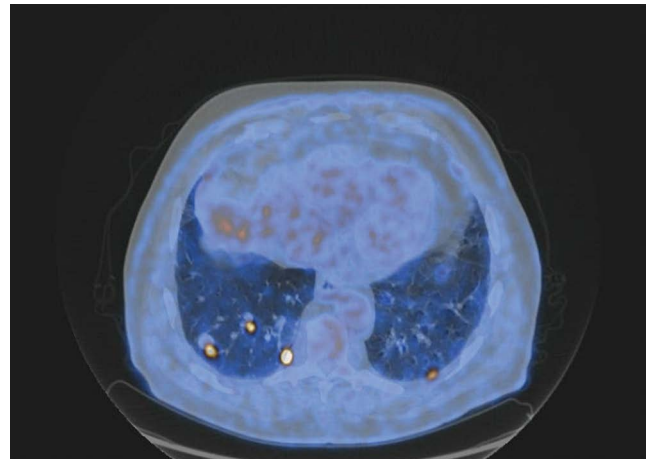


Figure 2B. PET/CT maximum intensity projection (MIP) performed under TSH suppression — multiple pulmonary metastasis



Figure 3A. PET/CT maximum intensity projection (MIP) performed under TSH stimulation — accumulation of the [18F]FDG in the right cervical lymph node

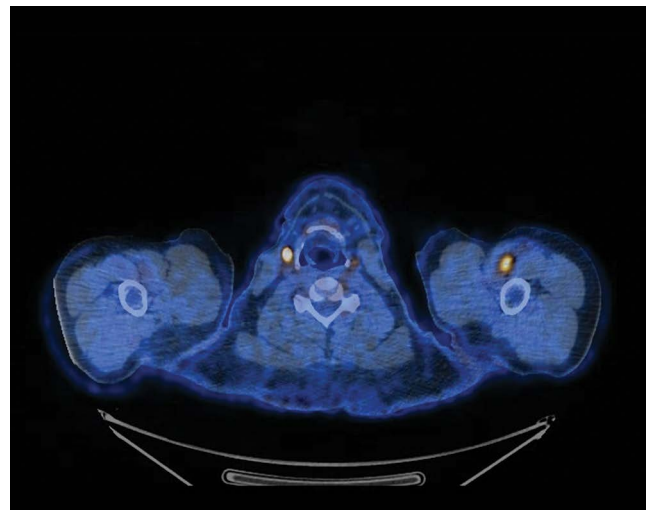


Figure 3B. PET/CT axial fusion projection performed under TSH stimulation — accumulation of the [18F]FDG in the right cervical lymph node

metastases of DTC (Fig. 3). The remaining studies in this group (12/22 — 55%) did not confirm the presence of foci of increased uptake of [18F]FDG (sPET/CT-). There were no statistically significant differences between both groups (natPET/CT and sPET/CT) to obtain a positive result of PET/CT (PET/CT+).

The mean maximum standardized uptake value (SUVmax) in the dominant lesion shown in the natPET/CT+ group was 6.08 ± 2.87 , and the tumour/background ratio for the reference point on mediastinal blood pool structures (MBPS) was 4.63 ± 2.35 . In the sPET/CT+ group, these values were respectively: 8.47 ± 5.38 and 6.36 ± 4.18 . However, these differences were not statistically significant ($p = 0.18$).

The median concentration of natTg and sTg measured during follow-up after ¹³¹I ablation treatment, which are the basis for qualification for PET/CT, in the natPET/CT group were, respectively: 1.07 ng/mL (0.04–190.3 ng/mL) and 6.87 ng/mL (1.45–882.0 ng/mL), and in the sPET/CT group: 0.54 ng/mL (0.04–3069 ng/mL) and 4.87 ng/mL (0.56–4405 ng/mL).

A statistically significant positive correlation was found both between the concentration of natTg and sTg and the number of lesions in PET/CT ($r = 0.71$; $p < 0.05$ and $r = 0.70$; $p < 0.05$, respectively). The analysis of ROC curves for the whole group (both natPET/CT and sPET/CT) showed that for obtaining a positive result of PET/CT, the optimal cut-off point for natTg and sTg

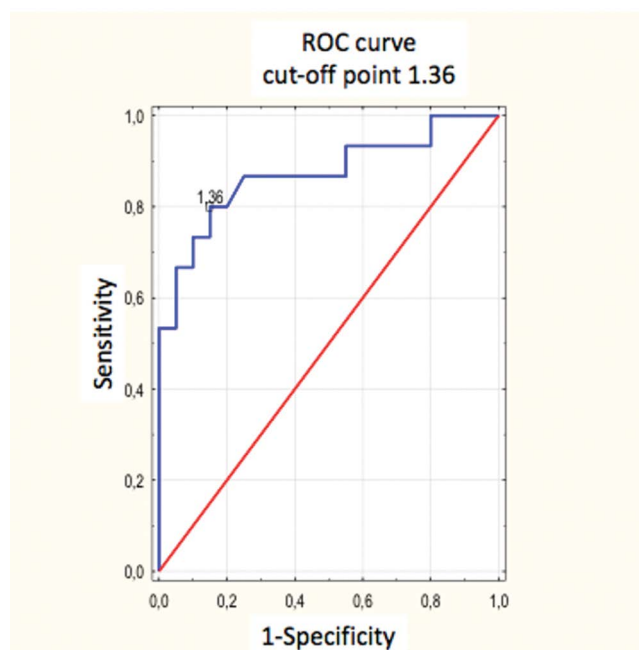


Figure 4. The ROC curve for natTg in the prediction of positive result of PET/CT

concentrations is: 1.36 ng/mL (sensitivity 80.0%, specificity 85.0%, accuracy 82.3%) and 7.05 ng/mL (sensitivity 81.3%, specificity 95.2%, accuracy 89.2%), respectively (Fig. 4, 5). However, the differences in the area under the ROC curves (AUC) between natTg and sTg were not statistically significant (0.872 vs 0.879; $p = 0.59$).

The analysis of the ROC curves for the natPET/CT group showed that to obtain a positive result of PET/CT, the optimal cut-off point for natTg and sTg concentrations is 2.7 ng/mL (sensitivity 100.0%, specificity 87.5%, accuracy 92.3%) and 11.03 ng/mL (sensitivity 100.0%, specificity 100.0%, accuracy 100.0%), respectively. For the sPET/CT group, the optimal cut-off point for natTg and sTg concentrations is 0.6ng/mL (sensitivity 80.0%, specificity 83.3%, accuracy 81.8%) and 6.3 ng/mL (sensitivity 80.0%, specificity 100.0%, accuracy 90.9%), respectively. Nevertheless, the differences in AUC for natTg and sTg between the groups (natPET/CT vs sPET/CT) were not statistically significant (0.925 vs 0.817; $p = 0.403$ vs 1.000 vs 0.833; $p = 0.124$).

Discussion

According to both the Polish recommendations and the American Thyroid Association (ATA) guidelines for the diagnosis and treatment of thyroid cancer, PET/CT with [18 F]FDG is recommended in patients with increased thyroglobulin concentration and no pathological lesions in 131 I WBS and/or ultrasound examination [1, 15]. The authors of these recommendations do not specify the thyroglobulin cut-off point above which PET/CT should be considered. Nevertheless, in the same guidelines, sTg concentration above 10 ng/mL indicates an incomplete biochemical response to the ablation treatment [1, 15].

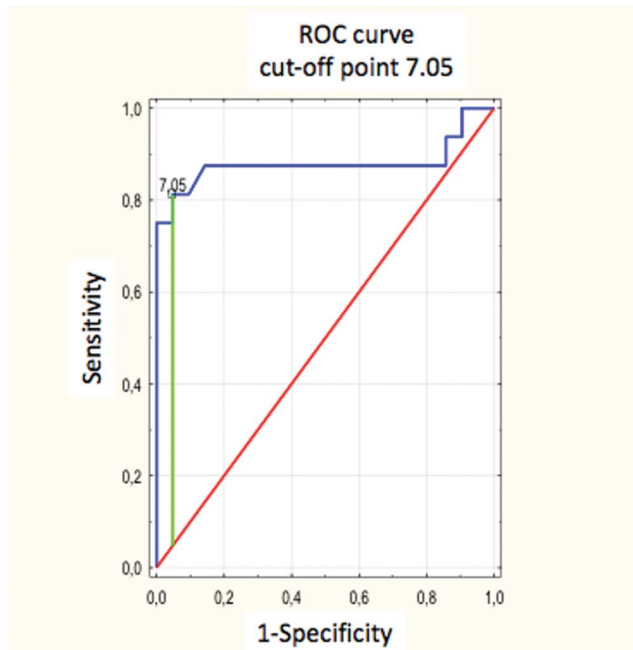


Figure 5. The ROC curve for sTg in the prediction of positive result of PET/CT

The present study found a positive correlation between both natTg and sTg concentration and the positive PET/CT result. Other authors confirmed the existence of such a correlation, but mainly concerning sTg. Trybek et al. [14] in 2014 showed that sTg has a strong and statistically significant accuracy in the diagnosis of recurrence and/or metastasis of differentiated thyroid cancer. Vural et al. [9] confirmed the relationship between the concentration of thyroglobulin under both suppression and stimulation of TSH, and the positive result of PET/CT. On the other hand, Shammam et al. [8] in a study from 2007 found that the sensitivity of PET/CT increases with the concentration of natTg. Similar conclusions, but regarding sTg, were reached by Stangierski et al. [16] in 2016, confirming that the probability of obtaining a positive PET/CT result, i.e. showing foci of pathological metabolism [18 F]FDG that may correspond to recurrence or metastasis of DTC, increases with sTg concentration. In previous years, many authors have tried to establish a cut-off point for the sTg concentration above which it is reasonable to perform PET/CT with [18 F]FDG. In a 2012 South Korean study, Na et al. [12] estimated it at 20 ng/mL. In the same year, in a study conducted on 105 patients, Vural et al. [9] found that the cut-off point for natTg is 1.9 ng/mL, while for sTg it is 38.2 ng/mL with a sensitivity of 94% and a specificity of 100%. In the Polish study by Trybek et al. [14], the concentration of sTg with a sensitivity and specificity equal to 100% was 28.5 ng/mL, while in a Chinese study from 2017, Chai et al. [17] with a sensitivity of 89.5% assessed was 49 ng/mL.

In the already cited Polish study by Stangierski et al. [16] the cut-off point for sTg was 32.9 ng/mL. This study found such correlation and established cut-off points for obtaining the positive result of PET/CT for both natTg and sTg at 1.36 ng/mL and

7.05 ng/mL, respectively. The threshold for natTg was lower, but similar to that obtained by Vural et al. [9], while the concentration of sTg determined by the authors was clearly lower than those mentioned in the above-cited studies, with a slightly lower, although still high, sensitivity. It was also lower than the values mentioned in the Polish and American recommendations for the diagnosis and treatment of DTC.

At the same time, the authors did not find statistically significant differences in the ROC curves for natTg with a cut-off point of 1.36 ng/mL and for sTg with a cut-off point of 7.05 ng/mL. Thus, the values of natTg and sTg in this study were comparable in predicting positive PET/CT in patients with non-radioiodine avid DTC. Therefore, it may be information that allows referring patients to PET/CT without prior assessment of sTg concentration. Due to the high costs of the rhTSH, basing the qualification of patients for PET/CT on the natTg concentrations performed in an outpatient setting should result in a lower burden for the health care system. Such an assumption was already made by the British group a few years ago, but then no useful cut-off point was found for natTg concentration [18].

The presented study did not find a statistically significant improvement in the detection of non-radioiodine avid recurrences and/or metastases of DTC using rhTSH stimulation before PET/CT, which is coherent with the observations of other authors [19, 20]. However, there are also data in the literature suggesting that the use of rhTSH stimulation before PET/CT may increase its sensitivity from 28% to 50% [21]. Dionigi et al. [4] found that administration of rhTSH before PET/CT increases its sensitivity in detecting recurrence of differentiated thyroid cancer from 81% to 95%. Furthermore, the Chinese meta-analysis of Ma et al. [22] covering 7 prospective studies with a total of 168 patients showed that the use of exogenous or endogenous TSH stimulation before PET/CT statistically significantly increases the chance of obtaining a positive result (OR = 2.45; 95% CI 1.23–4.9) and statistically influences the number of foci of radiotracer accumulation visible in PET/CT (OR = 4.92; 95% CI 2.7–8.95).

The present analysis of ROC curves in subgroups, separately for positive PET/CT results in the non-stimulated group (natPET/CT+) and after rhTSH stimulation (sPET/CT+), showed that the optimal cut-off point for sTg concentration to obtain a positive result of PET/CT is 11.03 ng/mL in the natPET/CT group and 6.3 ng/mL in the sPET/CT group, respectively. However, this difference was not statistically significant, perhaps due to the too-small size of both groups. Still, this may be indirect proof of the validity of using rhTSH before PET/CT in patients with slightly elevated sTg concentration (above 6.3 ng/mL). For the sTg concentration almost twice as high (11.03 ng/mL), it may be sufficient to perform a PET/CT under TSH suppression. There are no studies in the available literature that would deal with this issue in this aspect in a larger group of patients. Saab et al. [23] in a study involving a group of 15 sPET/CT stated that the use of TSH stimulation (exogenous or endogenous) allows for the identification of non-radioiodine avid metastases of DTC in PET/CT with relatively low sTg concentration, for which it was found to be 15 ng/mL. At the same time, these authors emphasize that PET/CT was useful regardless of the type of TSH stimulation. In the present study, all sPET/CT were performed with rhTSH, due to the proven equal, compared to endogenous, effectiveness of

this type of TSH stimulation in the treatment and diagnosis of DTC, with a simultaneously reduced risk of side effects of the withdrawal of levothyroxine treatment [24–26].

The work of Vera et al. [19], on the other hand, indicated low effectiveness of the sPET/CT at a natTg concentration below 10 ng/mL but did not take into the sTg concentration. The Brazilian study by Almeida et al. [27] compares the results of PET/CT before and after endogenous TSH stimulation (withdrawal of levothyroxine for 30 days). Due to the endogenous method of stimulation, the sTg concentration was measured only for the sPET/CT. In a German study, Petrich et al. [28] performed a head-to-head comparison of PET/CT before and after rhTSH stimulation in a group of 30 patients, but this work does not provide information on the analysis of ROC curves of sTg concentration for the natPET/CT and sPET/CT groups. On the other hand, these authors noticed that the use of rhTSH stimulation before PET/CT improved the tumour/background ratio of the identified lesions [28]. Other publications also indicate an improvement in the tumour/background ratio and an increase in SUVmax in PET/CT, which indicates better [¹⁸F]FDG uptake in metastatic lesions and leads to better PET/CT image quality [17, 20, 27]. The authors obtained similar results in their work, but they were not statistically significant. This may be due to the insufficient size of the analysed group, but their observations are preliminary and will be continued in the future.

The advantage and innovative approach to the presented work is not only to show a positive, statistically significant correlation between natTg and sTg and positive result of PET/CT but also to show a comparable value of natTg and sTg in predicting a positive PET/CT result, as well as determining the cut-off point for natTg and sTg separately for natPET/CT+ and sPET/CT+.

The main limitation of the present work is the small size of the analysed group, but it is a preliminary study. The analyses will be continued on a wider group of patients in the future.

Conclusions

1. PET/CT with [¹⁸F]FDG is a useful tool for detection of non-radioiodine avid recurrence and/or metastases of DTC.
2. The concentration of natTg and sTg is highly correlated with a positive result of PET/CT with [¹⁸F]FDG.
3. The concentration of natTg is comparable with sTg in predicting a positive result of PET/CT with [¹⁸F]FDG.
4. The cut-off point for a positive result of PET/CT for natTg was 1.36 ng/mL and for sTg was 7.05 ng/mL.

References

1. Jarzab B, Dedecjus M, Handkiewicz-Junak D, et al. Diagnostics and treatment of thyroid carcinoma. *Endokrynol Pol.* 2016; 67(1): 74–107, doi: [10.5603/EP.2016.0011](https://doi.org/10.5603/EP.2016.0011), indexed in Pubmed: [26884119](https://pubmed.ncbi.nlm.nih.gov/26884119/).
2. Załącznik nr 4 do Zarządzenia Nr 88/2013/DSOZ Prezesa Narodowego Funduszu Zdrowia z dnia 18 października 2013 roku.
3. Mu ZZ, Zhang X, Lin YS. Identification of radioactive iodine refractory differentiated thyroid cancer. *Chonnam Med J.* 2019; 55(3): 127–135, doi: [10.4068/cmj.2019.55.3.127](https://doi.org/10.4068/cmj.2019.55.3.127), indexed in Pubmed: [31598469](https://pubmed.ncbi.nlm.nih.gov/31598469/).
4. Dionigi G, Fama' F, Pignata SA, et al. Usefulness of PET-CT scan in recurrent thyroid cancer. *World J Otorhinolaryngol Head Neck Surg.* 2020; 6(3): 182–187, doi: [10.1016/j.wjorl.2020.02.008](https://doi.org/10.1016/j.wjorl.2020.02.008), indexed in Pubmed: [33073214](https://pubmed.ncbi.nlm.nih.gov/33073214/).

5. Schlumberger MJ. Papillary and follicular thyroid carcinoma. *N Engl J Med.* 1998; 338(5): 297–306, doi: [10.1056/NEJM199801293380506](https://doi.org/10.1056/NEJM199801293380506), indexed in Pubmed: [9445411](https://pubmed.ncbi.nlm.nih.gov/9445411/).
6. Nakada K, Hattori N, Sugie H, et al. Prognostic value of FDG PET/CT in radioiodine negative lung metastases from differentiated thyroid cancer. *J Nucl Med.* 2018; 59(Suppl 1): 241.
7. Davison JM, Stocker DJ, Montilla-Soler JL, et al. The added benefit of a dedicated neck F-18 FDG PET-CT imaging protocol in patients with suspected recurrent differentiated thyroid carcinoma. *Clin Nucl Med.* 2008; 33(7): 464–468, doi: [10.1097/RLU.0b013e31817792c9](https://doi.org/10.1097/RLU.0b013e31817792c9), indexed in Pubmed: [18580230](https://pubmed.ncbi.nlm.nih.gov/18580230/).
8. Shammas A, Degirmenci B, Mountz JM, et al. 18F-FDG PET/CT in patients with suspected recurrent or metastatic well-differentiated thyroid cancer. *J Nucl Med.* 2007; 48(2): 221–226, indexed in Pubmed: [17268018](https://pubmed.ncbi.nlm.nih.gov/17268018/).
9. Vural GU, Akkas BE, Ercakmak N, et al. Prognostic significance of FDG PET/CT on the follow-up of patients of differentiated thyroid carcinoma with negative 131I whole-body scan and elevated thyroglobulin levels: correlation with clinical and histopathologic characteristics and long-term follow-up data. *Clin Nucl Med.* 2012; 37(10): 953–959, doi: [10.1097/RLU.0b013e31825b2057](https://doi.org/10.1097/RLU.0b013e31825b2057), indexed in Pubmed: [22899202](https://pubmed.ncbi.nlm.nih.gov/22899202/).
10. Okuyucu K, Ince S, Alagoz E, et al. Risk factors and stratification for recurrence of patients with differentiated thyroid cancer, elevated thyroglobulin and negative I-131 whole-body scan, by restaging F-FDG PET/CT. *Hell J Nucl Med.* 2016; 19(3): 208–217, doi: [10.1967/s002449910402](https://doi.org/10.1967/s002449910402), indexed in Pubmed: [27824959](https://pubmed.ncbi.nlm.nih.gov/27824959/).
11. Bertagna F, Bosio G, Biasiotto G, et al. F-18 FDG-PET/CT evaluation of patients with differentiated thyroid cancer with negative I-131 total body scan and high thyroglobulin level. *Clin Nucl Med.* 2009; 34(11): 756–761, doi: [10.1097/RLU.0b013e3181b7d95c](https://doi.org/10.1097/RLU.0b013e3181b7d95c), indexed in Pubmed: [19851169](https://pubmed.ncbi.nlm.nih.gov/19851169/).
12. Na SJ, Yoo IR, O JH, et al. Diagnostic accuracy of (18)F-fluorodeoxyglucose positron emission tomography/computed tomography in differentiated thyroid cancer patients with elevated thyroglobulin and negative (131)I whole body scan: evaluation by thyroglobulin level. *Ann Nucl Med.* 2012; 26(1): 26–34, doi: [10.1007/s12149-011-0536-5](https://doi.org/10.1007/s12149-011-0536-5), indexed in Pubmed: [21971605](https://pubmed.ncbi.nlm.nih.gov/21971605/).
13. Mosci C, Iagaru A. PET/CT imaging of thyroid cancer. *Clin Nucl Med.* 2011; 36(12): e180–e185, doi: [10.1097/RLU.0b013e3182291d03](https://doi.org/10.1097/RLU.0b013e3182291d03), indexed in Pubmed: [22064103](https://pubmed.ncbi.nlm.nih.gov/22064103/).
14. Trybek T, Kowalska A, Lesiak J, et al. The role of 18F-Fluorodeoxyglucose Positron Emission Tomography in patients with suspected recurrence or metastatic differentiated thyroid carcinoma with elevated serum thyroglobulin and negative I-131 whole body scan. *Nucl Med Rev Cent East Eur.* 2014; 17(2): 87–93, doi: [10.5603/NMR.2014.0023](https://doi.org/10.5603/NMR.2014.0023), indexed in Pubmed: [25088108](https://pubmed.ncbi.nlm.nih.gov/25088108/).
15. Haugen B, Alexander E, Bible K, et al. 2015 American Thyroid Association Management guidelines for adult patients with thyroid nodules and differentiated thyroid cancer: the American Thyroid Association guidelines task force on thyroid nodules and differentiated thyroid cancer. *Thyroid.* 2016; 26(1): 1–133, doi: [10.1089/thy.2015.0020](https://doi.org/10.1089/thy.2015.0020).
16. Stangierski A, Kaznowski J, Wolinski K, et al. The usefulness of fluorine-18 fluorodeoxyglucose PET in the detection of recurrence in patients with differentiated thyroid cancer with elevated thyroglobulin and negative radioiodine whole-body scan. *Nucl Med Commun.* 2016; 37(9): 935–938, doi: [10.1097/MNM.0000000000000563](https://doi.org/10.1097/MNM.0000000000000563), indexed in Pubmed: [27383190](https://pubmed.ncbi.nlm.nih.gov/27383190/).
17. Chai H, Zhang Hu, Yu YL, et al. Optimal threshold of stimulated serum thyroglobulin level for F-FDG PET/CT imaging in patients with thyroid cancer. *J Huazhong Univ Sci Technol Med Sci.* 2017; 37(3): 429–432, doi: [10.1007/s11596-017-1752-6](https://doi.org/10.1007/s11596-017-1752-6), indexed in Pubmed: [28585147](https://pubmed.ncbi.nlm.nih.gov/28585147/).
18. Prestwich RJD, Viner S, Gerrard G, et al. Increasing the yield of recombinant thyroid-stimulating hormone-stimulated 2-(18-fluoride)-flu-2-deoxy-D-glucose positron emission tomography-CT in patients with differentiated thyroid carcinoma. *Br J Radiol.* 2012; 85(1018): e805–e813, doi: [10.1259/bjr/26733491](https://doi.org/10.1259/bjr/26733491), indexed in Pubmed: [22972977](https://pubmed.ncbi.nlm.nih.gov/22972977/).
19. Vera P, Kuhn-Lansoy C, Edet-Sanson A, et al. Does recombinant human thyrotropin-stimulated positron emission tomography with [18F]fluoro-2-deoxy-D-glucose improve detection of recurrence of well-differentiated thyroid carcinoma in patients with low serum thyroglobulin? *Thyroid.* 2010; 20(1): 15–23, doi: [10.1089/thy.2008.0416](https://doi.org/10.1089/thy.2008.0416), indexed in Pubmed: [20017617](https://pubmed.ncbi.nlm.nih.gov/20017617/).
20. Leboulleux S, Schroeder PR, Busaidy NL, et al. Assessment of the incremental value of recombinant thyrotropin stimulation before 2-[18F]-Fluoro-2-deoxy-D-glucose positron emission tomography/computed tomography imaging to localize residual differentiated thyroid cancer. *J Clin Endocrinol Metab.* 2009; 94(4): 1310–1316, doi: [10.1210/jc.2008-1747](https://doi.org/10.1210/jc.2008-1747), indexed in Pubmed: [19158200](https://pubmed.ncbi.nlm.nih.gov/19158200/).
21. Kukuliska A, Krajewska J, Kolasza Z, et al. The role of FDG-PET in localization of recurrent lesions of differentiated thyroid cancer (DTC) in patients with asymptomatic hyperthyroglobulinemia in a real clinical practice. *Eur J Endocrinol.* 2016; 175(5): 379–385, doi: [10.1530/EJE-16-0360](https://doi.org/10.1530/EJE-16-0360), indexed in Pubmed: [27511823](https://pubmed.ncbi.nlm.nih.gov/27511823/).
22. Ma C, Xie J, Lou Y, et al. The role of TSH for 18F-FDG-PET in the diagnosis of recurrence and metastases of differentiated thyroid carcinoma with elevated thyroglobulin and negative scan: a meta-analysis. *Eur J Endocrinol.* 2010; 163(2): 177–183, doi: [10.1530/EJE-10-0256](https://doi.org/10.1530/EJE-10-0256), indexed in Pubmed: [20484385](https://pubmed.ncbi.nlm.nih.gov/20484385/).
23. Saab G, Driedger AA, Pavlosky W, et al. Thyroid-stimulating hormone-stimulated fused positron emission tomography/computed tomography in the evaluation of recurrence in 131I-negative papillary thyroid carcinoma. *Thyroid.* 2006; 16(3): 267–272, doi: [10.1089/thy.2006.16.267](https://doi.org/10.1089/thy.2006.16.267), indexed in Pubmed: [16571089](https://pubmed.ncbi.nlm.nih.gov/16571089/).
24. Hasse-Lazar K, Handkiewicz-Junak D, Roskosz J, et al. Recombinant human TSH stimulation in radioiodine treatment of disseminated differentiated thyroid cancer — update of current and our own experiences [article in Polish]. *Endokrynol Pol.* 2006; 57(4): 445–450, indexed in Pubmed: [17006851](https://pubmed.ncbi.nlm.nih.gov/17006851/).
25. Suligowska A, Kowalska A, Nowalska M. Rating incidence of adverse effects after using recombinant TSH (rhTSH). *Medical Studies.* 2018; 34(2): 103–106, doi: [10.5114/ms.2018.76868](https://doi.org/10.5114/ms.2018.76868).
26. Robenshtok E, Tuttle RM. Role of recombinant human thyrotropin (rhtsh) in the treatment of well-differentiated thyroid cancer. *Indian J Surg Oncol.* 2012; 3(3): 182–189, doi: [10.1007/s13193-011-0115-1](https://doi.org/10.1007/s13193-011-0115-1), indexed in Pubmed: [23997506](https://pubmed.ncbi.nlm.nih.gov/23997506/).
27. Almeida LS, Araújo ML, Santos AO, et al. Head-to-head comparison of F-18 FDG PET/CT in radioiodine refractory thyroid cancer patients with elevated versus suppressed TSH levels a pilot study. *Heliyon.* 2020; 6(3): e03450, doi: [10.1016/j.heliyon.2020.e03450](https://doi.org/10.1016/j.heliyon.2020.e03450), indexed in Pubmed: [32154413](https://pubmed.ncbi.nlm.nih.gov/32154413/).
28. Petrich T, Börner AR, Otto D, et al. Influence of rhTSH on [(18)F]fluorodeoxyglucose uptake by differentiated thyroid carcinoma. *Eur J Nucl Med Mol Imaging.* 2002; 29(5): 641–647, doi: [10.1007/s00259-001-0745-6](https://doi.org/10.1007/s00259-001-0745-6), indexed in Pubmed: [11976802](https://pubmed.ncbi.nlm.nih.gov/11976802/).

SPECT-CT imaging with [^{99m}Tc]PSMA-T4 in patients with recurrent prostate cancer

Sonya Sergieva¹, Radoslav Mangalgiev², Milena Dimcheva¹, Kamen Nedev³, Zahary Zahariev⁴, Bozhil Robev⁵

¹Department of Nuclear Medicine, Sofia Cancer Centre, Sofia, Bulgaria

²Department of Medical Oncology, Sofia Cancer Centre, Sofia, Bulgaria

³Department of Radiotherapy, Acibadem City Clinic, Sofia, Bulgaria

⁴Department of Radiotherapy, UniHospital, Panagyurishte, Bulgaria

⁵Department of Medical Oncology, UH “St Ivan Rilsky”, Sofia, Bulgaria

[Received 12 II 2021; Accepted 19 VII 2021]

Abstract

Background: Prostate-specific membrane antigen (PSMA) is a cell surface glycoprotein with a large extracellular domain with overexpression of the prostatic tumour cells. Several small molecules of PSMA ligands of inhibitors binding to the active site of PSMA were developed. [^{99m}Tc]Tc-PSMA-T4 is a new radiopharmaceutical (Polatom) for imaging loco-regional metastases and/or local relapse in patients with prostate cancer.

The purpose of this work was to evaluate the clinical application of SPECT-CT imaging with [^{99m}Tc]Tc-PSMA-T4 in patients with recurrent prostate cancer.

Material and methods: Thirty-six patients with prostate cancer, aged 60–80 years with biochemical relapse of PSA (ranged from 0.1 to 73 ng/mL) were included. Three patients were studied after tru-cut biopsy, hormonal and cytoreductive radiotherapy and 33 patients out of 36 — after radical treatment (total prostatectomy or definitive radiotherapy of the tumour). All of them underwent whole-body imaging examinations with subsequent target SPECT-CT studies of the pelvis, abdomen and/or chest, 1–3 hrs post i.v. administration of [^{99m}Tc]Tc-PSMA-T4. The average activity dose was 6.3 MBq/kg in a man of 70 kg. A Dual-head SPECT-CT gamma camera with a low dose CT scan (Symbia T2, Siemens) was used. The images were interpreted based on all other clinical and radiological data. Follow-up could be conducted in 11/36 patients during that period.

Results: Normal biodistribution of the radiopharmaceutical with high activity background was observed in the liver, spleen, kidneys, lacrimal and salivary glands, bowels and urinary bladder. Positive imaging for local relapse in the prostate bad was imaged in 21 patients, lymph node metastases — in 16 cases, bone lesions — in 10 cases, pulmonary metastases – in 2 cases, hepatic lesions were visualised in one of them and in another — adrenal suprarenal metastasis with intensive tracer uptake significant for overexpression of PSMA. There was a suspicion for local recurrences in 4 patients with negative MRT studies who were followed up. In 3 cases, previously treated bone metastases were partially negative without tracer uptake, only some progressive bone lesions were positive. Five patients were with negative results. Sensitivity was 84.37% (27/32), specificity — 100% (4/4) and accuracy — 86.11% (31/36).

Conclusions: In conclusion SPECT-CT imaging with [^{99m}Tc]Tc-PSMA-T4 could be applied in patients with prostate cancer for the diagnosis of recurrent disease to determine personalized treatment for each patient. Specific uptake of this tracer, depicted by SPECT-CT images has clinical importance of identifying and assessing PSMA expression before consideration of Radio Ligand Therapy (RLT) with [¹⁷⁷Lu]Lu-PSMA. SPECT-CT imaging with [^{99m}Tc]PSMA is promising and reliable nuclear medicine approach to monitoring therapeutic effect after treatment and for restaging of the disease.

KEY words: recurrent prostate cancer; PSMA; [^{99m}Tc]Tc-PSMA-T4; SPECT-CT

Nucl Med Rev 2021; 24, 2: 70–81

Correspondence to: Sonya Sergieva
Department of Nuclear Medicine, Sofia Cancer Centre, Blvd.
“Andrey Saharov”22, Sofia — 1784, Bulgaria
e-mail: sergieva.sonya@yahoo.com

Introduction

Prostate cancer is the most common malignancy in men in Europe. According to forecast statistics for 2018, the number diagnosed with this disease is 450,000 men or 20% of all cases of malignancies in them [1]. This disease is socially significant both in Bulgaria and in the countries of the European Union. The incidence in 2018 (standardized indicator per 100,000 men) varies from 80.2 in Romania to 265.2 in Ireland. In Bulgaria, the incidence is 136.4, 14% lower than the European Union average, but with a tendency to increase. Mortality in 2018 varies from 22.7 in Italy to 73.9 in Estonia. In Bulgaria, the mortality rate is 40.1 and is 7% higher than the average for the European Union, with a tendency to increase, and the survival rate is the lowest among the European — 68% [1, 2]. Interpretation of these factual data points out that modern diagnostic and therapeutic methods have not yet shown their impact on epidemiological indicators in Bulgaria as well as in some other European countries. The reasons for this are complex and diverse for different countries.

One of the important clinical problems is the early detection and visualization of recurrences after prostatectomy, radiotherapy or other definitive local treatment, with PSA values above 0.2 ng/mL. Contrast-enhanced magnetic resonance imaging (MRI) and computed tomography (CT) scans are most commonly used, but they are not always of sufficient sensitivity and specificity, especially at low tumour marker values [3, 4].

With the introduction of molecular high sensitive imaging after administration of radiolabelled prostate-specific membrane antigen (PSMA), it has become possible to obtain early functional information for disease development and recurrence detection, which is more accurate than that of CT or MRI in many cases [5, 6].

Prostate-specific membrane antigen (PSMA) is a cell surface glycoprotein with a large extracellular domain with overexpression of the prostatic tumour cells. This membrane antigen is known as glutamate carboxypeptidase II (GCP II), a membrane-bound binuclear zinc metallopeptidase, which is available in low concentrations in normal kidney, intestinal tissue and salivary glands [7, 8]. PSMA overexpression is observed also in endothelial cells of tumour neovasculature of non-prostatic solid tumours and benign lesions: colon, gastric, breast, thyroid, ovary; Paget Disease, probably stimulated by secreted angiogenic factors. Upon ligand binding, PSMA is internalized via endocytosis in the tumour cell [7, 8].

In recent years in the clinical practice, a new concept was introduced for specific diagnosis and targeted effective radionuclide treatment of metastatic prostate cancer (PC) after administration of a target PSMA molecule, labelled with various radionuclides, on the principles of theranostics [9, 10].

The degree of intensity of PSMA overexpression epithelial cells in PC is proportional to the degree of malignant cell dedifferentiation and metastatic spread [7, 8]. The field of radiopharmacy and radiochemistry over the last decade is focused on the development of small ligand molecules or binding inhibitors with the active PSMA core, which are characterized by high specificity, good permeability in solid tumours, optimal pharmacokinetics in normal tissues, easily labelled and synthesized, no host-immune response in the recipient [7, 8].

Such PSMA ligands can be labelled with different radionuclides, respectively with ⁶⁸Ga, ¹⁸F, ^{99m}Tc, ^{123/124}I (emitting positron or gamma emission) for diagnostic purposes or with ¹⁷⁷Lu, ¹³¹I, ⁹⁰Y, ²²⁵Ac (emitting beta or alpha emissions) to conduct target radioligand therapy. The most used diagnostic radiopharmaceutical is the ⁶⁸Ga PSMA-11 inhibitor [6, 8, 10].

After intravenous application of gamma-emitting radiopharmaceutical [^{99m}Tc]PSMA or positron-emitting [⁶⁸Ga]PSMA, positive scans were significant for the presence of PSMA overexpression, this information is important for the assessment of malignant lesions and disease extension [5, 6].

Several small molecules of PSMA ligands or inhibitors were developed. One such small ligand binding to the active site of PSMA, namely PSMA-T4 (Glu-CO-Lys-L-Trp-4-Amc-HYNIC) and the kit formulation for its radiolabelling with technetium-99m resulting in the [^{99m}Tc]Tc-PSMA-T4 radiopharmaceutical were developed at Radioisotope Centre Polatom, National Centre for Nuclear Research in Otwock, Poland.

The purpose of this study was to evaluate the clinical role of [^{99m}Tc]Tc-PSMA-T4 for imaging of local relapse and/or loco-regional and distant metastases in patients with recurrent prostate cancer and biochemical disease progression.

Material and methods

Patients

This was a prospective study conducted in the period January 2019 — January 2020 after preliminary approval of this scientific project on the Local Ethics Committee. A cohort of 36 patients, aged 60–80 years/average of 69.44 years/ with prostate cancer was examined after obtaining written informed consent. Three patients underwent tru-cut biopsy, hormonal and cytoreductive radiotherapy; 33 patients out of 36 received radical treatment of primary cancer (total prostatectomy or definitive radiotherapy of the tumour). There was laboratory data on biochemical disease progression — serum value elevation of the tumour marker PSA and its doubling within 6 months. The average serum PSA level before SPECT-CT imaging was 6.73 ng/mL (ranged from 0.1 to 73 ng/mL) (Tab. 1).

All of the patients underwent whole-body imaging examinations with target SPECT-CT studies 1–3 hrs post intravenous administration of [^{99m}Tc]Tc-PSMA-T4.

Radiolabelling

PSMA-T4 (Glu-CO-Lys-L-Trp-4-Amc-HYNIC, 23 mcg) in the form of a dry kit for radiolabelling with technetium-99m has been obtained from National Centre for Nuclear Research (Polatom, Poland) and was radiolabelled with technetium-99m according to the procedure: to the kit vial, 1 to 2.5 mL of sodium pertechnetate solution (eluate from the ⁹⁹Mo/^{99m}Tc generator) with radioactivity in the range from 370 to 1500 MBq was added. The content of the vial was gently mixed for 30 seconds to allow complete dissolution, then heated in the boiling water bath for 15 min and afterwards cooled down at room temperature for 10 min. Radiolabelling yield was more than 95% as assessed by instant thin-layer chromatography (ITLC). The complex [^{99m}Tc]Tc-PSMA-T4 was stable for not less than 4 h.

The average activity dose injected intravenously was 6.3MBq/kg in a man of 70 kg.

Table 1. Clinical and pathological characteristics of the 36 patients with biochemical recurrence of prostate cancer

Pt No/Age	TNM Stage	Gleason Score	PSA at SPECT-CT Image	Primary Therapy
1/67 years	pT3bpN1M0	7 (4 + 3)	0.271 ng/mL	RP, RT, ADT
2/73 years	T3N0M0	7 (4 + 3)	12 ng/mL	RT, ADT
3/71 years	T3N0M0	8 (4 + 4)	73 ng/mL	RT, ADT, Chemotherapy
4/68 years	pT2pN0M0	7 (4 + 3)	0.30 ng/mL	RP
5/67 years	T3N1M0	9 (5 + 4)	9.68 ng/mL	RT,ADT
6/ 64 years	T3bN1M0	9 (5 + 4)	2.15 ng/mL	Cytoreductive RT, ADT, Chemotherapy
7/63 years	pT2pN0M0	7 (3 + 4)	0.12 ng/mL	RP
8/65 years	pT3pN0M0	6 (3 + 3)	0.36 ng/mL	RP
9/ 70 years	pT2pN0M0	7 (3 + 4)	0.24 ng/mL	RP, RT
10/64 years	pT2cpN0M1	7 (4 + 3)	0.82 ng/mL	RP, ADT
11/70 years	pT2pN0M0	7 (4 + 3)	0.69 ng/mL	RP,ADT
12/79 years	T3N0M0	10 (5 + 5)	10.87 ng/mL	RT, ADT, Chemotherapy
13/60 years	pT2pN0M0	5 (3 + 2)	0.50 ng/mL	RP
14/64 years	T3aN0M0	7 (4 + 3)	0.16 ng/mL	RP, ADT
15/74years	pT3bpN1M0	9 (5 + 4)	0.35 ng/mL	RP, RT, ADT, Chemotherapy
16/75years	pT2cpN0M0	7 (4 + 3)	0.57 ng/mL	RP, RT, ADT
17/75years	pT2cpN0M0	7 (4 + 3)	0.36 ng/mL	RP
18/70years	T3bN0M1	7 (3 + 4)	58 ng/mL	RT, ADT
19/62years	T3bN1M1	8 (4 + 4)	0.66 ng/mL	Cytoreductive RT, ADP
20/68years	T2NxM1	7 (4 + 3)	0.41 ng/mL	RT, ADT
21/63years	T3aN0M0	7 (4 + 3)	1.78 ng/mL	RT, ADT
22/77years	pT2pN0M0	7 (3 + 4)	1.5 ng/mL	RP, ADT
23/69years	T2NxM0	7 (4 + 3)	7.3 ng/mL	RT, ADT
24/79years	pT2pN0M0	6 (3 + 3)	1.42 ng/mL	RP, RT, ADT
25/64years	T4N1M1a	8 (4 + 4)	14 ng/mL	RT, ADT
26/77years	T3aN0M0	7 (3 + 4)	0.8 ng/mL	RT
27/66years	T2N0M0	8 (4 + 4)	1.88 ng/mL	RT
28/69years	pT2pN0M0	7 (4 + 3)	0.25 ng/mL	RP, RT
29/60years	pT2pN0M0	5 (3 + 2)	0.77 ng/mL	RP, ADT
30/78years	T1cN1M1	8 (4 + 4)	27 ng/mL	RT, ADP
31/69years	pT2N0M0	5 (3 + 2)	1.6 ng/mL	RP, ADP
32/70years	pT2N0M0	7 (4 + 3)	0.23 ng/mL	RP, RT
33/73years	T4N1M0	9 (4 + 5)	0.30 ng/mL	Cytoreductive RT, ADP
34/80years	T2N0M0	7 (4 + 3)	5.90 ng/mL	RT, ADP
35/70years	pT3bpN0M0	8 (4 + 4)	1.72 ng/mL	RP, ADP
36/71years	pT2cpN0M0	8 (5 + 3)	0.47 ng/mL	RT, ADP

RP — radical prostatectomy; RT — radiotherapy; ADT — androgen deprivation therapy

Imaging protocol

Whole-body imaging examinations with subsequent target SPECT-CT studies of the pelvis, abdomen and/or chest and were carried out 1–3 hrs. after tracer application. SPECT-CT gamma camera Symbia T2, Siemens, was used for topographic localization and morphological substratum of “hot” abnormal foci. Dual-head-SPECT acquisition included 64 projections, 25 s/projection, matrix 256 × 256. A low dose CT scan was performed in the helical mode. Acquisition parameters included settings at 130 kV, 30 mA; 3–5 mm slice thickness.

SPECT-CT images were analysed considering any focal abnormal uptake of [^{99m}Tc]Tc-PSMA-T4 above the surrounding background level, not associated with physiological biodistribution, suggestive of malignancy. The diagnostic differentiation between malignant and inflammatory lymph nodes is based not only on the intensity of tracer accumulation but also on the morphological structure of the nodule and the anatomical localization, especially if the accumulation is bilaterally symmetrical in the inguinal, hilar or axillary lymph nodes. The obtained SPECT-CT results were compared with the data from the

previously conducted diagnostic imaging studies — computed tomography, magnetic resonance tomography, bone scintigraphy. The images were interpreted based on all other clinical and radiological data.

Follow-up SPECT-CT studies with ^{99m}Tc Tc-PSMA-T4 were performed in 11/36 patients to monitor and evaluate the results of baseline scans and conducted treatment.

Results

Normal biodistribution of the radiopharmaceutical with high activity background was observed in the liver, spleen, kidneys, lacrimal and salivary glands, oral and nasal mucosa, bowels and urinary bladder (Fig. 1).

Positive imaging for local relapse in the prostate bed was imaged in 21 patients, pelvic and extra pelvic lymph node metastases — in 16 cases, bone lesions — in 10 cases, visceral lesions — in 3 cases: pulmonary metastases — in 2 cases, hepatic and adrenal suprarenal metastases — in one of them (Fig. 2–7). The smallest visualized positive lymph node was axial in size 9.2 mm (Fig. 2). All abnormal “hot” spots were scanned with intensive tracer uptake significant for PSMA overexpression.

There was a suspicion of local recurrence in the prostate bed in 4 patients with negative MRT imaging who were followed up after 6 months. The presence of the pathological findings was confirmed by the performed control studies with ^{99m}Tc Tc-PSMA-T4, as they were also positive by the computed tomography or magnetic resonance imaging carried out in parallel.

In 4 patients negative results were obtained for local recurrence of the prostate, no lymphogenic spread or hematogenous dissemination of the disease was observed. In these cases, the level of the tumour marker PSA decreased in the control studies, for these reasons, the data from the imaging ^{99m}Tc Tc-PSMA-T4 study were interpreted as truly negative (Fig. 4).

In 3 cases with multiple bone metastases, treated palliatively with radiotherapy and osteomodulators, tracer uptake was found only in some progressive bone lesions. There was a lack of activity in most osteosclerotic foci, probably due to a suppressed osteoblastic process after treatment (Figure 7). In one of these patients, the study with ^{99m}Tc Tc-PSMA-T4 was performed to exclude visceral and lymphogenic dissemination of the disease to plan treatment with Xofigo infusion (Fig. 8).

Targeted radiotherapy was performed in seven patients with a positive result for the development of local recurrence in the

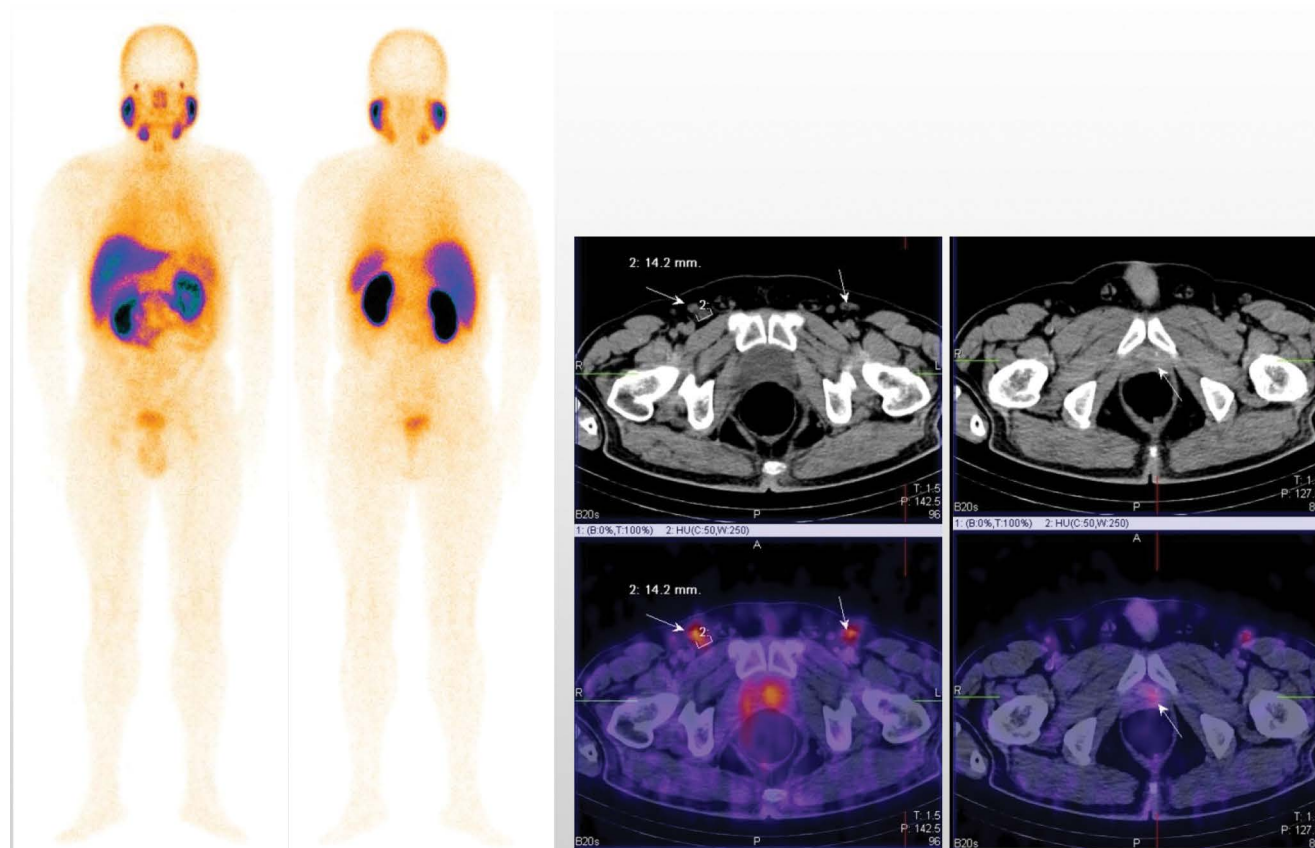


Figure 1. M/60yr with prostate cancer, pT2pN0M0, G2, Gl = 5 (3 + 2). Radical prostatectomy (2018). PSA = 0.5 ng/mL (01/2019). Whole-body scan and target ^{99m}Tc Tc-PSMA-T4 SPECT-CT imaging showed physiological tracer biodistribution in the liver, spleen, kidneys, lacrimal and salivary glands, oral and nasal mucosa, bowels and urinary bladder. Intensive ^{99m}Tc Tc-PSMA-T4 uptake was visualized in the prostatic bed suspicious for local recurrence, follow-up was required. There was moderate symmetrical activity in the inguinal bilateral lymph nodes, which were visualized with normal structure and size, with well-depicted lymphocytic sinus, interpreted as reactive lymph nodes

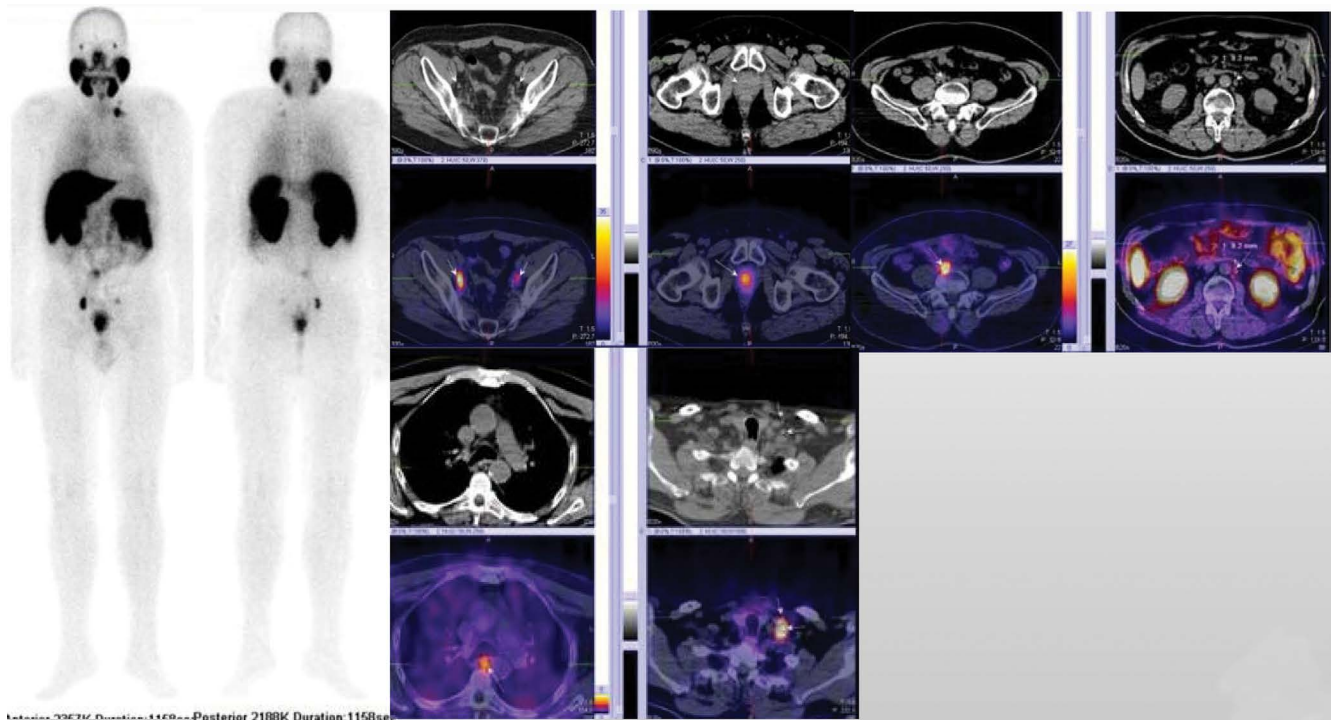


Figure 2. M/64yr with prostate cancer, pT3bpN1Mo, G3, Gl = 9 (5 + 4). Cytreoreductive radiotherapy (01/2018), androgen deprivation therapy, chemotherapy. PSA = 2.157 ng/mL (01/2019). Whole-body scan and target [^{99m}Tc]Tc-PSMA-T4 SPECT-CT imaging showed local recurrence and enlarged bilateral obturator lymph nodes, common iliac lymph node on the right, periaortic with diameter 9.2 mm lymph node, paraesophageal retrotracheal lymph node and supraclavicular lymph node metastases with intensive tracer uptake

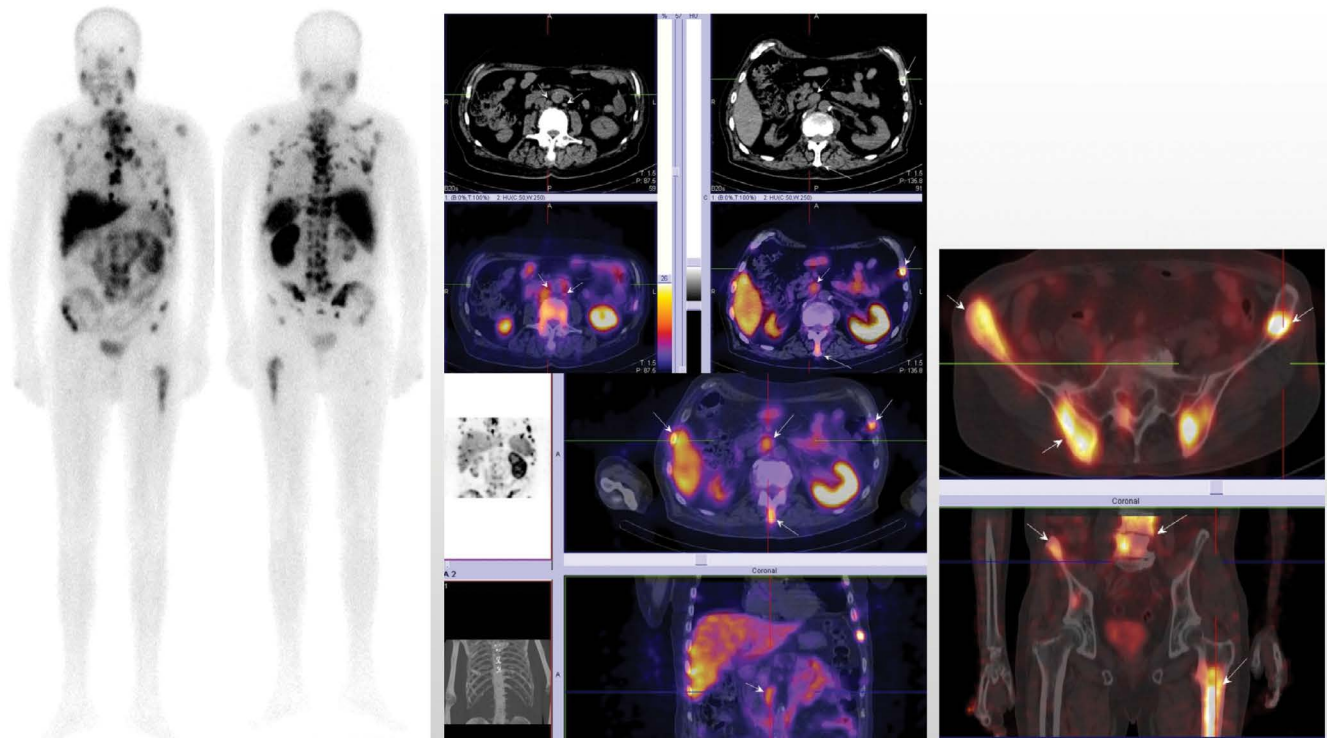


Figure 3. M/71yr with prostate cancer T3N0M0, G3, Gl = 8 (4 + 4). Radiotherapy definitive (09/2013). Androgen deprivation therapy. Chemotherapy and osteomodulators. PSA = 73ng/mL (02/2019). Whole-body scan and target [^{99m}Tc]Tc-PSMA-T4 SPECT-CT imaging showed multiple bone metastases and enlarged retroperitoneal lymph node metastases with intensive tracer uptake

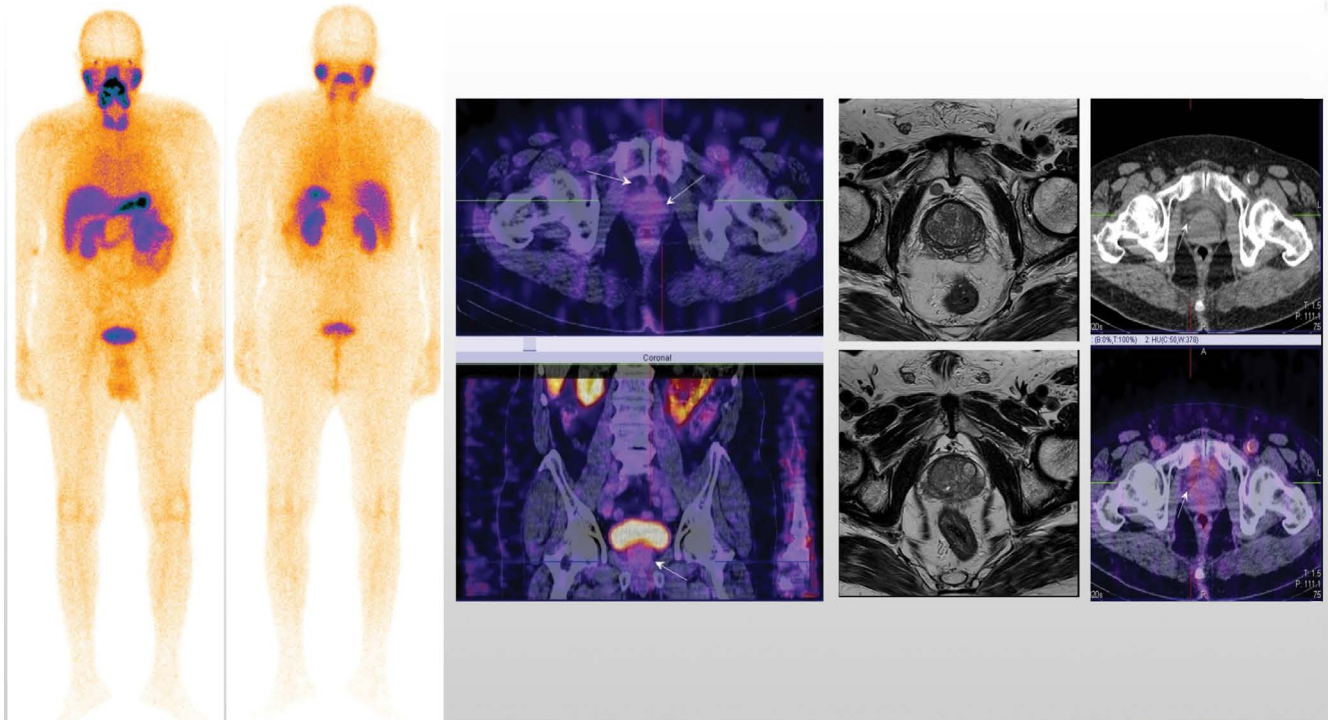


Figure 4. M/73yr with prostate cancer, T4N1M0, G3, GI = 9 (4 + 5). Cytoreductive radiotherapy (03/2019) and androgen deprivation therapy. PSA = 0.30 ng/mL (06/2019). Whole-body scan and target ^{99m}Tc Tc-PSMA-T4 SPECT-CT imaging showed enlarged prostatic gland and perivesical lymph nodes with intensive tracer uptake corresponding to MRT images. Disease persistence

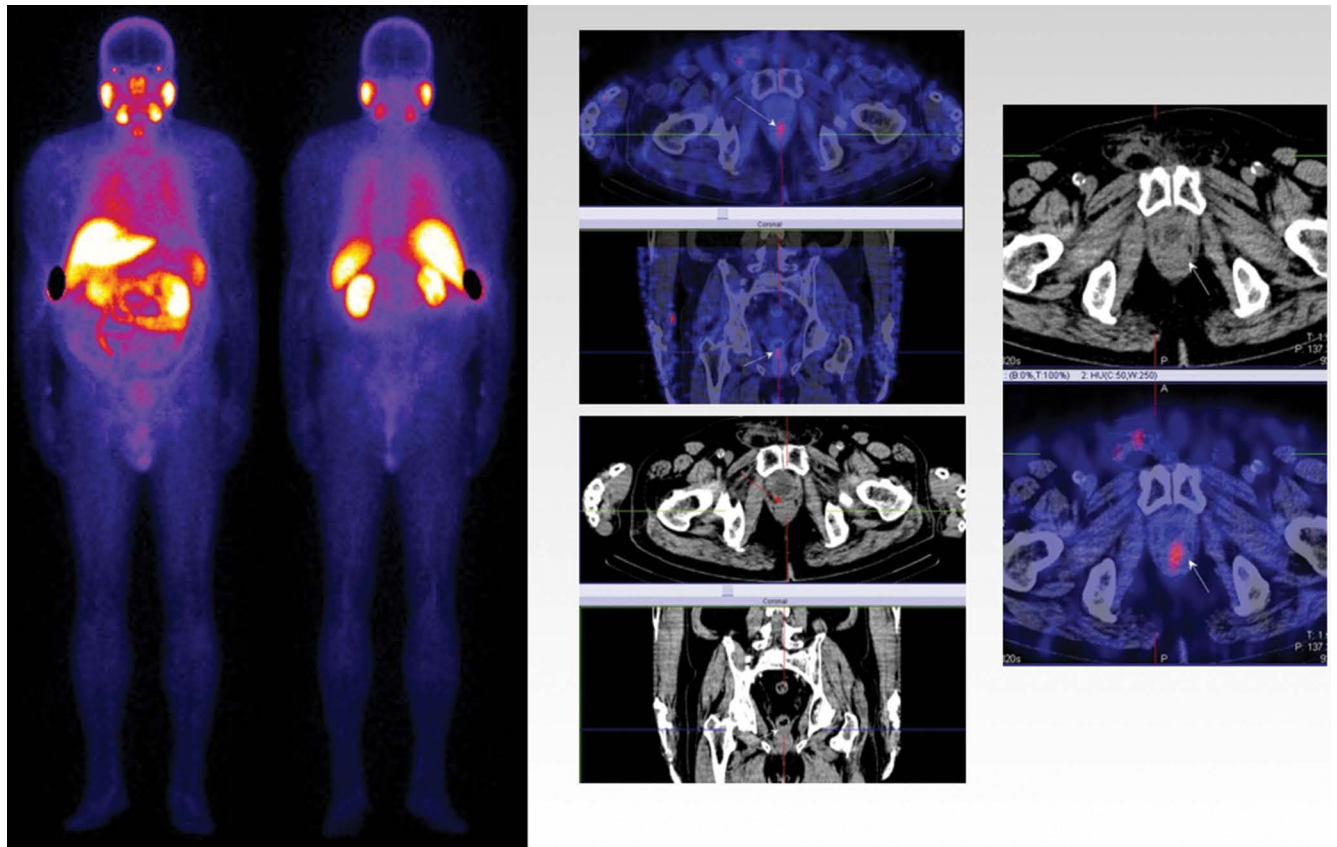


Figure 5. M/70yr with prostate cancer, pT2N0M0, G2, GI = 7 (3 + 4). Radical prostatectomy (2017) and radiotherapy. PSA = 0.24 ng/mL (06/2019). Whole-body scan and target ^{99m}Tc Tc-PSMA-T4 SPECT-CT imaging showed local recurrence in the prostatic bed with intensive tracer uptake. Disease progression

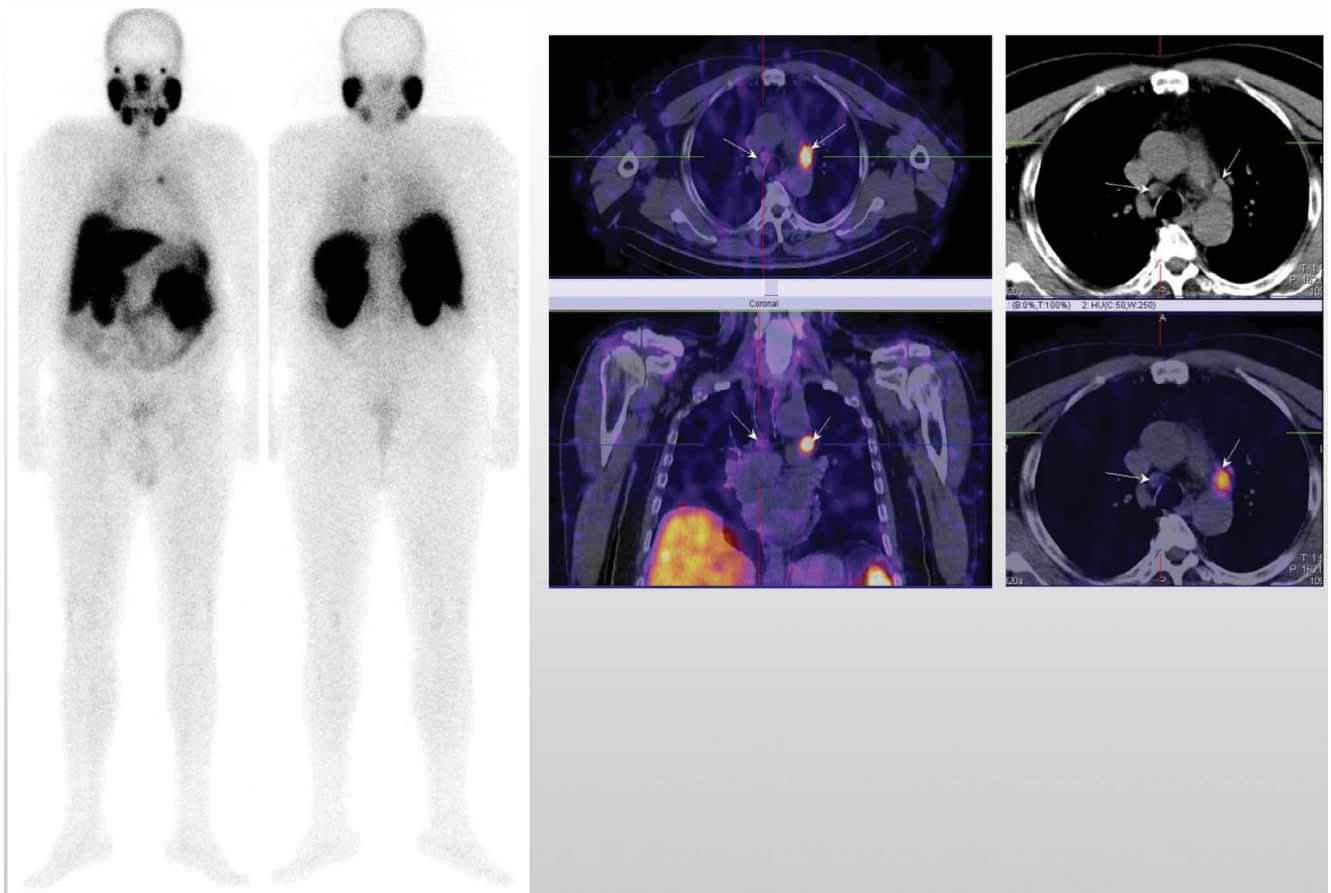


Figure 6. M/67yr with prostate cancer, pT3bpN1M0, G1 = 7 (4 + 3). Radical prostatectomy, radiotherapy (01/2018) and androgen deprivation therapy. PSA = 0.27 ng/mL (01/2019). Whole-body scan and target [^{99m}Tc]Tc-PSMA-T4 SPECT-CT imaging showed enlarged mediastinal lymph node metastases with intensive tracer uptake

prostate bed and pelvic lymphadenopathy. SPECT-CT images were used for contouring the gross tumour volume (GTV) and the clinical tumour volume (CTV) in the radiotherapy planning (Fig. 9, 10).

Negative results were found in 5 patients. They were followed up after 6 months, and no pathological lesions with tracer uptake were visualized in the second study. In this group, a continuing increase in serum PSA was observed:

- in the first patient the value of PSA before the baseline [^{99m}Tc]Tc-PSMA-T4 study was 0.12 ng/mL and 6 months later: PSA = 1.42 ng/mL;
- in the second patient, PSA levels were 0.23 ng/mL and 0.84 ng/mL respectively;
- in the third patient, PSA levels were 0.16 ng/mL and 0.25 ng/mL respectively;
- in the fourth patient, PSA levels were 0.50 ng/mL and 0.77 ng/mL respectively;
- in the fifth patient, PSA levels were 0.24 ng/mL and 0.47 ng/mL respectively.

Due to the continuing biochemical progression and negative scan of the [^{99m}Tc]Tc-PSMA-T4 study, the results in these cases were

interpreted as false-negative images. In all patients in this group, the baseline PSA was less than or equal to 0.50 ng/mL.

Sensitivity of SPECT-CT study with [^{99m}Tc]Tc-PSMA-T4 for imaging of recurrent prostate cancer in 36 involved patients was 84.37% (27/32), specificity — 100% (4/4) and accuracy — 86.11% (31/36). For the clinical application of this study, the following could be summarized:

1. SPECT-CT imaging with [^{99m}Tc]Tc-PSMA-T4 could be applied in patients with prostate cancer and biochemical progression if PSA \geq 0.50 ng/mL for the diagnosis of recurrent disease to determine personalized treatment for each patient.
2. To follow-up of patients after complex therapy for restaging of the disease in cases with unclear and uncertain findings from other imaging methods.
3. For imaging of local recurrence and/or metastases after therapy to perform target radiotherapy or SRT (salvage radiation therapy).
4. Specific uptake of this tracer, depicted by SPECT-CT images could have clinical importance of identifying and assessing PSMA expression before consideration of Radio Ligand Therapy (RLT) with [^{177}Lu]Lu-PSMA.

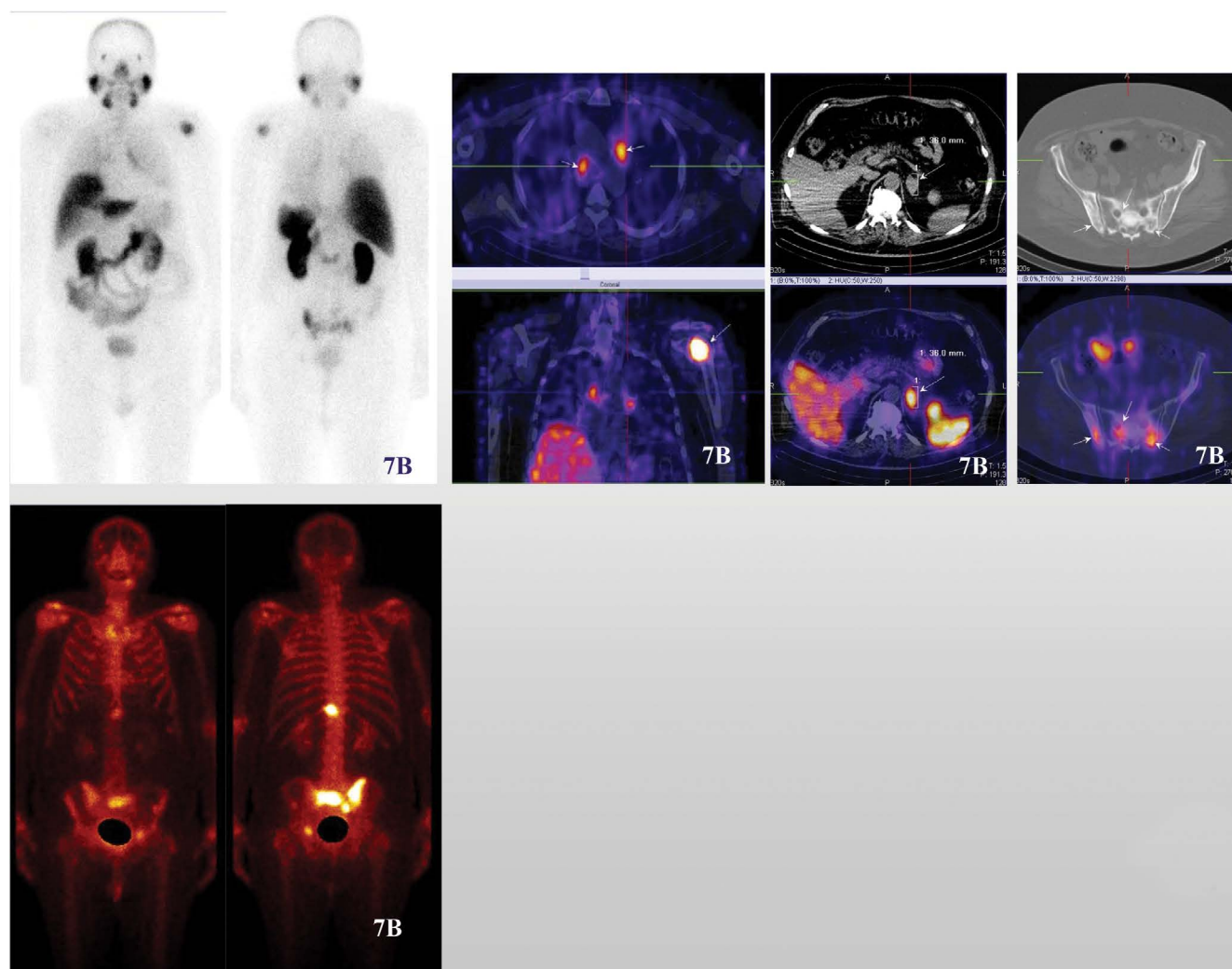


Figure 7A. M/79yr with prostate cancer, T3N0M0, G3, GI = 10 (35 + 5). Radiotherapy (2017), androgen deprivation therapy, chemotherapy. PSA = 10.87 ng/mL (03/2019). Whole-body scan and target [^{99m}Tc]Tc-PSMA-T4 SPECT-CT imaging showed multiple osteosclerotic bone lesions, partially negative due to prior treatment; **B.** Bone scan performed 6 months previously with a positive result for bone metastases in the pelvis, Th12 and left shoulder. New enlarged mediastinal lymph nodes and enlarged left adrenal gland, significant for metastases, were visualized. Disease progression

Discussion

The first results for clinical application of radiolabelled PSMA were published in 2013 [5] and this led to a qualitatively new nuclear medicine approach to this disease with the possibility of determining the optimal personalized therapy for patients [6, 10–12].

The cited sensitivity and specificity of the [⁶⁸Ga]Ga-PSMA-11 studies are very high due to the better spatial resolution of the PET-CT camera [13]. Compared to them, the images obtained by SPECT camera are characterized by lower spatial resolution, which is significantly improved in the combined multimodal SPECT-CT devices with greatly increased quality of the obtained images [14].

The results received in the present prospective study of the clinical use of [^{99m}Tc]Tc-PSMA-T4 in recurrent prostate cancer are comparable to those cited in the scientific literature [13, 15]. In a large study of 225 patients reported by Schmidkonz et al. [15], it was found that the detection capabilities of prostate cancer

with the biochemical progression of [^{99m}Tc]Tc-MIP-1404 SPECT-CT are comparable to those of [⁶⁸Ga]Ga-PSMA PET-CT at levels of PSA > 2 ng/mL. At lower than these values and a smaller volume of the tumour tissue substrate, the sensitivity of SPECT-CT studies is reduced to 54% [16]. Liu et al. [17], report that at lower PSA values < 0.5 ng/mL the diagnostic value of [^{99m}Tc]HYNIC-PSMA SPECT-CT is 48.6%.

Another study showed that [^{99m}Tc]PSMA scanning was as sensitive as [⁶⁸Ga]Ga-PSMA-11 in 28 prostate cancer patients in terms of visualization of bone and lymphogenic metastatic foci, with PSA levels > 2 ng/mL. SPECT-CT detection was lower when local recurrence was detected in the prostate bed in patients with evidence of biochemical progression with PSA < 0.5 ng/mL [15].

Goffin et al. [18], published data that the diagnostic value of SPECT-CT studies with [^{99m}Tc]Tc-MIP-1404 correlated with the degree of differentiation of the primary tumour — Gleason score. In patients at intermediate risk and high-risk disease with GI ≥ 7 (3 + 4) detection rate reached 94% (86% for MRT); for visualization

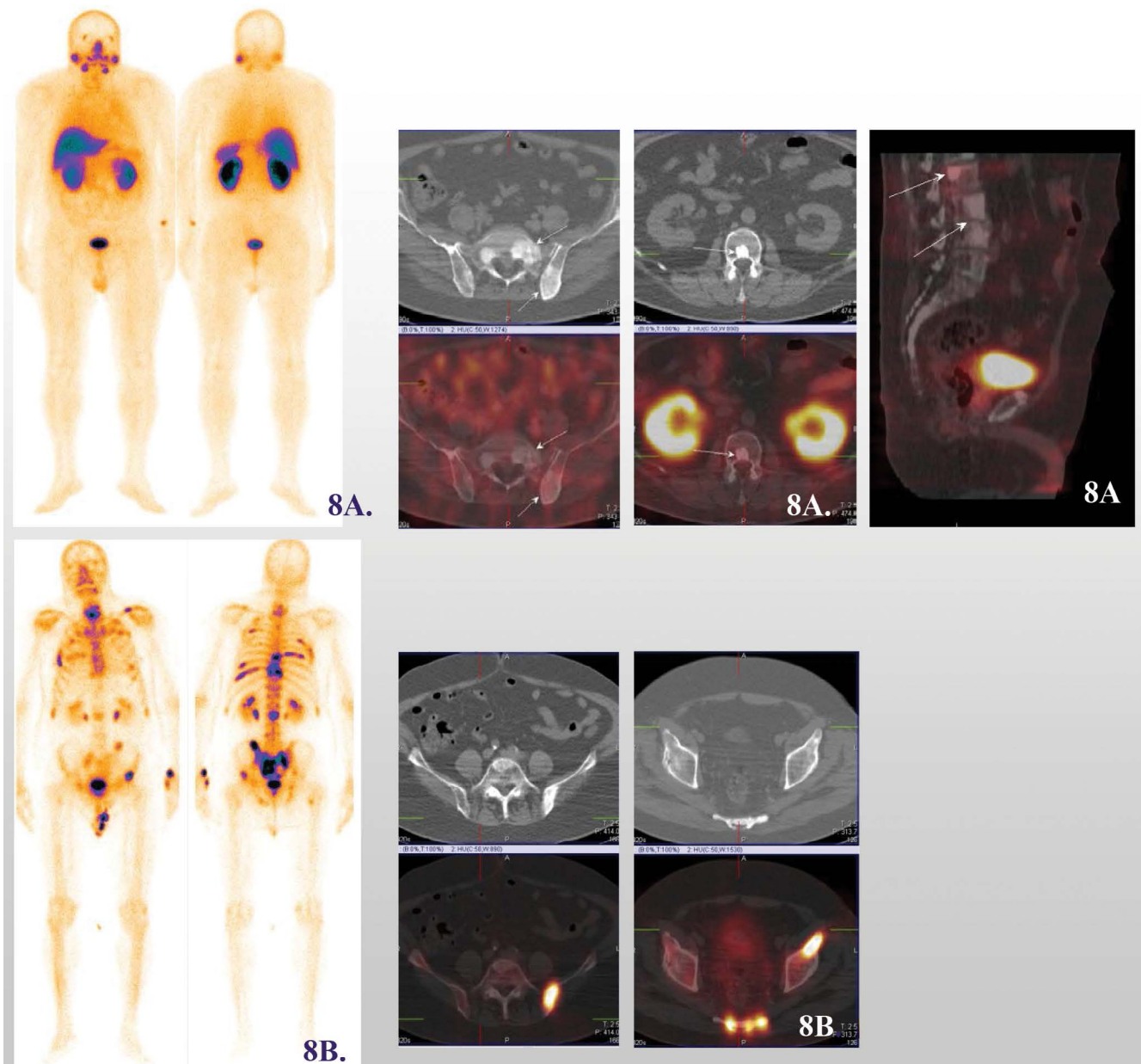


Figure 8A. M/62yr with prostate cancer, T3bN1M1, G3, GI = 10 (35 + 5). Radiotherapy (2017), androgen deprivation therapy, osteomodulators. PSA = 0.66 ng/mL (07/2019). Whole-body scan and target [^{99m}Tc]Tc-PSMA-T4 SPECT-CT imaging showed multiple osteosclerotic bone lesions, negative due to prior treatment; **B.** Bone scan was performed 6 months later due to increased PSA = 29 ng/mL, with a positive result for active multiple bone metastases in the thoracic and lumbar vertebrae, bilateral ribs, pelvic bones and synchondrosis, left shoulder. There were no evidence of local recurrence, lymphogenic and visceral targets. The patient was planned for Xofigo therapy

of metastatic lymph nodes, the sensitivity and specificity were 90% and 67% respectively [18].

In patients with treated skeletal metastases and a negative [^{99m}Tc]Tc-PSMA(I&T) scan without lymphogenic and visceral secondary lesions, but with a progressive PSA elevation, control whole-body bone scintigraphy or follow-up by other standard visual methods is recommended. It would be appropriate to discuss the possibility of treatment with Xofigo in these patients [19].

Another clinical application of [^{99m}Tc]PSMA SPECT-CT, which is not discussed in the present study but is cited in recently published scientific articles, is the introduction of this method for selective radio-guided surgery of metastatic lymph nodes and/or local recurrence in the bed of the prostate. Initial data are very encouraging for the future use of a gamma probe for intraoperative detection of metastatic foci in the pelvis, previously imaged by SPECT-CT using [^{99m}Tc]Tc-PSMA(I&T) and [^{99m}Tc]Tc-PSMA-ALUG [20, 21].

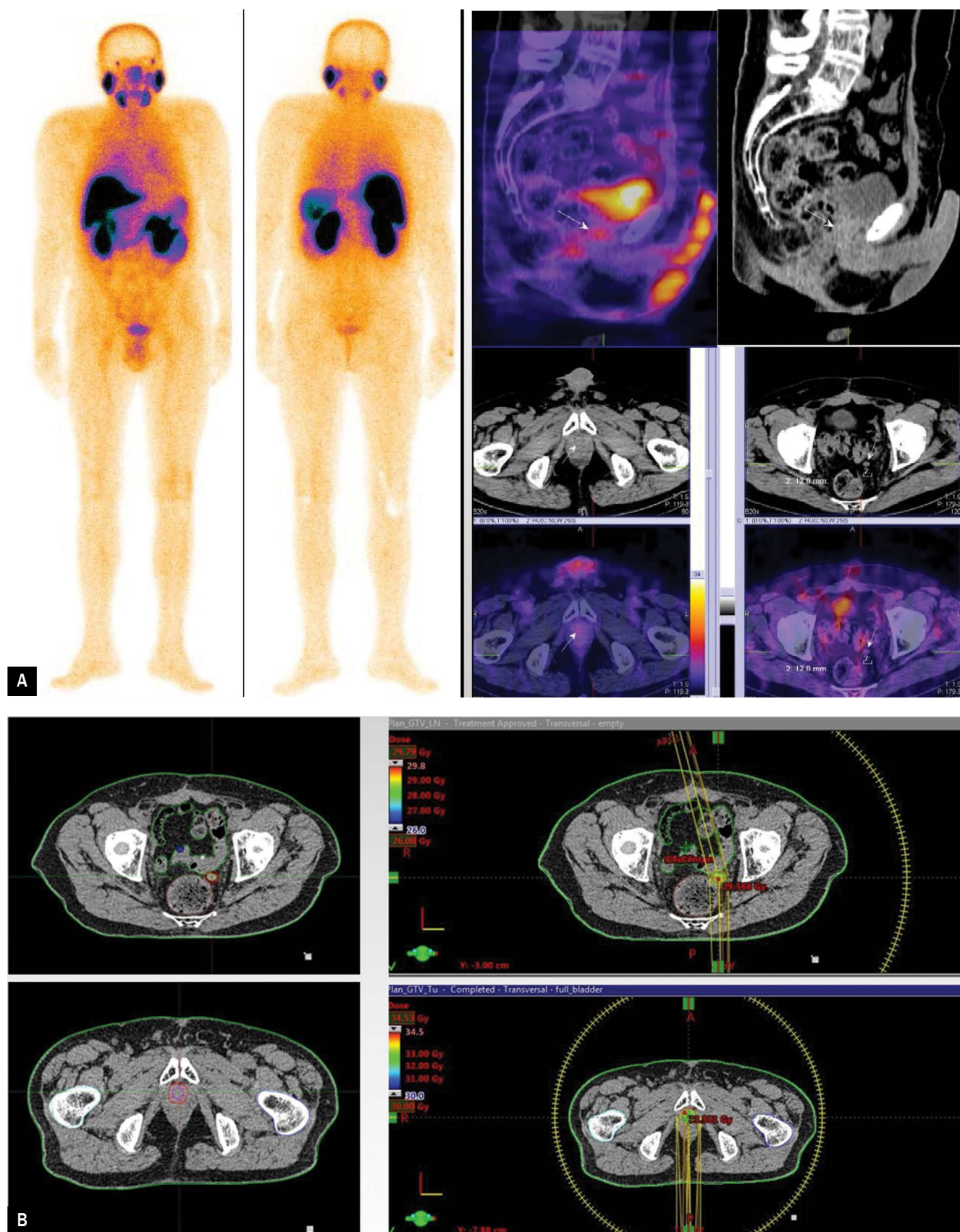


Figure 9A. M/75yr with prostate cancer, pT2cpN0M0, G2, GI = 7 (4 + 3). Radical prostatectomy, radiotherapy (2015) and androgen deprivation therapy. PSA = 0.57 ng/mL (03/2019). Whole-body scan and target [^{99m}Tc]Tc-PSMA-T4 SPECT-CT imaging showed local recurrence in the prostate bed and enlarged single perirectal lymph node on the left with intensive tracer uptake; **B.** Gross tumour volume (GTV) and Clinical Tumour Volume (CTV) delineation based on the [^{99m}Tc]Tc-PSMA-T4 imaging results in radiotherapy planning. Radiation dose distribution in the region of the local recurrence and the single enlarge perirectal lymph node on the left in the same patient

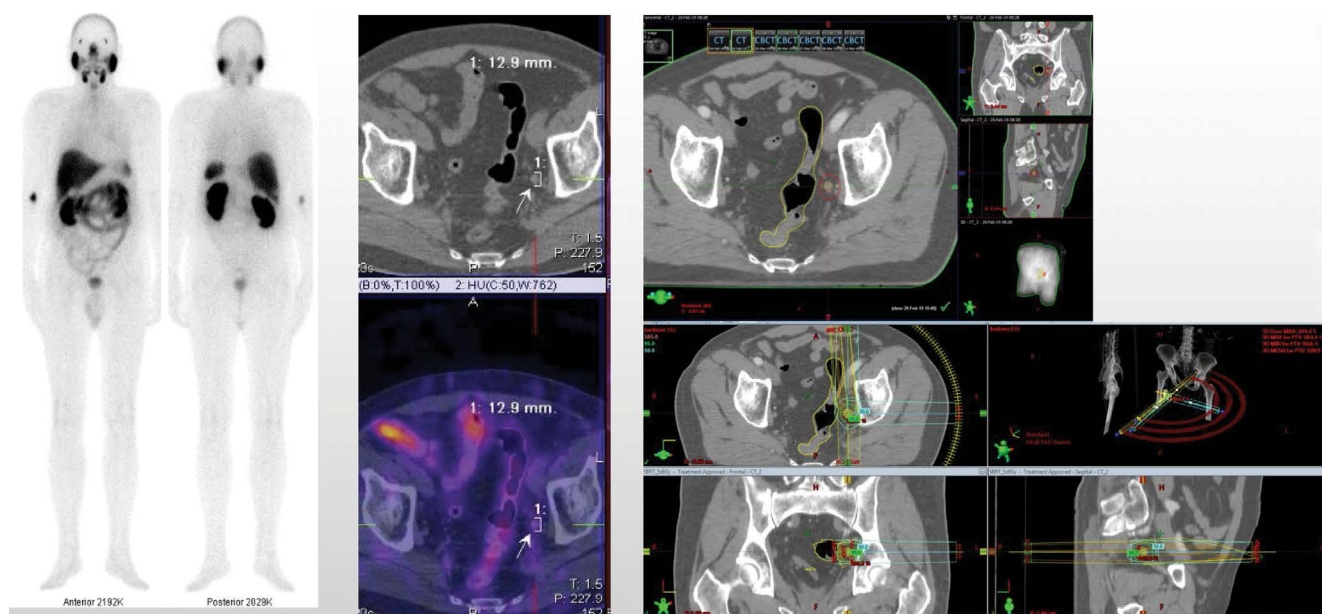


Figure 10. M/75yr with prostate cancer, pT2cpN0M0, Gl = 7 (4 + 3)_E. Radical prostatectomy/2016/ PSA = 0.36 ng/mL (02.2019) Whole-body scan and target [^{99m}Tc]Tc-PSMA-T4 SPECT-CT imaging showed enlarged single iliac lymph node on the left with intensive tracer uptake. Gross tumour volume (GTV) and Clinical Tumour Volume (CTV) delineation based on the [^{99m}Tc]Tc-PSMA-T4 imaging results in radiotherapy planning. Radiation dose distribution in the region of the single enlarged iliac lymph node on the left in the same patient. The PSA value decreased to 0.05 ng/mL (M.10.2019) after radiotherapy

Conclusions

Based on these results and the review of the published literature, it could be summarized that the new [^{99m}Tc]Tc-PSMA-T4 tracer was shown to have favourable biodistribution and kinetic behaviour. This radiopharmaceutical can be prepared in a short time, technically easy to perform radiolabelling and quality control, with a significantly lower radiation dose for the patient. A whole-body scan with subsequent SPECT-CT imaging is recommended within one to three hours after intravenous administration.

The use of [^{99m}Tc]Tc-PSMA-T4 is a very good alternative as a diagnostic method in patients with prostate cancer in nuclear medicine centres that cannot produce [⁶⁸Ga]Ga-PSMA.

SPECT-CT study with [^{99m}Tc]Tc-PSMA-T4 is a promising imaging tool showing high sensitivity and specificity with great diagnostic potential in patients with recurrent prostate cancer due to intensive target uptake in the local relapse of the prostate gland, lymphatic, bone and visceral metastases with a high diagnostic accuracy of 86.11%. These parameters make [^{99m}Tc]Tc-PSMA-T4 SPECT-CT studies an advanced visual method, cost-effective and widely applicable.

Conflict of interest

The authors report no conflicts of interest.

References

1. Ferlay J, Colombet M, Soerjomataram I, et al. Cancer incidence and mortality patterns in Europe: Estimates for 40 countries and 25 major cancers in 2018. *Eur J Cancer*. 2018; 103: 356–387, doi: [10.1016/j.ejca.2018.07.005](https://doi.org/10.1016/j.ejca.2018.07.005), indexed in Pubmed: [30100160](https://pubmed.ncbi.nlm.nih.gov/30100160/).
2. European Cancer Information System-ECIS, European Commission 2018. <https://ecis.jrc.ec.europa.eu/> (12.03.2019).
3. Kelloff GJ, Choyke P, Coffey DS, et al. Prostate Cancer Imaging Working Group. Challenges in clinical prostate cancer: role of imaging. *AJR Am J Roentgenol*. 2009; 192(6): 1455–1470, doi: [10.2214/AJR.09.2579](https://doi.org/10.2214/AJR.09.2579), indexed in Pubmed: [19457806](https://pubmed.ncbi.nlm.nih.gov/19457806/).
4. Engelbrecht MR, Jager GJ, Laheij RJ, et al. Local staging of prostate cancer using magnetic resonance imaging: a meta-analysis. *Eur Radiol*. 2002; 12(9): 2294–2302, doi: [10.1007/s00330-002-1389-z](https://doi.org/10.1007/s00330-002-1389-z), indexed in Pubmed: [12195484](https://pubmed.ncbi.nlm.nih.gov/12195484/).
5. Hillier SM, Maresca KP, Lu G, et al. 99mTc-labeled small-molecule inhibitors of prostate-specific membrane antigen for molecular imaging of prostate cancer. *J Nucl Med*. 2013; 54(8): 1369–1376, doi: [10.2967/jnumed.112.116624](https://doi.org/10.2967/jnumed.112.116624), indexed in Pubmed: [23733925](https://pubmed.ncbi.nlm.nih.gov/23733925/).
6. von Eyben FE, Picchio M, von Eyben R, et al. Ga-Labeled Prostate-specific Membrane Antigen Ligand Positron Emission Tomography/Computed Tomography for Prostate Cancer: A Systematic Review and Meta-analysis. *Eur Urol Focus*. 2018; 4(5): 686–693, doi: [10.1016/j.euf.2016.11.002](https://doi.org/10.1016/j.euf.2016.11.002), indexed in Pubmed: [28753806](https://pubmed.ncbi.nlm.nih.gov/28753806/).
7. Hupe MC, Philippi C, Roth D, et al. Expression of Prostate-Specific Membrane Antigen (PSMA) on Biopsies Is an Independent Risk Stratifier of Prostate Cancer Patients at Time of Initial Diagnosis. *Front Oncol*. 2018; 8: 623, doi: [10.3389/fonc.2018.00623](https://doi.org/10.3389/fonc.2018.00623), indexed in Pubmed: [30619757](https://pubmed.ncbi.nlm.nih.gov/30619757/).
8. Oliveira JM, Gomes C, Faria DB, et al. Ga-prostate-specific Membrane Antigen Positron Emission Tomography/Computed Tomography for Prostate Cancer Imaging: A Narrative Literature Review. *World J Nucl Med*. 2017; 16(1): 3–7, doi: [10.4103/1450-1147.198237](https://doi.org/10.4103/1450-1147.198237), indexed in Pubmed: [28217012](https://pubmed.ncbi.nlm.nih.gov/28217012/).
9. Kratochwil C, Giesel FL, Stefanova M, et al. PSMA-Targeted Radionuclide Therapy of Metastatic Castration-Resistant Prostate Cancer with 177Lu-Labeled PSMA-617. *J Nucl Med*. 2016; 57(8): 1170–1176, doi: [10.2967/jnumed.115.171397](https://doi.org/10.2967/jnumed.115.171397), indexed in Pubmed: [26985056](https://pubmed.ncbi.nlm.nih.gov/26985056/).

10. Jones W, Griffiths K, Barata PC, et al. PSMA Theranostics: Review of the Current Status of PSMA-Targeted Imaging and Radioligand Therapy. *Cancers (Basel)*. 2020; 12(6), doi: [10.3390/cancers12061367](https://doi.org/10.3390/cancers12061367), indexed in Pubmed: [32466595](https://pubmed.ncbi.nlm.nih.gov/32466595/).
11. Krimphove MJ, Theissen LH, Cole AP, et al. Performance and Impact of Prostate Specific Membrane Antigen-Based Diagnostics in the Management of Men with Biochemical Recurrence of Prostate Cancer and its Role in Salvage Lymph Node Dissection. *World J Mens Health*. 2020; 38(1): 32–47, doi: [10.5534/wjmh.180133](https://doi.org/10.5534/wjmh.180133), indexed in Pubmed: [30929322](https://pubmed.ncbi.nlm.nih.gov/30929322/).
12. Schwarzenboeck SM, Rauscher I, Bluemel C, et al. PSMA Ligands for PET Imaging of Prostate Cancer. *J Nucl Med*. 2017; 58(10): 1545–1552, doi: [10.2967/jnumed.117.191031](https://doi.org/10.2967/jnumed.117.191031), indexed in Pubmed: [28687599](https://pubmed.ncbi.nlm.nih.gov/28687599/).
13. Beheshti M, Manafi-Farid R, Geinitz H, et al. Multiphasic Ga-PSMA PET/CT in the Detection of Early Recurrence in Prostate Cancer Patients with a PSA Level of Less Than 1 ng/mL: A Prospective Study of 135 Patients. *J Nucl Med*. 2020; 61(10): 1484–1490, doi: [10.2967/jnumed.119.238071](https://doi.org/10.2967/jnumed.119.238071), indexed in Pubmed: [32060214](https://pubmed.ncbi.nlm.nih.gov/32060214/).
14. Mariani G, Bruselli L, Kuwert T, et al. A review on the clinical uses of SPECT/CT. *Eur J Nucl Med Mol Imaging*. 2010; 37(10): 1959–1985, doi: [10.1007/s00259-010-1390-8](https://doi.org/10.1007/s00259-010-1390-8), indexed in Pubmed: [20182712](https://pubmed.ncbi.nlm.nih.gov/20182712/).
15. Schmidkonz C, Hollweg C, Beck M, et al. Tc-MIP-1404-SPECT/CT for the detection of PSMA-positive lesions in 225 patients with biochemical recurrence of prostate cancer. *Prostate*. 2018; 78(1): 54–63, doi: [10.1002/pros.23444](https://doi.org/10.1002/pros.23444), indexed in Pubmed: [29105797](https://pubmed.ncbi.nlm.nih.gov/29105797/).
16. Liu C, Zhu Y, Su H, et al. Relationship between PSA kinetics and Tc-99m HYNIC PSMA SPECT/CT detection rates of biochemical recurrence in patients with prostate cancer after radical prostatectomy. *Prostate*. 2018; 78(16): 1215–1221, doi: [10.1002/pros.23696](https://doi.org/10.1002/pros.23696), indexed in Pubmed: [30027591](https://pubmed.ncbi.nlm.nih.gov/30027591/).
17. Albalooshi B, Al Sharhan M, Bagheri F, et al. Direct comparison of Tc-PSMA SPECT/CT and Ga-PSMA PET/CT in patients with prostate cancer. *Asia Ocean J Nucl Med Biol*. 2020; 8(1): 1–7, doi: [10.22038/ao-jnmb.2019.43943.1293](https://doi.org/10.22038/ao-jnmb.2019.43943.1293), indexed in Pubmed: [32064277](https://pubmed.ncbi.nlm.nih.gov/32064277/).
18. Goffin KE, Joniau S, Tenke P, et al. Phase 2 Study of Tc-Trofolostat SPECT/CT to Identify and Localize Prostate Cancer in Intermediate- and High-Risk Patients Undergoing Radical Prostatectomy and Extended Pelvic LN Dissection. *J Nucl Med*. 2017; 58(9): 1408–1413, doi: [10.2967/jnumed.116.187807](https://doi.org/10.2967/jnumed.116.187807), indexed in Pubmed: [28302763](https://pubmed.ncbi.nlm.nih.gov/28302763/).
19. Trabulsi EJ, Rumble RB, Jadvar H, et al. Optimum Imaging Strategies for Advanced Prostate Cancer: ASCO Guideline. *J Clin Oncol*. 2020; 38(17): 1963–1996, doi: [10.1200/JCO.19.02757](https://doi.org/10.1200/JCO.19.02757), indexed in Pubmed: [31940221](https://pubmed.ncbi.nlm.nih.gov/31940221/).
20. Maurer T, Robu S, Schottelius M, et al. Technetium-based Prostate-specific Membrane Antigen-radioguided Surgery in Recurrent Prostate Cancer. *Eur Urol*. 2019; 75(4): 659–666, doi: [10.1016/j.eururo.2018.03.013](https://doi.org/10.1016/j.eururo.2018.03.013), indexed in Pubmed: [29625755](https://pubmed.ncbi.nlm.nih.gov/29625755/).
21. Su HC, Zhu Y, Hu SL, et al. The Value of Tc-PSMA SPECT/CT-Guided Surgery for Identifying and Locating Lymph Node Metastasis in Prostate Cancer Patients. *Ann Surg Oncol*. 2019; 26(2): 653–659, doi: [10.1245/s10434-018-6805-y](https://doi.org/10.1245/s10434-018-6805-y), indexed in Pubmed: [30324468](https://pubmed.ncbi.nlm.nih.gov/30324468/).

State-of-the-art modalities in cardio-oncology: insight from a nuclear medicine approach

Narges Jokar¹, Abdullatif Amini², Mohammadreza Ravanbod³, Maryam Barekat⁴, Hossein Shooli⁵, Ali Gholamrezanezhad⁵, Majid Assadi¹

¹The Persian Gulf Nuclear Medicine Research Center, Department of Molecular Imaging and Radionuclide Therapy (MIRT), Bushehr Medical University Hospital, Bushehr University of Medical Sciences, Bushehr, Iran

²Medical Heart Center, Faculty of Medicine, Bushehr University of Medical Sciences, Bushehr, Iran

³Department of Internal Medicine, Persian Gulf Tropical Medicine Research Center, Bushehr University of Medical Sciences, Bushehr, Iran

⁴Department of Regenerative Medicine, Cell Science Research Center, Royan Institute for Stem Cell Biology and Technology, ACECR, Tehran, Iran

⁵Department of Radiology, Keck School of Medicine, University of Southern California, Los Angeles, United States

[Received 19 XI 2020; Accepted 16 III 2021]

Abstract

Cancer and cardiovascular disease are the most significant causes of morbidity and mortality worldwide. Although the cancer survival rate has increased due to improved treatment approaches, especially targeted therapy, some side effects such as cardiotoxicity decrease the efficiency of the clinical outcome. Radiation therapy and chemotherapy have a long-established history of potential cardiotoxic effects. A new multi-disciplinary and translational field known as cardio-oncology has been developed for the identification, prevention, and treatment of cardiovascular dysfunctions associated with cancer treatment approaches. One of the important tools for detecting and monitoring cardiotoxic effects is non-invasive nuclear cardiac imaging techniques. Cardiac nuclear imaging modalities especially recent findings positron emission tomography (PET) tracers have a quintessential role in the early detection of cardiovascular disorders. Moreover, comprehensive studies are required to investigate novel nuclear medicine treatment approaches such as peptide receptor radionuclide therapy (PRRT), fibroblast activation protein (FAP), and chemokine receptor (CXCR) targeting probes for possible cardiac side effects that play important roles in the treatment of malignancies.

KEY words: cardiotoxicity; cardio-oncology; PRRT-related cardiotoxicity; nuclear medicine; FAP; CXCR4; [^{99m}Tc]Sestamibi; [¹⁸F]MitoPhos; [⁶⁸Ga]Galmydar

Nucl Med Rev 2021; 24, 2: 82–92

Background

Cancer and cardiovascular disease are the most significant causes of morbidity and mortality worldwide [1]. Significant advances have been made in the early detection, treatment, and long-term survival of cancer patients. Importantly, each new therapeutic development has encountered specific challenges such as multi-organ adverse events [2]. Therefore, cardiovascular

diseases and malignancies may coexist in these patients because of using combination treatment approaches in molecular oncology for better patient management [3].

Cardiotoxicity as acute and occasionally lethal cardiac events (chronic) related to cancer therapeutic methods occurs either during or immediately following treatment in patients exposed to mediastinal radiation therapy (RT) and anti-cancer drugs as well as decreases the efficiency of the patient's health outcomes. It is categorized into different subtypes (Type I and II) including cardiomyopathy, thrombosis, hypertension, left ventricular dysfunction, QT prolongation, oedema, arrhythmias, metabolic abnormalities, and capillary leak syndrome, which might lead to cardiovascular abnormalities, especially in elderly patients with pre-existing cardiovascular disease [4–9]. Some chemotherapy agents such as vinblastine, anthracyclines, ramucirumab,

Correspondence to: Majid Assadi

The Persian Gulf Nuclear Medicine Research Center, Department of Molecular Imaging and Radionuclide Therapy (MIRT), Bushehr Medical University Hospital, Bushehr University of Medical Sciences, 45654775 Bushehr, Iran
e-mail: assadipoya@yahoo.com

This article is available in open access under Creative Common Attribution-Non-Commercial-No Derivatives 4.0 International (CC BY-NC-ND 4.0) license, allowing to download articles and share them with others as long as they credit the authors and the publisher, but without permission to change them in any way or use them commercially.

trastuzumab, cyclophosphamide, and 5-fluorouracil, can increase the risk of cardiovascular diseases in patients with different malignancies (breast, sarcoma, lung, bladder, gastric, prostate, leukaemia, lymphoma, etc.) [10]. Moreover, there are different reasons for radiation-induced cardiovascular dysfunction such as damage to cardiomyocytes as well as stimulating an inflammatory process in cardiac cells leading to the acceleration of atherosclerosis [11].

Cardio-oncology is a multidisciplinary clinical approach that improves awareness of monitoring and treatment methods in patients with cardiovascular complications related to cancer treatment [12]. According to The American Society of Echocardiography and the European Association of Cardiovascular Imaging, cardiotoxicity defines as a 10–15% early reduction in global longitudinal strain index [13].

One of the important tools for early detection and monitoring cardiotoxic effects are non-invasive imaging techniques. These techniques also give opportunities for the classification of therapeutic choices to improve patient management. Among these techniques, cardiac nuclear imaging modalities including planar multi-gated acquisition or multi-gated radionuclide angiography (MUGA), single-photon emission computed tomography (SPECT), and PET scans have demonstrated a significant role in the detection, screening during treatment, and monitoring of cancer treatment-related cardiotoxicities [14, 15].

Heretofore, chemotherapeutic agents were extensively assessed for cancer-therapy-related cardiotoxicity [9, 16]. On the other hand, recent developments in the field of nuclear medicine resulting in the introduction of new treatment modalities along with other common approaches require extensive investigations for probable side effects, including cardiotoxicity.

In this state-of-the-art review, the authors briefly present cancer treatment techniques that may induce cardiotoxicity and discuss nuclear cardiac imaging modalities used for detecting cardiotoxicity related to cancer treatment. New treatment modalities in the field of nuclear medicine are also evaluated in terms of potential cardiotoxic effects.

Cancer treatment approaches inducing cardiotoxicity

One of the unexpected adverse events of mediastinal RT is cardiotoxicity. The most important risk factors for radiation-associated heart failure include a delivered dose of more than 30–35 Gray (Gy), hyper-fractionated regimens including multiple dose fractions per day, exposure of an extensive volume of the heart to radiation, younger age, long-term survival, and some other patient characteristics such as obesity, family history of heart problems, diabetes, inactive lifestyle, dyslipidaemias, hypertension, and smoking [17]. Radiation-induced heart disease commonly occurs in patients with Hodgkin lymphoma, lung cancer, and breast cancer involving cardiac structures [18]. For many years, Hodgkin lymphoma patients used a traditional radiation therapy technique, known as the mantle technique, that induced cardiac disease and cardiotoxicity [19]. However, more developments resulted in less cardiac exposure to ionizing radiation, but cardiotoxicity remains a major concern in Hodgkin lymphoma [20]. Moreover, radiation therapy, as an adjuvant or neoadjuvant technique, has been used in more

than 50% of patients with breast cancer. In a meta-analysis carried out in 2005, the researchers found that cardiovascular-related mortality increased significantly (27%) in patients with combined treatment modalities including surgery and radiation therapy versus surgery as the only treatment modality [21]. Advanced modalities of high-precision RT techniques including intensity-modulated radiotherapy (IMRT), volumetric modulated arc therapy (VMAT), helical tomotherapy, prone and isocentric lateral decubitus (ILD) positions, breath-hold techniques, and proton therapy result in dose homogeneity, less cardiac exposure, and delivering lower doses to the heart and reduce adverse effects. The suitable selection of these techniques (alone or in combination) is based on the patient's characteristics, RT regions, and accessibility [22–33]. Although long-term follow-ups are needed to confirm the definitive role of these new techniques, clinical findings have been confirmed the positive effects of new radiation therapy techniques resulting in more precise treatment plans and decreased life-threatening effects including cardiotoxicity [34, 35].

Additionally, cardiac dysfunctions occur in a significant proportion of patients who receive chemotherapy. The pathophysiology of chemotherapeutic drug-induced cardiotoxicity is complex that involves multiple biochemical pathways and results in considerable efforts that have been made for early detection of cardiotoxic events. The most common drug classes that induce cardiotoxicity are anthracyclines (such as doxorubicin), alkaline agents (such as cyclophosphamide, ifosfamide), antimetabolite agents (such as 5-Fluorouracil (5-FU), and vinblastine [36]. Cardiac abnormalities mostly reduce left ventricular ejection fraction (LVEF) in more than 20% of the patients, which may not be detected until the final chemotherapy session [37, 38].

Monoclonal antibodies were developed as a basis for biological therapeutics for many cancers by Kohler and Milstein [39]. The main strategy of these drugs is anti-angiogenic treatment methods involving many factors such as vascular endothelial growth factor (VEGF). Bevacizumab, trastuzumab, ramucirumab, interleukin-2 (IL-2), and interferon-Alpha (INF) are the most common biological treatment agents for cancer patients that may cause cardiovascular toxicity (Tab. 1) [36, 40–43]. Some studies reported significant cardiotoxicity induced by bevacizumab in patients with breast cancer, renal cell carcinoma, and glioma [44–47]. Trastuzumab regimen is another monoclonal antibody that blocks the human epidermal growth factor receptor-2 (HER2 or ErbB2) in breast and gastric cancers including HER-2 positive receptors. In addition to improved disease-free survival, this drug induces acute cardiac disorders such as congestive heart failure and LV dysfunction as well as result in partial impairment in mitochondrial function and increased levels of oxidative stress (Fig. 1) [43, 48, 49].

Systematic studies and evidence-based recommendations are required to determine the early biomarkers of toxicity, risk-assessment models, monitoring, survivorship, prognostication of cardiotoxicity, and suitable treatment options for elderly people with malignancy that receive potentially cardiotoxic regimens.

Specifically, non-invasive and cost-effective diagnostic tools such as imaging have a high priority in detecting early cardiovascular disorders and play an important role in risk stratification and accurate management of elderly patients with cancer.

Table 1. Common anticancer agents with potential cardiotoxicity

Agent	Drug class	Cancer clinical use	Type of cardiotoxicity
Doxorubicin	Anthracyclines (Chemotherapeutic agent)	Breast, sarcoma, lung, bladder, gastric, prostate, leukemia, lymphoma, others	LV dysfunction
Cyclophosphamide	Alkylating (Chemotherapeutic agent)	Sarcoma, SCT, lymphoma, myeloma, breast	Myopericarditis, arrhythmias
Ifosfamide	Alkylating (Chemotherapeutic agent)	Testicular, sarcoma, lymphoma	Arrhythmias, LV dysfunction
5-Fluorouracil (5-FU)	Antimetabolites (Chemotherapeutic agent)	Colon, pancreatic, breast, head and neck	Coronary vasospasm, ischemia, arrhythmias
Vinblastine	Antimicrotubule (Chemotherapeutic agent)	Lymphoma, testicular, lung, melanoma	Ischemia, hypertension
Bevacizumab	Antibody VEGF (Biologic agents)	Colon, rectal, cervical, glioblastoma, ovarian, renal, endometrial, sarcoma	Hypertension, LV dysfunction
Trastuzumab	Antibody HER-2 (Biologic agents)	Breast, gastric, gastro-esophageal	LV dysfunction
Ramucirumab	Antibody VEGFR-2 (Biologic agents)	Colon, rectal, gastric, lung	Hypertension, thromboembolism
Interleukin-2 (IL-2)	Immune agent	Melanoma, renal	Capillary leak syndrome, hypotension, myocardial toxicity
Interferon-Alpha (INF)	Immune agent	Melanoma, renal, lymphoma	Arrhythmias, ischemia

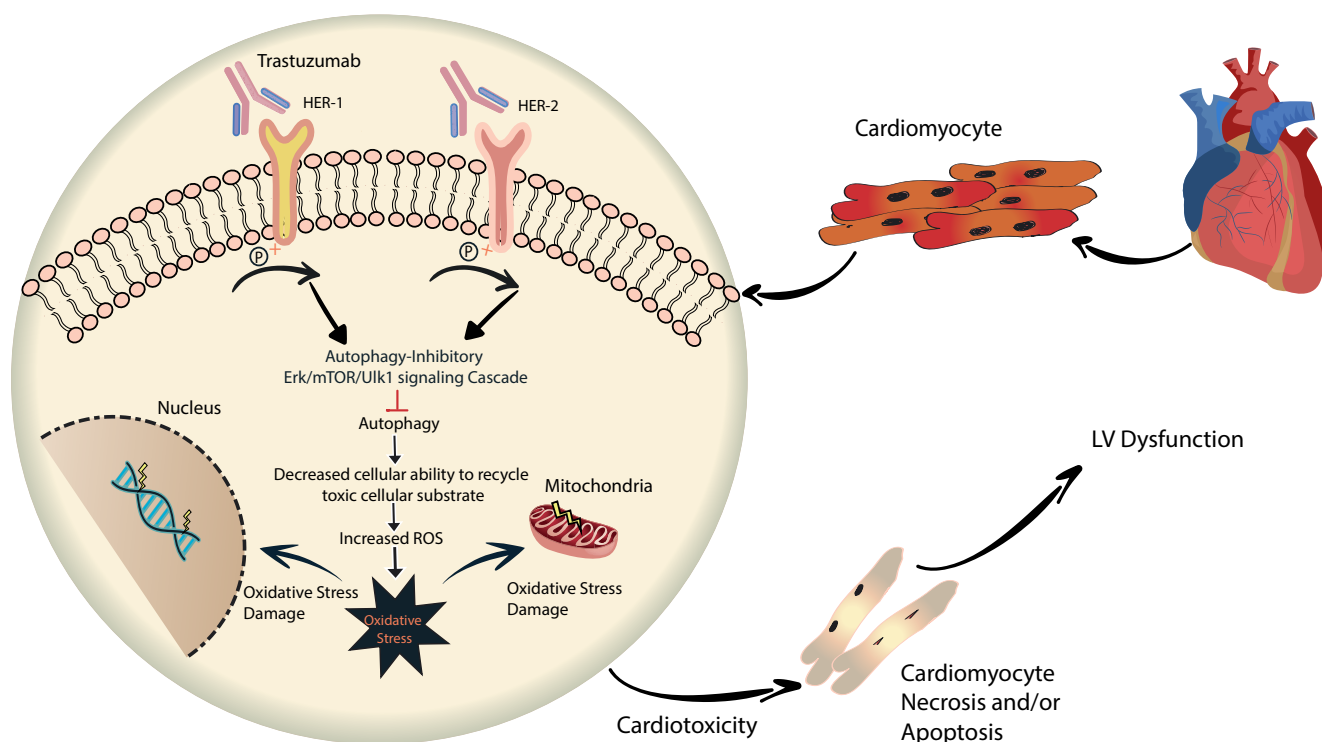


Figure 1. Trastuzumab is directed against the extracellular part of HER2 in HER-2 positive breast cancer patients. This agent causes the phosphorylation of tyrosine 845 (Y845) and 1248 (Y1248) at HER-1 and HER-2, respectively. This process activates the Erk/mTOR/ULK1 signalling cascade that inhibits autophagy in the primary cardiomyocytes. Subsequently, autophagy inhibition increases the intracellular level of reactive oxygen species (ROS) leading to oxidative stress in cardiomyocytes, resulting in apoptosis or necrosis of cardiomyocytes. Additionally, trastuzumab alters ultrastructural formation, and also expression profile of genes and DNA repair. These structural and genetic changes increase myocardial increased myocardial oxidative and nitrate stress and potentially activates apoptotic pathways in cardiomyocytes

Nuclear cardiac imaging in cardio-oncology

Cardio-oncology balances correct patient-centred treatment procedures and cardiovascular disorders. Therefore, it needs a multi-disciplinary team including cardiologists, oncologists, and nuclear medicine specialists for the best efficiency in understanding, treating, and preventing cardiovascular disease [10, 50].

Non-invasive cardiovascular imaging modalities with their versatility have caused a revolution in this field. There are many imaging techniques, but the most common practical procedures are two-dimensional echocardiography and multi-gated acquisition imaging, which evaluate resting left ventricle ejection fraction. Nuclear medicine using different radiotracers has a long history in the identification and management of myocardial cardiotoxicity (Tab. 2) [15].

Table 2. Important radiotracers in cardiac nuclear imaging for cardiotoxicity

Imaging modality	Radiotracer	Advantages	Disadvantages
Planar MUGA Scintigraphy	[^{99m} Tc]erythrocyte	Superior accuracy and highly reproducibility versus 2D echo	Limited structural and functional information beyond LVEF/radiation exposure
SPECT	[¹¹¹ In]antimyosin	Well-validated accuracy/Reproducibility/	Low sensitivity of EF for early diagnosis/ /less information about diastolic function
	[¹²³ I]MIBG	High sensitivity and specificity/No inter- and intra-observer variability	
	[^{99m} Tc]Sestamibi		
	[¹¹¹ In]Tz		
	[^{99m} Tc]annexin V		
	[¹²³ I]BMIP		
PET	[^{99m} Tc]tetrofosmin		
	[¹⁸ F]FDG	Quantification/	Limited availability/
	[¹¹ C]HED	Sensitivity/	High cost
	[¹¹ C]phenylephrine	Reproducibility/	
	[¹⁸ F]FDA	3-dimensional pharmacokinetic analysis	
	[¹⁸ F]MitoPhos	Spatial resolution/	
	[¹⁸ F]12	Myocardial metabolic and perfusion evaluation	
	[¹⁸ F]DHMT		
	[⁶⁸ Ga]Galmydar		
	[¹¹ C]HED		
	[¹¹ C]EPI		
	[¹¹ C]CGP12177		
	[¹¹ C]CGP12388		
[¹¹ C]GB67			

[^{99m}Tc]Multi-Gated Acquisition Scan (MUGAs)

A multi-gated acquisition scan is reproducible and provides the most accurate radionuclide ventriculography to visualize the cardiac blood pool. [^{99m}Tc]erythrocyte camera scintigraphy, also known as equilibrium radionuclide angiocardiology, assesses cardiac blood pool and its function for treatment response and collects prognostic information for patients with cardiac haemorrhage. One of the accepted cost-effective methods for cardiac monitoring of patients undergoing trastuzumab treatment is MUGAs. The results of the MUGA scan indicate cardiotoxicity if the LEVF decreases more than 10% (to a final ejection fraction of less than 50%) [51].

A study by Schwartz et al found the superiority of MUGA for monitoring cardiotoxicity and identifying cognitive heart failure in cancer survivors [52]. Additionally, MUGA is considered a promising choice for detecting the asymptomatic reduction of LVEF.

A serial cross-sectional study compared the use of three conventional cardiac imaging methods for chemotherapy-related cardiotoxicity. The major disadvantages of MUGA were high radiation exposure and the inability to provide information about the right ventricular, valvular, or pericardial disease [13]. The use of the MUGA scan decreased between 2011 and 2014 and two imaging methods including echo and cardiovascular magnetic resonance imaging were used instead. These results may be due to increased knowledge of patients and physicians about radiation risks associated with serial radionuclide ventriculography scans. Moreover, the findings of serial radionuclide ventriculography are similar to the findings of echocardiography and cardiac magnetic resonance imaging [53].

Single-photon emission computed tomography (SPECT)

Three-dimensional gated blood pool SPECT is similar to the previous method, but it has the potential to differentiate cardiac chambers better than planar radionuclide ventriculography. Automatic measurement of the LVEF by [^{99m}Tc]gated blood-pool SPECT (GBPS) provides accurate segmental wall motion analysis and estimates the cavity volume in a single examination [54, 55]. Nevertheless, there is a good agreement in the rough calculation of LVEF between MUGA and GBPS methods [56].

Anthracycline drugs are used to treat many different malignancies such as lymphoma, leukaemia, myeloma, breast carcinoma, lung, ovarian, and gastric. They are also induced cardiotoxicity inducing cardiomyopathy, valvular heart disease, coronary heart disease, and heart failure [57, 58]. Two important mechanisms correlated with anthracycline-cardiotoxicity are mitochondrial dysfunction and elevated oxidative stress [58, 59]. [^{99m}Tc]Sestamibi SPECT imaging is important in vivo molecular scan approach that enables interrogation of mitochondrial dysfunction and detection of doxorubicin-induced cardiotoxicity [60].

Moreover, myocardial abnormalities can be detected through ¹²³I-labeled metaiodobenzylguanidine ([¹²³I]MIBG) scan before causing permanent excessive left ventricular impairment. [¹²³I]MIBG is a norepinephrine analog radiotracer. This radiotracer shows appropriate reproducibility and sensitivity for the evaluation of myocardial adrenergic disorders.

In a study using myocardial perfusion imaging with [¹²³I]MIBG and [¹²³I]BMIPP for patients undergoing anthracycline treatment agents, the results showed early detection of anthracycline-related

cardiotoxicity through [¹²³I]MIBG. Early diagnosis results in a lower incidence and intensity of heart damage in these patients [61–63].

Indium-111 labelled antimyosin antibody as the main marker of myocardial cell necrosis has been introduced for direct visualization of myocyte damage. The myocardial uptake of this radiotracer correlates with the LVEF decrease in patients treated with an anthracycline. Additionally, ¹¹¹In-antimyosin SPECT imaging can identify cardiotoxicity associated with anthracycline chemotherapy regimens in breast cancer patients as well as the doxorubicin regimens in leukaemia, lymphoma, and other solid tumours [64–66].

Several preclinical results using the [^{99m}Tc]Annexin V scan confirmed the significant role of this radiotracer in the detection of myocardial apoptosis. [^{99m}Tc]Annexin V scintigraphy successfully detected apoptotic cells in myocarditis, acute myocardial infarction, the curative effect of anti-apoptosis medications in heart ischemia patients, unstable atherosclerotic plaque, cardiac transplant rejection, and a cardiotoxicity-related anthracycline [67–72]. Additional clinical studies are needed to assess the common use of this radiotracer, especially for early detection of myocardial damage associated with anticancer drugs.

Long-chain fatty acids, as a vital nutrient for the myocardium, are metabolized by β -oxidation. These fatty acids or related analogues can be used in specific imaging probes ([¹²³I]labelled fatty acids) to assess oxidative differentiation in multiple cardiac diseases [73]. Nevertheless, this radiotracer has not been used in SPECT imaging due to its instability in vivo. Therefore, novel tracers such as ¹²³I-15-(p-iodophenyl)-3-methyl pentadecanoic acid (BMIPP) have emerged, which have demonstrated promising results in nuclear cardiology [74, 75].

Some studies examined ¹¹¹In-DTPA-trastuzumab imaging techniques to visualize the human epidermal growth factor receptor 2 (HER2) expressed by myocytes in breast cancer patients. Trastuzumab has been used as a monoclonal antibody to bind to HER2 for curative purposes. This radiotracer has been used to detect patients potentially subject to trastuzumab-related cardiotoxicity. This technique may be helpful, especially in patients with high-risk cardiac failure [76–80]. Regardless of the predictive role of this radiotracer, the data are limited, and this method has not yet been used in conventional clinical practice.

Positron emission tomography (PET)

More common imaging procedures, such as computed tomography (CT) scan, nuclear magnetic resonance (NMR), and magnetic resonance imaging (MRI), define anatomic and physiological functional properties; nonetheless, they cannot determine the autogenetic myocardial biochemistry. Positron emission tomography (PET) assesses both myocardial metabolism and perfusion with a better resolution and higher sensitivity [81, 82]. Moreover, PET myocardial tracers provide an extensive and detailed evaluation of early and reversible cardiotoxic effects of anticancer treatment regimens. The uptake of fluorine-18-fluorodeoxyglucose ([¹⁸F]FDG) increases in cardiomyocytes before the LVEF decrease in patients treated with anthracyclines [83].

Reactive oxygen species (ROS) have been involved in cell signalling, homeostasis. However, a high number of ROS causes pathogenesis of a high number of human diseases and drug toxicities, so the development of imaging tools that able to characterize

ROS biology in vivo has been recently considered and turned into a big challenge [84]. The ¹⁸F-12 microPET imaging of the heart in mice with Doxorubicin-induced cardiac inflammation indicated 2-fold higher oxidation of this tracer compared to the control group. These findings showed that compound 12 is a suitable PET tracer for in vivo imaging of ROS [85]. Another PET tracer that evaluated superoxide production for early detection of doxorubicin-induced cardiotoxicity is ¹⁸F-DHMT. This tracer detected excessive production of reactive oxygen species before a decrease in LVEF that may give a good chance for early cardiotoxicity detection in patients with malignancies [86]. Moreover, [⁶⁸Ga]Galmydar is also evaluated as a potential radiotracer to monitor Doxorubicin-induced cardiomyopathy in different situations. MicroPET/CT scan showed a high-resolution non-invasive assessment of metabolic changes related to Doxorubicin treatment using ⁶⁸Ga-Galmydar at the earliest stages. Single-cell imaging and quantitative biodistribution demonstrated that Galmydar localized precisely in mitochondria of treated cells with Doxorubicin [87].

¹⁸F-MitoPhos as radiolabelled lipophilic cations was used for early detection of imaging cardiotoxicity in acute doxorubicin in the rat model. [¹⁸F]MitoPhos PET imaging demonstrated appropriate pharmacokinetic parameters for cardiac imaging and was introduced as a promising radiopharmaceutical for imaging chemotherapy-induced cardiotoxicity [88].

It has been recently demonstrated that [⁸²Rb]PET imaging could be a potential radiotracer for quantitative assessment of the myocardial blood flow in patients that are at high risk for anthracycline cardiotoxicity [15, 89]. Several studies are investigating nuclear cardiac imaging for the early detection of cardiotoxicity-related cancer therapy modalities. Important radiotracers used for investigating cardiotoxicity in cardiac nuclear imaging are summarized in Table 2.

Can treatment nuclear medicine modalities stimulate cancer therapy-related cardiotoxicity?

Another important modality for the treatment of malignancies is using injectable radiopharmaceuticals, which, similar to other treatment methods, require the assessment of possible side effects including cardiotoxicity.

One of the important approaches in nuclear medicine is theranostics, which combines diagnostic imaging and therapeutic methods through labelling the same molecule or the same agent with distinct radionuclides. More knowledge in genomics led to detecting theranostic biomaterials to diagnosis and treatment of malignancies along with molecular imaging tools. Cancer lesions are heterogeneous and therefore common treatment approaches may not provide favourable results. Nevertheless, these lesions can be detected through theranostics. Therefore, this characteristic can be used to determine which patient will benefit from therapy and which patient may not receive conventional treatments.

Theranostics is currently considered as the recommended modality not only for diagnosis and treatment of malignancies but also for staging, follow-up, monitoring response to treatment, and restaging. An important characteristic of this approach is delivering high doses to tumours while sparing non-targeted tissues.

Different theranostic probes have been developed from clinical experiments of radioactive iodine for evaluation of physiologic

metabolism and thyroid disorders to recent applications in neuroendocrine tumours and prostate cancer. Some pairs of radionuclides that have been used in theranostics include diagnostic gamma or positron emission radionuclides such as ^{123}I ($t_{1/2} = 13.22$ h), ^{124}I ($t_{1/2} = 4.2$ d), ^{68}Ga ($t_{1/2} = 68$ min), $^{99\text{m}}\text{Tc}$ ($t_{1/2} = 6$ h), ^{111}In ($t_{1/2} = 2.81$ d), and therapeutic high-dose radioactive materials such as ^{177}Lu ($t_{1/2} = 6.71$ d) and ^{90}Y ($t_{1/2} = 64.02$ h). Therapeutic radionuclides emit beta and alpha particles, causing damage to double-stranded DNA and death in cancer cells. The most common available pairs of theranostic radiopharmaceuticals include ^{68}Ga PSMA/ ^{177}Lu PSMA for prostate cancer and ^{68}Ga DOTATATE/ ^{177}Lu DOTATATE for neuroendocrine (NETs) (Fig. 2 and 3).

Theranostics is a form of systemic endo-radiotherapy that delivers toxic radiation to target cells but some side effects including severe hematotoxicity and nephrotoxicity have been reported. Many studies evaluated early and late side effects of radioligand therapy, especially peptide receptor radioligand therapy (PRRT), and found that side effects were almost entirely limited, predictable, and/or reversible [90–96]. Nonetheless, a recent case-report study found cardiotoxicity related PRRT in patients with metastatic neuroendocrine tumours.

Different radiotracers have been used in nuclear medicine to visualize and treat neuroendocrine tumours. These tumours develop in many tissues including the lungs, stomach, small intestine, appendix, colorectal tissue, and heart [97–99]. Somatostatin analogues are an inseparable component of diagnostic and treatment policies in metastatic carcinoid tumours. Neuroendocrine tumours have the potential to be targeted with radiopeptides due to peptide receptor expression. Peptide receptor radionuclide therapy using ^{90}Y DOTATAC and ^{177}Lu DOTATATE have successful results in the treatment of inoperative and metastases liver cancers. PRRT can cause renal or haematological adverse effects, but the timely application of appropriate precautionary measures and safe dose administration decrease these toxicities [100, 101].

More than 50% of patients with advanced carcinoid tumours are prone to carcinoid heart disease [102]. At the time of carcinoid cardiac metastases, due to the expression of somatostatin receptors in the cardiac tissue (sst1, sst2, sst4, and sst5), caution should be practised to target neuroendocrine tumour cells with somatostatin-radioisotope compounds. ^{177}Lu DOTATATE is confirmed as an effective option in inoperative metastases of neuroendocrine tumours with symptomatic cardiovascular impairment [103].

In a case report study, a 51-year-old-man was diagnosed with neuroendocrine tumour lesions and received somatostatin analogue therapy. After a while, a ^{68}Ga DOTATATE scan was used to evaluate the patient. Imaging demonstrated that metastatic lesions spread in the axial skeleton, liver, and spleen as well as the right and even the left myocardium. The ejection fraction was normal (62%) in the beginning. After receiving two cycles of ^{177}Lu labeled PRRT, an echocardiogram showed a serious decrease in the left ventricular systolic function and left ventricular ejection fraction (34%). Therefore, PRRT stopped but it started again because the cardiac function continued to decline. In this case, the cardiac function was normal before treatment, but the patient developed cardiotoxicity after treatment due to the delivery of the radioactive isotope to metastatic lesions. This cardiotoxic effect should be considered as a precaution in a patient with neuroendocrine tumour and cardiac metastases receiving PRRT [104].

Moreover, recent advances in nuclear medicine imaging and therapy have shown that fibroblast activation protein (FAP) and chemokine receptor (CXCR) are promising targets for nuclear-labelled tumour probes. Different reports have indicated an effective role of ^{68}Ga pentixafor chemokine-directed imaging in some solid tumours such as glioblastoma, ovarian cancer, renal cell cancer, small cell lung cancer, and adrenocortical carcinoma. However, a study by Vag et al. questioned its possibility in other tumours including pancreatic cancer, sarcoma, and breast cancer [105–109].

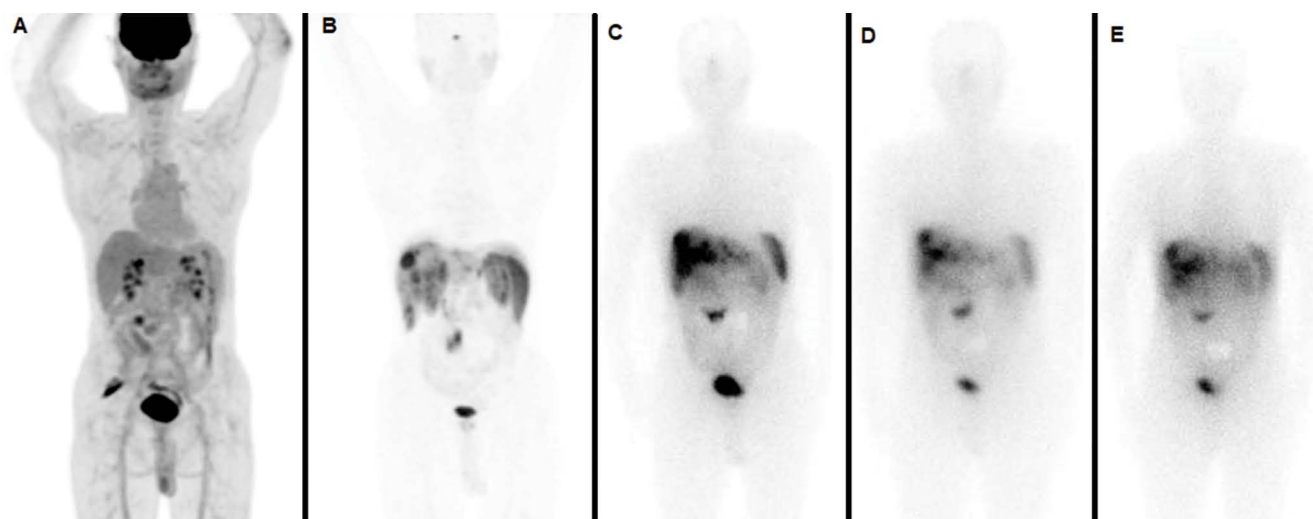


Figure 2. A 68-year-old man with metastatic neuroendocrine tumours refractory to chemotherapy presented for PRRT. Pre-treatment FDG PET (A) showed no abnormal radiotracer uptake, while all lesions in the liver and mid-abdomen revealed significant SSTR expression on pre-treatment ^{68}Ga -DOTATATE PET/CT (B). The patients underwent 3 cycles of PRRT (22.2 GBq). The post-treatment scintigraphy after the 1st cycle (C) indicated intensive uptake of radiotracer in the above regions, which decreased significantly in number and size in post-treatment scintigraphy after the 3rd cycle (D, E)

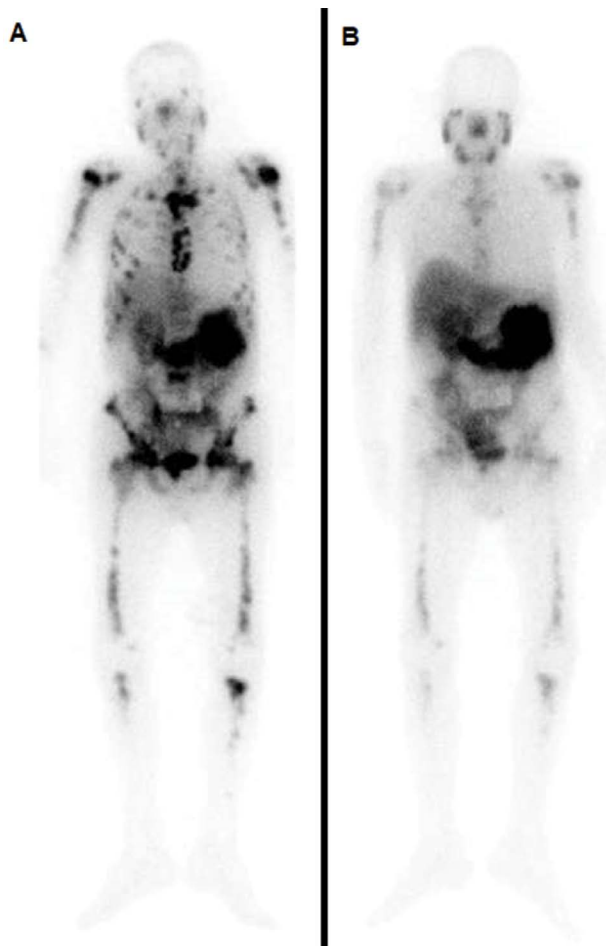


Figure 3. A 58-year-old man with metastatic castration-resistant prostate cancer refractory to different regimes of hormone therapy and chemotherapy presented for lutetium-177-labelled prostate-specific membrane antigen radioligand therapy. The patients underwent 3 cycles of [^{177}Lu]PSMA therapy (22.2 GBq). Post-treatment scintigraphy after the 1st cycle (A) indicated widespread uptake of radiotracer throughout the entire body which decreased significantly in number and size in post-treatment scintigraphy after the 3rd cycle (B)

^{177}Lu -pentixather has demonstrated outstanding CXCR4-targeting properties and a favourable pharmacokinetic profile. Additionally, [^{68}Ga]pentixafor/ ^{177}Lu -pentixather based CXCR4-targeted theranostic approach delivers high doses to the tumour sparing healthy non-targeted cells [110]. Several malignant cells including head and neck, breast, lung, pancreatic, and oesophageal, colorectal cancer have a high uptake of [^{68}Ga]FAPI that can be used for non-invasive molecular imaging, locating the primary site of unknown malignancies, and staging of tumours. On the other hand, [^{68}Ga]FAPI tracers contain universal DOTA chelators. This property makes it possible to label the ligand with a suitable therapeutic radionuclide for a theranostic approach [106, 111].

However, although no life-threatening side effects have been reported for these radioligands, concise studies should be performed to evaluate probable side effects and cardiotoxicity.

Conclusion

Cardio-oncology as a multi-modality approach has become a valuable strategy for improving treatment outcome and patient management through screening cardiotoxicity during cancer treatment. Several studies investigated cancer treatment cardiotoxicity in chemotherapy and external radiation therapy. In addition to the significant role of nuclear cardiac imaging procedures for early detection of cardiovascular changes, it is required to perform more comprehensive studies to investigate cancer treatment options such as PRRT, fibroblast activation protein, and chemokine receptor targeting probes for possible cardiac side effects that play important roles in the treatment of malignancies. Finally, it is required to establish a network of collaboration between oncologists, nuclear medicine specialists, and cardiologists to obtain optimal patient outcomes and decrease life-threatening cardiotoxicity.

Ethics approval and consent to participate

Not applicable.

Availability of data and materials

Not applicable.

Conflict of interests

The authors declare that they have no competing interests.

Acknowledgements

Not applicable.

References

1. Fuster V, Voûte J. MDGs: chronic diseases are not on the agenda. *The Lancet*. 2005; 366(9496): 1512–1514, doi: [10.1016/s0140-6736\(05\)67610-6](https://doi.org/10.1016/s0140-6736(05)67610-6).
2. Hofmann L, Forschner A, Loquai C, et al. Cutaneous, gastrointestinal, hepatic, endocrine, and renal side-effects of anti-PD-1 therapy. *Eur J Cancer*. 2016; 60: 190–209, doi: [10.1016/j.ejca.2016.02.025](https://doi.org/10.1016/j.ejca.2016.02.025), indexed in Pubmed: 27085692.
3. Sivapackiam J, Sharma M, Schindler TH, et al. PET radiopharmaceuticals for imaging chemotherapy-induced cardiotoxicity. *Curr Cardiol Rep*. 2020; 22(8): 62, doi: [10.1007/s11886-020-01315-z](https://doi.org/10.1007/s11886-020-01315-z), indexed in Pubmed: 32562004.
4. Herrmann J, Lerman A, Sandhu NP, et al. Evaluation and management of patients with heart disease and cancer: cardio-oncology. *Mayo Clin Proc*. 2014; 89(9): 1287–1306, doi: [10.1016/j.mayocp.2014.05.013](https://doi.org/10.1016/j.mayocp.2014.05.013), indexed in Pubmed: 25192616.
5. Lee CK, Aeppli D, Nierengarten ME. The need for long-term surveillance for patients treated with curative radiotherapy for Hodgkin's disease: University of Minnesota experience. *Int J Radiat Oncol Biol Phys*. 2000; 48(1): 169–179, doi: [10.1016/s0360-3016\(00\)00647-7](https://doi.org/10.1016/s0360-3016(00)00647-7), indexed in Pubmed: 10924987.
6. Jaworski C, Mariani JA, Wheeler G, et al. Cardiac complications of thoracic irradiation. *J Am Coll Cardiol*. 2013; 61(23): 2319–2328, doi: [10.1016/j.jacc.2013.01.090](https://doi.org/10.1016/j.jacc.2013.01.090), indexed in Pubmed: 23583253.
7. Aapro M, Bernard-Marty C, Brain EGC, et al. Anthracycline cardiotoxicity in the elderly cancer patient: a SIOG expert position paper. *Ann Oncol*.

- 2011; 22(2): 257–267, doi: [10.1093/annonc/mdq609](https://doi.org/10.1093/annonc/mdq609), indexed in Pubmed: [20956616](https://pubmed.ncbi.nlm.nih.gov/20956616/).
8. Serrano C, Cortés J, De Mattos-Arruda L, et al. Trastuzumab-related cardiotoxicity in the elderly: a role for cardiovascular risk factors. *Ann Oncol.* 2012; 23(4): 897–902, doi: [10.1093/annonc/mdr348](https://doi.org/10.1093/annonc/mdr348), indexed in Pubmed: [21828361](https://pubmed.ncbi.nlm.nih.gov/21828361/).
 9. Jain D, Russell RR, Schwartz RG, et al. Cardiac complications of cancer therapy: pathophysiology, identification, prevention, treatment, and future directions. *Curr Cardiol Rep.* 2017; 19(5): 36, doi: [10.1007/s11886-017-0846-x](https://doi.org/10.1007/s11886-017-0846-x), indexed in Pubmed: [28374177](https://pubmed.ncbi.nlm.nih.gov/28374177/).
 10. Russell RR, Alexander J, Jain D, et al. The role and clinical effectiveness of multimodality imaging in the management of cardiac complications of cancer and cancer therapy. *J Nucl Cardiol.* 2016; 23(4): 856–884, doi: [10.1007/s12350-016-0538-8](https://doi.org/10.1007/s12350-016-0538-8), indexed in Pubmed: [27251147](https://pubmed.ncbi.nlm.nih.gov/27251147/).
 11. Sardaro A, Petruzzelli MF, D'Errico MP, et al. Radiation-induced cardiac damage in early left breast cancer patients: risk factors, biological mechanisms, radiobiology, and dosimetric constraints. *Radiother Oncol.* 2012; 103(2): 133–142, doi: [10.1016/j.radonc.2012.02.008](https://doi.org/10.1016/j.radonc.2012.02.008), indexed in Pubmed: [22391054](https://pubmed.ncbi.nlm.nih.gov/22391054/).
 12. Hurtado-de-Mendoza D, Loaiza-Bonilla A, Bonilla-Reyes PA, et al. Cardio-oncology: cancer therapy-related cardiovascular complications in a molecular targeted era: new concepts and perspectives. *Cureus.* 2017; 9(5): e1258, doi: [10.7759/cureus.1258](https://doi.org/10.7759/cureus.1258), indexed in Pubmed: [28649481](https://pubmed.ncbi.nlm.nih.gov/28649481/).
 13. Plana JC, Galderisi M, Barac A, et al. Expert consensus for multimodality imaging evaluation of adult patients during and after cancer therapy: a report from the American Society of Echocardiography and the European Association of Cardiovascular Imaging. *J Am Soc Echocardiogr.* 2014; 27(9): 911–939, doi: [10.1016/j.echo.2014.07.012](https://doi.org/10.1016/j.echo.2014.07.012), indexed in Pubmed: [25172399](https://pubmed.ncbi.nlm.nih.gov/25172399/).
 14. Abdel-Qadir H, Austin PC, Lee DS, et al. A population-based study of cardiovascular mortality following early-stage breast cancer. *JAMA Cardiol.* 2017; 2(1): 88–93, doi: [10.1001/jamacardio.2016.3841](https://doi.org/10.1001/jamacardio.2016.3841), indexed in Pubmed: [27732702](https://pubmed.ncbi.nlm.nih.gov/27732702/).
 15. Makavos G, Ikonomidis I, Palios J, et al. Cardiac imaging in cardiotoxicity: a focus on clinical practice. *Heart Fail Rev.* 2020 [Epub ahead of print], doi: [10.1007/s10741-020-09952-w](https://doi.org/10.1007/s10741-020-09952-w), indexed in Pubmed: [32306221](https://pubmed.ncbi.nlm.nih.gov/32306221/).
 16. Pondé NF, Lambertini M, de Azambuja E. Twenty years of anti-HER2 therapy-associated cardiotoxicity. *ESMO Open.* 2016; 1(4): e000073, doi: [10.1136/esmoopen-2016-000073](https://doi.org/10.1136/esmoopen-2016-000073), indexed in Pubmed: [27843627](https://pubmed.ncbi.nlm.nih.gov/27843627/).
 17. Bovelli D, Plataniotis G, Roila F, et al. ESMO Guidelines Working Group. Cardiotoxicity of chemotherapeutic agents and radiotherapy-related heart disease: ESMO Clinical Practice Guidelines. *Ann Oncol.* 2010; 21(Suppl 5): v277–v282, doi: [10.1093/annonc/mdq200](https://doi.org/10.1093/annonc/mdq200), indexed in Pubmed: [20555097](https://pubmed.ncbi.nlm.nih.gov/20555097/).
 18. Donnellan E, Phelan D, McCarthy CP, et al. Radiation-induced heart disease: A practical guide to diagnosis and management. *Cleve Clin J Med.* 2016; 83(12): 914–922, doi: [10.3949/ccjm.83a.15104](https://doi.org/10.3949/ccjm.83a.15104), indexed in Pubmed: [27938516](https://pubmed.ncbi.nlm.nih.gov/27938516/).
 19. Aleman BMP, van den Belt-Dusebout AW, Klokmann WJ, et al. Long-term cause-specific mortality of patients treated for Hodgkin's disease. *J Clin Oncol.* 2003; 21(18): 3431–3439, doi: [10.1200/JCO.2003.07.131](https://doi.org/10.1200/JCO.2003.07.131), indexed in Pubmed: [12885835](https://pubmed.ncbi.nlm.nih.gov/12885835/).
 20. Cutter DJ, Darby SC, Yusuf SW. Risks of heart disease after radiotherapy. *Tex Heart Inst J.* 2011; 38(3): 257–258, indexed in Pubmed: [21720464](https://pubmed.ncbi.nlm.nih.gov/21720464/).
 21. Early Breast Cancer Trialists' Collaborative Group (EBCTCG). Effects of radiotherapy and of differences in the extent of surgery for early breast cancer on local recurrence and 15-year survival: an overview of the randomised trials. *The Lancet.* 2005; 366(9503): 2087–2106, doi: [10.1016/s0140-6736\(05\)67887-7](https://doi.org/10.1016/s0140-6736(05)67887-7).
 22. Popescu CC, Olivetto IA, Beckham WA, et al. Volumetric modulated arc therapy improves dosimetry and reduces treatment time compared to conventional intensity-modulated radiotherapy for locoregional radiotherapy of left-sided breast cancer and internal mammary nodes. *Int J Radiat Oncol Biol Phys.* 2010; 76(1): 287–295, doi: [10.1016/j.ijrobp.2009.05.038](https://doi.org/10.1016/j.ijrobp.2009.05.038), indexed in Pubmed: [19775832](https://pubmed.ncbi.nlm.nih.gov/19775832/).
 23. Osman SOS, Hol S, Poortmans PM, et al. Volumetric modulated arc therapy and breath-hold in image-guided locoregional left-sided breast irradiation. *Radiother Oncol.* 2014; 112(1): 17–22, doi: [10.1016/j.radonc.2014.04.004](https://doi.org/10.1016/j.radonc.2014.04.004), indexed in Pubmed: [24825176](https://pubmed.ncbi.nlm.nih.gov/24825176/).
 24. Sakumi A, Shiraishi K, Onoe T, et al. Single-arc volumetric modulated arc therapy planning for left breast cancer and regional nodes. *J Radiat Res.* 2012; 53(1): 151–153, doi: [10.1269/jrr.11159](https://doi.org/10.1269/jrr.11159), indexed in Pubmed: [22240941](https://pubmed.ncbi.nlm.nih.gov/22240941/).
 25. Lauche O, Kirova YM. Helical tomotherapy in breast cancer treatment. *Breast Cancer Management.* 2014; 3(5): 441–449, doi: [10.2217/bmt.14.34](https://doi.org/10.2217/bmt.14.34).
 26. Lohr F, El-Haddad M, Dobler B, et al. Potential effect of robust and simple IMRT approach for left-sided breast cancer on cardiac mortality. *Int J Radiat Oncol Biol Phys.* 2009; 74(1): 73–80, doi: [10.1016/j.ijrobp.2008.07.018](https://doi.org/10.1016/j.ijrobp.2008.07.018), indexed in Pubmed: [18973977](https://pubmed.ncbi.nlm.nih.gov/18973977/).
 27. Tan W, Wang X, Qiu D, et al. Dosimetric comparison of intensity-modulated radiotherapy plans, with or without anterior myocardial territory and left ventricle as organs at risk, in early-stage left-sided breast cancer patients. *Int J Radiat Oncol Biol Phys.* 2011; 81(5): 1544–1551, doi: [10.1016/j.ijrobp.2010.09.028](https://doi.org/10.1016/j.ijrobp.2010.09.028), indexed in Pubmed: [21470785](https://pubmed.ncbi.nlm.nih.gov/21470785/).
 28. Cao J, Roeske JC, Chmura SJ, et al. Calculation and prediction of the effect of respiratory motion on whole breast radiation therapy dose distributions. *Med Dosim.* 2009; 34(2): 126–132, doi: [10.1016/j.meddos.2008.07.002](https://doi.org/10.1016/j.meddos.2008.07.002), indexed in Pubmed: [19410141](https://pubmed.ncbi.nlm.nih.gov/19410141/).
 29. Borst GR, Sonke JJ, den Hollander S, et al. Clinical results of image-guided deep inspiration breath hold breast irradiation. *Int J Radiat Oncol Biol Phys.* 2010; 78(5): 1345–1351, doi: [10.1016/j.ijrobp.2009.10.006](https://doi.org/10.1016/j.ijrobp.2009.10.006), indexed in Pubmed: [20207496](https://pubmed.ncbi.nlm.nih.gov/20207496/).
 30. Lymberis SC, deWynngaert JK, Parhar P, et al. Prospective assessment of optimal individual position (prone versus supine) for breast radiotherapy: volumetric and dosimetric correlations in 100 patients. *Int J Radiat Oncol Biol Phys.* 2012; 84(4): 902–909, doi: [10.1016/j.ijrobp.2012.01.040](https://doi.org/10.1016/j.ijrobp.2012.01.040), indexed in Pubmed: [22494590](https://pubmed.ncbi.nlm.nih.gov/22494590/).
 31. Bradley JA, Dagan R, Ho MW, et al. Initial report of a prospective dosimetric and clinical feasibility trial demonstrates the potential of protons to increase the therapeutic ratio in breast cancer compared with photons. *Int J Radiat Oncol Biol Phys.* 2016; 95(1): 411–421, doi: [10.1016/j.ijrobp.2015.09.018](https://doi.org/10.1016/j.ijrobp.2015.09.018), indexed in Pubmed: [26611875](https://pubmed.ncbi.nlm.nih.gov/26611875/).
 32. Coon AB, Dickler A, Kirk MC, et al. Tomotherapy and multifield intensity-modulated radiotherapy planning reduce cardiac doses in left-sided breast cancer patients with unfavorable cardiac anatomy. *Int J Radiat Oncol Biol Phys.* 2010; 78(1): 104–110, doi: [10.1016/j.ijrobp.2009.07.1705](https://doi.org/10.1016/j.ijrobp.2009.07.1705), indexed in Pubmed: [20004529](https://pubmed.ncbi.nlm.nih.gov/20004529/).
 33. Kirova YM, Gambotti L, De Rycke Y, et al. Risk of second malignancies after adjuvant radiotherapy for breast cancer: a large-scale, single-institution review. *Int J Radiat Oncol Biol Phys.* 2007; 68(2): 359–363, doi: [10.1016/j.ijrobp.2006.12.011](https://doi.org/10.1016/j.ijrobp.2006.12.011), indexed in Pubmed: [17379448](https://pubmed.ncbi.nlm.nih.gov/17379448/).
 34. Lally BE, Detterbeck FC, Geiger AM, et al. The risk of death from heart disease in patients with nonsmall cell lung cancer who receive postoperative radiotherapy: analysis of the surveillance, epidemiology, and end results database. *Cancer.* 2007; 110(4): 911–917, doi: [10.1002/cncr.22845](https://doi.org/10.1002/cncr.22845), indexed in Pubmed: [17620279](https://pubmed.ncbi.nlm.nih.gov/17620279/).
 35. Wang K, Pearlstein KA, Patchett ND, et al. Heart dosimetric analysis of three types of cardiac toxicity in patients treated on dose-escalation trials for Stage III non-small-cell lung cancer. *Radiother Oncol.* 2017; 125(2): 293–300, doi: [10.1016/j.radonc.2017.10.001](https://doi.org/10.1016/j.radonc.2017.10.001), indexed in Pubmed: [29050957](https://pubmed.ncbi.nlm.nih.gov/29050957/).
 36. Kimmick GG, Lenihan DJ, Sawyer DB, Mayer EL, Hershman DL. Cardio-oncology: the clinical overlap of cancer and heart disease. Springer, Cham 2017.
 37. Luminari S, Montanini A, Caballero D, et al. Nonpegylated liposomal doxorubicin (Myocet™) combination (R-COMP) chemotherapy in elderly patients with diffuse large B-cell lymphoma (DLBCL): results from the phase II EURO18 trial. *Ann Oncol.* 2010; 21(7): 1492–1499, doi: [10.1093/annonc/mdp544](https://doi.org/10.1093/annonc/mdp544), indexed in Pubmed: [20007997](https://pubmed.ncbi.nlm.nih.gov/20007997/).

38. Cardinale D, Sandri MT, Martinoni A, et al. Left ventricular dysfunction predicted by early troponin I release after high-dose chemotherapy. *J Am Coll Cardiol*. 2000; 36(2): 517–522, doi: [10.1016/s0735-1097\(00\)00748-8](https://doi.org/10.1016/s0735-1097(00)00748-8), indexed in Pubmed: [10933366](https://pubmed.ncbi.nlm.nih.gov/10933366/).
39. Drews J. Drug discovery: a historical perspective. *Science*. 2000; 287(5460): 1960–1964, doi: [10.1126/science.287.5460.1960](https://doi.org/10.1126/science.287.5460.1960), indexed in Pubmed: [10720314](https://pubmed.ncbi.nlm.nih.gov/10720314/).
40. Ferrara N. Vascular endothelial growth factor: basic science and clinical progress. *Endocr Rev*. 2004; 25(4): 581–611, doi: [10.1210/er.2003-0027](https://doi.org/10.1210/er.2003-0027), indexed in Pubmed: [15294883](https://pubmed.ncbi.nlm.nih.gov/15294883/).
41. Ferrara N. VEGF and the quest for tumour angiogenesis factors. *Nat Rev Cancer*. 2002; 2(10): 795–803, doi: [10.1038/nrc909](https://doi.org/10.1038/nrc909), indexed in Pubmed: [12360282](https://pubmed.ncbi.nlm.nih.gov/12360282/).
42. Shabalala S, Muller CJF, Louw J, et al. Polyphenols, autophagy and doxorubicin-induced cardiotoxicity. *Life Sci*. 2017; 180: 160–170, doi: [10.1016/j.lfs.2017.05.003](https://doi.org/10.1016/j.lfs.2017.05.003), indexed in Pubmed: [28478263](https://pubmed.ncbi.nlm.nih.gov/28478263/).
43. Novo G, Cadeddu C, Sucato V, et al. Role of biomarkers in monitoring antineoplastic cardiotoxicity. *J Cardiovasc Med (Hagerstown)*. 2016; 17(Suppl 1): S27–S34, doi: [10.2459/JCM.0000000000000379](https://doi.org/10.2459/JCM.0000000000000379), indexed in Pubmed: [27183522](https://pubmed.ncbi.nlm.nih.gov/27183522/).
44. Hall PS, Harshman LC, Srinivas S, et al. The frequency and severity of cardiovascular toxicity from targeted therapy in advanced renal cell carcinoma patients. *JACC Heart Fail*. 2013; 1(1): 72–78, doi: [10.1016/j.jchf.2012.09.001](https://doi.org/10.1016/j.jchf.2012.09.001), indexed in Pubmed: [24621801](https://pubmed.ncbi.nlm.nih.gov/24621801/).
45. Qi WX, Fu S, Zhang Q, et al. Bevacizumab increases the risk of severe congestive heart failure in cancer patients: an up-to-date meta-analysis with a focus on different subgroups. *Clin Drug Investig*. 2014; 34(10): 681–690, doi: [10.1007/s40261-014-0222-1](https://doi.org/10.1007/s40261-014-0222-1), indexed in Pubmed: [25096848](https://pubmed.ncbi.nlm.nih.gov/25096848/).
46. Groarke JD, Choueiri TK, Slosky D, et al. Recognizing and managing left ventricular dysfunction associated with therapeutic inhibition of the vascular endothelial growth factor signaling pathway. *Curr Treat Options Cardiovasc Med*. 2014; 16(9): 335, doi: [10.1007/s11936-014-0335-0](https://doi.org/10.1007/s11936-014-0335-0), indexed in Pubmed: [25099086](https://pubmed.ncbi.nlm.nih.gov/25099086/).
47. Choueiri TK, Mayer EL, Je Y, et al. Congestive heart failure risk in patients with breast cancer treated with bevacizumab. *J Clin Oncol*. 2011; 29(6): 632–638, doi: [10.1200/JCO.2010.31.9129](https://doi.org/10.1200/JCO.2010.31.9129), indexed in Pubmed: [21205755](https://pubmed.ncbi.nlm.nih.gov/21205755/).
48. Moja L, Tagliabue L, Balduzzi S, et al. Trastuzumab containing regimens for early breast cancer. *Cochrane Database Syst Rev*. 2012(4): CD006243, doi: [10.1002/14651858.CD006243.pub2](https://doi.org/10.1002/14651858.CD006243.pub2), indexed in Pubmed: [22513938](https://pubmed.ncbi.nlm.nih.gov/22513938/).
49. Blackwell KL, Pegram MD, Tan-Chiu E, et al. Single-agent lapatinib for HER2-overexpressing advanced or metastatic breast cancer that progressed on first- or second-line trastuzumab-containing regimens. *Ann Oncol*. 2009; 20(6): 1026–1031, doi: [10.1093/annonc/mdn759](https://doi.org/10.1093/annonc/mdn759), indexed in Pubmed: [19179558](https://pubmed.ncbi.nlm.nih.gov/19179558/).
50. Patnaik JL, Byers T, DiGuseppi C, et al. Cardiovascular disease competes with breast cancer as the leading cause of death for older females diagnosed with breast cancer: a retrospective cohort study. *Breast Cancer Res*. 2011; 13(3): R64, doi: [10.1186/bcr2901](https://doi.org/10.1186/bcr2901), indexed in Pubmed: [21689398](https://pubmed.ncbi.nlm.nih.gov/21689398/).
51. Bellenger NG, Burgess MI, Ray SG, et al. Comparison of left ventricular ejection fraction and volumes in heart failure by echocardiography, radionuclide ventriculography and cardiovascular magnetic resonance; are they interchangeable? *Eur Heart J*. 2000; 21(16): 1387–1396, doi: [10.1053/euhj.2000.2011](https://doi.org/10.1053/euhj.2000.2011), indexed in Pubmed: [10952828](https://pubmed.ncbi.nlm.nih.gov/10952828/).
52. Schwartz RG, Jain D, Storozynsky E. Traditional and novel methods to assess and prevent chemotherapy-related cardiac dysfunction noninvasively. *J Nucl Cardiol*. 2013; 20(3): 443–464, doi: [10.1007/s12350-013-9707-1](https://doi.org/10.1007/s12350-013-9707-1), indexed in Pubmed: [23572315](https://pubmed.ncbi.nlm.nih.gov/23572315/).
53. Kolla BC, Roy SS, Duval S, et al. Cardiac imaging methods for chemotherapy-related cardiotoxicity screening and related radiation exposure: current practice and trends. *Anticancer Res*. 2017; 37(5): 2445–2449, doi: [10.21873/anticancer.11584](https://doi.org/10.21873/anticancer.11584), indexed in Pubmed: [28476812](https://pubmed.ncbi.nlm.nih.gov/28476812/).
54. Wexler O, Yoder SR, Elder JL, et al. Effect of gender on cardiovascular risk stratification with ECG gated SPECT left ventricular volume indices and ejection fraction. *J Nucl Cardiol*. 2009; 16(1): 28–37, doi: [10.1007/s12350-008-9000-x](https://doi.org/10.1007/s12350-008-9000-x), indexed in Pubmed: [19152126](https://pubmed.ncbi.nlm.nih.gov/19152126/).
55. Liu YH, Fazzone-Chettiar R, Sandoval V, et al. New approach for quantification of left ventricular function from low-dose gated bloodpool SPECT: Validation and comparison with conventional methods in patients. *J Nucl Cardiol*. 2019 [Epub ahead of print], doi: [10.1007/s12350-019-01823-8](https://doi.org/10.1007/s12350-019-01823-8), indexed in Pubmed: [31338796](https://pubmed.ncbi.nlm.nih.gov/31338796/).
56. Groch MW, DePuey EG, Belzberg AC, et al. Planar imaging versus gated blood-pool SPECT for the assessment of ventricular performance: a multicenter study. *J Nucl Med*. 2001; 42(12): 1773–1779, indexed in Pubmed: [11752072](https://pubmed.ncbi.nlm.nih.gov/11752072/).
57. Lipshultz SE, Karnik R, Sambatakos P, et al. Anthracycline-related cardiotoxicity in childhood cancer survivors. *Curr Opin Cardiol*. 2014; 29(1): 103–112, doi: [10.1097/HCO.0000000000000034](https://doi.org/10.1097/HCO.0000000000000034), indexed in Pubmed: [24284979](https://pubmed.ncbi.nlm.nih.gov/24284979/).
58. Cutter DJ, Schaapveld M, Darby SC, et al. Risk of valvular heart disease after treatment for Hodgkin lymphoma. *J Natl Cancer Inst*. 2015; 107(4): djv008, doi: [10.1093/jnci/djv008](https://doi.org/10.1093/jnci/djv008), indexed in Pubmed: [25713164](https://pubmed.ncbi.nlm.nih.gov/25713164/).
59. Ichikawa Y, Ghanefar M, Bayeva M, et al. Cardiotoxicity of doxorubicin is mediated through mitochondrial iron accumulation. *J Clin Invest*. 2014; 124(2): 617–630, doi: [10.1172/JCI72931](https://doi.org/10.1172/JCI72931), indexed in Pubmed: [24382354](https://pubmed.ncbi.nlm.nih.gov/24382354/).
60. Safee ZM, Baark F, Waters ECT, et al. Detection of anthracycline-induced cardiotoxicity using perfusion-corrected Tc sestamibi SPECT. *Sci Rep*. 2019; 9(1): 216, doi: [10.1038/s41598-018-36721-5](https://doi.org/10.1038/s41598-018-36721-5), indexed in Pubmed: [30659226](https://pubmed.ncbi.nlm.nih.gov/30659226/).
61. Carrió I, Estorch M, Berná L, et al. Indium-111-antimyosin and iodine-123-MIBG studies in early assessment of doxorubicin cardiotoxicity. *J Nucl Med*. 1995; 36(11): 2044–2049, indexed in Pubmed: [7472595](https://pubmed.ncbi.nlm.nih.gov/7472595/).
62. Russell RR, Zaret BL. Nuclear cardiology: present and future. *Curr Probl Cardiol*. 2006; 31(9): 557–629, doi: [10.1016/j.cpcardiol.2006.05.002](https://doi.org/10.1016/j.cpcardiol.2006.05.002), indexed in Pubmed: [16935694](https://pubmed.ncbi.nlm.nih.gov/16935694/).
63. Rosa GM, Gigli L, Tagliasacchi MI, et al. Update on cardiotoxicity of anti-cancer treatments. *Eur J Clin Invest*. 2016; 46(3): 264–284, doi: [10.1111/eci.12589](https://doi.org/10.1111/eci.12589), indexed in Pubmed: [26728634](https://pubmed.ncbi.nlm.nih.gov/26728634/).
64. Wenningmann N, Knapp M, Ande A, et al. Insights into Doxorubicin-induced Cardiotoxicity: Molecular Mechanisms, Preventive Strategies, and Early Monitoring. *Mol Pharmacol*. 2019; 96(2): 219–232, doi: [10.1124/mol.119.115725](https://doi.org/10.1124/mol.119.115725), indexed in Pubmed: [31164387](https://pubmed.ncbi.nlm.nih.gov/31164387/).
65. Jones RL, Swanton C, Ewer MS. Anthracycline cardiotoxicity. *Expert Opin Drug Saf*. 2006; 5(6): 791–809, doi: [10.1517/14740338.5.6.791](https://doi.org/10.1517/14740338.5.6.791), indexed in Pubmed: [17044806](https://pubmed.ncbi.nlm.nih.gov/17044806/).
66. Pepe A, Pizzino F, Gargiulo P, et al. Cardiovascular imaging in the diagnosis and monitoring of cardiotoxicity: cardiovascular magnetic resonance and nuclear cardiology. *J Cardiovasc Med (Hagerstown)*. 2016; 17(Suppl 1): S45–S54, doi: [10.2459/JCM.0000000000000380](https://doi.org/10.2459/JCM.0000000000000380), indexed in Pubmed: [27183525](https://pubmed.ncbi.nlm.nih.gov/27183525/).
67. Blankenberg FG. In vivo detection of apoptosis. *J Nucl Med*. 2008; 49(Suppl 2): 81S–95S, doi: [10.2967/jnumed.107.045898](https://doi.org/10.2967/jnumed.107.045898), indexed in Pubmed: [18523067](https://pubmed.ncbi.nlm.nih.gov/18523067/).
68. Wang X, Liu Y, Wang X, et al. The role of (99m)Tc-annexin V apoptosis scintigraphy in visualizing early stage glucocorticoid-induced femoral head osteonecrosis in the rabbit. *Biomed Res Int*. 2016; 7067259, doi: [10.1155/2016/7067259](https://doi.org/10.1155/2016/7067259), indexed in Pubmed: [26989689](https://pubmed.ncbi.nlm.nih.gov/26989689/).
69. Boersma HH, Kietselaer BL, Stolk LML, et al. Past, present, and future of annexin A5: from protein discovery to clinical applications. *J Nucl Med*. 2005; 46(12): 2035–2050, indexed in Pubmed: [16330568](https://pubmed.ncbi.nlm.nih.gov/16330568/).
70. Kietselaer BL, Reutelingsperger CPM, Boersma HH, et al. Noninvasive detection of programmed cell loss with 99mTc-labeled annexin A5 in heart failure. *J Nucl Med*. 2007; 48(4): 562–567, doi: [10.2967/jnumed.106.039453](https://doi.org/10.2967/jnumed.106.039453), indexed in Pubmed: [17401092](https://pubmed.ncbi.nlm.nih.gov/17401092/).
71. Taki J, Higuchi T, Kawashima A, et al. Effect of postconditioning on myocardial 99mTc-annexin-V uptake: comparison with ischemic preconditioning and caspase inhibitor treatment. *J Nucl Med*. 2007; 48(8): 1301–1307, doi: [10.2967/jnumed.106.037408](https://doi.org/10.2967/jnumed.106.037408), indexed in Pubmed: [17631551](https://pubmed.ncbi.nlm.nih.gov/17631551/).

72. Bennink RJ, van den Hoff MJ, van Hemert FJ, et al. Annexin V imaging of acute doxorubicin cardiotoxicity (apoptosis) in rats. *J Nucl Med.* 2004; 45(5): 842–848, indexed in Pubmed: [15136635](#).
73. Knapp FF, Kropp J. Iodine-123-labelled fatty acids for myocardial single-photon emission tomography: current status and future perspectives. *Eur J Nucl Med.* 1995; 22(4): 361–381, doi: [10.1007/BF00941855](#), indexed in Pubmed: [7607269](#).
74. Elmaleh DR, Fischman AJ, Shoup TM. Method for monitoring blood flow and metabolic uptake in tissue with radiolabeled alkanolic acid. Google Patents. 2009: US8268291B2.
75. Hashimura H, Kiso K, Yamada N, et al. Myocardial impairment detected by late gadolinium enhancement in hypertrophic cardiomyopathy: comparison with 99mTc-MIBI/tetrofosmin and 123I-BMIPP SPECT. *Kobe J Med Sci.* 2013; 59(3): E81–E92, indexed in Pubmed: [24045217](#).
76. Newshean S, Viscuse PV, O'Sullivan CC, et al. Incidence, diagnosis, and treatment of cardiac toxicity from trastuzumab in patients with breast cancer. *Curr Breast Cancer Rep.* 2017; 9(3): 173–182, doi: [10.1007/s12609-017-0249-4](#), indexed in Pubmed: [29225726](#).
77. Martín M, Esteva FJ, Alba E, et al. Minimizing cardiotoxicity while optimizing treatment efficacy with trastuzumab: review and expert recommendations. *Oncologist.* 2009; 14(1): 1–11, doi: [10.1634/theoncologist.2008-0137](#), indexed in Pubmed: [19147689](#).
78. McLarty K, Cornelissen B, Scollard DA, et al. Associations between the uptake of 111In-DTPA-trastuzumab, HER2 density and response to trastuzumab (Herceptin) in athymic mice bearing subcutaneous human tumour xenografts. *Eur J Nucl Med Mol Imaging.* 2009; 36(1): 81–93, doi: [10.1007/s00259-008-0923-x](#), indexed in Pubmed: [18712381](#).
79. Perik PJ, Lub-De Hooge MN, Gietema JA, et al. Indium-111-labeled trastuzumab scintigraphy in patients with human epidermal growth factor receptor 2-positive metastatic breast cancer. *J Clin Oncol.* 2006; 24(15): 2276–2282, doi: [10.1200/JCO.2005.03.8448](#), indexed in Pubmed: [16710024](#).
80. de Korte MA, de Vries EGE, Lub-de Hooge MN, et al. 111Indium-trastuzumab visualises myocardial human epidermal growth factor receptor 2 expression shortly after anthracycline treatment but not during heart failure: a clue to uncover the mechanisms of trastuzumab-related cardiotoxicity. *Eur J Cancer.* 2007; 43(14): 2046–2051, doi: [10.1016/j.ejca.2007.06.024](#), indexed in Pubmed: [17719768](#).
81. Bergmann SR, Fox KA, Geltman EM, et al. Positron emission tomography of the heart. *Prog Cardiovasc Dis.* 1985; 28(3): 165–194, doi: [10.1016/0033-0620\(85\)90014-3](#), indexed in Pubmed: [3877316](#).
82. Yoshinaga K, Klein R, Tamaki N. Generator-produced rubidium-82 positron emission tomography myocardial perfusion imaging-From basic aspects to clinical applications. *J Cardiol.* 2010; 55(2): 163–173, doi: [10.1016/j.jjcc.2010.01.001](#), indexed in Pubmed: [20206068](#).
83. Sarocchi M, Bauckneht M, Arboscello E, et al. An increase in myocardial 18-fluorodeoxyglucose uptake is associated with left ventricular ejection fraction decline in Hodgkin lymphoma patients treated with anthracycline. *J Transl Med.* 2018; 16(1): 295, doi: [10.1186/s12967-018-1670-9](#), indexed in Pubmed: [30359253](#).
84. Zhang W, Cai Z, Li L, et al. Optimized and automated radiosynthesis of [F] DHMT for translational imaging of reactive oxygen species with positron emission tomography. *Molecules.* 2016; 21(12): 1696, doi: [10.3390/molecules21121696](#), indexed in Pubmed: [27941676](#).
85. Chu W, Chepetan A, Zhou D, et al. Development of a PET radiotracer for non-invasive imaging of the reactive oxygen species, superoxide, in vivo. *Org Biomol Chem.* 2014; 12(25): 4421–4431, doi: [10.1039/c3ob42379d](#), indexed in Pubmed: [24847866](#).
86. Boutagy NE, Wu J, Cai Z, et al. In vivo reactive oxygen species detection with a novel positron emission tomography tracer, F-DHMT, allows for early detection of anthracycline-induced cardiotoxicity in rodents. *JACC Basic Transl Sci.* 2018; 3(3): 378–390, doi: [10.1016/j.jacbts.2018.02.003](#), indexed in Pubmed: [30062224](#).
87. Sivapackiam J, Kabra S, Speidel S, et al. 68Ga-Galmydar: A PET imaging tracer for noninvasive detection of Doxorubicin-induced cardiotoxicity. *PLoS One.* 2019; 14(5): e0215579, doi: [10.1371/journal.pone.0215579](#), indexed in Pubmed: [31120912](#).
88. McCluskey SP, Haslop A, Coello C, et al. Imaging of chemotherapy-induced acute cardiotoxicity with f-labeled lipophilic cations. *J Nucl Med.* 2019; 60(12): 1750–1756, doi: [10.2967/jnumed.119.226787](#), indexed in Pubmed: [31147403](#).
89. Laursen AH, Elming MB, Ripa RS, et al. Rubidium-82 positron emission tomography for detection of acute doxorubicin-induced cardiac effects in lymphoma patients. *J Nucl Cardiol.* 2020; 27(5): 1698–1707, doi: [10.1007/s12350-018-1458-6](#), indexed in Pubmed: [30298372](#).
90. Ahmadzadehfah H, Eppard E, Kürpig S, et al. Therapeutic response and side effects of repeated radioligand therapy with 177Lu-PSMA-DKFZ-617 of castrate-resistant metastatic prostate cancer. *Oncotarget.* 2016; 7(11): 12477–12488, doi: [10.18632/oncotarget.7245](#), indexed in Pubmed: [26871285](#).
91. Yordanova A, Mayer K, Brossart P, et al. Safety of multiple repeated cycles of Lu-octreotate in patients with recurrent neuroendocrine tumour. *Eur J Nucl Med Mol Imaging.* 2017; 44(7): 1207–1214, doi: [10.1007/s00259-017-3652-1](#), indexed in Pubmed: [28246882](#).
92. Bodei L, Kidd M, Paganelli G, et al. Long-term tolerability of PRRT in 807 patients with neuroendocrine tumours: the value and limitations of clinical factors. *Eur J Nucl Med Mol Imaging.* 2015; 42(1): 5–19, doi: [10.1007/s00259-014-2893-5](#), indexed in Pubmed: [25273832](#).
93. Sabet A, Haslerud T, Pape UF, et al. Outcome and toxicity of salvage therapy with 177Lu-octreotate in patients with metastatic gastroenteropancreatic neuroendocrine tumours. *Eur J Nucl Med Mol Imaging.* 2014; 41(2): 205–210, doi: [10.1007/s00259-013-2547-z](#), indexed in Pubmed: [24030668](#).
94. Sabet A, Ezziddin K, Pape UF, et al. Long-term hematotoxicity after peptide receptor radionuclide therapy with 177Lu-octreotate. *J Nucl Med.* 2013; 54(11): 1857–1861, doi: [10.2967/jnumed.112.119347](#), indexed in Pubmed: [24009272](#).
95. Sabet A, Ezziddin K, Pape UF, et al. Accurate assessment of long-term nephrotoxicity after peptide receptor radionuclide therapy with (177) Lu-octreotate. *Eur J Nucl Med Mol Imaging.* 2014; 41(3): 505–510, doi: [10.1007/s00259-013-2601-x](#), indexed in Pubmed: [24196919](#).
96. Ahmadzadehfah H, Rahbar K, Kürpig S, et al. Early side effects and first results of radioligand therapy with (177)Lu-DKFZ-617 PSMA of castrate-resistant metastatic prostate cancer: a two-centre study. *EJNMMI Res.* 2015; 5(1): 114, doi: [10.1186/s13550-015-0114-2](#), indexed in Pubmed: [26099227](#).
97. Skrabanek P, Cannon D, Kirrane J, et al. Substance P secretion by carcinoid tumours. *Ir J Med Sci.* 1978; 147(2): 47–49, doi: [10.1007/BF02939369](#), indexed in Pubmed: [632061](#).
98. van der Lely AJ, de Herder WW. Carcinoid syndrome: diagnosis and medical management. *Arq Bras Endocrinol Metabol.* 2005; 49(5): 850–860, doi: [10.1590/s0004-27302005000500028](#), indexed in Pubmed: [16444370](#).
99. Werner RA, Bundschuh RA, Bundschuh L, et al. Molecular imaging reporting and data systems (MI-RADS): a generalizable framework for targeted radiotracers with theranostic implications. *Ann Nucl Med.* 2018; 32(8): 512–522, doi: [10.1007/s12149-018-1291-7](#), indexed in Pubmed: [30109562](#).
100. Brabander T, van der Zwan WA, Teunissen JJM, et al. Long-term efficacy, survival, and safety of [177Lu, DOTA0, Tyr3] octreotate in patients with gastroenteropancreatic and bronchial neuroendocrine tumors. *Clin Cancer Res.* 2017; 23(16): 4617–4624, doi: [10.1158/1078-0432.CCR-16-2743](#), indexed in Pubmed: [28428192](#).
101. Bergsma H, van Lom K, Raaijmakers MH, et al. Persistent hematologic dysfunction after peptide receptor radionuclide therapy with 177Lu-DOTATATE: incidence, course, and predicting factors in patients with gastroenteropancreatic neuroendocrine tumors. *J Nucl Med.* 2018; 59(3): 452–458, doi: [10.2967/jnumed.117.189712](#), indexed in Pubmed: [28775205](#).

102. Hall R. Neoplastic heart disease. The heart, arteries and veins. McGraw-Hill, New York 1990: 1382–1403.
103. Smith WHT, Nair RU, Adamson D, et al. Somatostatin receptor subtype expression in the human heart: differential expression by myocytes and fibroblasts. *J Endocrinol.* 2005; 187(3): 379–386, doi: [10.1677/joe.1.06082](https://doi.org/10.1677/joe.1.06082), indexed in Pubmed: [16423817](https://pubmed.ncbi.nlm.nih.gov/16423817/).
104. Hendifar AE, Delpassand ES, Kittleson MM, et al. Cardiac toxicity in a patient receiving peptide receptor radionuclide therapy. *Pancreas.* 2018; 47(8): e55–e56, doi: [10.1097/MPA.0000000000001101](https://doi.org/10.1097/MPA.0000000000001101), indexed in Pubmed: [30113434](https://pubmed.ncbi.nlm.nih.gov/30113434/).
105. Chatterjee S, Azad BB, Nimmagadda S. The intricate role of CXCR4 in cancer. *Adv Cancer Res.* 2014; 124: 31–82, doi: [10.1016/B978-0-12-411638-2.00002-1](https://doi.org/10.1016/B978-0-12-411638-2.00002-1), indexed in Pubmed: [25287686](https://pubmed.ncbi.nlm.nih.gov/25287686/).
106. Kratochwil C, Flechsig P, Lindner T, et al. Ga-FAPI PET/CT: tracer uptake in 28 different kinds of cancer. *J Nucl Med.* 2019; 60(6): 801–805, doi: [10.2967/jnumed.119.227967](https://doi.org/10.2967/jnumed.119.227967), indexed in Pubmed: [30954939](https://pubmed.ncbi.nlm.nih.gov/30954939/).
107. Lapa C, Lückerrath K, Rudelius M, et al. [68Ga]Pentixafor-PET/CT for imaging of chemokine receptor 4 expression in small cell lung cancer-initial experience. *Oncotarget.* 2016; 7(8): 9288–9295, doi: [10.18632/oncotarget.7063](https://doi.org/10.18632/oncotarget.7063), indexed in Pubmed: [26843617](https://pubmed.ncbi.nlm.nih.gov/26843617/).
108. Kircher M, Herhaus P, Schottelius M, et al. CXCR4-directed theranostics in oncology and inflammation. *Ann Nucl Med.* 2018; 32(8): 503–511, doi: [10.1007/s12149-018-1290-8](https://doi.org/10.1007/s12149-018-1290-8), indexed in Pubmed: [30105558](https://pubmed.ncbi.nlm.nih.gov/30105558/).
109. Vag T, Gerngross C, Herhaus P, et al. First experience with chemokine receptor cxcr4-targeted PET imaging of patients with solid cancers. *J Nucl Med.* 2016; 57(5): 741–746, doi: [10.2967/jnumed.115.161034](https://doi.org/10.2967/jnumed.115.161034), indexed in Pubmed: [26769866](https://pubmed.ncbi.nlm.nih.gov/26769866/).
110. Schottelius M, Osl T, Poschenrieder A, et al. [Lu]pentixather: comprehensive preclinical characterization of a first cxcr4-directed endoradiotherapeutic agent. *Theranostics.* 2017; 7(9): 2350–2362, doi: [10.7150/thno.19119](https://doi.org/10.7150/thno.19119), indexed in Pubmed: [28744319](https://pubmed.ncbi.nlm.nih.gov/28744319/).
111. Giesel FL, Kratochwil C, Lindner T, et al. Ga-FAPI PET/CT: biodistribution and preliminary dosimetry estimate of 2 DOTA-containing FAP-targeting agents in patients with various cancers. *J Nucl Med.* 2019; 60(3): 386–392, doi: [10.2967/jnumed.118.215913](https://doi.org/10.2967/jnumed.118.215913), indexed in Pubmed: [30072500](https://pubmed.ncbi.nlm.nih.gov/30072500/).

Physical quantities useful for quality control of quantitative SPECT/CT imaging

Sara Kurkowska^{ORCID}, Bożena Birkenfeld^{ORCID}, Hanna Piwowarska-Bilska^{ORCID}

Department of Nuclear Medicine, Pomeranian Medical University, Szczecin, Poland

[Received 18 I 2021; Accepted 04 VI 2021]

Abstract

SPECT/CT imaging is transitioning from solely qualitative applications to quantitative analysis. Quantitative SPECT/CT systems require proper calibration, optimization and quality control. Various types of modern SPECT/CT scanners have different software for calibration and quality control (QC). There is still no standardization in this regard for quantitative SPECT/CT. This issue hinders the exchange of obtained results across centers and stunts the development of repeatable and reproducible measurements. The unification and standardization of calibration and quality control techniques for quantitative SPECT/CT systems is currently a pressing need for nuclear medicine departments.

The present study presents three selected physical quantities characterizing the quality of quantitative SPECT/CT system and seven quantities, currently used in the literature, to assess the quality of quantitative SPECT/CT images. The measurement of these parameters requires the use of standard gamma camera software for QC, external programs for quantitative analysis of recorded data and clinical software. The authors hope this will help physicists who are willing to perform quantitative SPECT/CT in their departments.

KEY words: SPECT/CT; quantitative SPECT/CT; SUV

Nucl Med Rev 2021; 24, 2: 93–98

Introduction

During the last decades, nuclear medicine is undergoing a significant change, emphasizing the quantitative quality of single photon emission computed tomography (SPECT) images. The introduction of hybrid devices, combining SPECT gamma cameras with a computed tomography (CT) scanner, enabled quantitative evaluation of images thanks to CT-based attenuation correction. New techniques of images reconstruction, based on iterative methods, reduced errors in absolute quantification in SPECT thanks to scatter and attenuation corrections. This permitted the introduction of quantification of radiopharmaceuticals uptake in healthy and pathological tissues and it is commonly expressed as standardized uptake value (SUV). Moreover, quantitative SPECT/CT images play a crucial role in internal dosimetry used for individualized radionuclide treatment planning.

For positron emission tomography (PET)/CT systems, the National Electrical Manufacturers Association (NEMA) has defined the standards which allow performing the quality control of quantitative images [1]. Such standards, though, are not defined for quantitative SPECT/CT imaging, yet. This issue hinders the exchange of obtained results across centres and stunts the development of repeatable and reproducible measurements.

While waiting for a set of standard procedures, active research is conducted to evaluate the accuracy and precision of quantitation [2–4]. To verify the quality of quantitative images obtained with SPECT/CT, many authors try to adopt the methods employed in PET or, if necessary, modify them as needed. According to Dickson et al. [5], now is the time to work together as a community to make this potential a reality.

The present study reviews physical quantities, currently used in literature, to assess the quality of quantitative SPECT/CT images. The authors hope this will help physicists who are willing to perform quantitative SPECT/CT in their departments.

Basic requirements for obtaining quantitative SPECT/CT images

The basic requirement for obtaining reliable results of quantitative image analysis is to perform acquisitions with SPECT/CT

Correspondence to: Sara Kurkowska
 Department of Nuclear Medicine, Pomeranian Medical University, Unii
 Lubelskiej 1, 71–344 Szczecin, Poland
 e-mail: sarakurkowska95@gmail.com

systems, which have the correct results of periodic quality control and calibration tests recommended by the manufacturer and compliant with NEMA guidelines. Standard instrument calibrations and quality control tests (including tests of uniformity, the centre of rotation, SPECT/CT spatial co-registration, as well as CT system tests) should be performed regularly, following the schedule recommended by producers. The clinical use of gamma cameras that do not show the stability of the measured parameters forces users to test and calibrate the systems more often.

Quantitative image reconstructions must be performed by iterative methods such as maximum likelihood expectation maximization or ordered subsets expectation maximization (OSEM), because only these reconstruction methods allow to perform attenuation and scatter corrections. The exact correction for attenuation is performed based on the attenuation maps, calculated from the transmission images of a patient, obtained with the CT component of the SPECT/CT system during one hybrid imaging session. Low-dose CT acquisitions, used to ensure radiological protection of the patient, are sufficient to correct the attenuation in SPECT images. The attenuation corrections are introduced at the stage of reconstruction of the scintigraphic slices.

A popular and relatively accurate method of scattered photon correction is acquisition with the triple energy window [6]. It allows evaluating the number of scattered photons based on the measurement of the counts in the projections collected in two additional energy windows, placed on both sides of the photopic. In the software of modern gamma cameras, the scattering correction is built directly into the reconstruction algorithm.

The correction of the gamma camera's resolution recovery is not necessary, because it does not affect the accuracy of the quantitative measurement of the activity distribution. Nevertheless, it is recommended since improving the resolution of the images facilitates the segmentation process.

Selected quantities characterizing the quality of quantitative SPECT/CT system

The physical quantities described in this work are the quantities most frequently reported in the literature that characterize the quantitative SPECT/CT quality.

Sensitivity

Each manufacturer of gamma cameras recommends a specified, repeatable technique for measuring the sensitivity of the gamma cameras. For example, Siemens, before the quantitative acquisition of scintigraphic images, requires a one-time volume sensitivity measurement using a cylindrical phantom filled with a homogeneous radioisotope solution. Afterwards, the monthly planar measurement of the sensitivity of the point source in a dedicated test tube should be performed. GE Healthcare recommends planar measurement of the detectors' sensitivity using a flat plastic dish (e.g., standard Petri dish), containing a homogeneous radioisotope solution. Commercial gamma camera software, within the set of programs for quality control, contains dedicated applications for measuring the sensitivity of the system. To compare the sensitivity of different types of gamma cameras, one should follow the recommendations of NEMA 1-2018 [7] regarding the measurements of

planar sensitivity test of detectors and volume sensitivity test of SPECT system.

Cross-calibration

To enable quantitative measurements, all SPECT images reconstructed in counts per pixel must be converted to the activity concentration (Bq/mL) units. In this way, it is possible to analyse the data by applying the SUV. There are two ways to convert it.

Firstly, the reconstructed counts in the SPECT volume can be directly related to the acquired counts in the projection data. In this situation, calibration is related to the absolute value of the camera sensitivity from the planar measurement, in units of counts per second per kBq (cps/kBq).

Another method uses the cross-calibration factor (CCF), which is determined from a reconstructed image, relating the counts to the radioactivity concentration. The CCF can be evaluated using a cylindrical homogeneous phantom and is defined by

$$CCF\left[\frac{\text{cps/ml}}{\text{Bq/ml}}\right] = \frac{\mu}{A_c \cdot t \times n \times v}, \quad (1)$$

where μ is the total counts in VOI in the reconstructed image, t is the time per projection, n is the number of projections, v is the VOI volume, A_c and is the true activity concentration in the phantom.

In the Q.Dose software [8], the calibration is performed using the Scaling Factor, which is the reciprocal of the CCF

$$SF\left[\frac{\text{Bq/ml}}{\text{cps/ml}}\right] = \frac{A_c}{\mu \cdot t \times n \times v}. \quad (2)$$

Spect reconstructed spatial resolution

An important quantity to assess the quality of quantitative tomographic imaging is the reconstructed spatial resolution, measured in air and a dispersion medium. The reconstructed spatial resolution of the SPECT system is defined as the full-width at half-maximum (FWHM) of the line spread function (LSF) or of the point spread function (PSF) with an imaging collimator installed. This measurement should be completed with the full width to the tenth of the maximum because the PSF or LSF may deviate from the Gaussian distribution. NEMA [7] recommends the use of 3 capillary tubes (e.g., syringe needles) with an inner diameter 1 mm as radioactive sources. They should be positioned parallel to the principal orthogonal axes of the camera to avoid broadening the LSF. Measuring the Reconstructed Spatial Resolution with Scatter requires placing 3 capillary tubes in a cylinder of water. Following NEMA guidelines, cross-sections through source centres (slices of thickness 10 ± 3 mm) should be reconstructed using the filtered back-projection technique with the ramp filter.

Dead-time

Imaging studies of patients who have just received radionuclide therapy, where relatively high activities of radionuclides are usually administered, may be affected by considerable dead time (DT) effects. These are caused mainly by the pile-up in the gamma camera detector and electronics. Therefore, for any post-therapy imaging study where quantitative information is required (e.g., for image-based dosimetry calculations, tumour staging and evaluation of therapy outcomes), DT corrections should be performed.

Ryu et al. [4] measured the DT effect of the SPECT system using a cylindrical phantom with high initial activity for ^{99m}Tc and ^{177}Lu . The DT constants were estimated based on the concepts of paralyzable (τ_p) and non-paralyzable (τ_{NP}) DTs and the corresponding two-component model introduced by Cranley et al. [9]. The DTs in the two-component model can be easily determined through a least-squares fitting for the decaying source method. To evaluate the paralyzable and non-paralyzable components of the system DT, the authors fitted eq. (3) to the observed data,

$$r' = \frac{r}{e^{r\tau_p} + \left(\frac{\tau_{NP}}{\tau_p} - 1\right) r\tau_p}, \quad (3)$$

where r' is the observed count rate, r is the true count rate, τ_p is the paralyzable and τ_{NP} the non-paralyzable constant. The fitting was stopped when R^2 -value was equal to 1.0.

Quantities describing the quality of the quantitative SPECT/CT image

Accuracy of activity recovery

The accuracy of activity recovery is simply the ratio between the activity concentration, measured in the reconstructed SPECT image (a_c), and the true activity concentration (A_c), measured during phantom preparation. This quantity can be measured for the cylindrical homogeneous and the anthropomorphic phantoms. Depending on the chosen phantom, the regions of interest (ROIs) can be defined in the background or in the spheres, when an anthropomorphic phantom, for example, NEMA/International Electrotechnical Commission (IEC) NU2 phantom, is used.

The background calibration factor ($Bg.cal$) is defined as

$$Bg.cal = \frac{a_{c,bg}}{A_{c,bg}}, \quad (4)$$

where $a_{c,bg}$ is the activity concentration measured in the reconstructed SPECT phantom background and $A_{c,bg}$ is true activity

concentration inside the phantom. Gnesin et al. [2] determined $a_{c,bg}$ as the average on 5 circular ROIs of 16 cm diameter centred on the cylinder axis, placed at different axial locations as in Figure 1.

For spheres, recovery coefficients (RCs) are defined as

$$RC_{j,max} = \frac{a_{c,sphj,max}}{A_{c,sph}}, \quad (5)$$

$$RC_{j,A50} = \frac{a_{c,sphj,A50}}{A_{c,sph}}, \quad (6)$$

where j is the number of the sphere, $a_{c,sphj,max}$ is the measured maximum voxel value (in terms of activity concentration) for a given spherical insert, $A_{c,sph}$ is the true activity concentration in the sphere, $a_{c,sphj,A50}$ is the average voxel value for each hot insert VOI defined by a 3D isocontour at 50% adapted for background [10].

In their study, Peters et al. [11] determined the RC for each sphere performing five measurements and, then, they evaluate the repeatability of these measurements using the median absolute deviation (MAD) for each sphere diameter according to

$$MAD = \text{median}(|RC_i - RC|), \quad (7)$$

where RC_i is the recovery coefficient of measurement i and RC is the median recovery coefficient of all five measurements.

The white paper published by GE Healthcare [12] shows a modified equation for the accuracy,

$$\text{Accuracy}(\%) = \left(1 - \frac{|A_{c,sphj} - a_{c,sphj}|}{A_{c,sphj}}\right) \times 100. \quad (8)$$

Image noise

The coefficient of variation (COV) is a parameter used to evaluate image noise. It is expressed as the ratio between the standard deviation (σ_{bg}) and the mean value of activity concentration measured in the phantom background ($\bar{a}_{c,bg}$),

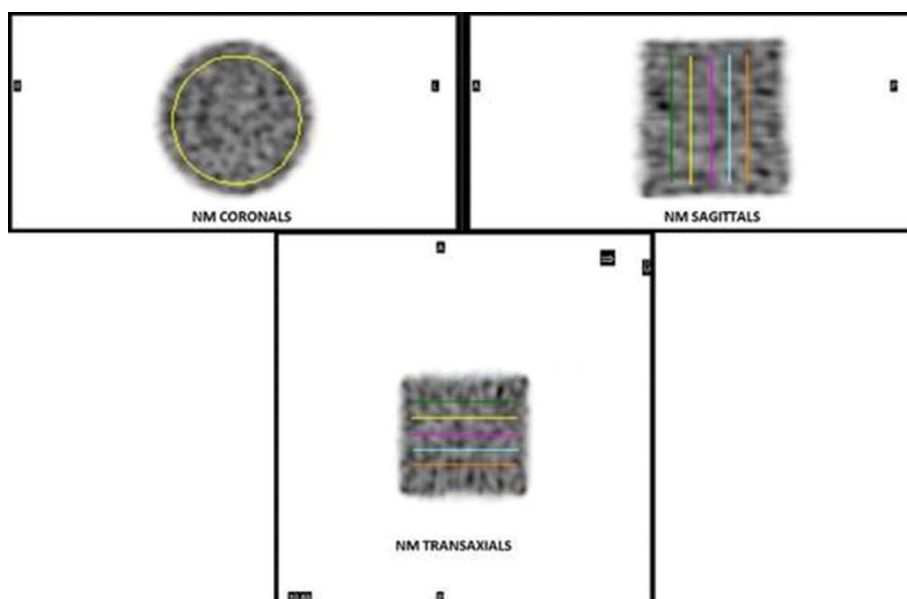


Figure 1. Reconstructed image of Phantom Well Counter Calibration Uniform Cylindrical performed in Q.Metrix software from GE Healthcare. 5 circular ROIs of 16 cm diameter centred on the cylinder axis were placed at different axial locations and used to calculate $Bg.cal$

$$COV(\%) = \frac{\sigma_{bg}}{\bar{a}_{c,bg}} \times 100. \quad (9)$$

The background mean value of activity concentration is determined as the mean value of several different ROIs and σ_{bg} is the standard deviation of the mean of these ROIs.

Koopman et al. [13] in placed three rectangular ROIs within the phantom background in three axial planes, obtaining nine ROIs. For each ROI, the image COV was determined using eq. (9). The COV for a reconstructed image was obtained by taking the average of the nine measured COVs. The technique of delineating ROIs is presented in Figure 2.

This quantity can be measure for the cylindrical homogeneous phantom and the NEMA/IEC NU2 phantom.

Total activity deviation

The total activity deviation is defined by

$$\Delta A_{tot}(\%) = \frac{A_{tot,rec} - A_{tot}}{A_{tot}} \times 100 \quad (10)$$

where $A_{tot,rec}$ is the total activity in the phantom measured in the reconstructed image, and A_{tot} is the true total activity of radionuclide measured during phantom preparation.

This quantity can be measured for the cylindrical homogeneous phantom and the NEMA/IEC NU2 phantom.

Contrast recovery

To evaluate the contrast recovery, the NEMA/IEC NU2 phantom with hot spheres should be used. The hot contrast for each hot sphere is calculated by

$$Q_{H,j}(\%) = \frac{(a_{c,sp,h,j}/a_{c,bg}) - 1}{(A_{c,sp,h,j}/A_{c,bg}) - 1} \times 100. \quad (11)$$

The ideal ratio is equal to 100%.

Residual error in scatter and attenuation corrections

The relative error in the lung, ΔC_{lung} , allows evaluating the residual error in scatter and attenuation corrections using an anthropomorphic phantom with lung insert and it is defined as

$$\Delta C_{lung}(\%) = \frac{a_{c,lung}}{A_{c,bg}} \times 100, \quad (12)$$

where $a_{c,lung}$ is the average activity concentration measured in a cylindrical VOI, with a 3 cm diameter and a length of 16 cm, placed into the lung insert [2].

Discussion

Quantitative analysis of SPECT/CT images is a difficult task. Many physical effects hinder proper quantification. Among the most important ones are blurring introduced by the collimator response function, the limited spatial resolution and associated partial volume effect, photon attenuation and the contribution in the images of events arising from photons scattered in the objects. There are, however, algorithms and methods used to compensate for these effects.

Despite these limitations, SPECT/CT is transitioning from solely qualitative applications to quantitative analysis.

Seret et al. [14] investigated four SPECT/CT systems focusing on their quantitative capabilities. They found that, in objects whose dimensions exceeded the SPECT spatial resolution by several times, quantification seemed to be feasible within 10% error limits. A partial-volume correction strategy remains necessary for smaller structures. In a study performed by Zeintl et al. [15], they report an average quantitative accuracy within 3.6% in phantoms with different-sized spheres and 1.1% in patients with a focus on the bladder when using [^{99m}Tc].

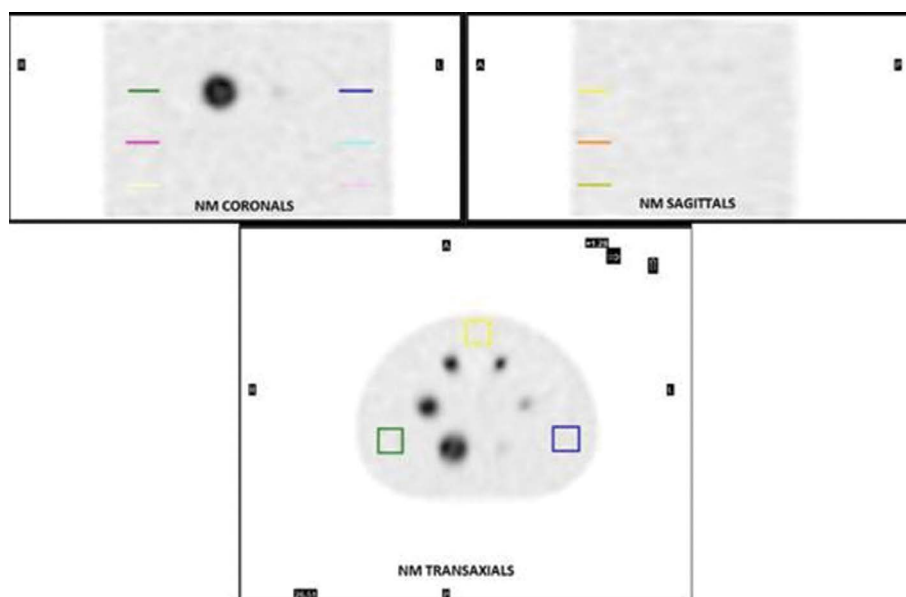


Figure 2. Reconstructed image of NEMA Body Phantom/IEC NU2 performed in Q.Metrix software from GE Healthcare. Three rectangular ROIs in three different axial planes within the phantom background were used to calculate COV. COV — coefficient of variation; IEC — International Electrotechnical Commission; NEMA — National Electrical Manufacturers Association

Dead-time is an important effect in quantitative SPECT. In terms of radionuclide therapy, where injected activities are very high, dead-time losses can be substantial and cause an underestimation of the doses received by organs. It is essential to correct for this effect during dosimetric studies. Dead-time correction is particularly important for radionuclides with multiple photon emissions such as ^{131}I , as photons not included in the energy window also contribute to dead time. In a study on the dosimetric impact of dead-time correction after a 4 GBq therapeutic injection of ^{131}I , correction for count losses led to an 11% increase in whole-body time-integrated activity [16]. For descriptions of practical methods for calculating corrections for DT effect for quantitative studies using high ^{177}Lu activities, see articles [17, 18].

In a study from 2012, Dewaraja et al. [19] showed that a planar measurement of a point source is sufficient for accurate calibration of the sensitivity of a gamma camera. It is necessary to use the same collimator and to set the same energy windows like the ones that will be used in the acquisition protocols of the examined patients. In a work from 2017, Matsumoto et al. [20] confirmed that the quantitative calibration of the gamma camera made based on a planar sensitivity measurement (using a Petri dish) is burdened with a lower measurement error than the calibration based on the measurement and reconstruction of a homogeneous cylindrical phantom (CCF method).

Even though a correct cross-calibration is performed, some differences in quantitative measurements might occur between centres because of the differences in applied image reconstruction parameters. Reconstructions should be performed with corrections for attenuation, scatter and resolution recovery. Therefore, it is necessary to standardize the method of image reconstruction for CCF and then to standardize the technique of quantitative SPECT/CT systems calibration.

The study performed by Gnesin et al. [2] shows that relative lung errors were comparable to PET levels, which suggest the efficient integration of attenuation and scatter corrections. Its value was less than 10% in the case of background activity concentrations > 12 kBq/mL. However, the value increased with lower statistic and was found to be approximately 20% for background activity concentrations of 1.5 kBq/mL.

Recovery coefficient (or Accuracy) is a very helpful quantity to assess the effectiveness of SPECT/CT quantitative analysis. By plotting RC curves for phantom hot spheres of various sizes, the optimal quantitative image reconstruction technique can be easily established. A phantom containing hot spheres is required to measure RC, Accuracy and contrast recovery measurements. A cylindrical phantom filled with a homogeneous radioisotope solution is sufficient to determine the background calibration factor, total activity and image noise. Relative error measurement requires the use of an anthropomorphic phantom with a lung insert.

The accuracy of the quantitative SPECT/CT technique has been evaluated with phantom experiments in many works. The results show that it is possible to obtain reproducible measurements. The study performed by Peters et al. [11] shows that absolute SPECT quantification is achievable in a multi-centre and multi-vendor setting. The variation between centres is mainly caused by the use of different reconstruction algorithms and/or settings. Based on their research, the authors confirmed that the OSEM iterative method with 5 iterations and 15 subsets, without the

3D post-reconstruction filter, is the optimal clinical method for the reconstruction of quantitative images obtained with the NM/CT850 gamma camera [21, 12]. On the other hand, for the gamma camera Symbia Intevo, Gnesin et al. [2] chose the iterative reconstruction technique with 16 iterations and 4 subsets and Gaussian smoothing of FWHM 7.5 mm (for foci with a diameter greater than 24 mm) as the optimal method.

The next step should be to establish the equivalence between the corresponding reconstruction techniques for gamma cameras from different manufacturers, for analogous acquisition parameters. The aim of the work should be focused on finding equivalent techniques of image reconstruction and filtering, which should ensure the same level of accuracy in the measurements of activity concentration for different SPECT/CT systems.

The further aim should be to unify and standardize calibration and quality control procedures for all types of new QSPECT/CT systems.

Summary

Quantitative SPECT/CT requires proper calibration, optimization and quality control. Various types of modern SPECT/CT scanners have different software for calibration and quality control of imaging. There is still no standardization in this regard for quantitative SPECT/CT. This paper presents three selected physical quantities characterizing the quality of quantitative SPECT/CT system: sensitivity, SPECT Reconstructed Spatial Resolution and dead-time. The measurement of these parameters requires the use of standard gamma camera software for image acquisition and, also, external programs for quantitative analysis of recorded data. Seven values characterizing the quality of quantitative SPECT/CT images were also presented: background calibration factor, recovery coefficient, the accuracy of measurements, coefficient of variation for image noise evaluating, total activity deviation, contrast recovery and residual error in scatter and attenuation corrections. All seven parameters can be determined using only clinical software.

The authors believe that the standardization of the quantitative SPECT/CT technique could be significantly accelerated by the unification of quantitative acquisition techniques, reconstruction, image analysis, as well as quality control procedures in all commercial quantitative SPECT/CT systems.

References

1. NEMA Standards Publication NU 2-2018. Performance measurements of positron emission tomographs (PETS) Rosslyn, 2018.
2. Gnesin S, Leite Ferreira P, Malterre J, et al. Phantom validation of Tc-99m absolute quantification in a SPECT/CT commercial device. *Comput Math Methods Med.* 2016; 2016: 4360371, doi: [10.1155/2016/4360371](https://doi.org/10.1155/2016/4360371), indexed in Pubmed: [28096891](https://pubmed.ncbi.nlm.nih.gov/28096891/).
3. Ferrando O, Chimenz A, Foppiano F, et al. SPECT/CT activity quantification in 99mTc-MAA acquisitions. *J Diag Imaging Ther.* 2018; 5(1): 32–36, doi: [10.17229/jdit.2018-0624-034](https://doi.org/10.17229/jdit.2018-0624-034).
4. Ryu H, Meikle SR, Willowson KP, et al. Performance evaluation of quantitative SPECT/CT using NEMA NU 2 PET methodology. *Phys Med Biol.* 2019; 64(14): 145017, doi: [10.1088/1361-6560/ab2a22](https://doi.org/10.1088/1361-6560/ab2a22), indexed in Pubmed: [31207583](https://pubmed.ncbi.nlm.nih.gov/31207583/).
5. Dickson J, Ross J, Vöö S. Quantitative SPECT: the time is now. *EJNMMI Phys.* 2019; 6(1): 4, doi: [10.1186/s40658-019-0241-3](https://doi.org/10.1186/s40658-019-0241-3), indexed in Pubmed: [30830530](https://pubmed.ncbi.nlm.nih.gov/30830530/).

6. Ogawa K, Harata Y, Ichihara T, et al. A practical method for position-dependent Compton-scatter correction in single photon emission CT. *IEEE Trans Med Imaging*. 1991; 10(3): 408–412, doi: [10.1109/42.97591](https://doi.org/10.1109/42.97591), indexed in Pubmed: [18222843](https://pubmed.ncbi.nlm.nih.gov/18222843/).
7. NEMA Standards Publication NU 1-2018. Performance measurements of gamma cameras Rosslyn, 2018.
8. QDOSE Dosimetry Software. User Manual. Version 1.1.14. 2020.
9. Cranley K, Millar R, Bell TK. Correction for deadtime losses in a gamma camera/data analysis system. *Eur J Nucl Med*. 1980; 5(4): 377–382, doi: [10.1007/BF00445626](https://doi.org/10.1007/BF00445626), indexed in Pubmed: [7398673](https://pubmed.ncbi.nlm.nih.gov/7398673/).
10. Boellaard R, O'Doherty MJ, Weber WA, et al. FDG PET and PET/CT: EANM procedure guidelines for tumour PET imaging: version 1.0. *Eur J Nucl Med Mol Imaging*. 2010; 37(1): 181–200, doi: [10.1007/s00259-009-1297-4](https://doi.org/10.1007/s00259-009-1297-4), indexed in Pubmed: [19915839](https://pubmed.ncbi.nlm.nih.gov/19915839/).
11. Peters SMB, van der Werf NR, Segbers M, et al. Towards standardization of absolute SPECT/CT quantification: a multi-center and multi-vendor phantom study. *EJNMMI Phys*. 2019; 6(1): 29, doi: [10.1186/s40658-019-0268-5](https://doi.org/10.1186/s40658-019-0268-5), indexed in Pubmed: [31879813](https://pubmed.ncbi.nlm.nih.gov/31879813/).
12. NM Quantification Q.Metrix for SPECT/CT Package. White Paper DOC1951185: GE Healthcare.
13. Koopman D, van Osch JAC, Jager PL, et al. Technical note: how to determine the FDG activity for tumour PET imaging that satisfies European guidelines. *EJNMMI Phys*. 2016; 3(1): 22, doi: [10.1186/s40658-016-0158-z](https://doi.org/10.1186/s40658-016-0158-z), indexed in Pubmed: [27682837](https://pubmed.ncbi.nlm.nih.gov/27682837/).
14. Seret A, Nguyen D, Bernard C. Quantitative capabilities of four state-of-the-art SPECT-CT cameras. *EJNMMI Res*. 2012; 2(1): 45, doi: [10.1186/2191-219X-2-45](https://doi.org/10.1186/2191-219X-2-45), indexed in Pubmed: [22925467](https://pubmed.ncbi.nlm.nih.gov/22925467/).
15. Zeintl J, Vija AH, Yahil A, et al. Quantitative accuracy of clinical ^{99m}Tc SPECT/CT using ordered-subset expectation maximization with 3-dimensional resolution recovery, attenuation, and scatter correction. *J Nucl Med*. 2010; 51(6): 921–928, doi: [10.2967/jnumed.109.071571](https://doi.org/10.2967/jnumed.109.071571), indexed in Pubmed: [20484423](https://pubmed.ncbi.nlm.nih.gov/20484423/).
16. Ferrer L, Delpon G, Lisbona A, et al. Dosimetric impact of correcting count losses due to deadtime in clinical radioimmunotherapy trials involving iodine-131 scintigraphy. *Cancer Biother Radiopharm*. 2003; 18(1): 117–124, doi: [10.1089/108497803321269395](https://doi.org/10.1089/108497803321269395), indexed in Pubmed: [12667314](https://pubmed.ncbi.nlm.nih.gov/12667314/).
17. Beauregard JM, Hofman MS, Pereira JM, et al. Quantitative (177)Lu SPECT (QSPECT) imaging using a commercially available SPECT/CT system. *Cancer Imaging*. 2011; 11(1): 56–66, doi: [10.1102/1470-7330.2011.0012](https://doi.org/10.1102/1470-7330.2011.0012), indexed in Pubmed: [21684829](https://pubmed.ncbi.nlm.nih.gov/21684829/).
18. Celler A, Piwowska-Bilska H, Shcherbinin S, et al. Evaluation of dead-time corrections for post-radionuclide-therapy (177)Lu quantitative imaging with low-energy high-resolution collimators. *Nucl Med Commun*. 2014; 35(1): 73–87, doi: [10.1097/MNM.000000000000011](https://doi.org/10.1097/MNM.000000000000011), indexed in Pubmed: [24131941](https://pubmed.ncbi.nlm.nih.gov/24131941/).
19. Dewaraja YK, Frey EC, Sgouros G, et al. MIRD pamphlet No. 23: quantitative SPECT for patient-specific 3-dimensional dosimetry in internal radionuclide therapy. *J Nucl Med*. 2012; 53(8): 1310–1325, doi: [10.2967/jnumed.111.100123](https://doi.org/10.2967/jnumed.111.100123), indexed in Pubmed: [22743252](https://pubmed.ncbi.nlm.nih.gov/22743252/).
20. Matsutomo N, Matsumoto S, Yamamoto T, et al. Validation of a calibration method using the cross-calibration factor and system planar sensitivity in quantitative single-photon emission computed tomography imaging. *Radiol Phys Technol*. 2017; 10(4): 439–445, doi: [10.1007/s12194-017-0416-3](https://doi.org/10.1007/s12194-017-0416-3), indexed in Pubmed: [28822095](https://pubmed.ncbi.nlm.nih.gov/28822095/).
21. Piwowska-Bilska H, Supińska A, Birkenfeld B. What validation tests can be done by the clinical medical physicist while waiting for the standardization of quantitative SPECT/CT imaging? , doi: [10.21203/rs.3.rs-118913/v1](https://doi.org/10.21203/rs.3.rs-118913/v1).

The role of [¹⁸F]FDG PET/CT for gastric cancer management

Ebru Salmanoglu 

Department of Nuclear Medicine, Kahramanmaraş Sutcu Imam University, Faculty of Medicine, Kahramanmaraş, Turkey

[Received 15 IV 2021; Accepted 28 VI 2021]

Abstract

Gastric cancer (GC) is a common cause of cancer-related deaths in the world. In addition to the patient's clinical history and clinical examination, nuclear medicine tools are required for diagnosis. [¹⁸F]FDG PET/CT has been commonly used for cancer patients for staging, restaging, evaluation of treatment response. This study aimed to review the current literature on the role of [¹⁸F]FDG PET/CT for GC management.

KEY words: gastric cancer; PET/CT; [¹⁸F]FDG

Nucl Med Rev 2021; 24, 2: 99–103

Introduction

Gastric cancer (GC) is a common neoplasm and GC is the third most widespread cause of cancer-related deaths worldwide. GC generally affects men higher than women. Various factors such as Helicobacter Pylori, bad diet habits and smoking give rise to GC [1]. GC is a cancer type usually diagnosed at an advanced stage. Patient history, physical examination, endoscopy and biopsy is essential for the diagnosis of this disease. Diagnostic imaging modalities including endoscopic ultrasound (EUS), computed tomography (CT), magnetic resonance imaging (MRI) and positron emission tomography/computed tomography (PET/CT) are used for the initial evaluation of GC. Fluorine-18 fluoro-2-deoxy-D-glucose ([¹⁸F]FDG) PET/CT is recommended if there is no evidence for metastasis and if clinically indicated according to National Comprehensive Cancer Network (NCCN) guidelines. PET/CT might be useful for the evaluation of therapy response before surgery, recurrence and determination of occult metastatic tumour [2]. In this review article, the role of [¹⁸F]FDG PET/CT for GC management is evaluated in light of the current literature.

Detection of primary tumours and prediction of prognosis

A cancer screening programme for detecting GC found that FDG-PET had 37.9% sensitivity. Furthermore, FDG-PET had lower

sensitivity than endoscopy. FDG-PET demonstrated early-stage GC in some cases. However, many of them were shown with a combination of endoscopy. Therefore, the combination of endoscopy was helpful for the detection of tumours at an early stage [3].

Dual time point imaging (DTPI) [¹⁸F]PET/CT was analysed to differentiate malignant and benign disease of GC patients (n = 74) with focal increased gastric uptake on imaging. The maximum standardized uptake value (SUVmax) of the early PET/CT imaging was 5.0 ± 1.4, the SUVmax of the delayed PET/CT imaging was 5.9 ± 2.7. The study concluded that DTPI can play an important role in differentiating malignant disease from the benign gastric disease [4].

The utility of [¹⁸F]FDG PET/CT was investigated for detecting primary GC in suspected GC patients (n = 68). After fasting whole-body PET/CT imaging, the patients drank a measured amount of milk with Diatrizoate Meglumine. Local gastric PET/CT imaging was also performed. Whole-body PET/CT had 92.9% sensitivity, 75.0% specificity, 94.5% PPV, and 69.0% negative predictive value (NPV) for detecting primary tumour. Local gastric PET/CT had 91.1% sensitivity, 91.7% specificity, 98.1% PPV, and 68.8% NPV. The mean ratio of the tumour's SUVmax/the adjacent gastric wall SUVmax was significantly increased with local gastric PET/CT. It was concluded that gastric distention might be useful for tumour visibility. However, gastric distention may not significantly improve diagnostic accuracy [5].

[¹⁸F]FDG uptake was investigated for the detection of regional lymph nodes (LNs) in preoperative GC patients (n = 156). Tumour size (≥ 3 cm) and LN metastasis were significantly associated with [¹⁸F]FDG uptake in LN. When the SUVmax of the primary tumour > 3.75, PET/CT had 73.5% sensitivity and 74.5% specificity for the detection of LN metastasis. While the SUVmax of the primary tumour > 4.35 and FDG uptake of LN was positive, PET/CT

Correspondence to: Ebru Salmanoglu
 Department of Nuclear Medicine, Kahramanmaraş Sutcu Imam University,
 Faculty of Medicine, Avsar Kampus 46040, Kahramanmaraş, Turkey
 e-mail: ebrusalmanoglu@yahoo.com

had 58.8% sensitivity and 91.6% specificity for the prediction of non-curative surgery [6].

Histopathologic characteristics of primary GC affect the FDG uptake and tumour detection rate on FDG PET/CT. In a study of 50 patients with preoperative locally advanced gastric adenocarcinoma (GA), FDG uptake of the primary tumour was investigated. Results were correlated with histopathologically. The poorly cohesive type according to the WHO classification, diffuse type according to the Lauren classification and infiltrative type according to the Ming classification had low FDG uptake in these patients. Therefore, the correlation between FDG uptake and histopathologic characteristics might be useful for FDG PET/CT imaging in GC patients [7].

Diagnostic accuracy of whole-body [¹⁸F]FDG PET/CT and regional [¹⁸F]FDG PET/CT after water gastric inflation was assessed in preoperative GC patients (n = 44). The sensitivity of whole-body PET/CT (50%) was augmented by regional PET/CT (75%) for primary tumour detection. Furthermore, the sensitivity of whole-body PET/CT (24.6%) for LN metastasis was significantly increased by regional PET/CT (36.1%). Regional PET/CT can be used to improve FDG uptake in GC patients [8].

The utility of [¹⁸F]FDG PET/CT was evaluated for progression-free survival (PFS) before therapy in GC patients (n = 321). The Low SUVmax group (≤ 5.74) had a longer mean PFS than that of the high SUVmax group (> 5.74). Stage, depth of tumour invasion, presence of LN metastasis and SUVmax (> 5.74 vs ≤ 5.74) were associated with recurrence. High SUVmax (> 5.74) and high metabolic tumour volume (MTV) (> 16.42) were poor prognostic factors for PFS [9].

The prognostic role of baseline and interim [¹⁸F]FDG PET/CT during chemotherapy was examined in patients (n = 44) with recurrent/metastatic advanced gastric cancer (AGC). Initial and change of metabolic parameters (MP)-MTV, tumour lesion glycolysis (TLG) and SUVmax and SUVmean were measured. Decreased percentage of SUVmax and SUVmean on interim PET/CT and initial values of volumetric parameters (MTV and TLG) were significant predicting factors for chemotherapy response. Furthermore, the decreased percentage values of metabolic parameters as well as maximum and mean SUV were important prognostic factors for overall survival (OS) and PFS [10].

The prediction of prognosis was investigated SUVmax of metastatic LNs using [¹⁸F]FDG PET/CT in preoperative GC patients (n = 151). Results were confirmed histologically. Nodal SUVmax was an independent prognostic factor for recurrence-free survival (RFS) and OS [11].

The metabolic affinity of primary tumours or metastatic LNs on [¹⁸F]FDG PET/CT was studied for the prediction of survival in patients (n = 168) with AGC. [¹⁸F]FDG PET/CT had 73.8% sensitivity for the detection of advanced pT ≥ 3 stages. Furthermore, [¹⁸F]FDG PET/CT had 92.2% specificity for the detection of the advanced pN (≥ 2) stage. Data showed that the [¹⁸F]FDG affinity of LNs was an independent prognostic factor for RFS [12].

TNM Staging

Imaging of LN metastasis and accurate staging is needed for effective therapy before surgery. However, accurate staging with conventional diagnostic imaging modalities such as CT is not enough due to its low sensitivity and low specificity. Therefore,

nuclear medicine imaging methods with high specificity such as [¹⁸F]FDG PET/CT are necessary to detect metastasis [13].

In a comparative retrospective study, the effect of FDG-PET for the staging of Gastric adenocarcinoma (GA) was analysed in 608 patients who had biopsy-proven GA and 207 patients who had both CT and FDG-PET. FDG-PET identified primary tumour (PT) (125 vs 120) more than CT alone. Furthermore, FDG detected distant lymph node disease (DLN) (41 vs 25) more than CT alone. In addition, FDG-PET up-staged 31 patients and down-staged 17 patients. PET/CT was more helpful than CT for the staging of GA [14].

In another comparative study, FDG PET/CT was researched in 97 histologically proven GC patients. It was reported that FDG uptake in both tumour and LN were related to poor OS. In contrast to FDG PET/CT, lymphadenomegaly was not related to OS on CT. FDG PET/CT had more prognostic importance than CT for staging [15].

A study (n = 90) reported that FDG PET/CT had 78.9% sensitivity for detecting primary GC. It was noted that T3/T4 disease had higher SUVmax than T1/T2 disease (9.0 vs 3.8) on PET/CT imaging. The SUVmax of the primary tumour was associated with tumour size. FDG-PET/CT had 64.5% sensitivity, 85.7% specificity, 71.1% accuracy, 90.9% PPV, and 52.2% NPV for evaluation of local LN metastasis [16].

[¹⁸F]FDG PET/CT was examined in non-junctional GC patients (n = 279). 80.6% of the primary tumour was FDG-avid. PET/CT detected 7% of patients that could not be shown with other imaging methods. For metastatic disease, PET/CT had 49.3% sensitivity, 97.1% specificity, 85.0% PPV, 85.4% NPV. This recent study reported that PET/CT should be used for staging and it should have a place in guidelines [17].

[¹⁸F]FDG PET/CT was analysed to image metabolically positive lymph nodes (MPLN) in patients (n = 50) with locally AGC. The numbers of MPLN were associated with the numbers of histologically positive LNs. The numbers of MPLN, PET/CT positive LN, SUVmax of LN (> 2.8), TNM stage were correlated with OS. Therefore, the number of MPLN is an important parameter for predicting the prognosis of locally AGC [18].

The relationship between FDG uptake in the primary tumour/LNs and clinicopathological factors, especially pStage III/IV were evaluated in AGC patients (n = 117). FDG uptake in primary tumour and LNs were related with pStage III/IV. FDG PET/CT had 22.7% sensitivity, 90.5% specificity for LN metastasis. FDG PET/CT had 80.4% sensitivity for the detection of pStage III/IV disease. As a result, PET/CT was a helpful modality for the evaluation of pStage III/IV [13].

In a retrospective study (n = 45), the role of F-FDG PET/CT for staging GC was compared with contrast-enhanced computed tomography (CECT). There was no significant statistical difference found between PET parameters and histotype, grading, and site of the gastric lesion. FDG PET/CT had higher specificity for both LN and distant metastasis [19].

In another retrospective study, clinicopathologic parameters that were related to [¹⁸F]FDG avidity was examined. Large tumour size, non-signet ring cell carcinoma type, and glucose transporter 1-positive expression on immunohistochemistry were strong predictive factors about [¹⁸F]FDG avidity. PET scoring system which was developed from these parameters detected [¹⁸F]FDG-avid cancer and it had 85% sensitivity and 71% specificity [20].

[¹⁸F]FDG PET/CT was compared with CECT in 45 GC patients for staging. While CECT had 92.11% sensitivity, 57.14% specificity; [¹⁸F]FDG PET/CT had 81.58% sensitivity, 85.71% specificity for detection of GC. Whereas CECT had 70.83% sensitivity, 61.90% specificity; [¹⁸F]FDG PET/CT had 58.33% sensitivity, 95.24% specificity for LN involvement. While CECT had 80% sensitivity, 62.86% specificity; [¹⁸F]FDG PET/CT had 60% sensitivity, 88.57% specificity for distant metastases. The authors stated that [¹⁸F]FDG PET/CT was helpful for the assessment of GC for the detection of the primary tumour, LN and distant metastasis [19].

[¹⁸F]FDG PET/CT was compared with CECT for staging in locally AGC patients (n=106). The combination of [¹⁸F]FDG PET/CT on CECT provided better diagnostic accuracy for imaging of both distant LN metastasis and bone metastasis [21].

Curability

The utility of FDG PET/CT was evaluated for predicting the curability of endoscopic submucosal dissection (ESD) for early GC in a first research study. EGCs (n = 210) of 199 patients were included. The detection rate of early GC with FDG PET/CT was 37.1%. In contrast to that, the detection of early GC which were not curable by ESD had 79% sensitivity, 91% specificity. It was concluded that FDG PET/CT might be a useful method secondary to endoscopy for this purpose [22].

Detection of recurrent tumours

Diagnostic performance of FDG PET/CT for surveillance was investigated in asymptomatic 190 GC patients (early GC patients: n = 115; AGC patients: n = 75) after surgery. FDG PET/CT had good diagnostic performance with 84.2% sensitivity and 87.7% specificity [23].

In another study, the diagnostic performance of [¹⁸F]FDG PET/CT was evaluated in AGC patients (n = 46) who were asymptomatic and negative on conventional imaging. Final verification was performed using clinical follow-up, tumour markers, CT, endoscopy and with/without a histopathologic diagnosis. [¹⁸F]FDG PET/CT had 100% sensitivity, 88.1% specificity, 44.4 % PPV and 100 % NPV in the patient-based analysis irrespective of the recurrence site [24].

FDG PET/CT was retrospectively compared with CECT to detect gastric carcinoma recurrence. The recurrence group (60 patients) and control group were (60 patients) were included. There was no significant difference found between these two methods for the detection of patient-based overall recurrence. On the other hand, CECT had higher sensitivity (96%) than PET/CT (50%) for imaging peritoneal carcinomatosis. Furthermore, on pathology-based analysis CECT had higher sensitivity (98%) than PET/CT (80%). Therefore, CECT might be a primary method for the detection of tumour recurrence [25].

Diagnostic performance of PET/CT was investigated in [¹⁸F]FDG-avid AGC patients (n = 368) for detection of recurrence. PET had higher sensitivity (81.0%) for [¹⁸F]FDG-avid tumours than both non-avid tumours and nonanastomosis site recurrences (52.4%). PET had high specificity (97.1% and 97.5%) in both groups [26].

In a meta-analysis study (828 patients in 14 studies) diagnostic accuracy of [¹⁸F]FDG PET for detection of GC recurrence

was examined. On a per-patient basis analysis, [¹⁸F]FDG PET had 85% sensitivity. On per-lesion basis analysis, [¹⁸F]FDG PET had 75% sensitivity [27].

The diagnostic utility of FDG PET/CT was evaluated in 279 patients. The primary tumour was FDG-avid in 80% of patients. PET/CT detected unsuspected metastases in 7% of patients. In addition, these metastases could not be detected by conventional staging without PET/CT in 5% of patients. Patients with FDG-avid nodes had an incurable disease. This retrospective study suggested that PET/CT should be considered in international recommendations [17].

Therapeutic response evaluation

Investigators evaluated the importance of PET imaging using [¹⁸F]FDG and [¹⁸F]fluoro-3'-deoxy-3'-L-fluorothymidine (FLT) for early metabolic response in AGC patients (n = 64) who were treated with chemotherapy. PET imaging was performed at baseline and 14 days after therapy beginning. FDG PET had 70% sensitivity and 83% specificity for predicting clinical response. FDG PET had 58% sensitivity and 100% specificity for predicting disease control status using with total uptake value reduction percentage (d-SUV) value. In contrast to FDG, the d-SUV value of FLT-PET was not useful for both predicting clinical response and disease control status. Decreased FDG uptake in liver metastasis helped predict both clinical response and disease control status [28].

The accuracy of FDG PET/CT to predict early pathologic response after neoadjuvant chemotherapy was analysed in 44 patients with locally advanced GC or esophagogastric junction II/III. PET/CT had 90.9% sensitivity, 47.3% specificity, and 63.3% accuracy for prediction of response [29].

Diffusion-weighted MRI (DW-MRI) and [¹⁸F]FDG PET/CT were compared for therapy response in patients with locally advanced GA (n = 17). Apparent diffusion coefficient (ADC) value and SUVmean corrected for partial volume effect were evaluated and compared with histopathological tumour regression grade. It was concluded that DW-MRI was more helpful than FDG-PET/CT for the evaluation of therapy response [30].

In a prospective study, therapy response in AGC patients (n = 74) who had lesions (n = 620) with > 1 cm on CT were included and each lesion was also assessed with [¹⁸F]FDG PET. Poorly cohesive carcinomas exhibited lower SUVmax than adenocarcinomas. Human epidermal growth factor receptor 2 (HER2)-positive tumours had higher SUVmax in comparison with HER2-negative tumours. The changes in SUVmax and total lesion glycolysis (TLG) owing to chemotherapy were associated with the changes in tumour size. Patients with a decrease in both tumour size and SUVmax had a better prognosis than patients who had only a decrease in tumour size or SUVmax [31].

Prediction of HER2 status

Surgery is often a part of the treatment of GC. However, surgery is not efficient especially for inoperable or metastatic GC patients. As a result of this, other therapy options are required for these patients [32]. Well or moderately differentiated GA, express HER2 more than poorly differentiated GA [33]. This is important to predict HER2 status for HER2-targeted molecular therapy.

PET/CT plays a leading role in predicting the therapy response of various cancers [32].

Association between [¹⁸F]FDG uptake and HER2 expression was evaluated in 64 GC patients. SUVmax and tumour differentiation was correlated with HER2 expression. When a SUVmax = 6.2 as a cut off value was used, [¹⁸F]FDG PET/CT had 64.4% accuracy for predicting the HER2 expression. [¹⁸F]FDG PET/CT also might help predict HER-2 targeted therapy response. However, further prospective studies are still needed to understand its potential [32].

In a research study, it was found that (n = 124) HER2-positive GCs had higher SUVmax (median = 12.1) than HER2-negative (median = 7.4) GCs. FDG PET/CT volume-based parameters can play a role in both HER2-positive GCs and HER2-negative cancers for predicting the prognosis of AGC [34]. However, in another study (n = 31), that firstly compared SUVmax and HER2 status in age-matched and sex-matched patients with GC and gastroesophageal junction adenocarcinomas (GEJC), SUVmax was not correlated with HER2 status of both cancer types. High SUVmax was correlated with decreased OS. Nonetheless, larger cohort studies are still needed to validate this result [35].

Conclusions

GC still has high mortality and is responsible for cancer-related deaths worldwide. Patients are asymptomatic at an early stage of GC. Early screening tests have vital importance for cancer patients. Unfortunately, there is no routine screening test for GC in daily clinical practice. On the other hand, new various screening biomarkers in the blood are still in progress and these studies are could not be applied to patients. Therefore, most of the cases diagnosed at the late stage which patients had an incurable disease. Even though diagnostic imaging modalities improved with current technology in this century, early and accurate detection of GC is still challenging for clinicians. Accurate staging and assessment of treatment response are important for a patient's lifetime. PET/CT is a noninvasive imaging modality that is important for TNM staging especially for detection of distant metastasis, evaluation of therapy response, curability, detection of recurrent tumours. However, some pathological types of gastric tumours are not FDG avid and these tumours may not be detectable on PET/CT images. Although this disadvantage, PET/CT hybrid imaging method has a great contribution to the management of these patients.

Acknowledgements

Not applicable.

Funding

Any support for the work in the form of grants, equipment or drugs: not applicable.

References

- Bray F, Ferlay J, Soerjomataram I, et al. Global cancer statistics 2018: GLOBOCAN estimates of incidence and mortality worldwide for 36 cancers in 185 countries. *CA Cancer J Clin*. 2018; 68(6): 394–424, doi: [10.3322/caac.21492](https://doi.org/10.3322/caac.21492), indexed in Pubmed: [30207593](https://pubmed.ncbi.nlm.nih.gov/30207593/).
- Ajani JA, D'Amico TA, Almhanna K, et al. Gastric cancer, version 3.2016, NCCN clinical practice guidelines in oncology. *J Natl Compr Canc Netw*. 2016; 14(10): 1286–1312, doi: [10.6004/jnccn.2016.0137](https://doi.org/10.6004/jnccn.2016.0137), indexed in Pubmed: [27697982](https://pubmed.ncbi.nlm.nih.gov/27697982/).
- Minamimoto R, Senda M, Jinnouchi S, et al. Performance profile of a FDG-PET cancer screening program for detecting gastric cancer: results from a nationwide Japanese survey. *Jpn J Radiol*. 2014; 32(5): 253–259, doi: [10.1007/s11604-014-0294-0](https://doi.org/10.1007/s11604-014-0294-0), indexed in Pubmed: [24562822](https://pubmed.ncbi.nlm.nih.gov/24562822/).
- Cui J, Zhao P, Ren Z, et al. Evaluation of dual time point imaging 18F-FDG PET/CT in differentiating malignancy from benign gastric disease. *Medicine (Baltimore)*. 2015; 94(33): e1356, doi: [10.1097/MD.0000000000001356](https://doi.org/10.1097/MD.0000000000001356), indexed in Pubmed: [26287421](https://pubmed.ncbi.nlm.nih.gov/26287421/).
- Ma Q, Xin J, Zhao Z, et al. Value of ¹⁸F-FDG PET/CT in the diagnosis of primary gastric cancer via stomach distension. *Eur J Radiol*. 2013; 82(6): e302–e306, doi: [10.1016/j.ejrad.2013.01.021](https://doi.org/10.1016/j.ejrad.2013.01.021), indexed in Pubmed: [23434453](https://pubmed.ncbi.nlm.nih.gov/23434453/).
- Choi JY, Shim KN, Kim SE, et al. The clinical value of 18F-fluorodeoxyglucose uptake on positron emission tomography/computed tomography for predicting regional lymph node metastasis and non-curative surgery in primary gastric carcinoma. *Korean J Gastroenterol*. 2014; 64(6): 340–347, doi: [10.4166/kjg.2014.64.6.340](https://doi.org/10.4166/kjg.2014.64.6.340), indexed in Pubmed: [25530585](https://pubmed.ncbi.nlm.nih.gov/25530585/).
- Kim HW, Won KS, Song BI, et al. Correlation of primary tumor FDG uptake with histopathologic features of advanced gastric cancer. *Nucl Med Mol Imaging*. 2015; 49(2): 135–142, doi: [10.1007/s13139-015-0327-3](https://doi.org/10.1007/s13139-015-0327-3), indexed in Pubmed: [26085859](https://pubmed.ncbi.nlm.nih.gov/26085859/).
- Lee SJ, Lee WW, Yoon HJ, et al. Regional PET/CT after water gastric inflation for evaluating loco-regional disease of gastric cancer. *Eur J Radiol*. 2013; 82(6): 935–942, doi: [10.1016/j.ejrad.2013.01.014](https://doi.org/10.1016/j.ejrad.2013.01.014), indexed in Pubmed: [23410909](https://pubmed.ncbi.nlm.nih.gov/23410909/).
- Kim J, Lim ST, Na CJ, et al. Pretreatment F-18 FDG PET/CT parameters to evaluate progression-free survival in gastric cancer. *Nucl Med Mol Imaging*. 2014; 48(1): 33–40, doi: [10.1007/s13139-013-0243-3](https://doi.org/10.1007/s13139-013-0243-3), indexed in Pubmed: [24900136](https://pubmed.ncbi.nlm.nih.gov/24900136/).
- Lee SY, Seo HJ, Kim S, et al. Prognostic significance of interim F-fluorodeoxyglucose positron emission tomography-computed tomography volumetric parameters in metastatic or recurrent gastric cancer. *Asia Pac J Clin Oncol*. 2018; 14(5): e302–e309, doi: [10.1111/ajco.12833](https://doi.org/10.1111/ajco.12833), indexed in Pubmed: [29226597](https://pubmed.ncbi.nlm.nih.gov/29226597/).
- Song BI, Kim HW, Won KS, et al. Preoperative standardized uptake value of metastatic lymph nodes measured by 18F-FDG PET/CT improves the prediction of prognosis in gastric cancer. *Medicine (Baltimore)*. 2015; 94(26): e1037, doi: [10.1097/MD.0000000000001037](https://doi.org/10.1097/MD.0000000000001037), indexed in Pubmed: [26131811](https://pubmed.ncbi.nlm.nih.gov/26131811/).
- Kwon HW, An L, Kwon HR, et al. Preoperative nodal F-FDG avidity rather than primary tumor avidity determines the prognosis of patients with advanced gastric cancer. *J Gastric Cancer*. 2018; 18(3): 218–229, doi: [10.5230/jgc.2018.18.e23](https://doi.org/10.5230/jgc.2018.18.e23), indexed in Pubmed: [30275999](https://pubmed.ncbi.nlm.nih.gov/30275999/).
- Kudou M, Kosuga T, Kubota T, et al. Value of preoperative PET-CT in the prediction of pathological stage of gastric cancer. *Ann Surg Oncol*. 2018; 25(6): 1633–1639, doi: [10.1245/s10434-018-6455-0](https://doi.org/10.1245/s10434-018-6455-0), indexed in Pubmed: [29626306](https://pubmed.ncbi.nlm.nih.gov/29626306/).
- Serrano OK, Love C, Goldman I, et al. The value of FDG-PET in the staging of gastric adenocarcinoma: A single institution retrospective review. *J Surg Oncol*. 2016; 113(6): 640–646, doi: [10.1002/jso.24190](https://doi.org/10.1002/jso.24190), indexed in Pubmed: [27115836](https://pubmed.ncbi.nlm.nih.gov/27115836/).
- Coupe NA, Karikios D, Chong S, et al. Metabolic information on staging FDG-PET-CT as a prognostic tool in the evaluation of 97 patients with gastric cancer. *Ann Nucl Med*. 2014; 28(2): 128–135, doi: [10.1007/s12149-013-0791-8](https://doi.org/10.1007/s12149-013-0791-8), indexed in Pubmed: [24297388](https://pubmed.ncbi.nlm.nih.gov/24297388/).
- Namikawa T, Okabayshi T, Nogami M, et al. Assessment of (18)F-fluorodeoxyglucose positron emission tomography combined with computed tomography in the preoperative management of patients with gastric cancer. *Int J Clin Oncol*. 2014; 19(4): 649–655, doi: [10.1007/s10147-013-0598-6](https://doi.org/10.1007/s10147-013-0598-6), indexed in Pubmed: [23877653](https://pubmed.ncbi.nlm.nih.gov/23877653/).

17. Findlay JM, Antonowicz S, Segaran A, et al. Routinely staging gastric cancer with F-FDG PET-CT detects additional metastases and predicts early recurrence and death after surgery. *Eur Radiol.* 2019; 29(5): 2490–2498, doi: [10.1007/s00330-018-5904-2](https://doi.org/10.1007/s00330-018-5904-2), indexed in Pubmed: [30643947](https://pubmed.ncbi.nlm.nih.gov/30643947/).
18. Wang X, Wei Y, Xue Y, et al. Predictive role of the number of 18f-fdg-positive lymph nodes detected by PET/CT for pre-treatment evaluation of locally advanced gastric cancer. *PLoS One.* 2016; 11(12): e0166836, doi: [10.1371/journal.pone.0166836](https://doi.org/10.1371/journal.pone.0166836), indexed in Pubmed: [27936109](https://pubmed.ncbi.nlm.nih.gov/27936109/).
19. Altini C, Niccoli Asabella A, Di Palo A, et al. 18F-FDG PET/CT role in staging of gastric carcinomas: comparison with conventional contrast enhancement computed tomography. *Medicine (Baltimore).* 2015; 94(20): e864, doi: [10.1097/MD.0000000000000864](https://doi.org/10.1097/MD.0000000000000864), indexed in Pubmed: [25997066](https://pubmed.ncbi.nlm.nih.gov/25997066/).
20. Kaneko Y, Murray WK, Link E, et al. Improving patient selection for 18F-FDG PET scanning in the staging of gastric cancer. *J Nucl Med.* 2015; 56(4): 523–529, doi: [10.2967/jnumed.114.150946](https://doi.org/10.2967/jnumed.114.150946), indexed in Pubmed: [25745094](https://pubmed.ncbi.nlm.nih.gov/25745094/).
21. Kawanaka Y, Kitajima K, Fukushima K, et al. Added value of pretreatment (18)F-FDG PET/CT for staging of advanced gastric cancer: Comparison with contrast-enhanced MDCT. *Eur J Radiol.* 2016; 85(5): 989–995, doi: [10.1016/j.ejrad.2016.03.003](https://doi.org/10.1016/j.ejrad.2016.03.003), indexed in Pubmed: [27130061](https://pubmed.ncbi.nlm.nih.gov/27130061/).
22. Chung HW, Kim JH, Sung IK, et al. FDG PET/CT to predict the curability of endoscopic resection for early gastric cancer. *J Cancer Res Clin Oncol.* 2019; 145(3): 759–764, doi: [10.1007/s00432-018-02832-9](https://doi.org/10.1007/s00432-018-02832-9), indexed in Pubmed: [30603905](https://pubmed.ncbi.nlm.nih.gov/30603905/).
23. Lee JW, Lee SM, Son MW, et al. Diagnostic performance of FDG PET/CT for surveillance in asymptomatic gastric cancer patients after curative surgical resection. *Eur J Nucl Med Mol Imaging.* 2016; 43(5): 881–888, doi: [10.1007/s00259-015-3249-5](https://doi.org/10.1007/s00259-015-3249-5), indexed in Pubmed: [26611426](https://pubmed.ncbi.nlm.nih.gov/26611426/).
24. Lee DY, Lee CH, Seo MJ, et al. Performance of (18)F-FDG PET/CT as a post-operative surveillance imaging modality for asymptomatic advanced gastric cancer patients. *Ann Nucl Med.* 2014; 28(8): 789–795, doi: [10.1007/s12149-014-0871-4](https://doi.org/10.1007/s12149-014-0871-4), indexed in Pubmed: [24965850](https://pubmed.ncbi.nlm.nih.gov/24965850/).
25. Kim JH, Heo SH, Kim JW, et al. Evaluation of recurrence in gastric carcinoma: Comparison of contrast-enhanced computed tomography and positron emission tomography/computed tomography. *World J Gastroenterol.* 2017; 23(35): 6448–6456, doi: [10.3748/wjg.v23.i35.6448](https://doi.org/10.3748/wjg.v23.i35.6448), indexed in Pubmed: [29085194](https://pubmed.ncbi.nlm.nih.gov/29085194/).
26. Kim SJ, Cho YS, Moon SH, et al. Primary tumor ¹ F-FDG avidity affects the performance of ¹ F-FDG PET/CT for detecting gastric cancer recurrence. *J Nucl Med.* 2016; 57(4): 544–550, doi: [10.2967/jnumed.115.163295](https://doi.org/10.2967/jnumed.115.163295), indexed in Pubmed: [26678615](https://pubmed.ncbi.nlm.nih.gov/26678615/).
27. Li P, Liu Q, Wang C, et al. Fluorine-18-fluorodeoxyglucose positron emission tomography to evaluate recurrent gastric cancer after surgical resection: a systematic review and meta-analysis. *Ann Nucl Med.* 2016; 30(3): 179–187, doi: [10.1007/s12149-016-1058-y](https://doi.org/10.1007/s12149-016-1058-y), indexed in Pubmed: [26830546](https://pubmed.ncbi.nlm.nih.gov/26830546/).
28. Wang C, Guo W, Zhou M, et al. The predictive and prognostic value of early metabolic response assessed by positron emission tomography in advanced gastric cancer treated with chemotherapy. *Clin Cancer Res.* 2016; 22(7): 1603–1610, doi: [10.1158/1078-0432.CCR-14-3235](https://doi.org/10.1158/1078-0432.CCR-14-3235), indexed in Pubmed: [26607599](https://pubmed.ncbi.nlm.nih.gov/26607599/).
29. Schneider PM, Eshmuninov D, Rordorf T, et al. FDG-PET-CT identifies histopathological non-responders after neoadjuvant chemotherapy in locally advanced gastric and cardia cancer: cohort study. *BMC Cancer.* 2018; 18(1): 548, doi: [10.1186/s12885-018-4477-4](https://doi.org/10.1186/s12885-018-4477-4), indexed in Pubmed: [29743108](https://pubmed.ncbi.nlm.nih.gov/29743108/).
30. Giganti F, De Cobelli F, Canevari C, et al. Response to chemotherapy in gastric adenocarcinoma with diffusion-weighted MRI and (18) F-FDG-PET/CT: correlation of apparent diffusion coefficient and partial volume corrected standardized uptake value with histological tumor regression grade. *J Magn Reson Imaging.* 2014; 40(5): 1147–1157, doi: [10.1002/jmri.24464](https://doi.org/10.1002/jmri.24464), indexed in Pubmed: [24214734](https://pubmed.ncbi.nlm.nih.gov/24214734/).
31. Park S, Ha S, Kwon HW, et al. Prospective evaluation of changes in tumor size and tumor metabolism in patients with advanced gastric cancer undergoing chemotherapy: association and clinical implication. *J Nucl Med.* 2017; 58(6): 899–904, doi: [10.2967/jnumed.116.182675](https://doi.org/10.2967/jnumed.116.182675), indexed in Pubmed: [28572288](https://pubmed.ncbi.nlm.nih.gov/28572288/).
32. Chen R, Zhou X, Liu J, et al. Relationship between 18F-FDG PET/CT findings and HER2 expression in gastric cancer. *J Nucl Med.* 2016; 57(7): 1040–1044, doi: [10.2967/jnumed.115.171165](https://doi.org/10.2967/jnumed.115.171165), indexed in Pubmed: [26966162](https://pubmed.ncbi.nlm.nih.gov/26966162/).
33. Laboissiere RS, Buzelin MA, Balabram D, et al. Association between HER2 status in gastric cancer and clinicopathological features: a retrospective study using whole-tissue sections. *BMC Gastroenterol.* 2015; 15: 157, doi: [10.1186/s12876-015-0384-1](https://doi.org/10.1186/s12876-015-0384-1), indexed in Pubmed: [26530403](https://pubmed.ncbi.nlm.nih.gov/26530403/).
34. Park JS, Lee N, Beom SH, et al. The prognostic value of volume-based parameters using F-FDG PET/CT in gastric cancer according to HER2 status. *Gastric Cancer.* 2018; 21(2): 213–224, doi: [10.1007/s10120-017-0739-0](https://doi.org/10.1007/s10120-017-0739-0), indexed in Pubmed: [28643145](https://pubmed.ncbi.nlm.nih.gov/28643145/).
35. Celli R, Colunga M, Patel N, et al. Metabolic signature on 18F-FDG PET/CT, HER2 status, and survival in gastric adenocarcinomas. *J Nucl Med Technol.* 2016; 44(4): 234–238, doi: [10.2967/jnmt.116.181479](https://doi.org/10.2967/jnmt.116.181479), indexed in Pubmed: [27789750](https://pubmed.ncbi.nlm.nih.gov/27789750/).

Presentation of genital tuberculosis detected on [¹⁸F]FDG PET-CT scan resembling a primary gynaecological tumour and metastases

Inci Uslu Biner¹, Ebru Tatci¹, Ozlem Ozmen¹, Mujgan Guler², Fatma Benli³

¹Department of Nuclear Medicine, Ataturk Chest Diseases and Thoracic Surgery Training and Research Hospital, Ankara, Turkey

²Department of Chest Diseases, Ataturk Chest Diseases and Thoracic Surgery Training and Research Hospital, Ankara, Turkey

³Department of Pathology, Ataturk Chest Diseases and Thoracic Surgery Training and Research Hospital, Ankara, Turkey

[Received 11 XII 2020; Accepted 04 VI 2021]

Abstract

This report presents [¹⁸F]Fluorodeoxyglucose ([¹⁸F]FDG) positron emission tomography-computed tomography (PET-CT) findings of a 33-year-old woman before and after tuberculostatic therapy. Tuberculosis (TB) should be kept in mind in the differential diagnosis of [¹⁸F]FDG avid lesions in the genital tract.

KEY words: genital tuberculosis; [¹⁸F]FDG PET/CT; extrapulmonary tuberculosis; therapeutic response to tuberculostatic treatment

Nucl Med Rev 2021; 24, 2: 104–105

A 33-year-old female presented at the hospital with a complaint of pelvic pain and tenderness in the right lower quadrant. Abdominal Computed Tomography (CT) revealed multiple enlarged abdominal lymph nodes.

¹⁸F-Fluorodeoxyglucose ([¹⁸F]FDG) positron emission tomography-computed tomography (PET-CT) was performed with suspicion of malignancy.

Maximum intensity projection (MIP) PET images (Fig. 1G) and sectional CT and PET-CT images showed increased radiotracer uptakes at right ovoid mass with a Maximum Standardised Uptake Value (SUV max) of 15.70 and endometrial wall thickening and intracavitary mass that extends to vagina with SUV max of 15.09. Additionally, several enlarged nodes with increased FDG uptakes prominently in abdominopelvic regions (Fig. 1A–D) and diffuse reticulonodular infiltrates and nodules randomly distributed in both lungs. prominently in upper lobes with mild FDG uptakes (Fig. 1E–F) were detected.

Histopathological examination of the cervical biopsy showed granulomatous inflammation (Fig. 2). Findings suggested multi-systemic tuberculosis.

Follow-up PET-CT examination after 9 months of tuberculostatic treatment showed diminished nodal uptakes and a complete metabolic response in endometrium and right adnexal mass. There was also regression in most of the lung parenchymal lesions (Fig. 3A–G).

Genital tuberculosis (TB) is frequently seen among women of reproductive age. It is mostly transmitted to the genital tract haematogenously from pulmonary or other sites of TB. The fallopian tubes are mostly affected organs followed by endometrial and ovarian involvement. Vagina, vulva and cervix are rarely involved. Atypical clinical signs such as infertility, menstrual irregularities and pelvic pain may be seen. Standard anti-tuberculous drugs are used to treat genital TB and higher response rates are reported.

[¹⁸F]FDG accumulates at the sites of infection and inflammation via increased glucose metabolism of activated inflammatory and infectious cells. So, [¹⁸F]FDG PET-CT is an additive, useful imaging modality in both diagnosis and monitoring response to therapy of infectious-inflammatory diseases such as tuberculosis. This case is discussed in order to emphasize the importance of considering the possibility of tuberculosis in the differential diagnosis of [¹⁸F]FDG avid malignant appearing lesions in the genital tract detected on [¹⁸F]FDG PET-CT scan.

Correspondence to: Inci Uslu Biner
Department of Nuclear Medicine, Ataturk Chest Diseases and Thoracic Surgery Training and Research Hospital, Sanatoryum Cad. 06280, Kecloren, Ankara, Turkey, phone: +90 312 567 73 42; +90 532 7932521
e-mail: inciustlu@yahoo.com

This article is available in open access under Creative Common Attribution-Non-Commercial-No Derivatives 4.0 International (CC BY-NC-ND 4.0) license, allowing to download articles and share them with others as long as they credit the authors and the publisher, but without permission to change them in any way or use them commercially.

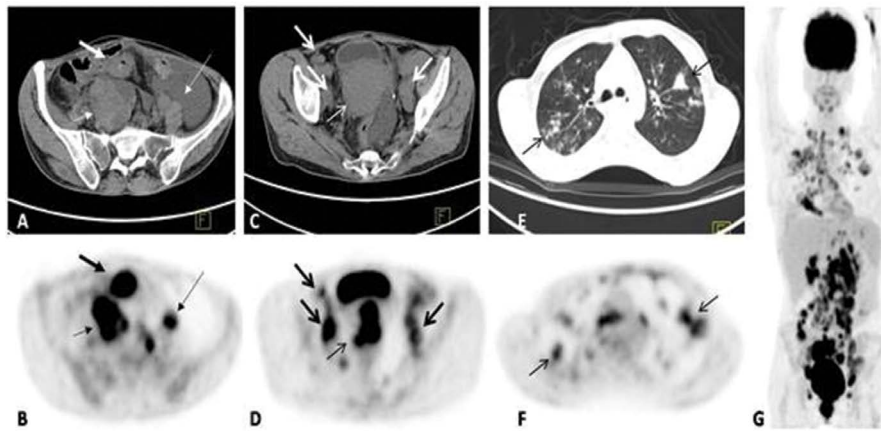


Figure 1. [¹⁸F]FDG PET-CT scan showing increased [¹⁸F]FDG uptakes at right ovo adnexal mass, endometrium [Maximum Standardised Uptake Value (SUVmax)] 15.70 and 15.09 respectively; **A–D.** Thin white and black arrows; lymph nodes at several regions prominently in abdominopelvic regions (SUVmax 13.16); **C, D.** White and black thick arrows and parenchymal lung lesions (SUVmax 9.96); **E, F.** Arrows; Intense accumulation of [¹⁸F]FDG in multiple lymph nodes, both lungs and genital tract can completely be seen on Maximum intensity projection image (MIP) of [¹⁸F]FDG PET/CT scan (**G**)

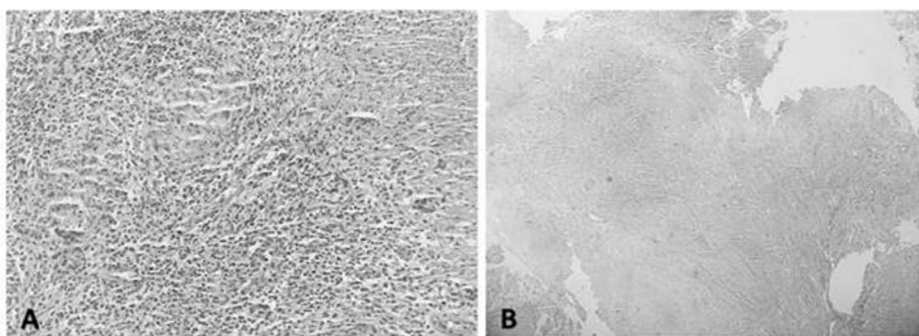


Figure 2. Cervical biopsy showing granulomatous inflammation

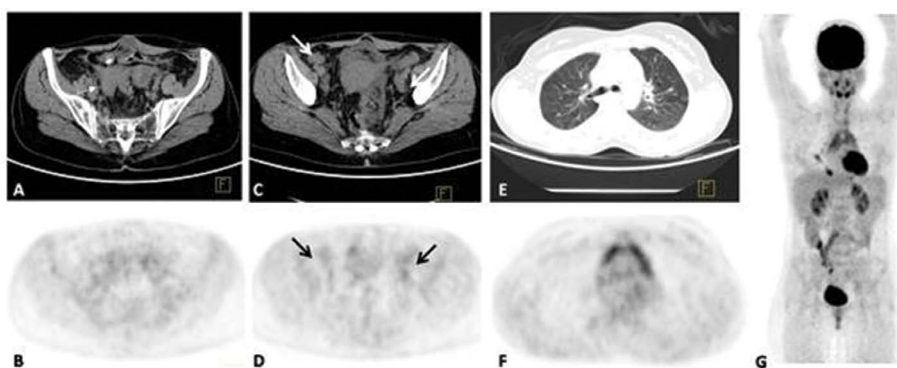


Figure 3. Follow-up [¹⁸F]FDG PET-CT scan showing prominent metabolic response to tuberculostatic treatment

Conflict of interest

The authors declare that they have no conflict of interest.

Informed consent

Informed consent was obtained from the patient included in this report.

Incidental finding of a dermoid cyst in a whole-body iodine scan: importance of using [¹³¹I]SPECT/CT in the differentiated thyroid carcinoma

Hadis Mohammadzadeh Kosari¹, Seyed Rasoul Zakavi¹, Somayeh Barashki¹, Hesamoddin Roustaei Firouzabad¹, Saeedeh Ataei Nakhai¹, Kamran Aryana¹

Nuclear Medicine Research Center, School of Medicine, Mashhad University of Medical Sciences, Mashhad, Iran

[Received 12 I 2021; Accepted 15 III 2021]

Abstract

A 33-year-old female with a history of total thyroidectomy for papillary thyroid carcinoma was referred to the nuclear medicine department for ablative radioiodine therapy. Post ablation scan showed an area of intense iodine uptake on the left side of the pelvic region, corresponding to the large well-defined heterogeneous mass in the left ovary in the SPECT/CT images. The radiologic features of this lesion were compatible with a dermoid cyst, previously unrecognized. Eventually, the lesion was laparoscopically removed, and a typical dermoid cyst was confirmed through histopathologic assessment.

KEY words: papillary thyroid carcinoma; whole-body radioiodine scan; dermoid cyst; false-positive

Nucl Med Rev 2021; 24, 2: 106–107

Introduction

A whole-body scan (WBS) with ¹³¹I-radioiodine is a sensitive procedure for detecting thyroid remnants and metastatic disease in differentiated thyroid cancer. However, there are several potential pitfalls that can cause misinterpretation. This report presents the incidental finding of a dermoid cyst with radioiodine uptake on post-ablation radioiodine scan. This case underlines the importance of performing a post-ablation SPECT/CT scan in finding the potential causes of abnormal or unusual uptake patterns in ¹³¹I-WBS.

Case report

The patient, a 33-year-old female with a history of total thyroidectomy for papillary thyroid carcinoma (pT1bN0aMx with extrathyroidal

extension), was referred to the nuclear medicine department for ablative radioiodine therapy. At the time of radioiodine therapy (RIT), stimulated serum thyroglobulin and anti-thyroglobulin antibodies were 21 ng/mL and 36, respectively. Eight days after oral administration of 150 mCi (5550 MBq) of I-131, WBS was performed by a dual-head variable angle gamma camera (GE Healthcare) equipped with a high-energy parallel-hole collimator. The post-therapy WBS showed areas of intense iodine uptake in the midline of the neck and on the left side of the pelvic region (Fig. 1). SPECT/CT images confirmed central neck uptake in the thyroid tissue and the thyroglossal duct remnant (Fig. 2) and also localized a focal intense uptake in the left pelvic fossa to the well-defined heterogeneously mass (5 × 6 cm) in the left ovary, which was containing fat, fluid, and calcification. The radiologic features of this lesion were compatible with the teratoma ovary, previously unrecognized (Fig. 3).

In this case, due to ectopic thyroid tissue, the level of serum thyroglobulin was unreliable in the follow of the thyroid carcinoma. The metastatic papillary thyroid carcinoma or malignant transformation of the ectopic thyroid tissue cannot be distinguished from normal thyroid tissue in the ovarian cyst [1–3]. Considering this issue and unpredictable thyroglobulin level, the patient was referred

Correspondence to: Kamran Aryana
Nuclear Medicine Research Center, School of Medicine, Mashhad
University of Medical Sciences, Mashhad, Iran
e-mail: aryanak@mums.ac.ir

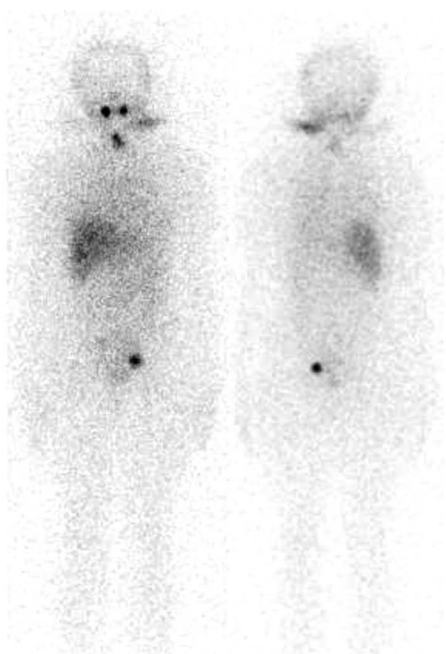


Figure 1. A whole-body iodine scan demonstrated two focal zones of radio-iodine uptake in the midline of the neck and left side of the pelvic region. Also, the scan showed Horizontal line uptake on both sides of the neck, compatible with the hair contamination in the SPECT/CT images

for surgery. The lesion was laparoscopically removed, and a typical dermoid cyst was confirmed by histopathologic assessment. Serum thyroglobulin dropped to normal levels about one month after the surgery (< 0.04 ng/mL).

Conflict of interest

The authors declare that they do not have any conflict of interest.

References

1. Campenni A, Giovinazzo S, Tuccari G, et al. Abnormal radioiodine uptake on post-therapy whole body scan and sodium/iodine symporter expression in a dermoid cyst of the ovary: report of a case and review of the literature. *Arch Endocrinol Metab.* 2015; 59(4): 351–354, doi: [10.1590/2359-3997000000087](https://doi.org/10.1590/2359-3997000000087), indexed in Pubmed: [26331324](https://pubmed.ncbi.nlm.nih.gov/26331324/).
2. Mebarki M, Menemani A, Medjahedi A, et al. Radioiodine accumulation in a giant ovarian cystadenofibroma detected incidentally by ^{131}I whole body scans. *Case Rep Radiol.* 2012; 2012: 295617, doi: [10.1155/2012/295617](https://doi.org/10.1155/2012/295617), indexed in Pubmed: [23119215](https://pubmed.ncbi.nlm.nih.gov/23119215/).
3. Oporto M, Orta N, Cepa F, et al. Captación de yoduro sódico ^{131}I en un teratoma ovárico. *Revista Española de Medicina Nuclear e Imagen Molecular.* 2018; 37(1): 50–51, doi: [10.1016/j.remnm.2017.06.005](https://doi.org/10.1016/j.remnm.2017.06.005).



Figure 2. SPECT/CT images revealed a focal zone of iodine uptake in the midline of the upper cervical region, compatible with the thyroglossal duct remnant

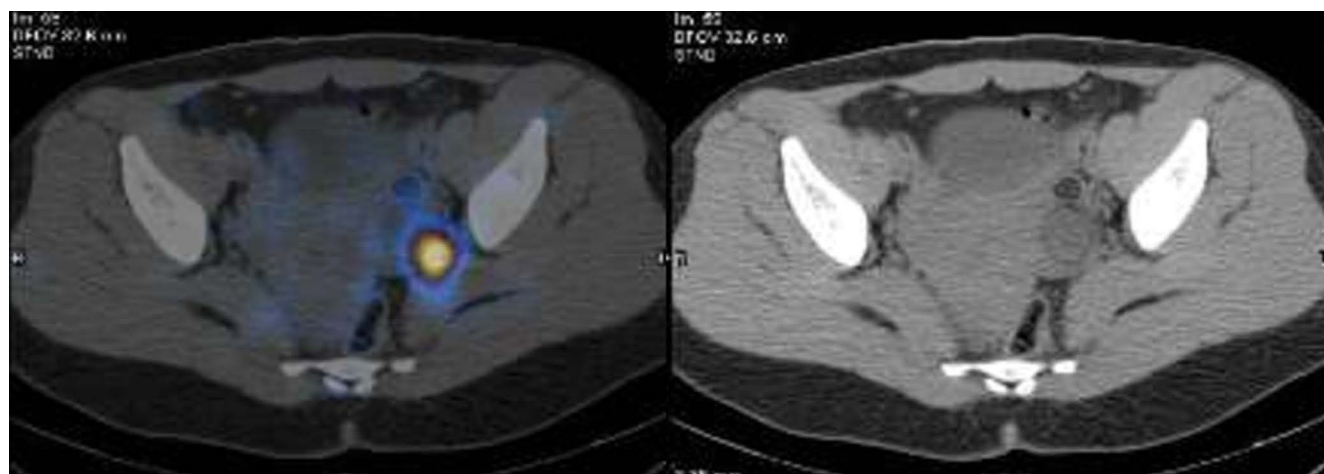


Figure 3. SPECT/CT images revealed a focal zone of iodine uptake on the left side of the pelvic cavity, corresponding to the well-defined heterogeneous mass (5 × 6 cm), which was containing fat, fluid, and amorphous calcification in the left ovary in the CT slices

[¹⁸F]FDG PET-CT findings in an unusual case of synchronous double primary lung cancer of different histologies

Punit Sharma¹ , Indranil Ghosh²

¹Department of Nuclear Medicine and PET-CT, Apollo Gleneagles Hospitals, Kolkata, India

²Department of Medical Oncology, Apollo Gleneagles Hospital, Kolkata, India

[Received 6 II 2021; Accepted 15 III 2021]

Abstract

Double primary lung cancer (DPLC) is a rare occurrence of primaries of different histologies or the same histology in different lobes in absence of advanced nodal or distant metastasis. It could be synchronous or metachronous. They are frequently misdiagnosed as metastasis or recurrence. This study presents the staging [¹⁸F]Fluorodeoxyglucose positron emission tomography-computed tomography findings in a case of a 74-year-old man with DPLC of different histologies.

KEY words: [¹⁸F]FDG; PET-CT; lung cancer; double primary; staging

Nucl Med Rev 2021; 24, 2: 108–109

A 74-year-old man presented at the hospital with a history of cough of 6-week duration. There was no fever or weight loss. He was a heavy smoker but had quit smoking 18 years back. Chest X-ray showed two large, rounded lung opacities, one in the left lower zone and another in the right lung mid-zone. A transbronchial needle sampling was performed from the left lung mass, which showed small cell lung cancer (SCLC), positive for synaptophysin and chromogranin A. Bronchoalveolar lavage from the left lung was negative for malignant cells. Contrast-enhanced [¹⁸F]Fluorodeoxyglucose ([¹⁸F]FDG) positron emission tomography-computed tomography (PET-CT) was subsequently performed for staging. Maximum intensity projection PET images (A) showing two rounded areas of intense [¹⁸F]FDG uptake in the thorax, one in the right lung (arrow) and another in the left lung, close to mediastinum (broken arrow) (Fig 1). No other abnormal focus of [¹⁸F]FDG uptake is seen in the rest of the body. Transaxial CT (B) and PET-CT (C) images of the thorax showing a peripheral, thick-walled, cavitary mass in the posterior segment of the right lung upper lobe, measuring 3.4 × 2.5 cm and showing intense [¹⁸F]FDG uptake (arrow, SUV max 15.4). Transaxial CT (D) and PET-CT (E) images of the

thorax also show another solid soft tissue mass in the left lung lower lobe anteromedial segment, measuring 4.9 × 4.5 cm with intense [¹⁸F]FDG uptake (broken arrow, SUV max 16.3). There was no nodal or distant metastasis. Based on the PET-CT findings, especially because of different morphological characteristics of two lung masses and lack of nodal or distant metastasis, suspicion of double primary lung carcinoma (DPLC) was raised. A CT guided biopsy from the right lung mass was then performed which showed non-small cell lung carcinoma (NSCLC), squamous cell type. Thus, the final diagnosis was synchronous DPLC with different histologies, SCLC of the left lung (limited stage) and NSCLC of the right lung (stage IB). The patient was treated with chemo-radiotherapy for right lung squamous cell carcinoma and chemotherapy followed by primary cranial irradiation for left lung SCLC.

DPLC is an unusual occurrence of either primary lung cancers of different histologies and/or molecular features, or the appearance of the same histological lung primary in different lobes, but without N2/3 nodal or distant metastasis. Depending on the temporal evolution, DPLC can be either synchronous or metachronous. The reported incidence of synchronous DPLC is about 0.5%. It is often misdiagnosed as metastasis or recurrence. Since these patients usually don't have advanced nodal or distant metastasis, this misdiagnosis puts them into therapeutic arms with palliative rather than curative intent. It has been shown that aggressive treatment in DPLC can yield good survival. [¹⁸F]FDG PET-CT is now an integral part of the management of lung carcinoma for staging, response evaluation, restaging and surveillance. Therefore, when

Correspondence to: Punit Sharma
Department of Nuclear Medicine and PET-CT, Apollo Gleneagles Hospitals,
Kolkata, India
e-mail: dr_punitsharma@yahoo.com

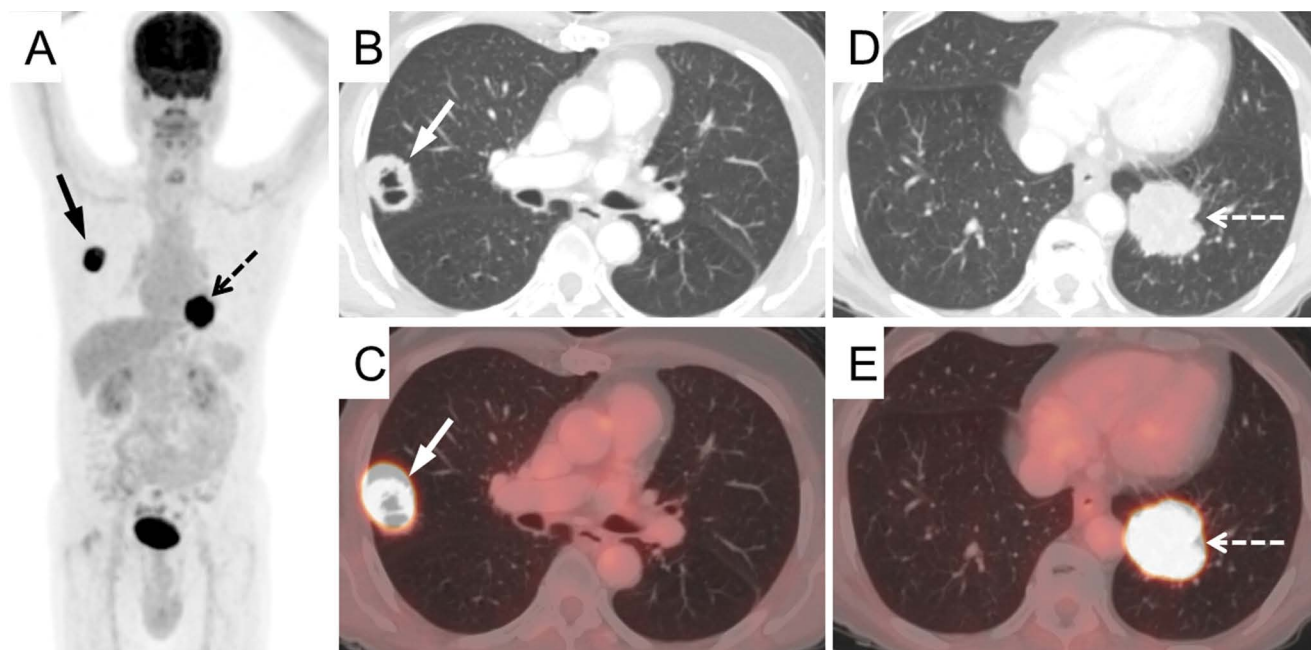


Figure 1. Positron emission tomography-computed tomography (PET-CT) images of the patient

evaluating PET-CT images in such clinical scenarios, the possibility of DPLC should be kept in mind and pointed out as was done in the present case, as that can have a significant impact on management and prognosis.

Conflict of interest

The authors declare that they do not have any conflict of interest.

Incidental detection of COVID-19 associated pneumonia by [^{99m}Tc]UBI scintigraphy

Fariba Jafari¹ , Mehrosadat Alavi^{1,2}

¹Department of Nuclear Medicine, Medicine School, Shiraz University of Medical Sciences, Shiraz, Iran

²Ionizing and Nonionizing Radiation Protection Research Center (INIRPRC), Shiraz University of Medical Sciences, Shiraz, Iran

[Received 14 II 2021; Accepted 15 III 2021]

Abstract

A 31-year-old woman who had multiple orthopedic surgeries on the left lower limb and recently suffered from pain and redness in the lateral left lower thigh was referred to the hospital to rule out osteomyelitis by [^{99m}Tc]UBI scintigraphy. Except soft tissue inflammation in the mentioned region, the scan showed significant and diffuse both lungs uptake incidentally. The patient had experienced symptoms of COVID-19 disease recently. Chest HRCT scan also revealed multiple segmental ground-glass opacities (GGOs) which were typical features for lung involvement of COVID-19 associated pneumonia.

KEY words: COVID-19; pneumonia; UBI scintigraphy

Nucl Med Rev 2021; 24, 2: 110–112

The authors report a case of a 31-year-old woman with a history of multiple orthopaedic surgeries on the left lower extremity and insertion of hardware implant in the left femur due to limb deformity in the past years. She surgically had been removed femoral device about 4 years ago. Recently she developed pain, redness and oedema in the lateral left lower thigh. Laboratory assays revealed high erythrocyte sedimentation rate (ESR) (68 mm/h) and C Reactive Protein (CRP) (21 Mg/L) levels, normal WBC count, without specific finding on plain radiography of left femur and knee. She was referred to rule out osteomyelitis by [^{99m}Tc]Ubiquidine (UBI) scintigraphy.

UBI scan was performed immediately after IV injection of 740 MBq (20 mCi) [^{99m}Tc]UBI, dynamic images of bilateral femora and knees were obtained for 30 minutes followed by whole-body and static images in 30 minutes, 1 and 2 hours. The scan revealed soft tissue inflammation of the lateral aspect of the left lower thigh, without evidence of osteomyelitis. In whole-body planar images significant, diffuse [^{99m}Tc]UBI uptake in both lungs fields was observed incidentally. (Fig. 1A, B) Regarding the patient's history, she and her family had experienced typical symptoms of COVID-19 in the

last 2 months. The patient underwent an HRCT scan of the chest. Multiple segmental ground-glass opacities (GGOs) with superimposed inter- and intralobular septal thickening were noticed in both lungs which were interpreted as a typical feature for COVID-19 pneumonia (Fig. 2) [1, 2].

In December 2019 an aggressive disease emerged and caused severe acute respiratory syndrome (SARS-CoV-2) and spread globally, becoming a pandemic [3]. A combination of clinical features, imaging findings and laboratory results of COVID-19 (RT-PCR) should be used for confident diagnosis [4]. Although nuclear medicine modalities don't play an important role in the primary diagnosis of COVID-19, the disease may be detected incidentally in asymptomatic but infected patients undergoing routine imaging (SPECT or PET scans) for other indications [5]. Here, COVID-19 — associated pneumonia was found in an asymptomatic patient who underwent UBI scintigraphy for another reason, by chance. The aim of this case presentation was to make nuclear medicine physicians aware of this possibility to improve their knowledge about COVID-19 findings features in different imaging, especially in regions with high COVID-19 prevalence [6–8].

Correspondence to: Fariba Jafari
Department of Nuclear Medicine, Medicine School, Shiraz University of
Medical Sciences, Shiraz, Iran
e-mail: fariba.jafarinm@gmail.com

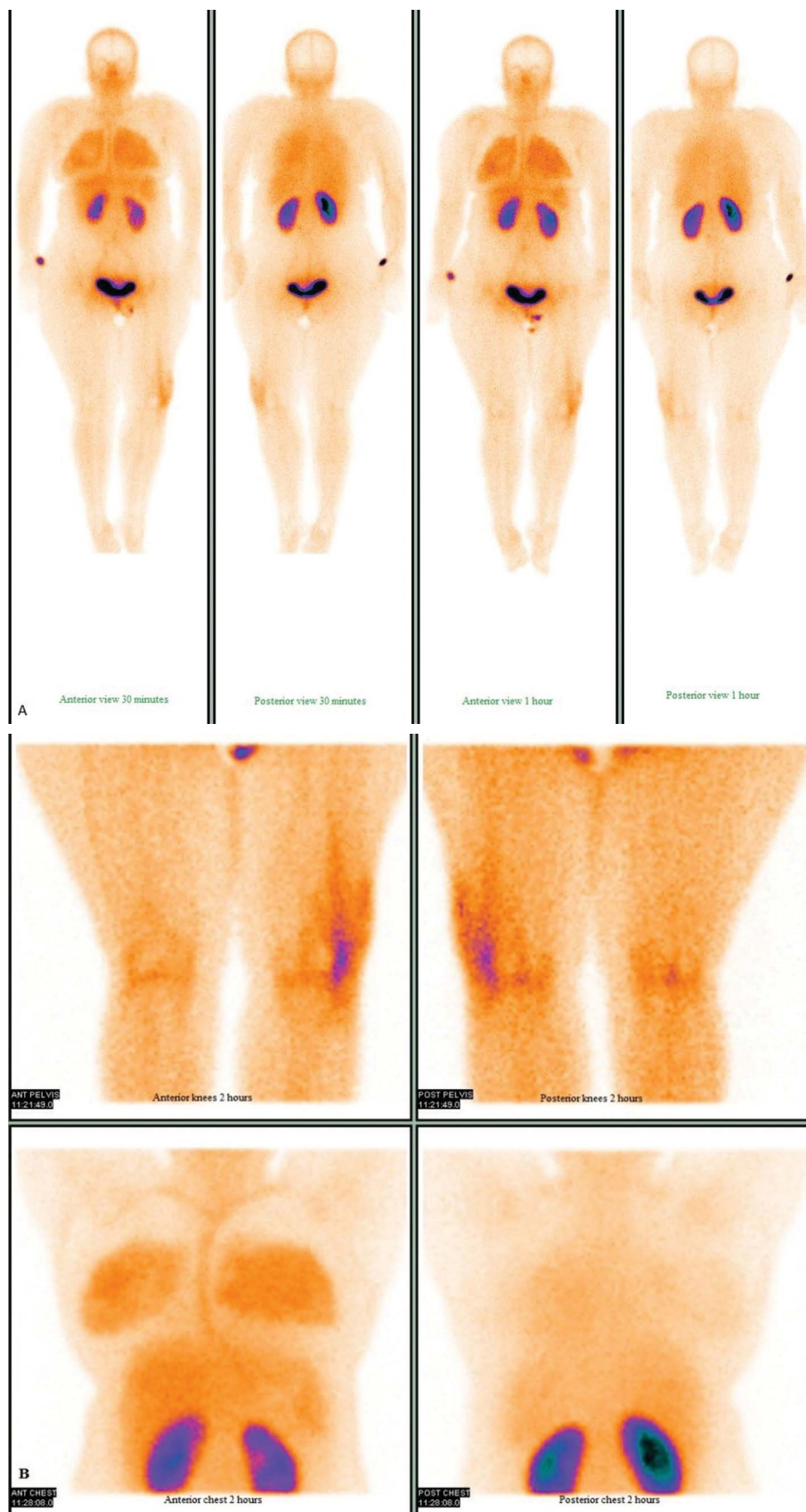


Figure 1. A. Whole-body planar images in anterior and posterior views (30 minutes and 1 hour) of UBI scintigraphy showed significant bilateral and diffuse lungs uptake (red arrows). Also mild soft tissue inflammation in the lateral aspect of the left lower thigh (blue arrow). **B.** Delayed 2 hours static images of chest and knees confirm the activity of lungs and lateral aspect of left lower thigh

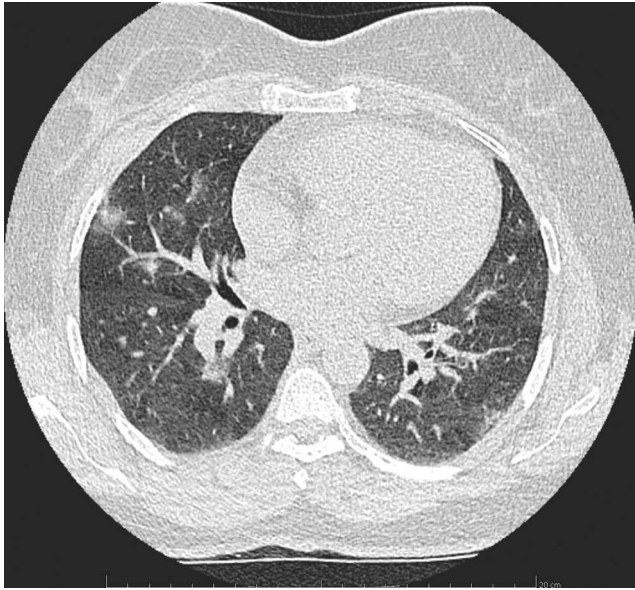


Figure 2. Trans axial Chest HRCT showed multiple bilateral ground-glass opacities (GGOs) with superimposed inter- and intralobular septal thickening, more located peripherally


Conflict of interest

The authors declare that they do not have any conflict of interest.

References

1. Zheng Q, Lu Y, Lure F, et al. Clinical and radiological features of novel coronavirus pneumonia. *J Xray Sci Technol.* 2020; 28(3): 391–404, doi: [10.3233/XST-200687](https://doi.org/10.3233/XST-200687), indexed in Pubmed: [32538893](https://pubmed.ncbi.nlm.nih.gov/32538893/).
2. Jiang F, Deng L, Zhang L, et al. Review of the clinical characteristics of coronavirus disease 2019 (COVID-19). *J Gen Intern Med.* 2020; 35(5): 1545–1549, doi: [10.1007/s11606-020-05762-w](https://doi.org/10.1007/s11606-020-05762-w), indexed in Pubmed: [32133578](https://pubmed.ncbi.nlm.nih.gov/32133578/).
3. Huang C, Wang Y, Li X, et al. Clinical features of patients infected with 2019 novel coronavirus in Wuhan, China. *Lancet.* 2020; 395(10223): 497–506, doi: [10.1016/S0140-6736\(20\)30183-5](https://doi.org/10.1016/S0140-6736(20)30183-5), indexed in Pubmed: [31986264](https://pubmed.ncbi.nlm.nih.gov/31986264/).
4. Lan L, Xu D, Ye G, et al. Positive RT-PCR test results in patients recovered from COVID-19. *JAMA.* 2020; 323(15): 1502–1503, doi: [10.1001/jama.2020.2783](https://doi.org/10.1001/jama.2020.2783), indexed in Pubmed: [32105304](https://pubmed.ncbi.nlm.nih.gov/32105304/).
5. Albano D, Bertagna F, Bertoli M, et al. Incidental findings suggestive of COVID-19 in asymptomatic patients undergoing nuclear medicine procedures in a high-prevalence region. *J Nucl Med.* 2020; 61(5): 632–636, doi: [10.2967/jnumed.120.246256](https://doi.org/10.2967/jnumed.120.246256), indexed in Pubmed: [32238429](https://pubmed.ncbi.nlm.nih.gov/32238429/).
6. Habouzit V, Sanchez A, Dehbi S, et al. Incidental finding of COVID-19 lung infection in 18F-FDG PET/CT: what should we do? *Clin Nucl Med.* 2020; 45(8): 649–651, doi: [10.1097/RLU.0000000000003135](https://doi.org/10.1097/RLU.0000000000003135), indexed in Pubmed: [32558722](https://pubmed.ncbi.nlm.nih.gov/32558722/).
7. Zheng J, Liu Y. 99mTc-Leukocyte scintigraphy revealed viral pulmonary infection in a COVID-19 patient. *Clin Nucl Med.* 2020; 45(10): 821–823, doi: [10.1097/RLU.0000000000003219](https://doi.org/10.1097/RLU.0000000000003219), indexed in Pubmed: [32701817](https://pubmed.ncbi.nlm.nih.gov/32701817/).
8. Czernin J, Fanti S, Meyer PT, et al. Nuclear medicine operations in the times of COVID-19: strategies, precautions, and experiences. *J Nucl Med.* 2020; 61(5): 626–629, doi: [10.2967/jnumed.120.245738](https://doi.org/10.2967/jnumed.120.245738), indexed in Pubmed: [32238430](https://pubmed.ncbi.nlm.nih.gov/32238430/).

Incidental detection of COVID-19 associated pneumonia by thyroid scintigraphy

Mehrosadat Alavi^{1,2}, Fariba Jafari¹ 

¹Department of Nuclear Medicine, Medicine School, Shiraz University of Medical Sciences, Shiraz, Iran

²Ionizing and NonIonizing Radiation Protection Research Center (INIRPRC), Shiraz University of Medical Sciences., Shiraz, Iran

[Received 14 II 2021; Accepted 15 III 2021]

Abstract

This report presents a case of a 49-year-old woman with complaint of sore throat and front neck pain, who referred to a hospital for thyroid scan due to suppressed TSH level (0.005 mU/L). Diffuse and bilateral lungs uptake in the scan was noticed incidentally. The patient had positive history of covid-19 symptoms. Multifocal and bilateral ground-glass opacities (GGOs) in both lungs were compatible with typical features of lung involvement in COVID-19-associated pneumonia.

KEY words: COVID-19; pneumonia; thyroid scintigraphy

Nucl Med Rev 2021; 24, 2: 113–114

A 49-year-old female was presented with complaints of sore throat and front neck pain for 1 month. She referred to the nuclear medicine department to perform a thyroid scan. The thyroid gland was tender on physical examination. Also, the laboratory assay showed suppressed TSH level (0.005 mU/L). 15 minutes after

Intravenous injection of 185 MBq [^{99m}Tc] pertechnetate, an anterior planar image of the neck was obtained. The scan revealed diffusely decreased radiotracer uptake throughout the thyroid with poor delineation of the thyroid gland which was suggestive of subacute thyroiditis (Fig. 1). Moreover, significant, diffuse and bilateral [^{99m}Tc]

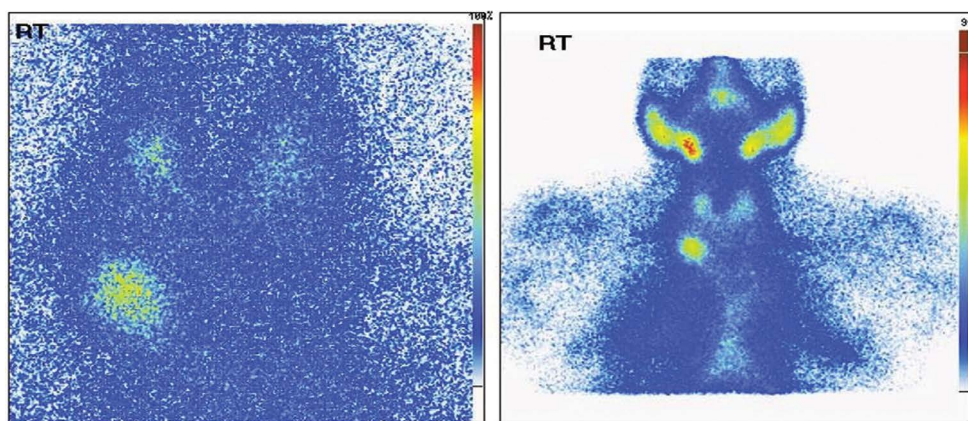


Figure 1. [^{99m}Tc] pertechnetate thyroid scan. Anterior planar image of the neck revealed diffusely decreased radiotracer uptake throughout the thyroid with poor delineation of the thyroid gland and decreased thyroid to background ratio. Also, significant, diffuse and bilateral uptake in both lungs is noted

Correspondence to: Fariba Jafari
 Department of Nuclear Medicine, Medicine School, Shiraz University of
 Medical Sciences, Shiraz, Iran
 e-mail: fariba.jafarinm@gmail.com

This article is available in open access under Creative Common Attribution-Non-Commercial-No Derivatives 4.0 International (CC BY-NC-ND 4.0) license, allowing to download articles and share them with others as long as they credit the authors and the publisher, but without permission to change them in any way or use them commercially.

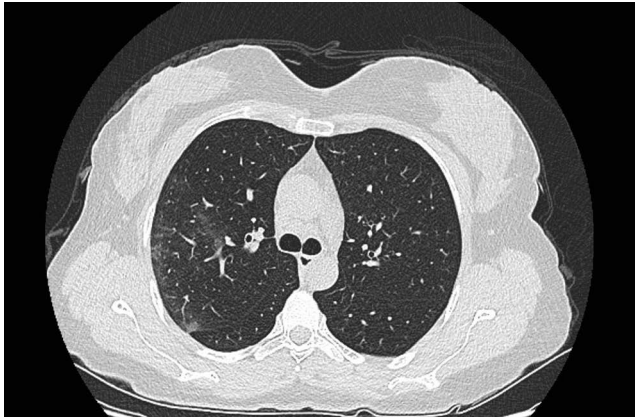


Figure 2. Transaxial chest HRCT scan showed bilateral and multifocal patchy ground-glass opacities (GGOs), (more in the right lung), predominantly located in the peripheral of the chest

per technetate in both lungs fields caught our attention. After that, the patient was asked about experiencing any infectious symptoms. She had fever, cough, dyspnoea and myalgia for the past 40 days, which were typical symptoms of COVID-19 pneumonia [1, 2]. The patient underwent a chest high-resolution CT scan (HRCT) that revealed multifocal and bilateral ground-glass opacities (GGOs), predominantly distributed in the peripheral. These findings were compatible with typical findings of COVID-19-associated pneumonia (Fig. 2) [3, 4].

COVID-19 disease causes severe acute respiratory syndrome. SARS-CoV-2 was first recognized at the end of 2019 and became a global concern very soon [5]. Nowadays, many people around the world have experienced a range of clinical manifestation, from no symptoms to critical illness. The purpose of this presentation is to spread awareness among nuclear medicine physicians to develop their knowledge about incidental detection of COVID-19 disease in

patients who undergo routine SPECT/CT or PET/CT scans during this pandemic, especially in high COVID-19 prevalence areas [6–8].

Conflict of interest

The authors declare that they do not have any conflict of interest.

References

1. Huang C, Wang Y, Li X, et al. Clinical features of patients infected with 2019 novel coronavirus in Wuhan, China. *Lancet*. 2020; 395(10223): 497–506, doi: [10.1016/S0140-6736\(20\)30183-5](https://doi.org/10.1016/S0140-6736(20)30183-5), indexed in Pubmed: [31986264](https://pubmed.ncbi.nlm.nih.gov/31986264/).
2. Jiang F, Deng L, Zhang L, et al. Review of the clinical characteristics of coronavirus disease 2019 (COVID-19). *J Gen Intern Med*. 2020; 35(5): 1545–1549, doi: [10.1007/s11606-020-05762-w](https://doi.org/10.1007/s11606-020-05762-w), indexed in Pubmed: [32133578](https://pubmed.ncbi.nlm.nih.gov/32133578/).
3. Ali SA, Abdelkawi MM. Incidentally recognized COVID-19 pneumonia in routine oncologic 18F-FDG PET/CT examinations: a local experience during pandemic era. *Egyptian Journal of Radiology and Nuclear Medicine*. 2020; 51(1), doi: [10.1186/s43055-020-00333-9](https://doi.org/10.1186/s43055-020-00333-9).
4. Fang Y, Zhang H, Xie J, et al. Sensitivity of chest CT for COVID-19: comparison to RT-PCR. *Radiology*. 2020; 296(2): E115–E117, doi: [10.1148/radiol.2020200432](https://doi.org/10.1148/radiol.2020200432), indexed in Pubmed: [32073353](https://pubmed.ncbi.nlm.nih.gov/32073353/).
5. Zhou P, Yang XL, Wang XG, et al. A pneumonia outbreak associated with a new coronavirus of probable bat origin. *Nature*. 2020; 579(7798): 270–273, doi: [10.1038/s41586-020-2012-7](https://doi.org/10.1038/s41586-020-2012-7), indexed in Pubmed: [32015507](https://pubmed.ncbi.nlm.nih.gov/32015507/).
6. Tulchinsky M, Fotos JS, Slonimsky E. Incidental CT findings suspicious for covid-19-associated pneumonia on nuclear medicine examinations: recognition and management plan. *Clin Nucl Med*. 2020; 45(7): 531–533, doi: [10.1097/RLU.00000000000003100](https://doi.org/10.1097/RLU.00000000000003100), indexed in Pubmed: [32502091](https://pubmed.ncbi.nlm.nih.gov/32502091/).
7. Hindle-Katel W, Oen-Hsiao J, Lussnig E, et al. Incidental finding of COVID-19 pulmonary infiltrates on SPECT/CT attenuation correction CT. *J Nucl Cardiol*. 2020; 27(4): 1385–1386, doi: [10.1007/s12350-020-02178-1](https://doi.org/10.1007/s12350-020-02178-1), indexed in Pubmed: [32394407](https://pubmed.ncbi.nlm.nih.gov/32394407/).
8. Cohen F, Chiche L, Rebaudet S, et al. Incidental pneumonia on PET imaging. *Rev Med Interne*. 2021; 42(3): 225–226, doi: [10.1016/j.revmed.2020.09.003](https://doi.org/10.1016/j.revmed.2020.09.003), indexed in Pubmed: [33160705](https://pubmed.ncbi.nlm.nih.gov/33160705/).

Infection of aortobifemoral bypass graft implanted 20 years ago proved by labeled leukocytes SPECT-CT

Olgierd Chrabanski¹ , Tomasz Golab²

¹Department of Radiodiagnostics, Invasive Radiology and Nuclear Medicine, Faculty of Medical Sciences in Katowice, Medical University of Silesia, Katowice, Poland

²Clinica Medica, Tychy, Poland

[Received 30 III 2021; Accepted 7 V 2021]

KEY words: infection; aortobifemoral; graft; labeled leukocytes; SPECT-CT

Nucl Med Rev 2021; 24, 2: 115–117

Aortic graft infections are very serious complications of arterial reconstructive surgery. The described in literature longest interval between primary reconstruction and aortic graft infections was 20 years [1].

This research reports a case of a 60-year-old man with a suspected infection of an aortobifemoral bypass graft implanted 20 years ago due to an aneurysm of the abdominal aorta. He was referred to a nuclear medicine department for scintigraphic detection or exclusion of active infection within the stent-graft.

The patient had many comorbidities: renal failure, arterial hypertension, hypertensive cardiomyopathy, ischemic heart disease. This year, the patient underwent thrombosis of the left saphenous vein with cellulitis of the left leg and was treated surgically due to an abscess of the left buttock. Laboratory tests revealed: leukocytosis, significantly elevated CRP and anaemia. Enterococcus faecalis susceptible to ampicillin, teicoplanin and vancomycin were grown on venous blood cultures. Despite the implementation of antibiotic therapy, no significant improvement in the patient's clinical condition was achieved. The computed tomography examination showed changes suggesting infection of the vascular prosthesis.

Due to the high risk of the surgery, it was decided to operate after obtaining scintigraphic detection of infection within the stent-graft.

The examination was performed with Technetium-99m labeled leukocytes using HMPAO.

The patient was examined 1, 4 and 24 hours after radiotracer injection using Symbia Intevo with a protocol including SPECT/CT with LEHR collimator, low-dose CT.

Correspondence to: Olgierd Chrabanski, Department of Radiodiagnostics, Invasive Radiology and Nuclear Medicine, Faculty of Medical Sciences in Katowice, Medical University of Silesia, Katowice, Poland, e-mail: olgierdchrabanski@gmail.com

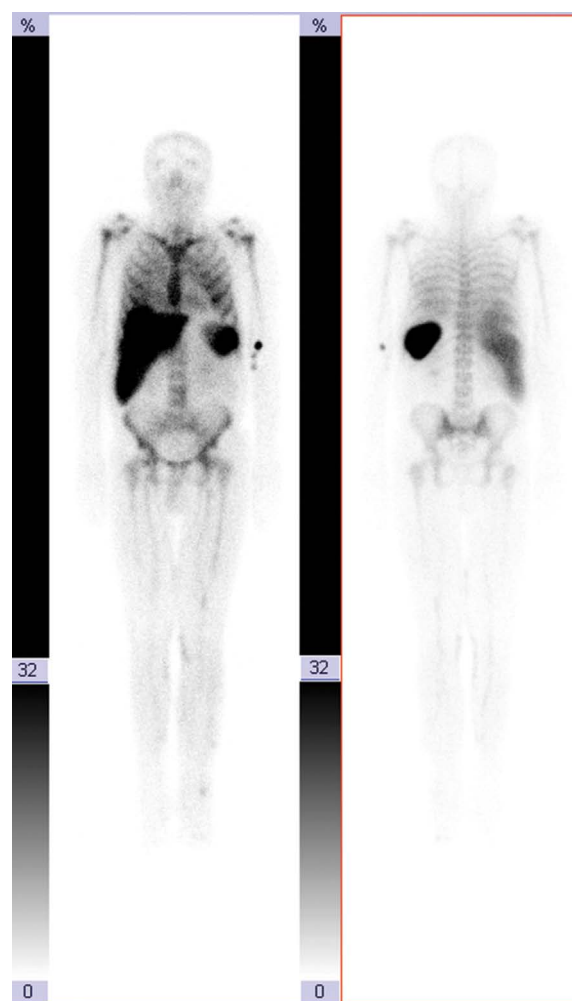


Figure 1. Whole-body WBC scan performed 4 hours after the administration of the radiotracer, no obvious foci of pathological accumulation ^{99m}Tc-HMPAO labeled leukocytes in stent-graft

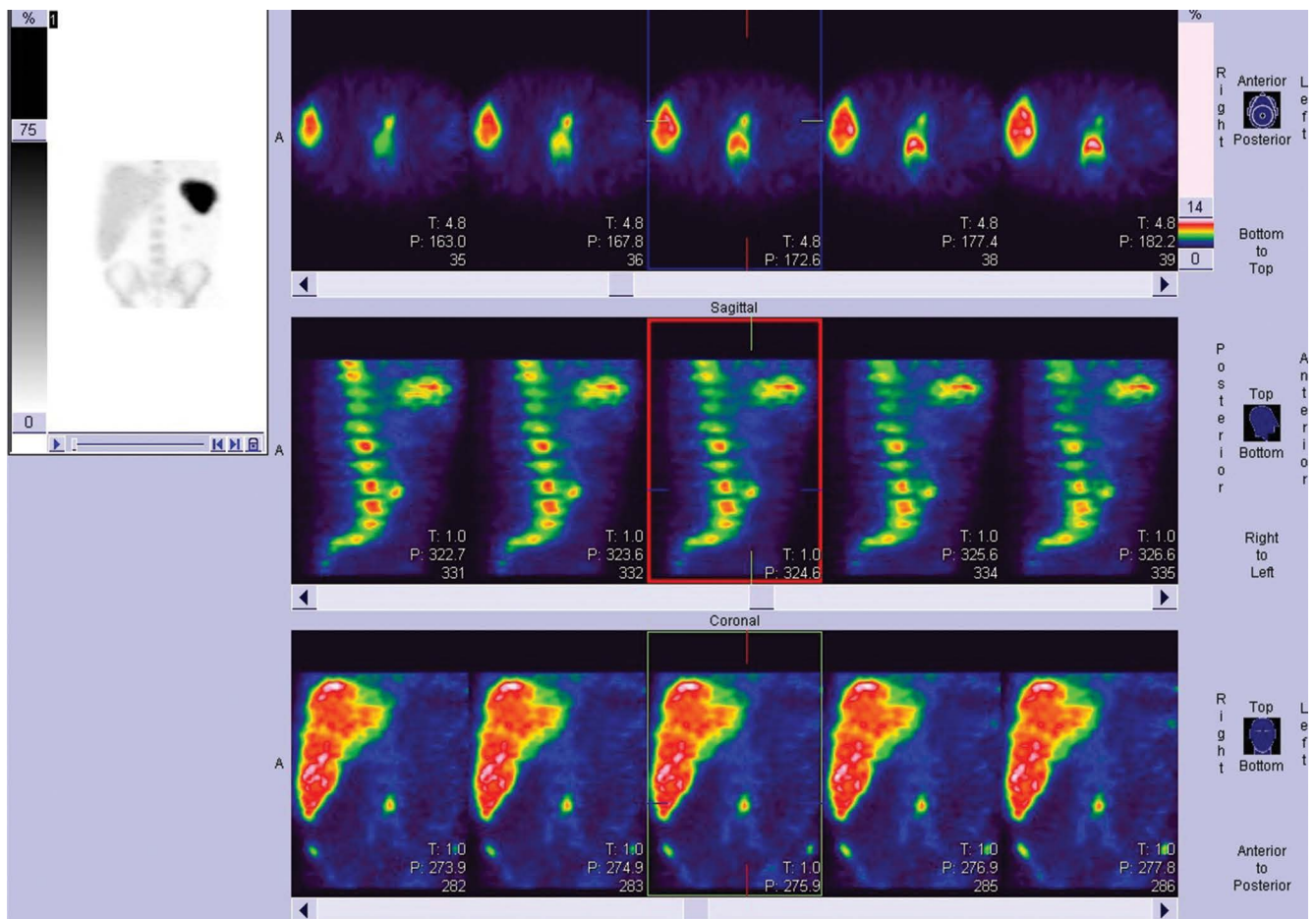


Figure 2. SPECT after 4 hours there was a small focus on the level of L4/L5 intervertebral space and slightly to the left of the midline of the body

Planar examination of the whole body performed 4 hours after the administration of the radiotracer — no obvious foci of pathological accumulation of the radiotracer in stent-graft. Discreet accumulation of labelled leukocytes was visible in the projection of the left shank, which might be a consequence of the patient's history of left saphenous vein thrombosis. The enlarged liver was also visible in Figure 1.

On SPECT after 4 hours there was a small focus on the level of L4/L5 intervertebral space and slightly to the left of the midline of the body Figure 2.

In SPECT-CT acquisition, pathological accumulation of the radiotracer localized in the aorta (within the stent-graft) was detected in Figure 3 A–C.

After scintigraphic examination, the patient was operated on. During the operation, infection of stent-graft was confirmed. Modern gamma camera using high-resolution SPECT/CT can detect small foci invisible on the planar scan. It can be essential for final diagnosis.

Conflict of interest

The authors report no conflicts of interest.

References

1. Treska V, Certik B, Molacek J. Management of aortic graft infections - the present strategy and future perspectives. *Bratisl Lek Listy*. 2016; 117(3): 125–132, doi: [10.4149/bll_2016_024](https://doi.org/10.4149/bll_2016_024), indexed in Pubmed: [26925740](https://pubmed.ncbi.nlm.nih.gov/26925740/).

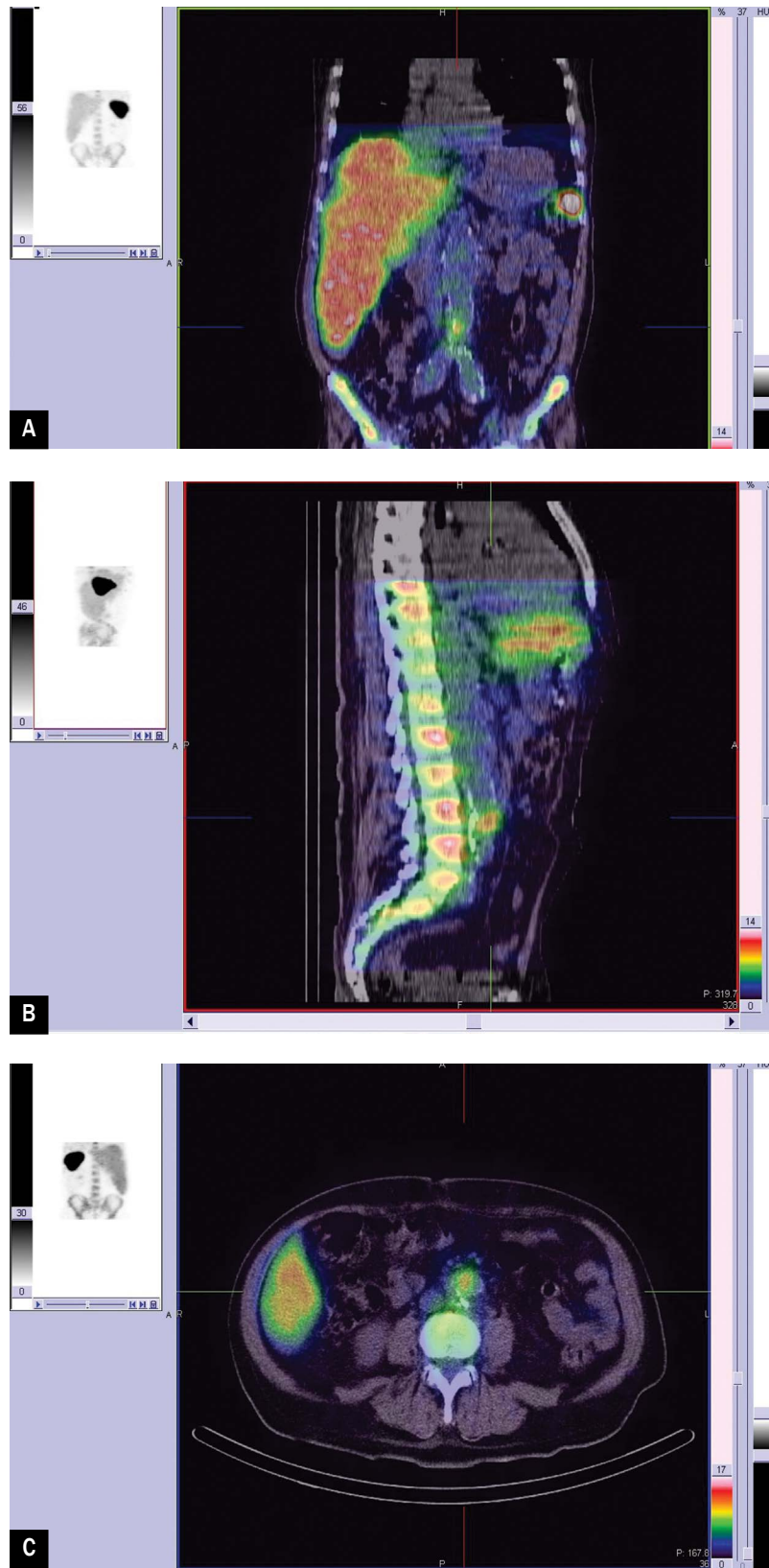


Figure 3 A-C. In SPECT-CT acquisition after 4 h, pathological accumulation of labelled leukocytes localized in the aorta stent-graft confirm infection

[^{99m}Tc]MIBI scintigraphy in a patient with thyroid follicular neoplasm: a case report and review of literature

Mohsen Arabi¹ , Hanieh Zamani¹ , Masume Soltanabadi² , Leila Kalhor¹ 

¹Department of Nuclear Medicine, Alborz University of Medical Sciences, Karaj, Iran

²Department of Nuclear Medicine, Shahrekord University of Medical Sciences, Shahrekord, Iran

[Received 24 II 2021; Accepted 15 III 2021]

Abstract

[^{99m}Tc]MIBI thyroid scintigraphy is a useful tool to differentiate benign from malignant thyroid nodules. This report aims to show the diagnostic performance of [^{99m}Tc]MIBI scintigraphy used in an 83-year-old woman who had a thyroidectomy about 7 years ago. She had a mass of thyroid which was very large, non-homogenous and painless. [^{99m}Tc]MIBI scintigraphy could be a pre-surgical method to investigate the follicular nodules and predicting the malignant form of thyroid nodules. Also, it will provide tissue information for [^{99m}Tc]MIBI images in thyroid lesions.

KEY words: [^{99m}Tc]MIBI scintigraphy; patient; thyroid follicular neoplasm

Nucl Med Rev 2021; 24, 2: 118–119

Introduction

The prevalence of thyroid nodules is about 5% even in areas with adequate iodine intake [1]. The risk of thyroid nodules is about 3–5% [2]. Thyroid cancer has been one of the most diagnosed forms of cancers around the world in the past few decades [3]. The 2nd most common thyroid cancer is follicular thyroid cancer, and it is a higher incidence of distant metastases. Therefore, the prognosis is worse than the more common papillary thyroid carcinoma [4–6]. Thyroid gland follicular neoplasm comprises follicular carcinoma and adenoma.

Case presentation

An 83-year-old woman came for a nuclear thyroid scan. After examination of her neck, the mass of thyroid was non-homogenous, enlarged, difficult to be examined and firm and painless. She had a thyroidectomy 7 years ago but did not know the details of whether it was a total or hemithyroidectomy. After 4 years of recurrence, the physician advised her to have another surgery, but the patient was not satisfied. After scanning of the patient's thyroid with [^{99m}Tc]pertechnetate, it was observed that this mass had no uptake,

Therefore, performing a [^{99m}Tc]MIBI was decided. In this case report were performed both [^{99m}Tc]pertechnetate and ^{99m}Tc-MIBI scintigraphy in anterior projection. The study showed poor delineation of the thyroid gland in [^{99m}Tc]pertechnetate thyroid scan (Fig. 1). In the [^{99m}Tc]MIBI scan, an area of increased uptake is noticed on the left lobe of the thyroid corresponding to a palpable nodule. The left lobe of the thyroid was enlarged with a rather in-homogenous radiotracer uptake. There was no significant radiotracer activity in the right lobe of the thyroid (due to previous surgery) (Fig. 2). With the patient's history (previous thyroidectomy), scan findings (MIBI avid lesions of the left lobe) showed highly tumour recurrence and after following up she was diagnosed with follicular carcinoma.

[^{99m}Tc]MIBI and [^{99m}Tc]pertechnetate scintigraphy

Twenty minutes after IV injection of 111 MBq (3 MCI) [^{99m}Tc]pertechnetate and twenty minutes after IV injection of 148 MBq (4 MCI) [^{99m}Tc]MIBI, thyroid imaging was performed in anterior projection.

Discussion

[^{99m}Tc]MIBI scans have been used to study myocardial perfusion since 1989, but the uptake of this radiopharmaceutical into tumours has led to its use in the study of breast, bone, thyroid, parathyroid, and brain tumours [7]. Numerous studies examining

Correspondence to: Leila Kalhor
Department of Nuclear Medicine, Alborz University of Medical Sciences,
Karaj, Iran
e-mail: kalhorleila169@gmail.com

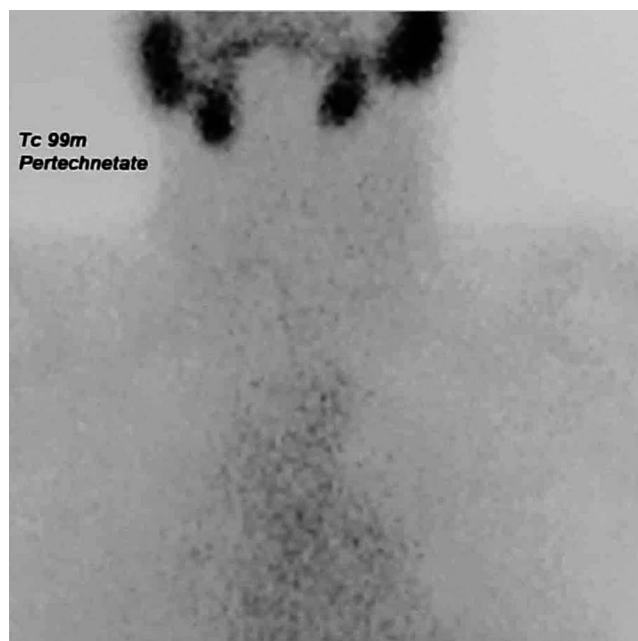


Figure 1. Non-visualized of thyroid gland with thyroid scan and [^{99m}Tc]pertechnetate

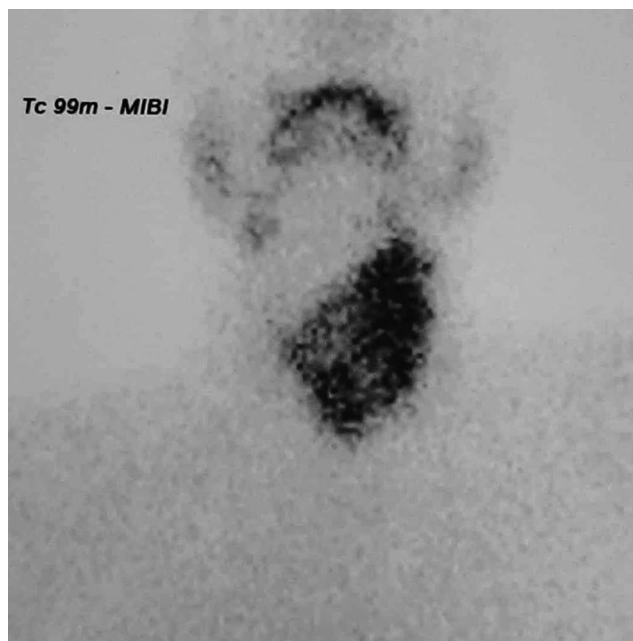


Figure 2. Left lobe of the thyroid

thyroid scans with [^{99m}Tc]MIBI show conflicting results [8]. In a study of 34 operated thyroid nodules, it was concluded that the rate of absorption of [^{99m}Tc]MIBI in the thyroid nodule is mainly a sign of thyroid tissue viability and is not specific to malignancy [9]. But another study [7] on thyroid nodules found that high uptake of [^{99m}Tc]MIBI significantly increased the risk of malignancy. The researchers suggested routine use of [^{99m}Tc]MIBI scan with fine-needle aspiration in the diagnosis of cold thyroid.

Nowadays, fewer than 25% of nodules (follicular neoplasm) show malignant features at histological examination [10, 11]. Some studies expressed that [^{99m}Tc]MIBI scintigraphy is a reliable procedure to improve the accuracy of diagnostic thyroid fine-needle aspiration cytology (FNAC) [2, 12–13]. Several authors observed that [^{99m}Tc]MIBI scintigraphy is positive in both malignant and benign thyroid lesions [13, 14] and [^{99m}Tc]MIBI thyroid scintigraphy is highly accurate in the differential diagnosis of nodules with indeterminate cytology finding [15].

We can conclude that [^{99m}Tc]MIBI scintigraphy could be a pre-surgical method to investigate follicular nodules and predicting the malignant thyroid nodules. Therefore, the scintigraphy of [^{99m}Tc]MIBI provides tissue information for these scintigraphy images in thyroid nodules.

Conflict of interest

The authors declare that they do not have any conflict of interest.

References

- Schlumberger MJ, Feletti S, Hay I. Nontoxic goiter and thyroid neoplasm In: Williams text book of endocrinology. 10th edition. Philadelphia: Saunders. 2003: 465.
- Hegedüs L, Bonnema SJ, Bennedbaek FN. Management of simple nodular goiter: current status and future perspectives. *Endocr Rev.* 2003; 24(1): 102–132, doi: [10.1210/er.2002-0016](https://doi.org/10.1210/er.2002-0016), indexed in Pubmed: 12588812.
- Howlader N, et al. SEER Cancer Statistics Review, Populations, National Cancer Institute. 1975.
- Podda M, Saba A, Porru F, et al. Follicular thyroid carcinoma: differences in clinical relevance between minimally invasive and widely invasive tumors. *World J Surg Oncol.* 2015; 13: 193, doi: [10.1186/s12957-015-0612-8](https://doi.org/10.1186/s12957-015-0612-8), indexed in Pubmed: 26041024.
- Brennan M, Bergstralh E, van Heerden J, et al. Follicular Thyroid Cancer Treated at the Mayo Clinic, 1946 Through 1970: Initial Manifestations, Pathologic Findings, Therapy, and Outcome. *Mayo Clinic Proceedings.* 1991; 66(1): 11–22, doi: [10.1016/s0025-6196\(12\)61170-7](https://doi.org/10.1016/s0025-6196(12)61170-7).
- Hundahl SA, Fleming ID, Fremgen AM, et al. A National Cancer Data Base report on 53,856 cases of thyroid carcinoma treated in the U.S., 1985–1995 *Cancer.* 1998; 83(12): 2638–2648, doi: [10.1002/\(sici\)1097-0142\(19981215\)83:12<2638::aid-cnrc31>3.0.co;2-1](https://doi.org/10.1002/(sici)1097-0142(19981215)83:12<2638::aid-cnrc31>3.0.co;2-1), indexed in Pubmed: 9874472.
- Mezosi E, Bajnok L, Gyory F, et al. The role of technetium-99m methoxy-isobutylisonitrile scintigraphy in the differential diagnosis of cold thyroid nodules. *European Journal of Nuclear Medicine and Molecular Imaging.* 1999; 26(8): 798–803, doi: [10.1007/s002590050451](https://doi.org/10.1007/s002590050451).
- Kim N, Lavertu P. Evaluation of a thyroid nodule. *Otolaryngologic Clinics of North America.* 2003; 36(1): 17–33, doi: [10.1016/s0030-6665\(02\)00130-5](https://doi.org/10.1016/s0030-6665(02)00130-5).
- Alonso O, Lago G, Mut F, et al. Thyroid imaging with Tc-99m MIBI in patients with solitary cold single nodules on pertechnetate imaging. *Clin Nucl Med.* 1996; 21(5): 363–367, doi: [10.1097/00003072-199605000-00002](https://doi.org/10.1097/00003072-199605000-00002), indexed in Pubmed: 8732828.
- Schlumberger M, Pacini F. *Thyroid Tumors.* 2nd ed. Paris, France: Editions Nucléon. 2003: 18–24.
- Erdil TY, Ozker K, Kabasakal L, et al. Correlation of technetium-99m MIBI and thallium-201 retention in solitary cold thyroid nodules with post-operative histopathology. *Eur J Nucl Med.* 2000; 27(6): 713–720, doi: [10.1007/s002590050567](https://doi.org/10.1007/s002590050567), indexed in Pubmed: 10901459.
- Chamnanrabiabkij E, Welch A, Jayapaul MK, et al. Detection of Hurthle cell carcinoma using sestamibi. *Thyroid.* 2008; 18(5): 575–576, doi: [10.1089/thy.2007.0200](https://doi.org/10.1089/thy.2007.0200), indexed in Pubmed: 18044993.
- Campenni A, Siracusa M, Ruggeri RM, et al. Differentiating malignant from benign thyroid nodules with indeterminate cytology by Tc-MIBI scan: a new quantitative method for improving diagnostic accuracy. *Sci Rep.* 2017; 7(1): 6147, doi: [10.1038/s41598-017-06603-3](https://doi.org/10.1038/s41598-017-06603-3), indexed in Pubmed: 28733644.

Findings in [^{99m}Tc]MAA SPECT/CT in the diagnosis and follow-up of pulmonary embolism after infection by SARS-CoV-2 (COVID-19)

Marylin Acuña Hernández¹, Tatiana Morales Avellaneda^{1,2}, Jorge Andres Narvaez Gomez¹, Liset Sanchez Orduz²

¹Universidad Autónoma De Bucaramanga, Santander, Colombia

²Spect Medicina Nuclear S.A.S, Centro medico carlos ardila Lulle, Bucaramanga, Colombia

[Received 5 III 2021; Accepted 15 III 2021]

Abstract

SARS-CoV-2 (COVID-19) infection is a current public health problem that has been shown to cause multiple complications, including pulmonary thromboembolism. The first presented case is a 59-year-old woman with a history of COPD, paroxysmal atrial fibrillation and COVID-19 infection in September 2020, consultation in December 2020 for atypical chest pain with suspected PE, AngioCT of pulmonary vessels was performed negative for emboli, subsequently [^{99m}Tc]Tc MAA SPECT/CT was indicated with a report of multiple triangular defects concerning acute pulmonary thromboembolism. A second case is a 70-year-old man with a history of dyslipidaemia, presented COVID-19 infection in September 2020 with a complication of PE with involvement of the left pulmonary artery, followed by [^{99m}Tc]Tc MAA SPECT/CT report multiple triangular and not triangles defects concerning pulmonary thromboembolism with signs of reperfusion.

KEY words: pulmonary embolism; coronavirus infections; ventilation-perfusion scan; diagnosis

Nucl Med Rev 2021; 24, 2: 120–121

SARS-CoV-2 (COVID-19) infection is a current public health problem that has been shown multiple complications, including pulmonary embolism. This study presents the case of a 59-year-old woman with a history of COPD, paroxysmal atrial fibrillation and COVID-19 infection in September 2020, consultation in December 2020 for atypical chest pain, ruling out cardiac, vascular and infectious ischemic causes, finding in TT echocardiogram sign of precapillary pulmonary hypertension. PE was suspected and therefore negative AngioCT of pulmonary vessels was indicated, although the clinical doubt persisted, starting anticoagulation and 7 days later [^{99m}Tc]Tc MAA planar images and SPECT/CT were indicated (Fig. 1 A, B) evidence of triangular defects in the left upper lobe apicoposterior segment, upper and lower lingular and non-triangular hypoperfusion areas of the lower left lobe posterior basal

segment and upper right lobe apical and lateral segments without related morphological alterations, making a diagnosis of acute PE according to MSKCC Q-SPECT/CT Criteria [1] with signs of reperfusion.

The second case is a 70-year-old man with a history of dyslipidaemia, presented COVID-19 infection in September 2020 during hospitalization. AngioCT of pulmonary vessels was made evidence pulmonary embolisms in the left pulmonary artery, anticoagulation was started and in December 2020 requested control with [^{99m}Tc]Tc MAA planar images and SPECT/CT (Fig. 2 A–B) triangular defect in right upper lobe apical segment and non-triangular upper left lobe apicoposterior segment without morphological alterations concerning PE according to MSKCC Q-SPECT/CT Criteria [1] with signs of reperfusion.

It is currently known that viral infections, especially by SARS-CoV-2 (COVID-19), can predispose to pulmonary thromboembolic events, the active systemic inflammatory cascade that leads to a procoagulant state due to endothelial dysfunction and hypoxia, in the case of pulmonary involvement generates bronchoalveolar haemostasis with a generation of microthrombi [2, 3].

Correspondence to: Marylin Acuña Hernández
Universidad Autónoma De Bucaramanga, Santander, Colombia
e-mail: macuna766@unab.edu.co

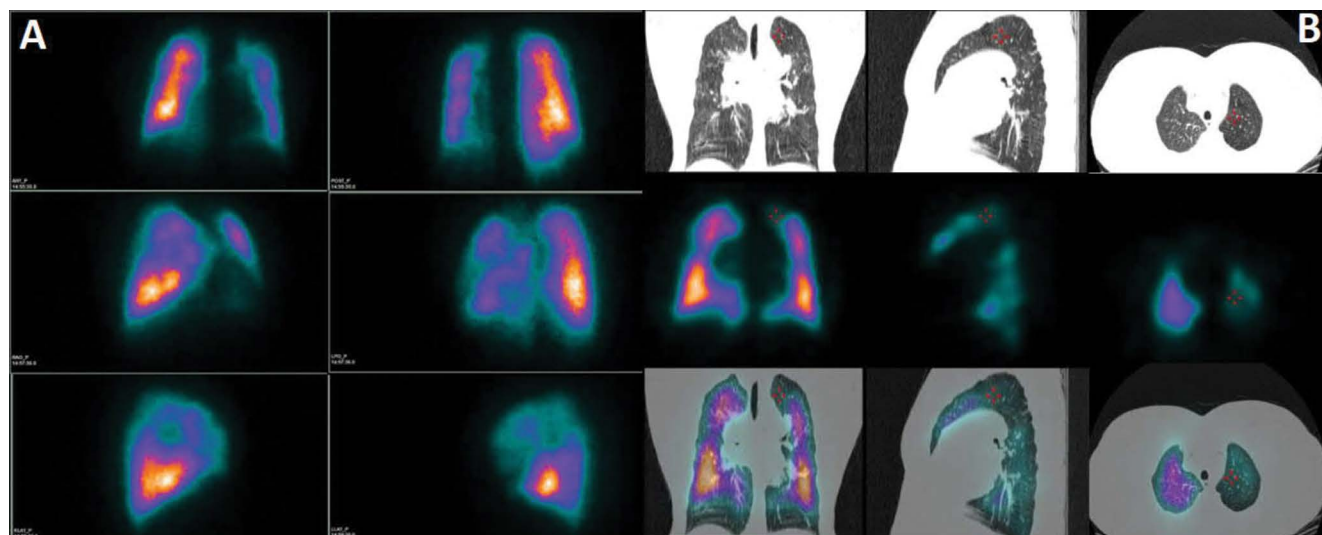


Figure 1. Triangular defects in the left upper lobe apicoposterior segment, upper and lower lingular and non-triangular hypoperfusion areas of the lower left lobe posterior basal segment and upper right lobe apical and lateral segments without related morphological alterations

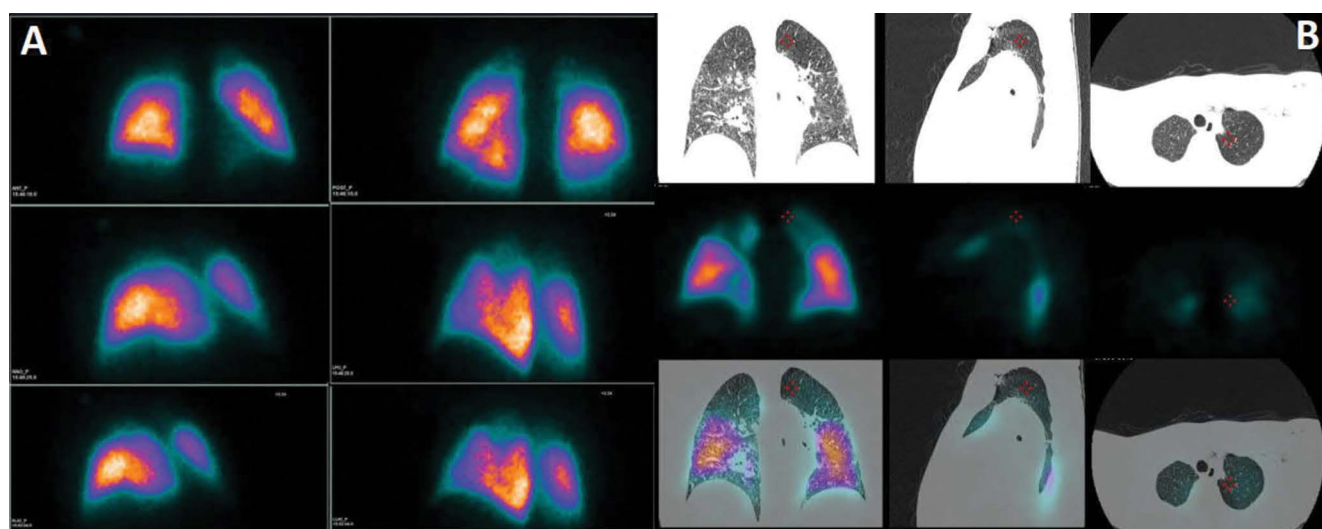


Figure 2. Triangular defect in right upper lobe apical segment and non-triangular upper left lobe apicoposterior segment without morphological alterations

In the same way, it has been described that the affection in these individuals is due to pulmonary artery thrombosis secondary to the phenomena referred to in the previous paragraph that generates severe pulmonary inflammation that triggers a hypercoagulable state instead of serious thromboembolism, venous aetiology [3].

Conflict of interest

The authors declare that they do not have any conflict of interest.

References

1. Lu Y, Macapinlac HA. Perfusion SPECT/CT to diagnose pulmonary embolism during COVID-19 pandemic. *Eur J Nucl Med Mol Imaging*. 2020; 47(9): 2064–2065, doi: [10.1007/s00259-020-04851-6](https://doi.org/10.1007/s00259-020-04851-6), indexed in Pubmed: [32383092](https://pubmed.ncbi.nlm.nih.gov/32383092/).
2. Sakr Y, Giovini M, Leone M, et al. Pulmonary embolism in patients with coronavirus disease-2019 (COVID-19) pneumonia: a narrative review. *Ann Intensive Care*. 2020; 10(1): 124, doi: [10.1186/s13613-020-00741-0](https://doi.org/10.1186/s13613-020-00741-0), indexed in Pubmed: [32936400](https://pubmed.ncbi.nlm.nih.gov/32936400/).
3. Cavagna E, Muratore F, Ferrari F. Pulmonary Thromboembolism in COVID-19: Venous Thromboembolism or Arterial Thrombosis? *Radiol Cardiothorac Imaging*. 2020; 2(4): e200289, doi: [10.1148/ryct.2020200289](https://doi.org/10.1148/ryct.2020200289), indexed in Pubmed: [33778609](https://pubmed.ncbi.nlm.nih.gov/33778609/).

False-positive radioiodine uptake in breasts in a female haemodialysis patient

Aleksandra Ledwon¹, Przemysław Soczomski¹, Ewa Paliczka-Cieślak¹, Aleksandra Blewaska¹, Daria Handkiewicz-Junak¹
Department of Nuclear Medicine and Endocrine Oncology, Maria Skłodowska-Curie National Research Institute of Oncology, Gliwice branch, Poland

[Received 25 III 2021; Accepted 7 V 2021]

KEY words: radioiodine uptake; breasts; hemodialysis

Nucl Med Rev 2021; 24, 2: 122–123

Introduction

The Na⁺/I⁻ symporter (NIS) is an intrinsic plasma membrane glycoprotein that mediates the active uptake of I⁻ in the thyroid and other tissues such as salivary glands, gastric mucosa and lactating mammary gland. Physiologically, NIS is expressed in the breast exclusively during gestation and lactation. In vitro and in vivo studies confirmed that lactogenic hormones, including prolactin, can induce functional NIS expression in mammary tissue. Hyperprolactinemia is common in patients with end-stage renal disease (ESRD).

Clinical case

A 42-year-old woman with papillary thyroid cancer and ESRD treated with haemodialysis underwent ¹³¹I adjuvant therapy after rh-TSH (Thyrogen®) stimulation.

After ¹³¹I application, the patient underwent dialysis sessions in the nephrology department every second day after ¹³¹I therapy. A posttherapy whole-body scan performed 96 hours after administration of 100 mCi/3700MBq ¹³¹I showed radioiodine accumulation in thyroid bed and chest (Fig. 1), that in single-photon emission computed tomography fusion imaging (SPECT/CT) was confirmed as intense and symmetrical breasts uptake (Fig. 2). The patient had her last menstruation 5 years ago and denied galactorrhoea. The prolactin level measured after ¹³¹I therapy was 100.98 ng/mL (reference range 5.18–26.53 ng/mL).

The ultrasound of the mammary glands and conventional mammography was without any abnormalities.

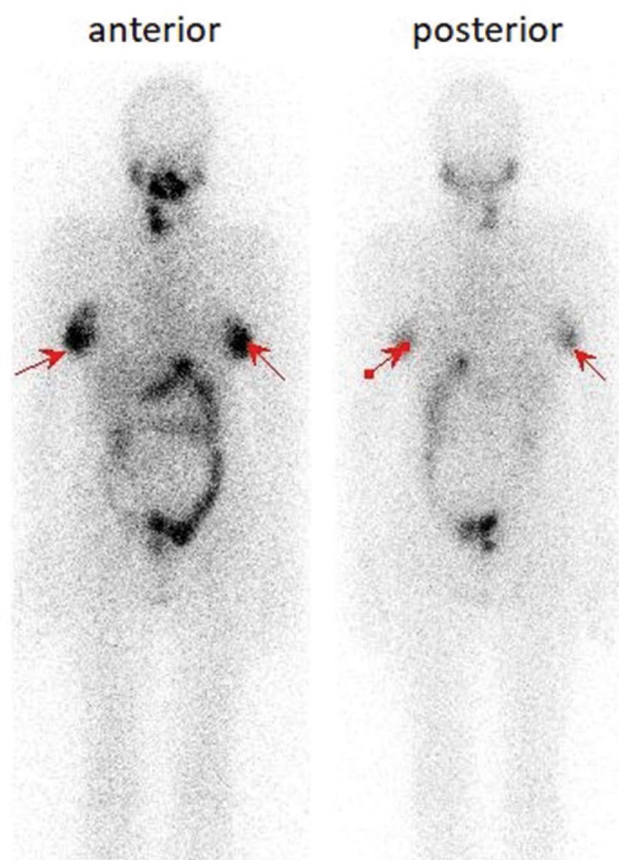


Figure 1. Post therapeutic ¹³¹I planar whole-body scan showed symmetric and intense iodine uptake in mammary glands

Correspondence to: Aleksandra Ledwon, Department of Nuclear Medicine and Endocrine Oncology, Maria Skłodowska-Curie National Research Institute of Oncology, Gliwice branch, Wybrzeże Armii Krajowej Street 15, 44–101 Gliwice, Poland, phone: +48 32278 99 28, fax: +4832 278 9310, e-mail: aleksandra.ledwon@io.gliwice.pl



Figure 2. Image fusion of CT and iodine SPECT scan of the thoracic region clearly demonstrated the radioiodine uptake in the breasts

Discussion

Due to NIS expression in lactating mammary tissue breastfeeding is an absolute contraindication to radioiodine therapy. The time interval between completed breastfeeding and radioiodine treatment should be at least six weeks. NIS expression has been also demonstrated in benign and malignant breast lesions, however, that was not the case of the presented patient.

The major causes of hyperprolactinemia in patients with ESRD is the reduced renal clearance of prolactin (which level does not decrease significantly in response to haemodialysis) and enhanced prolactin secretion by the pituitary due to lactotrophic resistance. Although each year about 10 patients on haemodialysis are treated with radioiodine, this was the first patient on haemodialysis and radioiodine uptake in breasts. The explanation for it could be the young age of the patient since the other ones were much older (median 60 years of age). One cannot exclude that the mammary gland in younger women is more sensitive to prolactin stimulation due to the increased amount of epithelial tissue.

Prolactin measurement and stimulation of the D2 receptor with dopamine agonists should be considered in young female patients with ESRD who are planned for radioiodine treatment.

Conflict of interest

The authors report no conflicts of interest.

Cholethorax with biliopleural communication detected on [^{99m}Tc]mebrofenin hepatobiliary scintigraphy

Georgios Meristoudis¹, Ioannis Ilias², Evangelia Zaromytidou¹, Emmanouil Alevroudis³, Athanasios Notopoulos¹

¹Department of Nuclear Medicine, Hippokraton General Hospital, Thessaloniki, Greece

²Elena Venizelou General Hospital, Athens, Greece

³Second Department of Radiology, Nuclear Medicine Unit, National and Kapodistrian University of Athens, Attikon University General Hospital, Athens, Greece

[Received 30 III 2021; Accepted 7 V 2021]

Abstract

Bilious pleural effusion or cholethorax is a rare type of exudative pleural effusion. Here is presented a case of right-sided cholethorax, in which the direct communication between the pleural effusion with the biliary duct was visible only on the posterior images of dynamic hepatobiliary scintigraphy with [^{99m}Tc]mebrofenin.

KEY words: cholethorax; biliopleural communication; hepatobiliary scintigraphy

Nucl Med Rev 2021; 24, 2: 124–125

Cholethorax (ChT, bilious pleural effusion; biliothorax) is very rare. The authors report a case of right-sided ChT in which the continuity of intrathoracic fluid collection with the biliary ductal system was visualized only in posterior images of dynamic hepatobiliary scintigraphy (HBS) with technetium-99m [^{99m}Tc]mebrofenin.

A 51-year-old male with a history of decompensated alcoholic cirrhosis underwent orthotopic liver transplantation. Four weeks after the procedure, the patient presented with right upper abdominal and pleuritic chest pain, mild dyspnoea, and fever. Chest X-ray revealed a new right-sided pleural effusion (confirmed by computed tomography; CT, which also showed unspecific intraabdominal fluid collections, Fig. 1). The patient underwent HBS after intravenous administration of 185 MBq of [^{99m}Tc]mebrofenin. Synchronous dynamic imaging in anterior and posterior projections was performed with a dual-head γ -camera

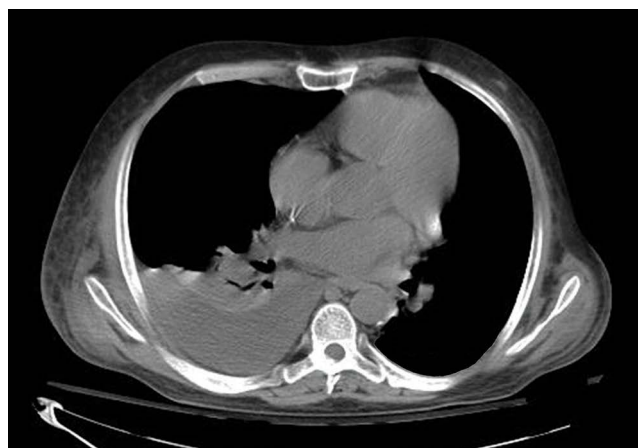


Figure 1. Axial CT image of the lung bases (mediastinal window) shows right pleural fluid collection

Correspondence to: Georgios Meristoudis, Department of Nuclear Medicine, Hippokraton General Hospital, 49 Konstantinoupoleos Str, 54642 Thessaloniki, Greece, e-mail: meristoudis@yahoo.gr



Figure 2. Anterior dynamic images of [^{99m}Tc]mebrofenin HBS (reformatted for display at 3 min/frame) reveal increased tracer activity extending from the superolateral surface of the right hepatic lobe to the right chest. In the last row of images, the findings are much more pronounced in the thorax (which is included in the field of view)

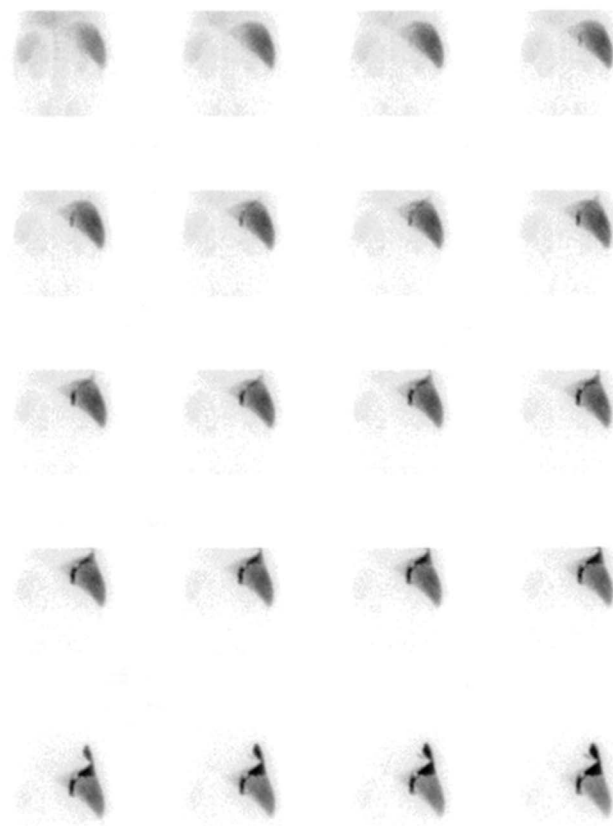


Figure 3. Posterior dynamic images of [^{99m}Tc]mebrofenin HBS directly delineate the presence of biliopleural communication. Tracer accumulation is clearly visible from the region of the bile duct, ascending to the superior segments of the right hepatic lobe, and extending into the right chest cavity

at a rate of 1 min/frame for 48 min focused on the abdomen, followed by the second acquisition of dynamic images, to include the entire chest in the field of view, for an additional 12 min. The anterior views revealed a linear area of increased tracer accumulation extending from the superolateral aspect of the right hepatic lobe to the right hemithorax, confirming the diagnosis of ChT. In these views, there was no evidence of a direct connection between the pleural effusion with the biliary tract (Fig. 2). However, the posterior images demonstrated the presence of biliopleural communication, showing radiopharmaceutical emanating from the region of the biliary duct to the superior segments of the right lobe of the liver with subsequent passage into the right chest cavity (Fig. 3). Right-sided thoracentesis was performed; biochemical analysis revealed an exudative pleural effusion with bilirubin at 16.5 mg/dL (serum 0.5 mg/dL),

a finding consistent with ChT. A chest drain was placed, and the patient's symptoms improved.

Despite the rarity of its occurrence, ChT should not be overlooked in the differential diagnosis of patients with pleural effusion, particularly after biliary or hepatic surgery or abdominal trauma. This case illustrates the clinical usefulness of [^{99m}Tc]mebrofenin HBS for the etiological diagnosis of pleural fluid collection. It also highlights the importance of simultaneous dynamic anterior and posterior imaging, compared with the standard anterior views; in the presented case, the posterior views defined the direct communication between the pleural space with the biliary pathway.

Conflict of interest

The authors declare no conflicts of interest.

Erratum

In the Original Article entitled "Patterns of vascular graft infection in 18F-FDG PET/CT" published in the Nuclear Medicine Review 2020, 23, 2: 63–70 there were errors in the fourth and fifth row of the Table 2. The authors apologize for these errors.

The corrected table is attached below.

Table 2. SUV max in the area of suspected of infection

Prosthesis	n	SUV max in area suspected of infection		
		median	MAX	MIN
All	24	9.0	21.5	4.2
EVAR	7	8.3	13.0	4.2
Open mode	17	14.4	21.5	4.8
Abdominal	20	10.2	21.5	4.2
Thoracic	4	9.3	12.5	4.8

EVAR — endovascular aortic repair